INL/EXT-09-15794

Evaluation of the Start-Up Core Physics Tests at Japan's High Temperature Engineering Test Reactor (Annular Core Loadings)

John D. Bess
Nozomu Fujimoto
James W. Sterbentz
Luka Snoj
Atsushi Zukeran

March 2010

The INL is a U.S. Department of Energy National Laboratory
operated by Battelle Energy Alliance

INL/EXT-09-15794

Evaluation of the Start-Up Core Physics Tests at Japan's High Temperature Engineering Test Reactor (Annular Core Loadings)

John D. Bess
Nozomu Fujimoto[1]
James W. Sterbentz
Luka Snoj[2]
Atsushi Zukeran[3]

[1]Japan Atomic Energy Agency
[2]Jozef Stefan Institute
[3]Senior Reactor Physics Consultant

March 2010

Idaho National Laboratory
Idaho Falls, Idaho 83415

http://www.inl.gov

Prepared for the
U.S. Department of Energy
Office of Nuclear Energy
Under DOE Idaho Operations Office
Contract DE-AC07-05ID14517

NEA/NSC/DOC(2006)1

Gas Cooled (Thermal) Reactor - GCR

HTTR-GCR-RESR-002
CRIT-REAC-RRATE

EVALUATION OF THE START-UP CORE PHYSICS TESTS AT JAPAN'S HIGH TEMPERATURE ENGINEERING TEST REACTOR
(ANNULAR CORE LOADINGS)

Evaluators

John D. Bess
Idaho National Laboratory

Nozomu Fujimoto
Japan Atomic Energy Agency

Internal Reviewers
James W. Sterbentz
Idaho National Laboratory

Independent Reviewers

Luka Snoj
Jozef Stefan Institute

Atsushi Zukeran
Senior Reactor Physics Consultant

Gas Cooled (Thermal) Reactor - GCR

HTTR-GCR-RESR-002
CRIT-REAC-RRATE

Status of Compilation / Evaluation / Peer Review

Section 1	Compiled	Independent Review	Working Group Review	Approved
1.0 DETAILED DESCRIPTION	YES	YES	YES	YES
1.1 Description of the Critical and / or Subcritical Configuration	YES	YES	YES	YES
1.2 Description of Buckling and Extrapolation Length Measurements	NA	NA	NA	NA
1.3 Description of Spectral Characteristics Measurements	NA	NA	NA	NA
1.4 Description of Reactivity Effects Measurements	YES	YES	YES	YES
1.5 Description of Reactivity Coefficient Measurements	NA	NA	NA	NA
1.6 Description of Kinetics Measurements	NA	NA	NA	NA
1.7 Description of Reaction-Rate Distribution Measurements	YES	YES	YES	YES
1.8 Description of Power Distribution Measurements	NA	NA	NA	NA
1.9 Description of Isotopic Measurements	NA	NA	NA	NA
1.10 Description of Other Miscellaneous Types of Measurements	NA	NA	NA	NA
Section 2	**Evaluated**	**Independent Review**	**Working Group Review**	**Approved**
2.0 EVALUATION OF EXPERIMENTAL DATA	YES	YES	YES	YES
2.1 Evaluation of Critical and / or Subcritical Configuration Data	YES	YES	YES	YES
2.2 Evaluation of Buckling and Extrapolation Length Data	NA	NA	NA	NA
2.3 Evaluation of Spectral Characteristics Data	NA	NA	NA	NA
2.4 Evaluation of Reactivity Effects Data	YES	YES	YES	YES
2.5 Evaluation of Reactivity Coefficient Data	NA	NA	NA	NA
2.6 Evaluation of Kinetics Measurements Data	NA	NA	NA	NA
2.7 Evaluation of Reaction Rate Distributions	YES	YES	YES	YES
2.8 Evaluation of Power Distribution Data	NA	NA	NA	NA
2.9 Evaluation of Isotopic Measurements	NA	NA	NA	NA
2.10 Evaluation of Other Miscellaneous Types of Measurements	NA	NA	NA	NA

Gas Cooled (Thermal) Reactor - GCR

HTTR-GCR-RESR-002
CRIT-REAC-RRATE

Section 3	Compiled	Independent Review	Working Group Review	Approved
3.0 BENCHMARK SPECIFICATIONS	YES	YES	YES	YES
3.1 Benchmark-Model Specifications for Critical and / or Subcritical Measurements	YES	YES	YES	YES
3.2 Benchmark-Model Specifications for Buckling and Extrapolation Length Measurements	NA	NA	NA	NA
3.3 Benchmark-Model Specifications for Spectral Characteristics Measurements	NA	NA	NA	NA
3.4 Benchmark-Model Specifications for Reactivity Effects Measurements	YES	YES	YES	YES
3.5 Benchmark-Model Specifications for Reactivity Coefficient Measurements	NA	NA	NA	NA
3.6 Benchmark-Model Specifications for Kinetics Measurements	NA	NA	NA	NA
3.7 Benchmark-Model Specifications for Reaction-Rate Distribution Measurements	YES	YES	YES	YES
3.8 Benchmark-Model Specifications for Power Distribution Measurements	NA	NA	NA	NA
3.9 Benchmark-Model Specifications for Isotopic Measurements	NA	NA	NA	NA
3.10 Benchmark-Model Specifications of Other Miscellaneous Types of Measurements	NA	NA	NA	NA
Section 4	**Compiled**	**Independent Review**	**Working Group Review**	**Approved**
4.0 RESULTS OF SAMPLE CALCULATIONS	YES	YES	YES	YES
4.1 Results of Calculations of the Critical or Subcritical Configurations	YES	YES	YES	YES
4.2 Results of Buckling and Extrapolation Length Calculations	NA	NA	NA	NA
4.3 Results of Spectral Characteristics Calculations	NA	NA	NA	NA
4.4 Results of Reactivity Effect Calculations	YES	YES	YES	YES
4.5 Results of Reactivity Coefficient Calculations	NA	NA	NA	NA
4.6 Results of Kinetics Parameter Calculations	NA	NA	NA	NA
4.7 Results of Reaction-Rate Distribution Calculations	YES	YES	YES	YES
4.8 Results of Power Distribution Calculations	NA	NA	NA	NA
4.9 Results of Isotopic Calculations	NA	NA	NA	NA
4.10 Results of Calculations of Other Miscellaneous Types of Measurements	NA	NA	NA	NA
Section 5	**Compiled**	**Independent Review**	**Working Group Review**	**Approved**
5.0 REFERENCES	YES	YES	YES	YES
Appendix A: Computer Codes, Cross Sections, and Typical Input Listings	YES	YES	YES	YES

Gas Cooled (Thermal) Reactor - GCR

HTTR-GCR-RESR-002
CRIT-REAC-RRATE

EVALUATION OF THE START-UP CORE PHYSICS TESTS AT JAPAN'S HIGH TEMPERATURE ENGINEERING TEST REACTOR (ANNULAR CORE LOADINGS)

IDENTIFICATION NUMBER: HTTR-GCR-RESR-002
CRIT-REAC-RRATE

KEY WORDS: annular cores, critical configurations, graphite-moderated, graphite-reflected, helium coolant, HTTR, low enriched uranium (LEU), pin-in-block fuel, prismatic fuel, thermal reactor, TRISO, uranium oxide fuel

SUMMARY INFORMATION

1.0 DETAILED DESCRIPTION

The High Temperature Engineering Test Reactor (HTTR) of the Japan Atomic Energy Agency (JAEA) is a 30 MWth, graphite-moderated, helium-cooled reactor that was constructed with the objectives to establish and upgrade the technological basis for advanced high-temperature gas-cooled reactors (HTGRs) as well as to conduct various irradiation tests for innovative high-temperature research. The core size of the HTTR represents about one-half of that of future HTGRs, and the high excess reactivity of the HTTR, necessary for compensation of temperature, xenon, and burnup effects during power operations, is similar to that of future HTGRs. During the start-up core physics tests of the HTTR, various annular cores were formed to provide experimental data for verification of design codes for future HTGRs (Ref. 1, p. 310).

The Japanese government approved construction of the HTTR in the 1989 fiscal year budget; construction began at the Oarai Research and Development Center in March 1991 and was completed May 1996. Fuel loading began July 1, 1998, from the core periphery. The first criticality was attained with an annular core on November 10, 1998 at 14:18, followed by a series of start-up core physics tests (Figure 1.1) until a fully-loaded core was developed on December 16, 1998. Criticality tests were carried out into January 1999. The first full power operation with an average core outlet temperature of 850ºC was completed on December 7, 2001, and operational licensing of the HTTR was approved on March 6, 2002. The HTTR attained high temperature operation at 950 ºC in April 19, 2004. After a series of safety demonstration tests, it will be used as the heat source in a hydrogen production system by 2015 (Ref. 3, pp. 12-14).

Hot zero-power critical,[a] rise-to-power,[b] irradiation,[c] and safety demonstration testing[de] have also been performed with the HTTR, representing additional means for computational validation efforts. Power tests were performed in steps from 0 to 30 MW, with various tests performed at each step to confirm core

---

[a] J. C. Kuijper, X. Raepsaet, J. B. M. de Haas, W. von Lensa, U. Ohlig, H-J. Ruetten, H. Brockmann, F. Damian, F. Dolci, W. Bernnat, J. Oppe, J. L. Kloosterman, N. Cerullo, G. Lomonaco, A. Negrini, J. Magill, and R. Seiler, "HTGR Reactor Physics and Fuel Cycle Studies," *Nucl. Eng. Des.*, **236**: 615-634 (2006).

[b] S. Nakagawa, Y. Tachibana, K. Takamatsu, S. Ueta, and S. Hanawa, "Performance Test of HTTR," *Nucl. Eng. Des.*, **233**: 291-300 (2004).

[c] T. Shibata, T. Kikuchi, S. Miyamoto, and K. Ogura, "Assessment of Irradiation Temperature Stability of the First Irradiation Test Rig in the HTTR," *Nucl. Eng. Des.*, **223**: 133-143 (2003).

[d] Y. Tachibana, S. Nakagawa, T. Takeda, A. Saikusa, T. Furusawa, K. Takamatsu, K. Sawa, and T. Iyoku, "Plan for the First Phase of Safety Demonstration Tests of the High Temperature Engineering Test Reactor (HTTR)," *Nucl. Eng. Des.*, **224**: 179-197 (2003).

[e] S. Nakagawa, K. Takamatsu, Y. Tachibana, N. Sakaba, and T. Iyoku, "Safety Demonstration Tests using High Temperature Engineering Test Reactor," *Nucl. Eng. Des.*, **233**: 301-308 (2004).

characteristics, thermal-hydraulic properties, and radiation shielding (Ref. 4, p. 284). The high-temperature test operation at 950 ºC represented the fifth and final phase of the rise-to-power tests.[a] The safety tests demonstrated inherent safety features of the HTTR such as slow temperature response during abnormal events due to the large heat capacity of the core and the negative reactivity feedback.[b]

The experimental benchmark performed and currently evaluated in this report pertains to the data available for the annular core criticals from the initial six isothermal, annular and fully-loaded, core critical measurements performed at the HTTR. Evaluation of the start-up core physics tests specific to the fully-loaded core is compiled elsewhere (HTTR-GCR-RESR-001).

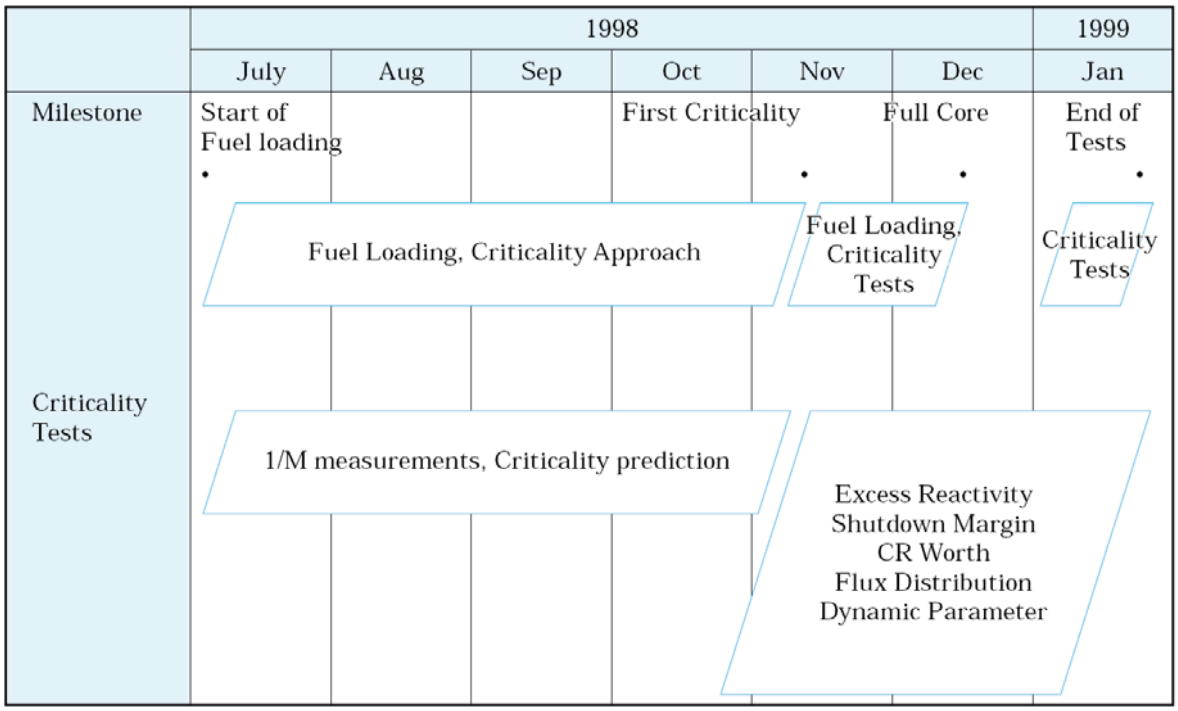

Figure 1.1. Progress of Start-Up Core Physics Tests.[c]

1.1 Description of the Critical and / or Subcritical Configuration

1.1.1 Overview of Experiment

The initial start-up core physics tests for the High Temperature Engineering Test Reactor were performed between the months of July 1998 and January 1999. The HTTR facility is at the Oarai Research and Development Center of the JAEA.

[a] S. Fujikawa, H. Hayashi, T. Nakazawa, K. Kawasaki, T. Iyoku, S. Nakagawa, and N. Sakaba, "Achievement of Reactor-Outlet Coolant Temperature of 950 ºC in HTTR," *J. Nucl. Sci. Tech.*, **41**(12): 1245-1254 (December 2004).

[b] S. Nakagawa, D. Tochio, K. Takamatsu, M. Goro, and T. Takeda, "Improvement of Analysis Technology for High Temperature Gas-Cooled Reactor by using Data Obtained in High Temperature Engineering Test Reactor," *J. Power Energy Syst.*, **2**(1): 83-91 (2008).

[c] "Present Status of HTGR Research and Development," Japan Atomic Energy Research Institute, Tokaimura, March 2004.

First criticality was attained on November 10, 1998, and the core was fully loaded in December 1998. During the fuel loading period, various tests were conducted under cold clean conditions as the start-up core physics tests. During these tests, the power was limited to below 30 W and the helium pressure was 1 bar. The tests for the critical approach, excess reactivity, shutdown margin, neutron flux distribution and control rod worth were conducted (Ref. 4, p. 284). Elsewhere the pressure is listed as 1 atmosphere (Ref. 1, p. 312). One atmosphere is equal to 1.01325×10^5 Pa, or 1.01325 bar.

Of the initial six isothermal, annular and fully-loaded, core critical measurements that were performed, only the annular core loadings were evaluated in this benchmark analysis. The maximum uncertainty range is between -1.03 and +1.00 % Δk (1σ) for the 19-fuel-column core, with a decrease in the uncertainty as graphite dummy blocks are replaced by fuel blocks in the core. Dominant uncertainties are the impurities in the IG-110 graphite blocks, PGX graphite reflector blocks, and IG-11 graphite dummy blocks. Comprehensive biases could not be completed for all aspects of this experiment.

Currently the calculations performed using the benchmark models have a k_{eff} between 1.4 to 2.7 % of the experimental benchmark value and within 3σ, except for configuration 4, which is within 4σ. It is currently difficult to obtain the necessary information to further improve the confidence in the benchmark model and effectively reduce the overall uncertainty; the necessary data is proprietary and its released is being restricted, because the benchmark configuration of the HTTR core is the same that is currently in operation. Once this information is made available, the HTTR benchmark can be adjusted as appropriate.

1.1.2 Geometry of the Experiment Configuration and Measurement Procedure

The geometric information publicly available for this benchmark can be found compiled in Section 1.1.2 of HTTR-GCR-RESR-001.

1.1.2.1 Description of Criticality Measurements

Before fuel loading, the whole region in the core was filled with graphite dummy blocks. Helium gas was filled up to 1 atm at room temperature. Dummy blocks were replaced with fuel blocks, column by column, in the fuel loading, starting from the core periphery to the center, as shown in Figure 1.2.

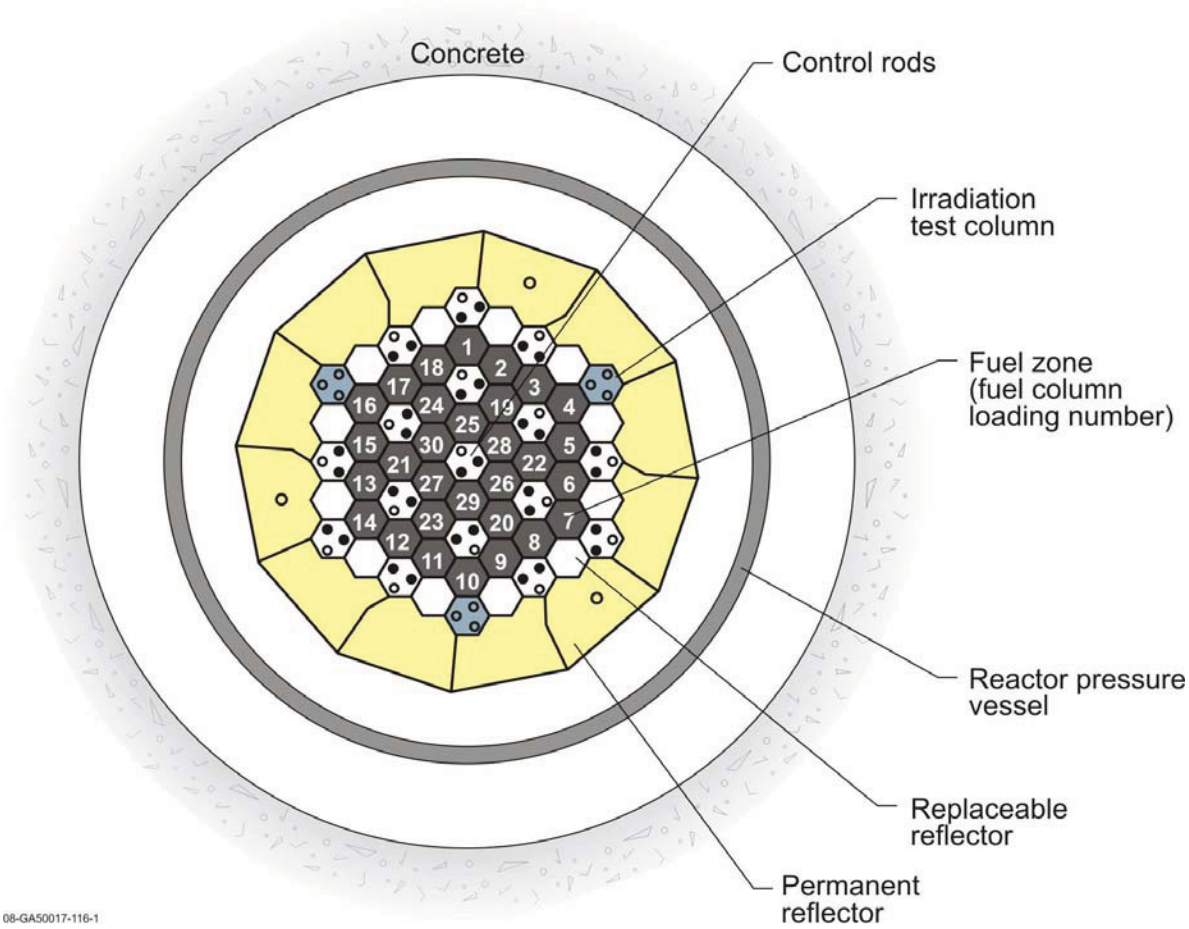

Figure 1.2. Loading Pattern of the HTTR (Redrawn from Ref. 1, p. 313).

In the first phase of fuel loading, six fuel columns were loaded consecutively. In the second phase, three fuel columns were loaded at a time, until a total of 15 columns were in the core. In the third phase of fuel loading, columns were loaded one at a time, so as to identify the number of fuel columns needed for the first criticality. In every loading phase, all control rods were withdrawn from the core after each fuel loading, and inverse multiplication factors were measured. Initial criticality was achieved with 19 fuel columns loaded. Symmetric annular cores were formed at 21-, 24-, and 27-fuel-column loaded cores. The fully-loaded core consists of 30 fuel columns. Figure 1.3 shows some of the fuel-loading steps during the initial core loading (Ref. 4, p. 285).

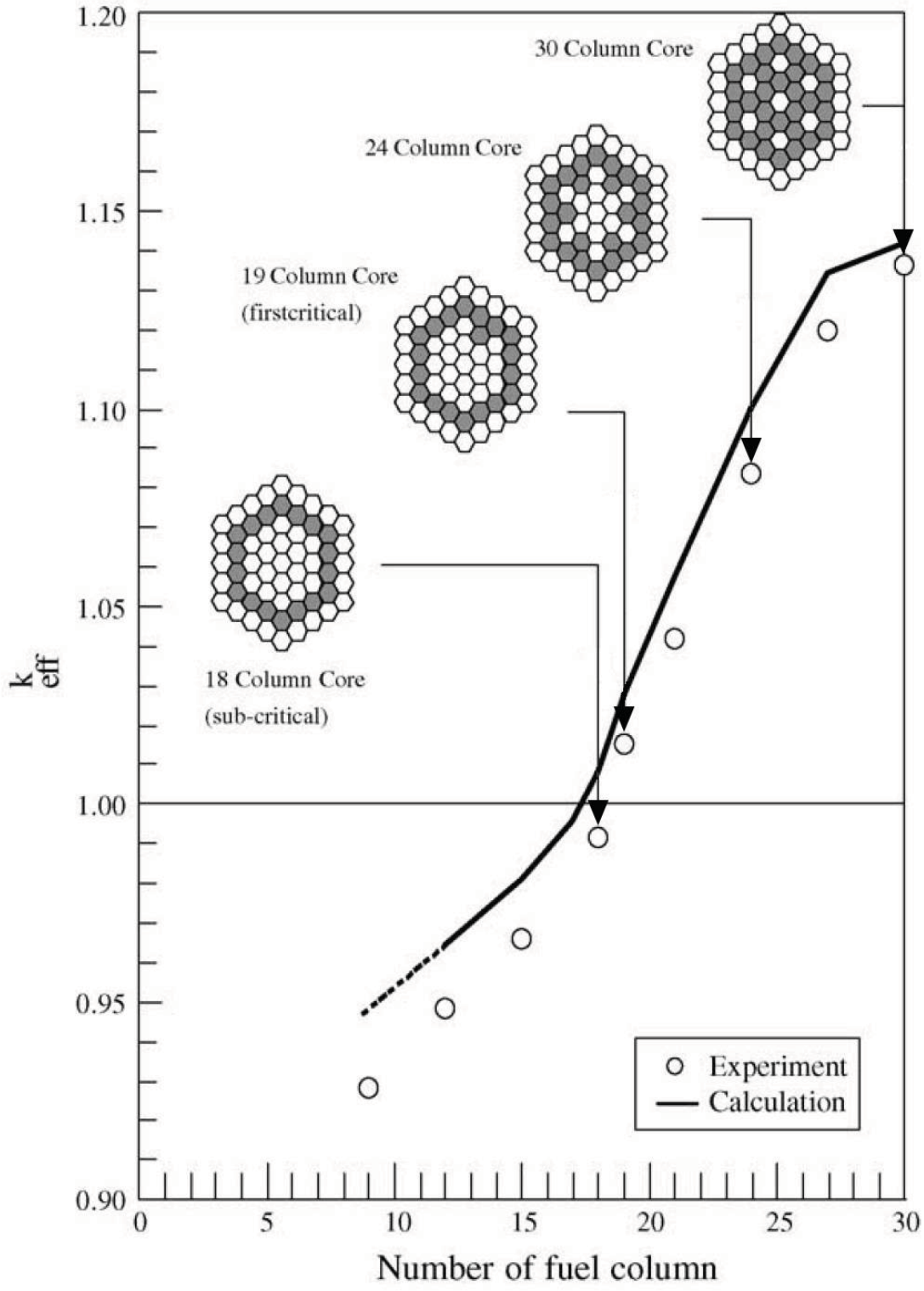

Figure 1.3. Critical Approach at Room Temperature using the Fuel Addition Method (Ref. 4, p. 285).

The inverse neutron multiplication factor was monitored in order to observe the approach to criticality; the core was regarded as critical when the neutron flux was self-sustained after removing the temporary neutron source. After the initial criticality, reactivity increase was measured using the IK (Inverse Kinetics) method. The excess reactivity of the core was then obtained by adding all increments of the reactivity from the first criticality to the fully-loaded core (Ref. 2, p. 14).

Inverse multiplication factors were evaluated at 0, 6, 9, 12, 15, 16, 17, and 18 fuel-column-loaded cores to predict the first criticality (Ref. 2, p. 39). The inverse multiplication data were recorded and are shown in Figure 1.4.

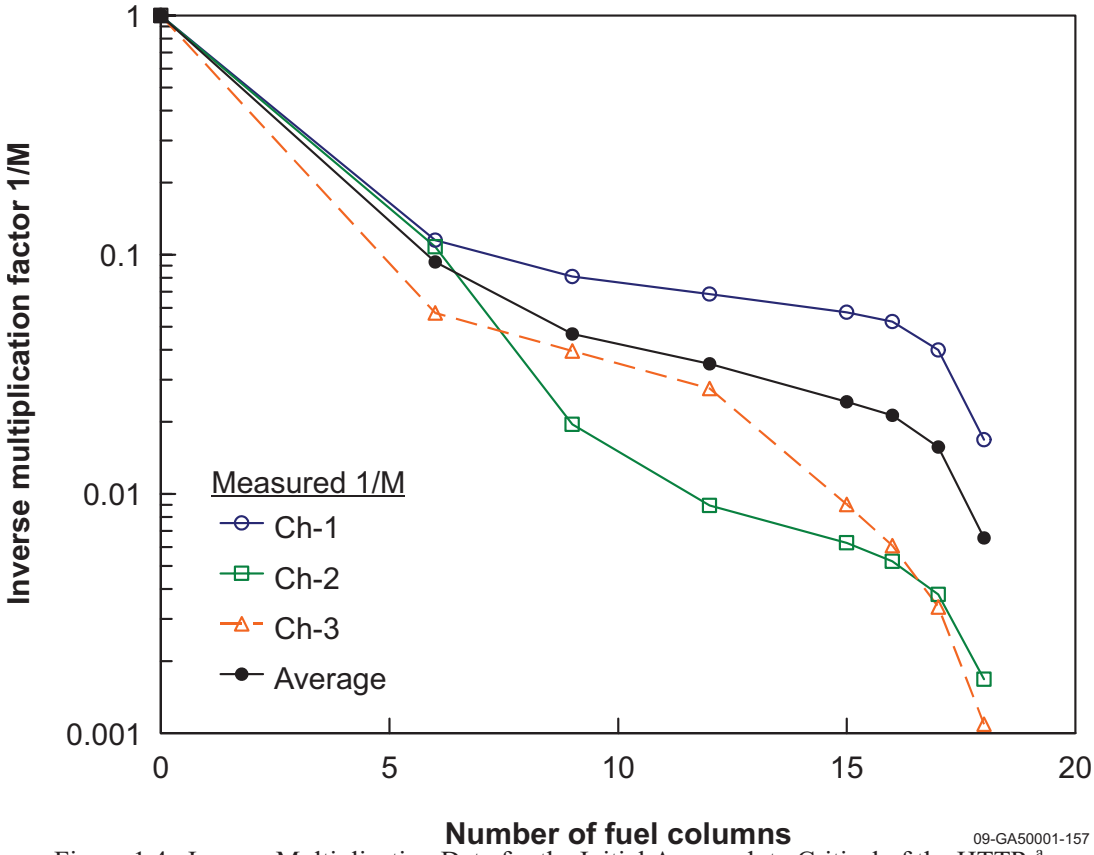

Figure 1.4. Inverse Multiplication Data for the Initial Approach to Critical of the HTTR.[a]

During the first approach to critical (after loading the 19th fuel assembly) the source criticality at very low power was achieved. Then the neutron source was removed and the central control rod moved to compensate for the change in reactivity. The first criticality of the reactor was attained on November 10, 1998. Figure 1.5 shows the result of the reactivity measurements during this approach to critical (Ref. 2, p. 113).

[a] "Present Status of HTGR Research and Development," Japan Atomic Energy Research Institute, Tokaimura, March 2004.

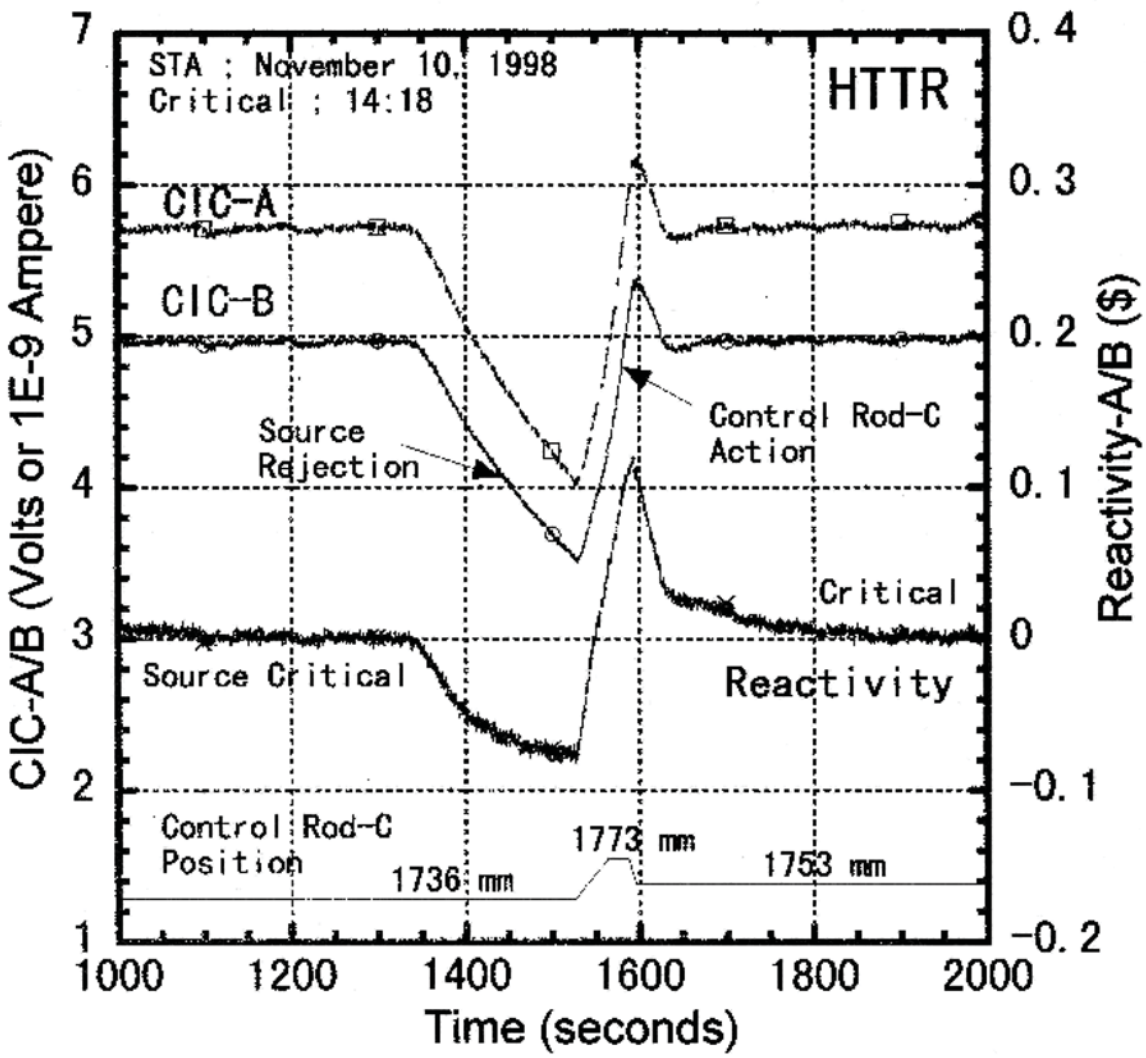

Figure 1.5. Initial Approach to Criticality Reactivity Measurements (Ref 2, p. 114).

The control rod (CR) positions are provided in Table 1.1 for the critical conditions of the annular and fully-loaded cores. The CR pairs were named center (C), ring 1 (R1), ring 2 (R2), and ring 3 (R3) from the center to the outside as shown in Figure 1.2 (also see Section 3.1.2.11 and Figure 3.17). Both R2 and R3 CRs are in the replaceable reflector region surrounding the core, where the six CR pairs on the sides of the hexagonal loading pattern are R2 CRs and the three remaining CR pairs at corners of the hex are R3 CRs. The C-CR was inserted into the 19-column core to adjust initial criticality while the other CRs were fully withdrawn (Ref. 1, p. 317).

All control rod insertion levels are adjusted on the same level except for the three pairs of control rods in the most outer region in the side reflectors. These three pairs of CRs are usually fully withdrawn (Ref. 2, p. 40).

There were two CR patterns used for the 24-fuel-column core. The first was the flat standard (FS) pattern, where the C, R1, and R2 CRs were inserted into the core at the same height, and the R3 CRs were fully withdrawn. The second pattern was the F23 pattern, where the R2 and R3 CRs in the side reflector were inserted into the core at the same height and the C and R1 CRs were fully withdrawn. The F23 pattern was used to simulate the control of future HTGRs, where the reflector CRs would mainly be

used for reactivity control. The effective multiplication factors for the measured CR positions at critical conditions were evaluated for different annular cores and temperatures. The results in Table 1.1 are adjusted such that the multiplication factors could be evaluated at 27 ºC, 300 K (Ref. 1, pp. 317-318).

A simpler statement for control rod positions of four of the critical cases is shown in Table 1.2, representing the average for rods C, R1, and R2 (with R3 completely withdrawn).

Effective corrections to critical rod position in the core include a sinking effect from the CR driving mechanism of about -14 mm and a temperature expansion effect of about +2 mm from 25 to 27 ºC (Ref. 2, p. 46). Reported Japanese data typically had the sinking effect already accounted for in the reported rod positions.

Control rods positions were defined with distance from the bottom of the fifth fuel layer (Ref. 1, p. 317).

Table 1.1. Measured Control Rod Positions for Critical Conditions (Ref. 1, p. 318).

Case	Fuel Columns	Temperature (ºC)	k_m [(a)]	Critical Rod Position (mm)[(b)]				Remark[(c)]
				C	R1	R2	R3	
1	19	23	1.00049	1739	4050	3325	4050	C
2	21	24	1.00037	2647	2645	2646	4049	FS
3	24	24	1.00037	2213	2215	2215	4049	FS
4	24	24	1.00037	4051	4050	1593	1592	F23
5	27	24	1.00037	1901	1899	1899	4050	FS
6	30	25	1.00025	1775	1775	1775	4049	FS

(a) Measured k_m has been corrected with the measured temperature coefficient (TC) for the 30-fuel-column core [-1.23×10^{-4} ($\Delta k/k/ºC$) to 27 ºC (300 K)]. It was assumed that use of the TC for the 30-fuel-column core was practically still useful for the other cores because of the small temperature difference of <4 ºC.

(b) Nominally fully withdrawn positions of C, R1, and R3 CRs are 4060 mm and that of the R2 CRs is 3335 mm.

(c) C = criticality obtained using central control rod only. FS = flat standard pattern where C, R1, and R2 CRs were inserted into the core at the same levels while R3 CRs were fully withdrawn. F23 = only R2 and R3 CRs were used for control while C and R1 CRs were fully withdrawn.

Table 1.2. Average Control Rod Positions for Critical Conditions (Ref. 2, p. 40).

Fuel Column	21 (Case 2)	24 (Case 3)	27 (Case 5)	30 (Case 6)
Rod Position (mm)	2646 ± 5	2215 ± 5	1899 ± 5	1775 ± 5

1.1.3 Material Data

The material data publicly available for this benchmark can be found compiled in Section 1.1.3 of HTTR-GCR-RESR-001.

1.1.4 Temperature Data

The core is at room temperature (Ref. 2, p. 14). Table 1.1 provides the temperature of the experiment for each of the six critical configurations, ranging between 23 and 25ºC.

1.1.5 Additional Information Relevant to Critical and Subcritical Measurements

Additional information is not available.

1.2 Description of Buckling and Extrapolation Length Measurements

Buckling and extrapolation length measurements were not made.

1.3 Description of Spectral Characteristics Measurements

Spectral characteristics measurements were not made.

1.4 Description of Reactivity Effects Measurements

After the initial criticality the excess reactivity of the core was then obtained by adding all increments of the reactivity from the first criticality to the fully-loaded core (Ref. 2, p. 14).

Further information regarding the measurement of excess reactivity of the annular core configurations is provided in Section 1.4.2.1 of HTTR-GCR-RESR-001.

1.5 Description of Reactivity Coefficient Measurements

Reactivity coefficient measurements were not made.

1.6 Description of Kinetics Measurements

Kinetics measurements were not made.

1.7 Description of Reaction-Rate Distribution Measurements

1.7.1 Overview of Experiment

The axial reaction rate profile in the instrumentation columns has been evaluated for this benchmark configuration.

1.7.2 Geometry of the Experiment Configuration and Measurement Procedure

The geometry of the core is that of the fully-loaded core configuration in Section 1.1.2 with modifications as stated below.

1.7.2.1 Axial Reaction Rate Distribution

The fission reaction rate of ^{235}U was regarded as a neutron flux distribution because the neutron flux distribution could not be directly measured in the HTTR core. The three micro fission chambers (FCs) placed in the irradiation test columns were used to measure the axial reaction rate. The FCs are 5 cm long with a diameter of 0.6 cm. A FC was connected to the end of a long aluminum stick such that it could be axially traversed by moving the stick in the aluminum tube well inserted into the holes of the irradiation test columns. The temporary neutron source was withdrawn from the core during measurements. The reaction rates were then measured at several points around the peak of the reaction rate distribution to search for the peak. The reactor power was changed by the movement of the FC because reactivity was added by movement of the attached stick and cable, which caused a change in the reaction rates of the FCs. The reaction rate of the traversing FC was then normalized with the reaction rate of the FC fixed in another irradiation test column. The axial fission reaction rate distributions were measured for the 24- and 30-fuel-column cores. Both FS and F23 patterns were formed in the 24-fuel-column core. The experimental error of the neutron flux was ~0.2 %, and was evaluated from the number of FC pulse counts. Measured distributions are shown (compared with some of Japan's calculated results) in Figure 1.6 (Ref. 1, pp. 317-318).

The reaction rate for the 30-fuel-column core configuration is evaluated in HTTR-GCR-RESR-001, as it represents measurements performed using the fully-loaded core configuration of the HTTR.

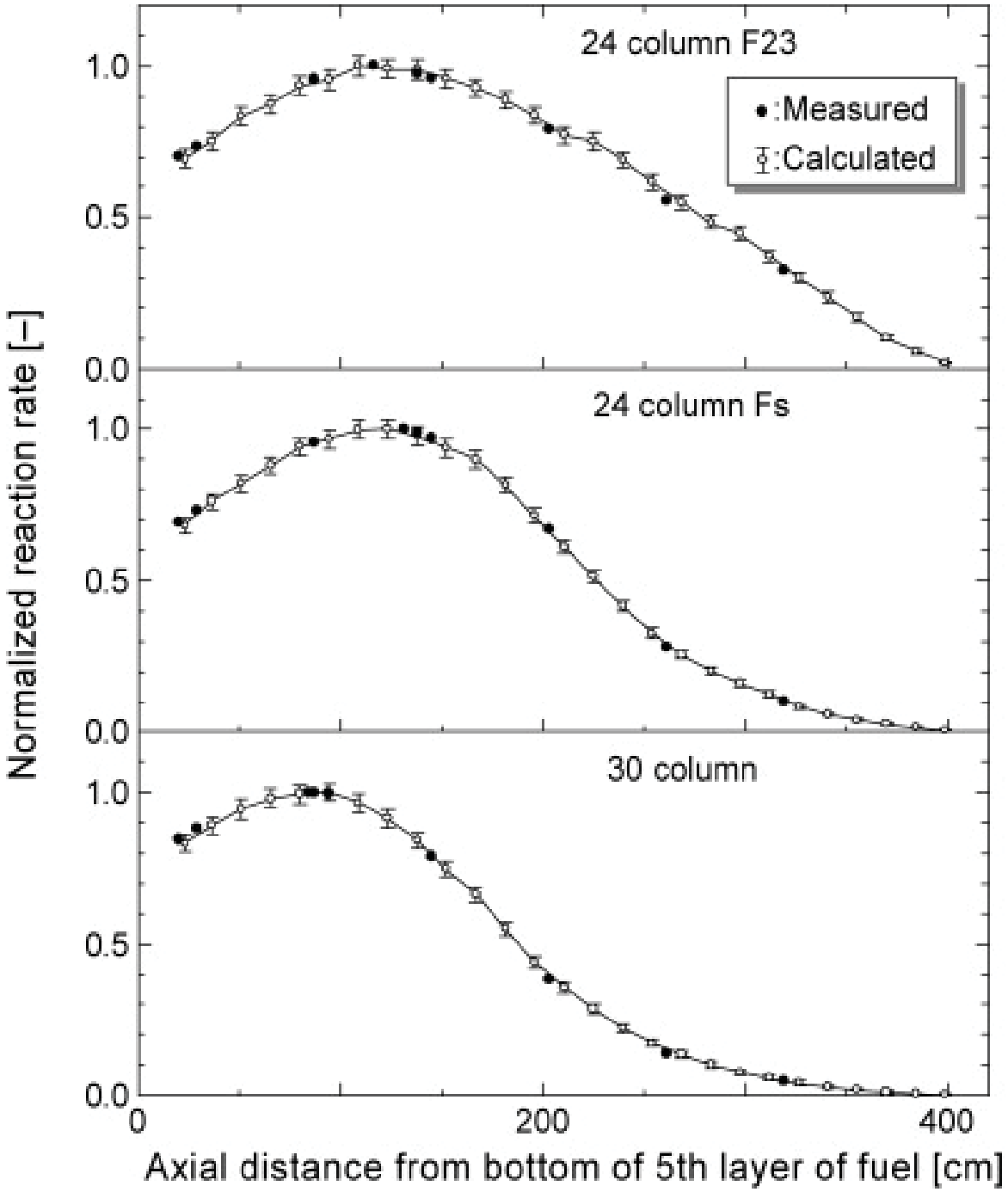

Figure 1.6. Axial Reaction Rate Distribution in Irradiation Column for 24- and 30-Fuel-Column Cores (Ref. 1, p. 318). F23 and FS are defined in the footnote of Table 1.1. The 30-fuel-column core reaction-rate measurements are evaluated in HTTR-GCR-RESR-001.

1.7.3 Material Data

The materials in the core were those described in the fully-loaded core configuration in Section 1.1.3 with modifications as stated below.

1.7.4 Temperature Data

Experiments were essentially performed at room temperature.

1.7.5 Additional Information Relevant to Reaction-Rate Distribution Measurements

Additional information is not available.

1.8 Description of Power Distribution Measurements

Power distribution measurements were not made.

1.9 Description of Isotopic Measurements

Isotopic measurements were not made.

1.10 Description of Other Miscellaneous Types of Measurements

Other miscellaneous types of measurements were not made.

2.0 EVALUATION OF EXPERIMENTAL DATA

The overall uncertainty in the calculated value of k_{eff}, which is a function of multiple input parameters, is given by[a]

$$u_c^2(k_{eff}) = \sum_{i=1}^{N} (\Delta k_i)^2 + 2\sum_{i=1}^{N-1} \sum_{j=i+1}^{N} (\Delta k_i)(\Delta k_j) r_{i,j} \,. \tag{2.1}$$

In Equation 2.1, Δk_i is the change in k_{eff} when parameter i is changed by the standard deviation in the parameter, and $r_{i,j}$ is the correlation coefficient for parameters i and j.

Where standard deviations are available, they are used for calculating the effects these uncertainties might have on k_{eff}, in terms of Δk_i. Where observed ranges are given, but not standard deviations, the limiting values of the observed ranges are usually applied, and plausible distribution functions are assumed for finding Δk_i. Where only tolerances are given, their limiting values are used, along with plausible distribution functions. Where no guidance is given on the variability of a parameter, engineering judgment is used to select a range of variation that will produce the largest reasonable uncertainty in k_{eff}. The bounding values in this range are then applied in the uncertainty analysis. If the overall uncertainty in k_{eff} predicted by this approach is small enough that the experiment can be judged an acceptable benchmark, one can be confident that the real experiment is actually even better. All uncertainties are adjusted to values of one standard deviation (1σ). No information is available on correlations among parameters, so all parameters and their uncertainties are assumed to be uncorrelated.

Usually, no information is publicly available about the distribution function of the deviation of a parameter from its nominal value. In most cases, it is reasonably assumed that the most relevant quantity is uniformly distributed. For example, if the change in k_{eff} from its nominal value is dependent on the change in the volume of a spatial region, then it is assumed that the deviation of the volume of that region from its nominal value is uniformly distributed.

The uncertainty analyses were performed in accordance with guidance provided in the ICSBEP Handbook.

It should be noted that assuming a uniform distribution of a parameter between its limits leads to overprediction of the effect on k_{eff}.

These observations are used repeatedly in the following analysis.

The following sections discuss the calculation of the effects of uncertainties in the parameters listed in tables in each section. The values of the tabulated parameters are computed in the benchmark critical configuration and in the configuration with each parameter assigned its maximum variation (or its standard deviation when available), one parameter at a time. The bases for the choices of the parameter values are discussed.

In all cases where tolerances or observed variations apply to large numbers of objects, such as TRISO fuel particles, both deterministic (or systematic) uncertainties (applying to all the objects equally) and random uncertainties (different from one object to the next) will occur. For the fuel particles and their subregions especially, the random uncertainties are extremely small (i.e., the tolerance limit for the random uncertainty divided by the square root of the number of fuel particles in the core). In all cases, division by such large numbers would make the random component of the uncertainty negligible.

[a] *International Handbook of Evaluated Criticality Safety Benchmark Experiments,* NEA/NSC/DOC(95)03/I-VIII, OECD-NEA, "ICSBEP Guide to the Expression of Uncertainties," Revision 1, p. 29, September 30, 2004.

Positional dependence of objects within the assembly also influences the effective proportional effect on the resultant uncertainty and bias calculations. However, since no information is available about how the uncertainties are divided between the systematic and random components, it is assumed throughout that the uncertainties are 25 % systematic and 75 % random for all uncertainties that exhibit a random component.

This assumption provides a basic prediction of the effect on k_{eff} until additional information regarding systematic uncertainties can be better evaluated. The 25 % systematic uncertainty is bound by the fact that most systematic uncertainties would be below 50 % of the total uncertainty and above the historic approach of ignoring the unknown systematic components (i.e., treat it with a 0 % probability). In actuality, careful experimenters may have an unknown systematic uncertainty that is approximately 10-15 % of their total reported uncertainty. Evaluated uncertainties are listed as calculated, such that the readers may themselves adjust results according to some desired systematic-to-random uncertainty ratio. The summary in Section 2.1.7 does list the systematic and random components of the uncertainty as separate entities based on the assumption that uncertainties with random components have 25 % systematic uncertainty.

It is important to note that most parameters regarding the TRISO particles are normally distributed.

2.1 Evaluation of Critical and / or Subcritical Configuration Data

In the preliminary Japanese computational evaluation, the predicted number of fuel columns to achieve criticality was 16±1, much less than the experimental result of 19. It was regarded that the neglect of nitrogen in the porous graphite led to this discrepancy. Two reevaluations were carried out after the initial criticality experiment (Ref. 1, pp. 313-314). The first reevaluation examined the air content in the graphite, simplification of graphite geometry, and impurity concentration in the dummy blocks. The predicted number of fuel columns for initial criticality was changed to 18±1.[a] The second reevaluation wasn't performed until after the full power tests at 30 MW and 850 ºC. Heterogeneity effects and air composition in the graphite was analyzed; the reevaluation also predicted 18±1 fuel columns for initial criticality.[b]

Monte Carlo n-Particle (MCNP) version 5.1.40 calculations were utilized to estimate the biases and uncertainties associated with the experimental results for HTTR critical configurations in this evaluation. MCNP is a general-purpose, continuous-energy, generalized-geometry, time-dependent, coupled n-particle Monte Carlo transport code.[c] The Evaluated Neutron Data File library, ENDF/B-VII.0,[d] was utilized in analysis of the experiment and benchmark model biases and uncertainties.

Elemental data such as molecular weights and isotopic abundances were taken from the 16th edition of the Chart of the Nuclides.[e] These values are summarized in Appendix C.

---

[a] Fujimoto, N., Nakano, M., Takeuchi, M., Fujisaki, S., and Yamashita, K., "Start-Up Core Physics Tests of High Temperature Engineering Test Reactor (HTTR), (II): First Criticality by an Annular Form Fuel Loading and Its Criticality Prediction Method," *J. Atomic Energy Society Japan*, **42**(5), 458-464 (2000).

[b] Yamashita, K., Fujimoto, N., Takeuchi, M., Fujisaki, S., Nakano, M., Umeda, M., Takeda, T., Mogi, H., and Tanaka, T., "Startup Core Physics Tests of High Temperature Engineering Test Reactor (HTTR), (I): Test Plan, Fuel Loading and Nuclear Characteristics Tests," *J. Atomic Energy Society Japan*, **42**(1), 30-42 (2000).

[c] X-5 Monte Carlo Team, "MCNP – a General Monte Carlo n-Particle Transport Code, version 5," LA-UR-03-1987, Los Alamos National Laboratory (2003).

[d] M. B. Chadwick, et al., "ENDF/B-VII.0: Next Generation Evaluated Nuclear Data Library for Nuclear Science and Technology," *Nucl. Data Sheets*, **107**: 2931-3060 (2006).

[e] Nuclides and Isotopes: Chart of the Nuclides, 16th edition, (2002).

Only the primary components of the HTTR active core and surrounding reflector region were included in the analysis of uncertainties in this evaluation. The uncertainty analysis was performed using a model temperature of approximately 300 K. Five configurations, or cases, representing the HTTR annular cores, created during initial fuel loading, are analyzed in this benchmark. The fully-loaded core configuration is analyzed in a separate report (HTTR-GCR-RESR-001). The difference between the different cases is the number of loaded fuel columns in the core; these are identified in Table 1.1.

For all impurity assessments, only the equivalent natural-boron content is utilized in the evaluation. In the compositions used in the evaluation models, the natural-boron content is adjusted to include only the primary absorber ^{10}B, according to an isotopic abundance of 19.9 at.%.

All MCNP calculations of k_{eff} have statistical uncertainties between 0.00011 and 0.00012, resulting in Δk statistical uncertainties of approximately 0.00016, assuming no correlation between the individual MCNP results.

Some of the calculated uncertainties are poorly estimated because they are very small and on the order of the statistical uncertainty of the analysis method. However, these uncertainties are insignificant in magnitude compared to the total benchmark uncertainty. Reanalysis of most of these parameters with larger variations would not significantly reduce their uncertainties below the statistical uncertainty of the Monte Carlo calculations.

Uncertainties less than 0.00001 are reported as negligible (neg). When calculated uncertainties in Δk_{eff} are less than their statistical uncertainties, the statistical uncertainties are used in the calculation of the total uncertainty.

The term "Scaling Factor" denotes the necessary correction to adjust the evaluated uncertainty in k_{eff} to a 1σ value. Often a larger uncertainty is evaluated such that the calculated Δk value is greater than the statistical uncertainty in the analysis method.

2.1.1 Experimental Uncertainties

2.1.1.1 Temperature

Temperature coefficients were not determined for the annular core configurations. The experimenters assumed that the temperature coefficient for the fully-loaded core configuration applies toward all HTTR configurations. Various temperature coefficients of reactivity are reported, ranging from -1.23×10^{-4} $\Delta k/k$-ºC (Table 1.17 of HTTR-GCR-RESR-001) to -14.2 pcm/ºC (Ref. 2, p. 113 and 132). An average of -13.25 pcm/ºC with a deviation of ±0.95 (1σ) was selected to represent the effective change in reactivity with temperature adjustment. The experiments were performed near room temperature, and an uncertainty of ±1 ºC (1σ) was selected to represent the uncertainty in the temperature of the experiment. Results are shown in Table 2.1.

The uncertainty in the temperature is considered all systematic with no random component.

Table 2.1. Effect of Uncertainty in Temperature.

Deviation	Δk	±	$\sigma_{\Delta k}$	Scaling Factor	Δk_{eff} (1σ)	±	$\sigma_{\Delta keff}$
-1 ºC	0.00013	±	0.00001	1	0.00013	±	0.00001
+1 ºC	-0.00013	±	0.00001	1	-0.00013	±	0.00001

2.1.1.2 Control Rod Position

Control rod positions were varied ±15 mm (3σ), as shown in Table 1.2, to determine the effective change in k_{eff}. The "sinking effect" of -14 mm that was described in Section 1.1.2.1 (just prior to Table 1.1) had already been applied to the rod position shown in Tables 1.1 and 1.2. It is unconfirmed whether temperature expansion effect of ±2 mm (reported at the end of Section 1.1.2.4 in HTTR-GCR-RESR-001) applies uniformly to all control rods, how it was obtained, or that is was even applied to the reported experimental positions. Therefore it is applied with the ±5 mm in a root mean square approach, the overall uncertainty in the height remains approximately ±5 mm. No additional bias or bias uncertainty was evaluated for the sinking effect of the control rods. Results are shown in Table 2.2.

The total number of control rods used in the core is 32 (16 pairs). For determining the random component of the uncertainty in Section 2.1.7, the results in Table 2.2 are divided by $\sqrt{16}$.

Table 2.2. Effect of Uncertainty in Control Rod Position.

Case	Deviation	Δk	±	$\sigma_{\Delta k}$	Scaling Factor	Δk_{eff} (1σ)	±	$\sigma_{\Delta keff}$
1	-15 mm (3σ)	-0.00036	±	0.00017	3	-0.00012	±	0.00006
	+15 mm (3σ)	0.00041	±	0.00017	3	0.00014	±	0.00006
2	-15 mm (3σ)	-0.00133	±	0.00017	3	-0.00044	±	0.00006
	+15 mm (3σ)	0.00142	±	0.00016	3	0.00047	±	0.00005
3	-15 mm (3σ)	-0.00175	±	0.00016	3	-0.00058	±	0.00005
	+15 mm (3σ)	0.00156	±	0.00017	3	0.00052	±	0.00006
4	-15 mm (3σ)	-0.00111	±	0.00017	3	-0.00037	±	0.00006
	+15 mm (3σ)	0.00076	±	0.00017	3	0.00025	±	0.00006
5	-15 mm (3σ)	-0.00169	±	0.00016	3	-0.00056	±	0.00005
	+15 mm (3σ)	0.00187	±	0.00016	3	0.00062	±	0.00005

2.1.1.3 Measured Value of k_{eff}

There is no additional information regarding the accuracy of the k_{eff} measurements for the critical core conditions reported in Table 1.1. Typically the uncertainty and its effect are relatively insignificant.

2.1.2 Geometrical Properties

2.1.2.1 Coated Fuel Particles

When adjusting the diameters of the TRISO particle coatings, the other diameters are held constant. This in turn would increase or decrease the mass of the remaining layers. Whereas the diameters of the different layers appeared to be documented with more detail (see Table 1.14 and Figure 1.48 of HTTR-GCR-RESR-001), this approach seemed appropriate. The uncertainty in the mass is then evaluated as part of the density uncertainty Section 2.1.3.1.

Kernel Diameter

Because of the overspecification of the TRISO particles in Table 1.14 (HTTR-GCR-RESR-001) and the correlation of uranium kernel diameter, density, TRISO packing fraction, and mass, the effect of the

uncertainty in the kernel diameter is not included in the total uncertainty. However, an analysis of the uncertainty based upon the fuel mass is performed in Section 2.1.6.

Buffer Diameter

The buffer thickness was varied ±12 μm (3σ) from the nominal value of 60 μm (Tables 1.12 and 1.14, and Figure 1.48 of HTTR-GCR-RESR-001) to determine the effective change in k_{eff}. All other thicknesses in the TRISO particle were maintained the same. The packing fraction of the TRISO particles in the fuel was not conserved, so as to conserve fuel mass, but remained within 1σ of the nominal value of 30 vol. % (±3 % in Table 1.14 of HTTR-GCR-RESR-001). Results are shown in Table 2.3.

The total number of TRISO particles used in the fully-loaded core is approximately 868,140,000. For determining the random component of the uncertainty, the results in Table 2.3 would be divided by √N, where N for each case is shown in Table 2.3.

Table 2.3. Effect of Uncertainty in Buffer Diameter.

Case	Deviation	Δk	±	$\sigma_{\Delta k}$	Scaling Factor	Δk_{eff} (1σ)	±	$\sigma_{\Delta keff}$	N
1	-12 μm (3σ)	0.00009	±	0.00016	3	0.00003	±	0.00005	5.38×10^8
	+12 μm (3σ)	0.00000	±	0.00017	3	0.00000	±	0.00006	
2	-12 μm (3σ)	-0.00005	±	0.00016	3	-0.00002	±	0.00006	5.98×10^8
	+12 μm (3σ)	-0.00016	±	0.00017	3	-0.00005	±	0.00006	
3	-12 μm (3σ)	-0.00019	±	0.00016	3	-0.00006	±	0.00005	6.88×10^8
	+12 μm (3σ)	-0.00015	±	0.00017	3	-0.00005	±	0.00006	
4	-12 μm (3σ)	0.00002	±	0.00017	3	0.00001	±	0.00006	6.88×10^8
	+12 μm (3σ)	-0.00043	±	0.00017	3	-0.00014	±	0.00006	
5	-12 μm (3σ)	0.00028	±	0.00016	3	0.00009	±	0.00005	7.78×10^8
	+12 μm (3σ)	-0.00022	±	0.00016	3	-0.00007	±	0.00005	

IPyC Diameter

The IPyC thickness was varied ±6 μm (3σ) from the nominal value of 30 μm (Tables 1.12 and 1.14, and Figure 1.48 of HTTR-GCR-RESR-001) to determine the effective uncertainty in k_{eff}. All other thicknesses in the TRISO particle were maintained the same. The packing fraction of the TRISO particles in the fuel was not conserved but remained within 1σ of the nominal value of 30 vol. % (±3 % in Table 1.14 of HTTR-GCR-RESR-001). Results are shown in Table 2.4.

The total number of TRISO particles used in the fully-loaded core is approximately 868,140,000. For determining the random component of the uncertainty, the results in Table 2.4 would be divided by √N, where N for each case is shown in Table 2.4.

Table 2.4. Effect of Uncertainty in IPyC Diameter.

Case	Deviation	Δk	±	$\sigma_{\Delta k}$	Scaling Factor	Δk_{eff} (1σ)	±	$\sigma_{\Delta keff}$	N
1	-6 µm (3σ)	0.00003	±	0.00017	3	0.00001	±	0.00006	5.38×10^8
	+6 µm (3σ)	0.00014	±	0.00016	3	0.00005	±	0.00005	
2	-6 µm (3σ)	-0.00002	±	0.00016	3	-0.00001	±	0.00005	5.98×10^8
	+6 µm (3σ)	-0.00002	±	0.00017	3	-0.00001	±	0.00006	
3	-6 µm (3σ)	-0.00017	±	0.00017	3	-0.00006	±	0.00006	6.88×10^8
	+6 µm (3σ)	0.00007	±	0.00017	3	0.00002	±	0.00006	
4	-6 µm (3σ)	-0.00008	±	0.00017	3	-0.00003	±	0.00006	6.88×10^8
	+6 µm (3σ)	0.00003	±	0.00017	3	0.00001	±	0.00006	
5	-6 µm (3σ)	0.00010	±	0.00016	3	0.00003	±	0.00005	7.78×10^8
	+6 µm (3σ)	0.00004	±	0.00016	3	0.00001	±	0.00005	

SiC Diameter

The SiC thickness was varied ±12 µm (3σ) from the nominal value of 30 µm (Tables 1.12 and 1.14, and Figure 1.48 of HTTR-GCR-RESR-001) to determine the effective uncertainty in k_{eff}. Although there is a negative component to the deviation in the thickness (Figure 1.48 of HTTR-GCR-RESR-001), TRISO particles with SiC thicknesses less than 25 µm are not acceptable for use as a final product. The thickness of 25 µm for the thickness appears to be a manufacturing limit while the thickness of 30 µm is more likely to be the actual thickness of the SiC layer. All other thicknesses in the TRISO particle were maintained the same. The packing fraction of the TRISO particles in the fuel was not conserved but remained within 1σ of the nominal value of 30 vol. % (±3 % in Table 1.14 of HTTR-GCR-RESR-001). Results are shown in Table 2.5.

The total number of TRISO particles used in the fully-loaded core is approximately 868,140,000. For determining the random component of the uncertainty, the results in Table 2.5 would be divided by √N, where N for each case is shown in Table 2.5.

Table 2.5. Effect of Uncertainty in SiC Diameter.

Case	Deviation	Δk ± $\sigma_{\Delta k}$	Scaling Factor	Δk_{eff} (1σ) ± $\sigma_{\Delta keff}$	N
1	-12 μm (3σ)	0.00019 ± 0.00017	3	0.00006 ± 0.00006	5.38×10^8
	+12 μm (3σ)	-0.00062 ± 0.00017	3	-0.00021 ± 0.00006	
2	-12 μm (3σ)	0.00070 ± 0.00017	3	0.00023 ± 0.00006	5.98×10^8
	+12 μm (3σ)	-0.00021 ± 0.00016	3	-0.00007 ± 0.00005	
3	-12 μm (3σ)	0.00062 ± 0.00016	3	0.00021 ± 0.00005	6.88×10^8
	+12 μm (3σ)	-0.00057 ± 0.00017	3	-0.00019 ± 0.00006	
4	-12 μm (3σ)	0.00025 ± 0.00016	3	0.00008 ± 0.00005	6.88×10^8
	+12 μm (3σ)	-0.00080 ± 0.00017	3	-0.00027 ± 0.00006	
5	-12 μm (3σ)	0.00068 ± 0.00016	3	0.00023 ± 0.00005	7.78×10^8
	+12 μm (3σ)	-0.00074 ± 0.00016	3	-0.00025 ± 0.00005	

OPyC Diameter

The OPyC thickness was varied ±6 μm (3σ) from the nominal value of 45 μm (Tables 1.12 and 1.14, and Figure 1.48 of HTTR-GCR-RESR-001) to determine the effective uncertainty in k_{eff}. All other thicknesses in the TRISO particle were maintained the same. The packing fraction of the TRISO particles in the fuel was not conserved but remained within 1σ of the nominal value of 30 vol. % (±3 % in Table 1.14 of HTTR-GCR-RESR-001). Results are shown in Table 2.6.

The total number of TRISO particles used in the fully-loaded core is approximately 868,140,000. For determining the random component of the uncertainty, the results in Table 2.6 would be divided by √N, where N for each case is shown in Table 2.6.

Table 2.6. Effect of Uncertainty in OPyC Diameter.

Case	Deviation	Δk ± $\sigma_{\Delta k}$	Scaling Factor	Δk_{eff} (1σ) ± $\sigma_{\Delta keff}$	N
1	-6 μm (3σ)	-0.00002 ± 0.00016	3	-0.00001 ± 0.00005	5.38×10^8
	+6 μm (3σ)	0.00000 ± 0.00017	3	0.00000 ± 0.00006	
2	-6 μm (3σ)	0.00019 ± 0.00016	3	0.00006 ± 0.00005	5.98×10^8
	+6 μm (3σ)	0.00032 ± 0.00017	3	0.00011 ± 0.00006	
3	-6 μm (3σ)	-0.00018 ± 0.00017	3	-0.00006 ± 0.00006	6.88×10^8
	+6 μm (3σ)	0.00011 ± 0.00017	3	0.00004 ± 0.00006	
4	-6 μm (3σ)	-0.00014 ± 0.00017	3	-0.00005 ± 0.00006	6.88×10^8
	+6 μm (3σ)	-0.00031 ± 0.00017	3	-0.00010 ± 0.00006	
5	-6 μm (3σ)	-0.00003 ± 0.00016	3	-0.00001 ± 0.00005	7.78×10^8
	+6 μm (3σ)	-0.00002 ± 0.00016	3	-0.00001 ± 0.00005	

Overcoat Diameter

Because insufficient data is available for the final composition and density of the graphite overcoat, this layer is being treated with equal properties to that of the surrounding compact graphite matrix (Table 1.14 of HTTR-GCR-RESR-001). Therefore modification of the overcoat diameter would not generate an effective uncertainty in k_{eff} beyond statistical uncertainty.

2.1.2.2 Prismatic Fuel Compact

Dimensions

The inner and outer diameters (ID and OD) of a fuel compact were each individually varied ±0.3 mm and the height (H) was varied ±0.5 mm to determine the effective uncertainty in k_{eff}. For the effective change in height, the fuel stack height was adjusted by ±7.0 mm and the effect from a height change in a single fuel compact was then determined by dividing by 14 for the number of compacts in a fuel rod. The nominal values for the inner diameter, outer diameter, and height of the fuel compacts are 10.0, 26.0, and 39.0 mm, respectively (Table 1.14 of HTTR-GCR-RESR-001). Results are shown in Tables 2.7 through 2.9. In essence, changing the dimensions of the fuel compact without changing the number of TRISO particles would slightly adjust the packing fraction, but within the uncertainty limits.

Later information was obtained regarding manufacturing tolerances for the fuel compacts. The ±0.1 mm of the ID and OD represents a bounding limit (with assumed uniform probability) and the effective stack height has a bounding limit (with assumed uniform probability) of ±1.0 mm.[a] The appropriate corrections to the scaling factors have been incorporated into the uncertainty analysis of these parameters.

The total number of fuel compacts used in the fully-loaded core is 66,780. For determining the random component of the uncertainty, the results in Tables 2.7 through 2.9 would be divided by √N, where N for each case is shown in Tables 2.7 through 2.9.

Table 2.7. Effect of Uncertainty in Compact Dimensions (Inner Diameter).

Case	Deviation	Δk	±	$\sigma_{\Delta k}$	Scaling Factor	Δk_{eff} (1σ)	±	$\sigma_{\Delta keff}$	N
1	-0.3 mm (3 × limit)	0.00016	±	0.00016	3√3	0.00003	±	0.00003	41,370
	+0.3 mm (3 × limit)	-0.00003	±	0.00017	3√3	-0.00001	±	0.00003	
2	-0.3 mm (3 × limit)	0.00014	±	0.00016	3√3	0.00003	±	0.00003	45,990
	+0.3 mm (3 × limit)	-0.00020	±	0.00016	3√3	-0.00004	±	0.00003	
3	-0.3 mm (3 × limit)	0.00014	±	0.00017	3√3	0.00003	±	0.00003	52,920
	+0.3 mm (3 × limit)	-0.00008	±	0.00017	3√3	-0.00002	±	0.00003	
4	-0.3 mm (3 × limit)	-0.00004	±	0.00017	3√3	-0.00001	±	0.00003	52,920
	+0.3 mm (3 × limit)	-0.00037	±	0.00017	3√3	-0.00007	±	0.00003	
5	-0.3 mm (3 × limit)	0.00012	±	0.00016	3√3	0.00002	±	0.00003	59,850
	+0.3 mm (3 × limit)	-0.00023	±	0.00016	3√3	-0.00004	±	0.00003	

[a] S. Maruyama, K. Yamashita, N. Fujimoto, I. Murata, R. Shindo, and Y. Sudo, "Determination of Hot Spot Factors for Calculation of the Maximum Fuel Temperatures in the Core Thermal and Hydraulic Design of HTTR," JAERI-M 88-250, JAEA (November 18, 1988). [in Japanese].

Table 2.8. Effect of Uncertainty in Compact Dimensions (Outer Diameter).

Case	Deviation	Δk	±	$\sigma_{\Delta k}$	Scaling Factor	Δk_{eff} (1σ)	±	$\sigma_{\Delta keff}$	N
1	-0.3 mm (3 × limit)	-0.00048	±	0.00017	3√3	-0.00009	±	0.00003	41,370
	+0.3 mm (3 × limit)	0.00060	±	0.00016	3√3	0.00012	±	0.00003	
2	-0.3 mm (3 × limit)	-0.00050	±	0.00016	3√3	-0.00010	±	0.00003	45,990
	+0.3 mm (3 × limit)	0.00049	±	0.00016	3√3	0.00009	±	0.00003	
3	-0.3 mm (3 × limit)	-0.00087	±	0.00016	3√3	-0.00017	±	0.00003	52,920
	+0.3 mm (3 × limit)	0.00068	±	0.00016	3√3	0.00013	±	0.00003	
4	-0.3 mm (3 × limit)	-0.00081	±	0.00017	3√3	-0.00016	±	0.00003	52,920
	+0.3 mm (3 × limit)	0.00057	±	0.00017	3√3	0.00011	±	0.00003	
5	-0.3 mm (3 × limit)	-0.00066	±	0.00016	3√3	-0.00013	±	0.00003	59,850
	+0.3 mm (3 × limit)	0.00059	±	0.00016	3√3	0.00011	±	0.00003	

Table 2.9. Effect of Uncertainty in Compact Dimensions (Height).

Case	Deviation	Δk	±	$\sigma_{\Delta k}$	Scaling Factor	Δk_{eff} (1σ)	±	$\sigma_{\Delta keff}$	N
1	-7.0 mm (7 × limit)	-0.00262	±	0.00016	7√3	-0.00022	±	0.00001	41,370
	+7.0 mm (7 × limit)	0.00246	±	0.00017	7√3	0.00020	±	0.00001	
2	-7.0 mm (7 × limit)	-0.00236	±	0.00017	7√3	-0.00019	±	0.00001	45,990
	+7.0 mm (7 × limit)	0.00216	±	0.00017	7√3	0.00018	±	0.00001	
3	-7.0 mm (7 × limit)	-0.00260	±	0.00017	7√3	-0.00021	±	0.00001	52,920
	+7.0 mm (7 × limit)	0.00191	±	0.00017	7√3	0.00016	±	0.00001	
4	-7.0 mm (7 × limit)	-0.00282	±	0.00017	7√3	-0.00023	±	0.00001	52,920
	+7.0 mm (7 × limit)	0.00201	±	0.00017	7√3	0.00017	±	0.00001	
5	-7.0 mm (7 × limit)	-0.00268	±	0.00016	7√3	-0.00022	±	0.00001	59,850
	+7.0 mm (7 × limit)	0.00201	±	0.00016	7√3	0.00017	±	0.00001	

Packing Fraction

Because of the overspecification of the TRISO particles in Table 1.14 (HTTR-GCR-RESR-001) and the correlation of uranium kernel diameter, density, TRISO packing fraction, and mass, the effect of the uncertainty in the packing fraction is not included in the total uncertainty. However, an analysis of the uncertainty based upon the fuel mass is performed in Section 2.1.6.

2.1.2.3 Graphite Sleeves

The uncertainty in the sleeve thickness was unreported. An inner diameter uncertainty of ±0.5 mm, which is limited by the 0.25 mm gap width between the sleeve and fuel compacts (Table 1.13 of HTTR-GCR-RESR-001), and an outer diameter uncertainty of ±2 mm were assumed; their effects on the

uncertainty of k_{eff} were determined. Figure 1.51 of HTTR-GCR-RESR-001 shows an inner diameter of 26.25 mm for the graphite sleeves, which would only provide a gap space of 0.125 mm. The assumed uncertainty encompasses the discrepancy in this value. Results are shown in Tables 2.10 and 2.11.

The fuel sleeve height was varied ±0.5 mm from the nominal value of 577 mm (Table 1.14 and Figure 1.51 of HTTR-GCR-RESR-001) and the effect on the uncertainty of k_{eff} was determined. Results are shown in Table 2.12.

Later information was obtained regarding manufacturing tolerances for the fuel sleeves. The ±0.1 mm of the ID and OD represents a bounding limit (with assumed uniform probability) and the height is then assumed to have a bounding limit (with assumed uniform probability) also of ±0.1 mm.[a] The appropriate corrections to the scaling factors have been incorporated into the uncertainty analysis of these parameters.

The total number of graphite sleeves used in the fully-loaded core is 4,770. For determining the random component of the uncertainty, the results in Tables 2.10 through 2.12 would be divided by √N, where N for each case is shown in Tables 2.10 through 2.12.

Table 2.10. Effect of Uncertainty in Graphite Sleeve Dimensions (Inner Diameter).

Case	Deviation	Δk	±	$\sigma_{\Delta k}$	Scaling Factor	Δk_{eff} (1σ)	±	$\sigma_{\Delta keff}$	N
1	-0.5 mm	0.00079	±	0.00017	5√3	0.00009	±	0.00002	2,955
	+0.5 mm	-0.00089	±	0.00017	5√3	-0.00010	±	0.00002	
2	-0.5 mm	0.00077	±	0.00017	5√3	0.00009	±	0.00002	3,285
	+0.5 mm	-0.00074	±	0.00016	5√3	-0.00009	±	0.00002	
3	-0.5 mm	0.00083	±	0.00016	5√3	0.00010	±	0.00002	3,780
	+0.5 mm	-0.00102	±	0.00016	5√3	-0.00012	±	0.00002	
4	-0.5 mm	0.00111	±	0.00017	5√3	0.00013	±	0.00002	3,780
	+0.5 mm	-0.00103	±	0.00017	5√3	-0.00012	±	0.00002	
5	-0.5 mm	0.00110	±	0.00016	5√3	0.00013	±	0.00002	4,275
	+0.5 mm	-0.00125	±	0.00016	5√3	-0.00014	±	0.00002	

[a] S. Maruyama, K. Yamashita, N. Fujimoto, I. Murata, R. Shindo, and Y. Sudo, "Determination of Hot Spot Factors for Calculation of the Maximum Fuel Temperatures in the Core Thermal and Hydraulic Design of HTTR," JAERI-M 88-250, JAEA (November 18, 1988). [in Japanese].

Table 2.11. Effect of Uncertainty in Graphite Sleeve Dimensions (Outer Diameter).

Case	Deviation	Δk	±	$\sigma_{\Delta k}$	Scaling Factor	Δk_{eff} (1σ)	±	$\sigma_{\Delta keff}$	N
1	-2 mm	-0.00499	±	0.00016	20√3	-0.00014	±	0.00000	2,955
	+2 mm	0.00574	±	0.00016	20√3	0.00017	±	0.00000	
2	-2 mm	-0.00555	±	0.00017	20√3	-0.00016	±	0.00000	3,285
	+2 mm	0.00587	±	0.00017	20√3	0.00017	±	0.00000	
3	-2 mm	-0.00622	±	0.00016	20√3	-0.00018	±	0.00000	3,780
	+2 mm	0.00640	±	0.00016	20√3	0.00018	±	0.00000	
4	-2 mm	-0.00692	±	0.00017	20√3	-0.00020	±	0.00000	3,780
	+2 mm	0.00715	±	0.00017	20√3	0.00021	±	0.00000	
5	-2 mm	-0.00675	±	0.00016	20√3	-0.00019	±	0.00000	4,275
	+2 mm	0.00700	±	0.00016	20√3	0.00020	±	0.00000	

Table 2.12. Effect of Uncertainty in Graphite Sleeve Dimensions (Height).

Case	Deviation	Δk	±	$\sigma_{\Delta k}$	Scaling Factor	Δk_{eff} (1σ)	±	$\sigma_{\Delta keff}$	N
1	-0.5 mm (1σ)	-0.00047	±	0.00016	5√3	-0.00005	±	0.00002	2,955
	+0.5 mm (1σ)	0.00039	±	0.00017	5√3	0.00005	±	0.00002	
2	-0.5 mm (1σ)	-0.00042	±	0.00017	5√3	-0.00005	±	0.00002	3,285
	+0.5 mm (1σ)	0.00036	±	0.00016	5√3	0.00004	±	0.00002	
3	-0.5 mm (1σ)	-0.00035	±	0.00017	5√3	-0.00004	±	0.00002	3,780
	+0.5 mm (1σ)	0.00025	±	0.00016	5√3	0.00003	±	0.00002	
4	-0.5 mm (1σ)	-0.00058	±	0.00017	5√3	-0.00007	±	0.00002	3,780
	+0.5 mm (1σ)	0.00026	±	0.00017	5√3	0.00003	±	0.00002	
5	-0.5 mm (1σ)	-0.00068	±	0.00016	5√3	-0.00008	±	0.00002	4,275
	+0.5 mm (1σ)	0.00022	±	0.00016	5√3	0.00003	±	0.00002	

2.1.2.4 Burnable Poisons

The uncertainty in the diameters of the BPs and BP insertion holes was unreported. A BP diameter uncertainty of ±1 mm from the nominal diameter (D) of 14 mm and a BP insertion hole diameter uncertainty of ±1 mm from the nominal diameter of 15 mm were assumed and their effects on the uncertainty of k_{eff} were determined. Results are shown in Tables 2.13 and 2.15.

The uncertainty in the height stack of the BPs was unreported. A stack height (H) uncertainty of ±1 mm from the nominal height of 200 mm was assumed (approximately ±0.1 mm per BP pellet) and the effective uncertainty in k_{eff} was determined. The height of the BP insertion hole was adjusted to accommodate the change in BP stack height. Results are shown in Table 2.14.

The uncertainty in the dimensions of the graphite disks was unreported. A diameter uncertainty of ±1 mm from the nominal diameter of 14 mm and a height uncertainty of ±1 mm from the nominal stack height of 100 mm were assumed and their effects on the uncertainty of k_{eff} were determined. The height of the BP insertion hole was adjusted to accommodate the change in graphite-disk stack height. Results are shown in Tables 2.16 and 2.17.

Because of the tight manufacturing tolerances of the fuel compacts and graphite sleeves (Sections 2.1.2.2 and 2.1.2.3, respectively) it is believed that similar tolerances apply to other graphite and boron carbide components of the HTTR. Therefore, the BP and graphite disk diameters are treated with a tolerance (with uniform probability) of ±0.1 mm and a stack height tolerance (with uniform probability) of ±1.0 mm. The appropriate corrections to the scaling factors have been incorporated into the uncertainty analysis of these parameters.

The total number of burnable poison pellets used in the fully-loaded core is 5,520. For determining the random component of the uncertainty, the results in Tables 2.13 through 2.17 would be divided by $\sqrt{N}$, where N for each case is shown in Tables 2.13 through 2.17. The total number of BP stacks is 600, of BP insertion holes is 450, and of graphite disk stacks is 300, in the fully-loaded core configuration.

Table 2.13. Effect of Uncertainty in BP Pin Dimensions (Diameter).

Case	Deviation	Δk	±	$\sigma_{\Delta k}$	Scaling Factor	Δk_{eff} (1σ)	±	$\sigma_{\Delta keff}$	N
1	-1 mm (10 × limit)	0.01047	±	0.00017	10√3	0.00060	±	0.00001	3,496
	+1 mm (10 × limit)	-0.00974	±	0.00017	10√3	-0.00056	±	0.00001	
2	-1 mm (10 × limit)	0.01125	±	0.00016	10√3	0.00065	±	0.00001	3,864
	+1 mm (10 × limit)	-0.01045	±	0.00016	10√3	-0.00060	±	0.00001	
3	-1 mm (10 × limit)	0.01198	±	0.00016	10√3	0.00069	±	0.00001	4,416
	+1 mm (10 × limit)	-0.01149	±	0.00016	10√3	-0.00066	±	0.00001	
4	-1 mm (10 × limit)	0.01202	±	0.00017	10√3	0.00069	±	0.00001	4,416
	+1 mm (10 × limit)	-0.01171	±	0.00016	10√3	-0.00068	±	0.00001	
5	-1 mm (10 × limit)	0.01287	±	0.00016	10√3	0.00074	±	0.00001	4,968
	+1 mm (10 × limit)	-0.01234	±	0.00016	10√3	-0.00071	±	0.00001	

Table 2.14. Effect of Uncertainty in BP Pin Dimensions (Stack Height).

Case	Deviation	Δk	±	$\sigma_{\Delta k}$	Scaling Factor	Δk_{eff} (1σ)	±	$\sigma_{\Delta keff}$	N
1	-1 mm	0.00061	±	0.00017	√3	0.00035	±	0.00010	380
	+1 mm	-0.00050	±	0.00017	√3	-0.00029	±	0.00010	
2	-1 mm	0.00056	±	0.00017	√3	0.00032	±	0.00010	420
	+1 mm	-0.00065	±	0.00016	√3	-0.00038	±	0.00009	
3	-1 mm	0.00044	±	0.00017	√3	0.00025	±	0.00010	480
	+1 mm	-0.00077	±	0.00017	√3	-0.00044	±	0.00010	
4	-1 mm	0.00050	±	0.00017	√3	0.00029	±	0.00010	480
	+1 mm	-0.00088	±	0.00017	√3	-0.00051	±	0.00010	
5	-1 mm	0.00055	±	0.00016	√3	0.00032	±	0.00009	520
	+1 mm	-0.00065	±	0.00016	√3	-0.00038	±	0.00009	

Table 2.15. Effect of Uncertainty in BP Insertion Hole Diameter.

Case	Deviation	Δk	±	$\sigma_{\Delta k}$	Scaling Factor	Δk_{eff} (1σ)	±	$\sigma_{\Delta keff}$	N
1	-1 mm (10 × limit)	0.00102	±	0.00017	10√3	0.00006	±	0.00001	285
	+1 mm (10 × limit)	-0.00092	±	0.00017	10√3	-0.00005	±	0.00001	
2	-1 mm (10 × limit)	0.00116	±	0.00016	10√3	0.00007	±	0.00001	315
	+1 mm (10 × limit)	-0.00076	±	0.00016	10√3	-0.00004	±	0.00001	
3	-1 mm (10 × limit)	0.00076	±	0.00017	10√3	0.00004	±	0.00001	360
	+1 mm (10 × limit)	-0.00104	±	0.00016	10√3	-0.00006	±	0.00001	
4	-1 mm (10 × limit)	0.00069	±	0.00016	10√3	0.00004	±	0.00001	360
	+1 mm (10 × limit)	-0.00122	±	0.00016	10√3	-0.00007	±	0.00001	
5	-1 mm (10 × limit)	0.00109	±	0.00016	10√3	0.00006	±	0.00001	405
	+1 mm (10 × limit)	-0.00098	±	0.00016	10√3	-0.00006	±	0.00001	

Table 2.16. Effect of Uncertainty in Graphite Disk Dimensions (Diameter).

Case	Deviation	Δk	±	$\sigma_{\Delta k}$	Scaling Factor	Δk_{eff} (1σ)	±	$\sigma_{\Delta keff}$	N
1	-1 mm (10 × limit)	-0.00018	±	0.00017	10√3	-0.00001	±	0.00001	190
	+1 mm (10 × limit)	0.00008	±	0.00017	10√3	0.00000	±	0.00001	
2	-1 mm (10 × limit)	0.00008	±	0.00016	10√3	0.00000	±	0.00001	210
	+1 mm (10 × limit)	-0.00005	±	0.00017	10√3	0.00000	±	0.00001	
3	-1 mm (10 × limit)	-0.00002	±	0.00016	10√3	0.00000	±	0.00001	240
	+1 mm (10 × limit)	0.00011	±	0.00017	10√3	0.00001	±	0.00001	
4	-1 mm (10 × limit)	-0.00011	±	0.00017	10√3	-0.00001	±	0.00001	240
	+1 mm (10 × limit)	-0.00008	±	0.00017	10√3	0.00000	±	0.00001	
5	-1 mm (10 × limit)	-0.00004	±	0.00016	10√3	0.00000	±	0.00001	270
	+1 mm (10 × limit)	-0.00012	±	0.00016	10√3	-0.00001	±	0.00001	

Table 2.17. Effect of Uncertainty in Graphite Disk Dimensions (Stack Height).

Case	Deviation	Δk	±	$\sigma_{\Delta k}$	Scaling Factor	Δk_{eff} (1σ)	±	$\sigma_{\Delta keff}$	N
1	-1 mm	-0.00001	±	0.00017	√3	-0.00001	±	0.00010	190
	+1 mm	0.00022	±	0.00016	√3	0.00013	±	0.00009	
2	-1 mm	0.00008	±	0.00016	√3	0.00005	±	0.00009	210
	+1 mm	-0.00005	±	0.00017	√3	-0.00003	±	0.00010	
3	-1 mm	-0.00004	±	0.00016	√3	-0.00002	±	0.00009	240
	+1 mm	0.00001	±	0.00017	√3	0.00001	±	0.00010	
4	-1 mm	0.00000	±	0.00017	√3	0.00000	±	0.00010	240
	+1 mm	-0.00009	±	0.00017	√3	-0.00005	±	0.00010	
5	-1 mm	-0.00015	±	0.00016	√3	-0.00009	±	0.00009	270
	+1 mm	0.00021	±	0.00016	√3	0.00012	±	0.00009	

2.1.2.5 Control Rods

Absorber Dimensions

The uncertainty in the absorber dimensions was unreported. Assumed inner and outer diameter (ID and OD) uncertainties are ±5 mm each from the nominal values of 75 and 105 mm (Table 1.15 of HTTR-GCR-RESR-001), respectively, and their effects on the uncertainty of k_{eff} were determined. The uncertainty in the pellet height was assumed to be ±1 cm from the nominal stack height (H) of 29 cm. The alternate value of 115 mm provided for the outer diameter of the absorber material is believed to be a typographical error (see footnote of Table 1.15 of HTTR-GCR-RESR-001). Results are shown in Tables 2.18 through 2.20.

Because of the tight manufacturing tolerances of the fuel compacts and graphite sleeves (Sections 2.1.2.2 and 2.1.2.3, respectively) it is believed that similar tolerances apply to other graphite and boron carbide components of the HTTR. Therefore, the absorber diameters are treated with a tolerance (with uniform probability) of ±0.1 mm and a stack height tolerance (with uniform probability) of ±1.0 mm. The appropriate corrections to the scaling factors have been incorporated into the uncertainty analysis of these parameters.

The total number of control rod absorber pellets used in the fully-loaded core is approximately 975, as approximately 30% of the control rods are actually inserted into the core. For determining the random component of the uncertainty, the results in Tables 2.18 through 2.20 would be divided by $\sqrt{N}$, where N for each case is shown in Tables 2.18 through 2.20.

Table 2.18. Effect of Uncertainty in CR Absorber Dimensions (Inner Diameter).

Case	Deviation	Δk	±	$\sigma_{\Delta k}$	Scaling Factor	Δk_{eff} (1σ)	±	$\sigma_{\Delta keff}$	N
1	-5 mm (50 × limit)	-0.00026	±	0.00017	50√3	0.00000	±	0.00000	225
	+5 mm (50 × limit)	0.00003	±	0.00017	50√3	0.00000	±	0.00000	
2	-5 mm (50 × limit)	-0.00021	±	0.00017	50√3	0.00000	±	0.00000	585
	+5 mm (50 × limit)	0.00037	±	0.00017	50√3	0.00000	±	0.00000	
3	-5 mm (50 × limit)	-0.00033	±	0.00017	50√3	0.00000	±	0.00000	780
	+5 mm (50 × limit)	0.00014	±	0.00017	50√3	0.00000	±	0.00000	
4	-5 mm (50 × limit)	-0.00042	±	0.00016	50√3	0.00000	±	0.00000	720
	+5 mm (50 × limit)	0.00037	±	0.00017	50√3	0.00000	±	0.00000	
5	-5 mm (50 × limit)	-0.00032	±	0.00016	50√3	0.00000	±	0.00000	910
	+5 mm (50 × limit)	0.00035	±	0.00016	50√3	0.00000	±	0.00000	

Table 2.19. Effect of Uncertainty in CR Absorber Dimensions (Outer Diameter).

Case	Deviation	Δk	±	$\sigma_{\Delta k}$	Scaling Factor	Δk_{eff} (1σ)	±	$\sigma_{\Delta keff}$	N
1	-5 mm (50 × limit)	0.00072	±	0.00016	50√3	0.00001	±	0.00000	225
	+5 mm (50 × limit)	-0.00083	±	0.00017	50√3	-0.00001	±	0.00000	
2	-5 mm (50 × limit)	0.00130	±	0.00017	50√3	0.00002	±	0.00000	585
	+5 mm (50 × limit)	-0.00100	±	0.00016	50√3	-0.00001	±	0.00000	
3	-5 mm (50 × limit)	0.00135	±	0.00017	50√3	0.00002	±	0.00000	780
	+5 mm (50 × limit)	-0.00145	±	0.00017	50√3	-0.00002	±	0.00000	
4	-5 mm (50 × limit)	0.00226	±	0.00017	50√3	0.00003	±	0.00000	720
	+5 mm (50 × limit)	-0.00275	±	0.00017	50√3	-0.00003	±	0.00000	
5	-5 mm (50 × limit)	0.00160	±	0.00016	50√3	0.00002	±	0.00000	910
	+5 mm (50 × limit)	-0.00187	±	0.00016	50√3	-0.00002	±	0.00000	

Table 2.20. Effect of Uncertainty in CR Absorber Dimensions (Stack Height).

Case	Deviation	Δk	±	$\sigma_{\Delta k}$	Scaling Factor	Δk_{eff} (1σ)	±	$\sigma_{\Delta keff}$	N
1	-1 cm (10 × limit)	0.00024	±	0.00017	10√3	0.00001	±	0.00001	22.5
	+1 cm (10 × limit)	-0.00023	±	0.00016	10√3	-0.00001	±	0.00001	
2	-1 cm (10 × limit)	0.00085	±	0.00016	10√3	0.00005	±	0.00001	58.5
	+1 cm (10 × limit)	-0.00089	±	0.00017	10√3	-0.00005	±	0.00001	
3	-1 cm (10 × limit)	0.00039	±	0.00017	10√3	0.00002	±	0.00001	78.0
	+1 cm (10 × limit)	-0.00099	±	0.00017	10√3	-0.00006	±	0.00001	
4	-1 cm (10 × limit)	0.00059	±	0.00017	10√3	0.00003	±	0.00001	72.0
	+1 cm (10 × limit)	-0.00073	±	0.00017	10√3	-0.00004	±	0.00001	
5	-1 cm (10 × limit)	0.00042	±	0.00016	10√3	0.00002	±	0.00001	91.0
	+1 cm (10 × limit)	-0.00111	±	0.00016	10√3	-0.00006	±	0.00001	

Clad Dimensions

The uncertainty in the clad dimensions was unreported, and detailed dimensions for anything similar to the diagram shown in Figure 1.60 of HTTR-GCR-RESR-001were unavailable. Therefore a solid clad material encasing the control rod absorber was defined without detail for the end caps. Inner and outer thicknesses were varied ±5 mm from the nominal values of 65 and 113 mm (Table 1.15 of HTTR-GCR-RESR-001), respectively, to determine their effects on the uncertainty of k_{eff}. The spine diameter was varied ±10 mm from the nominal value of 10 mm (Table 1.15 of HTTR-GCR-RESR-001) and its effect on the uncertainty of k_{eff} was determined. The clad height of a single control rod section was varied ±1 cm. The reported clad thickness of 3.5 mm does not appear to conform to the difference between reported diameters of the clad and absorber materials. It is unclear whether a gap exists or there is rounding of values in the original table. The uncertainties evaluated encompass the overall uncertainty in this discrepancy. The control rod diameters are chosen as the more appropriate dimensions for modeling, such that inner and outer clad thicknesses are approximately 5 and 4 mm, respectively. Results are shown in Tables 2.21 through 2.24.

Height change of clad also affects the effective height of each control rod segment.

Because of the tight manufacturing tolerances of the fuel compacts and graphite sleeves (Sections 2.1.2.2 and 2.1.2.3, respectively) it is believed that tighter tolerances apply to the absorber cladding. Therefore, the diameters are treated with a tolerance (with uniform probability) of ±0.5 mm and a height tolerance (with uniform probability) of ±1.0 mm. The appropriate corrections to the scaling factors have been incorporated into the uncertainty analysis of these parameters.

The total number of control rod sections used in the fully-loaded core is approximately 97.5, as approximately 30% of the control rods are actually inserted into the core. For determining the random component of the uncertainty, the results in Tables 2.21 through 2.24 would be divided by √N, where N for each case is shown in Tables 2.21 through 2.24.

Table 2.21. Effect of Uncertainty in CR Clad Dimensions (Inner Diameter).

Case	Deviation	Δk	±	$\sigma_{\Delta k}$	Scaling Factor	Δk_{eff} (1σ)	±	$\sigma_{\Delta keff}$	N
1	-5 mm (10 × limit)	-0.00004	±	0.00016	10√3	0.00000	±	0.00001	22.5
	+5 mm (10 × limit)	-0.00018	±	0.00017	10√3	-0.00001	±	0.00001	
2	-5 mm (10 × limit)	-0.00003	±	0.00017	10√3	0.00000	±	0.00001	58.5
	+5 mm (10 × limit)	0.00021	±	0.00016	10√3	0.00001	±	0.00001	
3	-5 mm (10 × limit)	-0.00003	±	0.00016	10√3	0.00000	±	0.00001	78.0
	+5 mm (10 × limit)	-0.00019	±	0.00017	10√3	-0.00001	±	0.00001	
4	-5 mm (10 × limit)	-0.00007	±	0.00017	10√3	0.00000	±	0.00001	72.0
	+5 mm (10 × limit)	-0.00011	±	0.00017	10√3	-0.00001	±	0.00001	
5	-5 mm (10 × limit)	-0.00002	±	0.00016	10√3	0.00000	±	0.00001	91.0
	+5 mm (10 × limit)	-0.00006	±	0.00016	10√3	0.00000	±	0.00001	

Table 2.22. Effect of Uncertainty in CR Clad Dimensions (Outer Diameter).

Case	Deviation	Δk	±	$\sigma_{\Delta k}$	Scaling Factor	Δk_{eff} (1σ)	±	$\sigma_{\Delta keff}$	N
1	-5 mm (10 × limit)	-0.00033	±	0.00017	10√3	-0.00002	±	0.00001	22.5
	+5 mm (10 × limit)	0.00018	±	0.00017	10√3	0.00001	±	0.00001	
2	-5 mm (10 × limit)	-0.00053	±	0.00017	10√3	-0.00003	±	0.00001	58.5
	+5 mm (10 × limit)	0.00028	±	0.00016	10√3	0.00002	±	0.00001	
3	-5 mm (10 × limit)	-0.00082	±	0.00017	10√3	-0.00005	±	0.00001	78.0
	+5 mm (10 × limit)	0.00055	±	0.00016	10√3	0.00003	±	0.00001	
4	-5 mm (10 × limit)	-0.00169	±	0.00017	10√3	-0.00010	±	0.00001	72.0
	+5 mm (10 × limit)	0.00108	±	0.00017	10√3	0.00006	±	0.00001	
5	-5 mm (10 × limit)	-0.00087	±	0.00016	10√3	-0.00005	±	0.00001	91.0
	+5 mm (10 × limit)	0.00058	±	0.00016	10√3	0.00003	±	0.00001	

Table 2.23. Effect of Uncertainty in CR Clad Dimensions (Height).

Case	Deviation	Δk	±	$\sigma_{\Delta k}$	Scaling Factor	Δk_{eff} (1σ)	±	$\sigma_{\Delta keff}$	N
1	-1 cm (10 × limit)	0.00036	±	0.00016	10√3	-0.00002	±	0.00001	22.5
	+1 cm (10 × limit)	-0.00046	±	0.00016	10√3	-0.00003	±	0.00001	
2	-1 cm (10 × limit)	0.00188	±	0.00017	10√3	-0.00011	±	0.00001	58.5
	+1 cm (10 × limit)	-0.00192	±	0.00017	10√3	-0.00011	±	0.00001	
3	-1 cm (10 × limit)	0.00243	±	0.00017	10√3	-0.00014	±	0.00001	78.0
	+1 cm (10 × limit)	-0.00231	±	0.00017	10√3	-0.00013	±	0.00001	
4	-1 cm (10 × limit)	0.00136	±	0.00017	10√3	-0.00008	±	0.00001	72.0
	+1 cm (10 × limit)	-0.00130	±	0.00017	10√3	-0.00008	±	0.00001	
5	-1 cm (10 × limit)	0.00235	±	0.00016	10√3	-0.00014	±	0.00001	91.0
	+1 cm (10 × limit)	-0.00258	±	0.00016	10√3	-0.00015	±	0.00001	

Table 2.24. Effect of Uncertainty in CR Clad Dimensions (Spine Diameter).

Case	Deviation	Δk	±	$\sigma_{\Delta k}$	Scaling Factor	Δk_{eff} (1σ)	±	$\sigma_{\Delta keff}$	N
1	-10 mm (20 × limit)	-0.00002	±	0.00017	20√3	0.00000	±	0.00000	22.5
	+10 mm (20 × limit)	0.00001	±	0.00017	20√3	0.00000	±	0.00000	
2	-10 mm (20 × limit)	0.00008	±	0.00017	20√3	0.00000	±	0.00000	58.5
	+10 mm (20 × limit)	0.00014	±	0.00016	20√3	0.00000	±	0.00000	
3	-10 mm (20 × limit)	-0.00002	±	0.00017	20√3	0.00000	±	0.00000	78.0
	+10 mm (20 × limit)	-0.00017	±	0.00017	20√3	0.00000	±	0.00000	
4	-10 mm (20 × limit)	-0.00010	±	0.00017	20√3	0.00000	±	0.00000	72.0
	+10 mm (20 × limit)	0.00010	±	0.00016	20√3	0.00000	±	0.00000	
5	-10 mm (20 × limit)	-0.00026	±	0.00016	20√3	-0.00001	±	0.00000	91.0
	+10 mm (20 × limit)	0.00007	±	0.00016	20√3	0.00000	±	0.00000	

2.1.2.6 Instrumentation

Insufficient information is available to comprehensively model and evaluate the uncertainties and biases related to the utility of instrumentation in the HTTR. Neglect of instrumentation inclusion in the model would be a bias; uncertainty in the dimensions and composition of the instrumentation would provide uncertainty in that bias or uncertainty in the model should it have been included in the benchmark model. An approximation of the instrumentation in the HTTR was modeled using information from Section 1.1.2.3 of HTTR-GCR-RESR-001 and approximate diagrams shown in a presentation at the IAEA CRP-

5 Meeting.[a] The expected bias in the instrumentation, from the aforementioned reference, is ~0.2 % Δk/k.

Figures 2.1 through 2.4 provide basic geometric descriptions of the instrumentation utilized in the HTTR core. Figure 2.1 shows the respective heights. Figure 2.2, 2.3, and 2.4 provide additional information regarding channels 1, 2, and 3, respectively (columns E05, E13, and E21, respectively, in Figure 2.5). The 5-cm long 0.6-cm diameter BF_3 counters were modeled containing gas at 1 atm with 100 at.% ^{10}B content. All metallic components were modeled as aluminum. Approximate dimensions were used based on scaling of the Figures 2.2 through 2.4 and the known hole diameter of 123 mm.

Approximate biases were calculated for the annular core configurations (Table 3.1). The bias for the fully-loaded core critical was calculated to be 0.254 ± 0.073 % Δk/k (HTTR-GCR-RESR-001 Section 3.1.1.1), which is similar to the previously reported value. The uncertainty in the biases was approximated by dividing the biases in half, and then treating it as a bounding uncertainty and dividing by √3. The uncertainty in the instrumentation is included in the total benchmark model uncertainty, and is provided in Table 3.1. The instrumentation is not included in the benchmark model but the bias in used to correct the experimental k_{eff}. Because the actual dimensions and material properties are approximated, this uncertainty is treated as completely systematic with no random components.

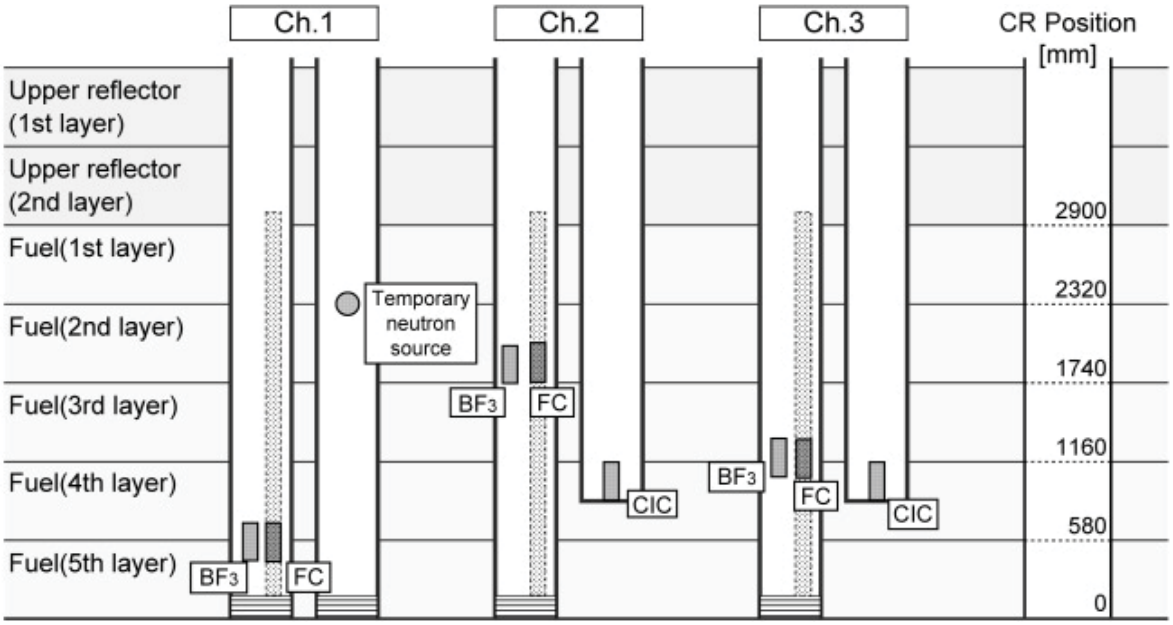

Figure 2.1. Vertical Position of the Temporary Neutron Detectors (Ref 1, p. 314).
BF_3 = boron-trifluoride neutron detector
CIC = gamma-ray compensated ionization chamber
FC = micro-fission chamber

[a] N. Fujimoto, N. Nojiri, and K. Yamashita, "HTTR's Benchmark Calculation of Start-Up Core Physics Tests," Report of the 3rd Research Coordiation Meeting on the CRP, IAEA, Oarai, Japan, March 12-16 (2001).

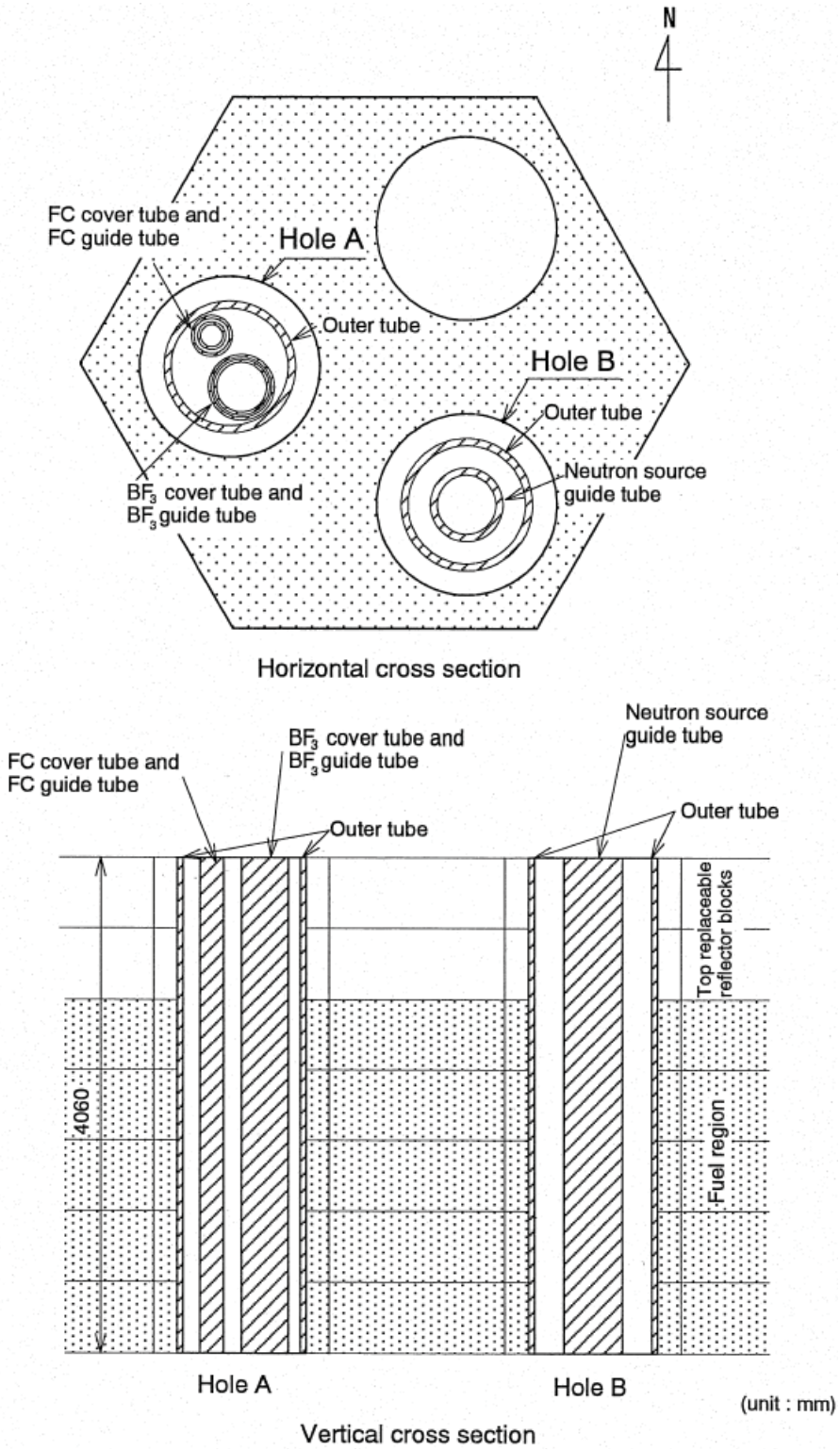

Figure 2.2. Approximation of Instrumentation Channel 1 (Column E05).[a]

[a] N. Fujimoto, N. Nojiri, and K. Yamashita, "HTTR's Benchmark Calculation of Start-Up Core Physics Tests," Report of the 3rd Research Coordination Meeting on the CRP, IAEA, Oarai, Japan, March 12-16 (2001).

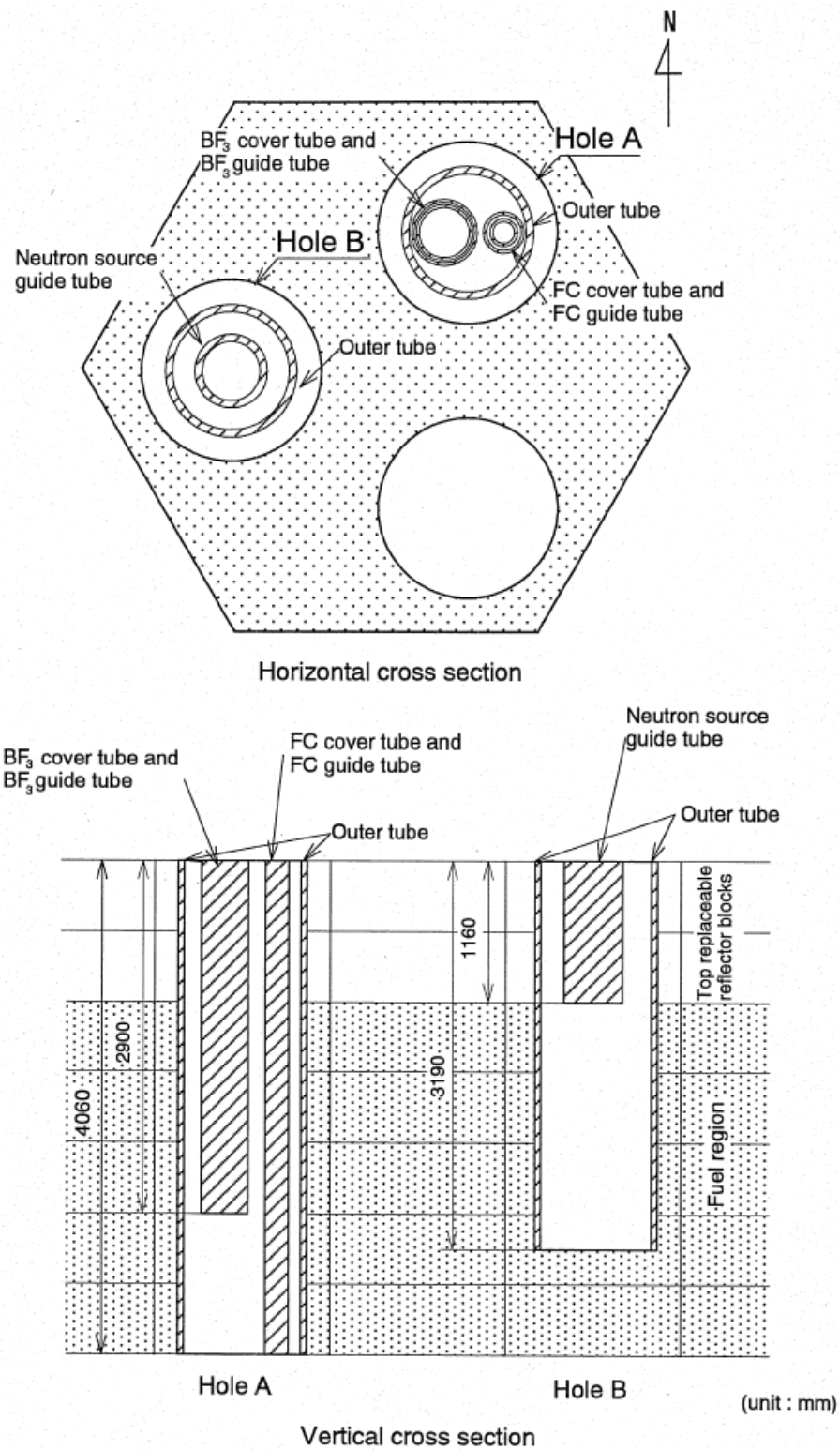

Figure 2.3. Approximation of Instrumentation Channel 2 (Column E13).[a]

[a] N. Fujimoto, N. Nojiri, and K. Yamashita, "HTTR's Benchmark Calculation of Start-Up Core Physics Tests," Report of the 3rd Research Coordination Meeting on the CRP, IAEA, Oarai, Japan, March 12-16 (2001).

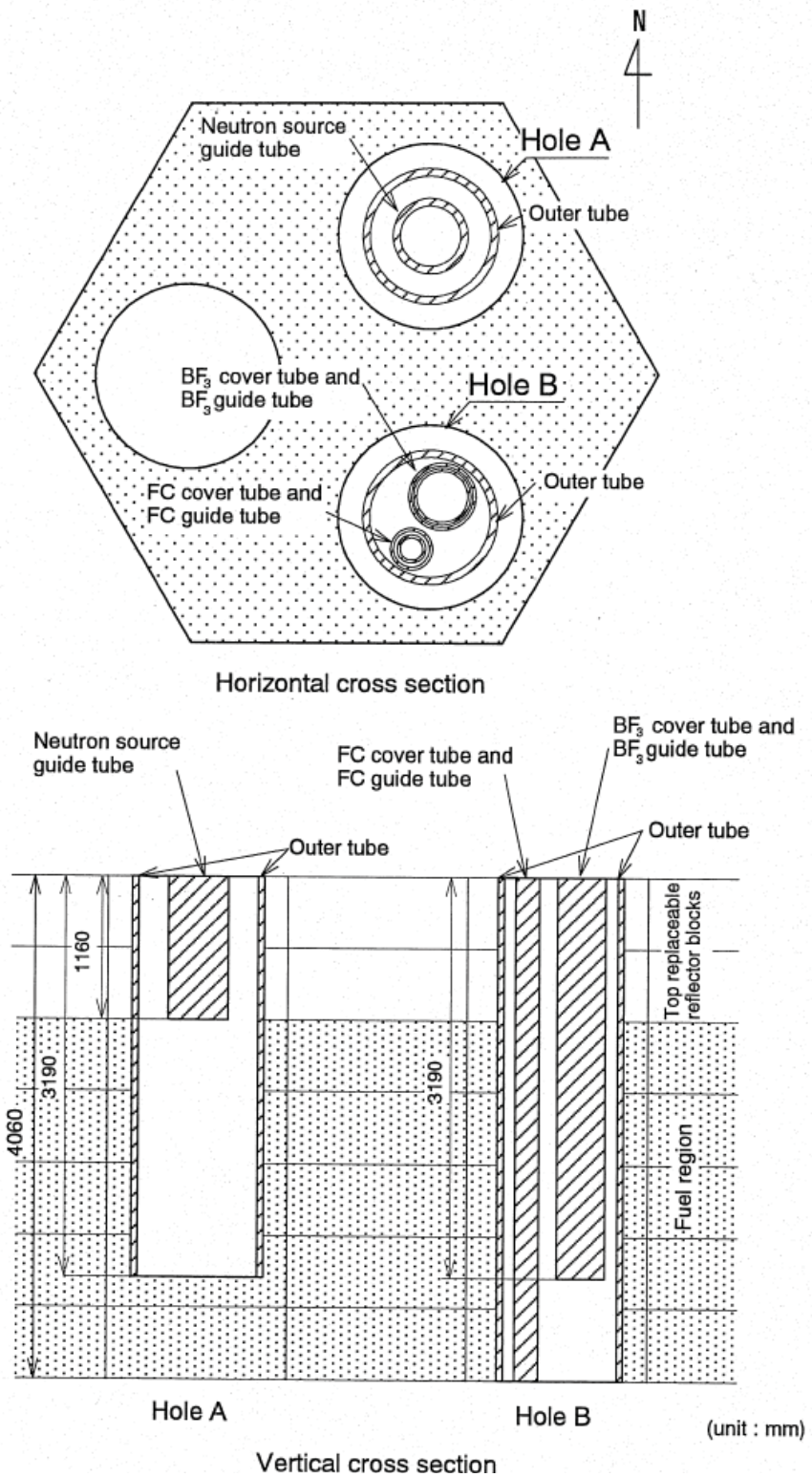

Figure 2.4. Approximation of Instrumentation Channel 3 (Column E21).[a]

[a] N. Fujimoto, N. Nojiri, and K. Yamashita, "HTTR's Benchmark Calculation of Start-Up Core Physics Tests," Report of the 3rd Research Coordination Meeting on the CRP, IAEA, Oarai, Japan, March 12-16 (2001).

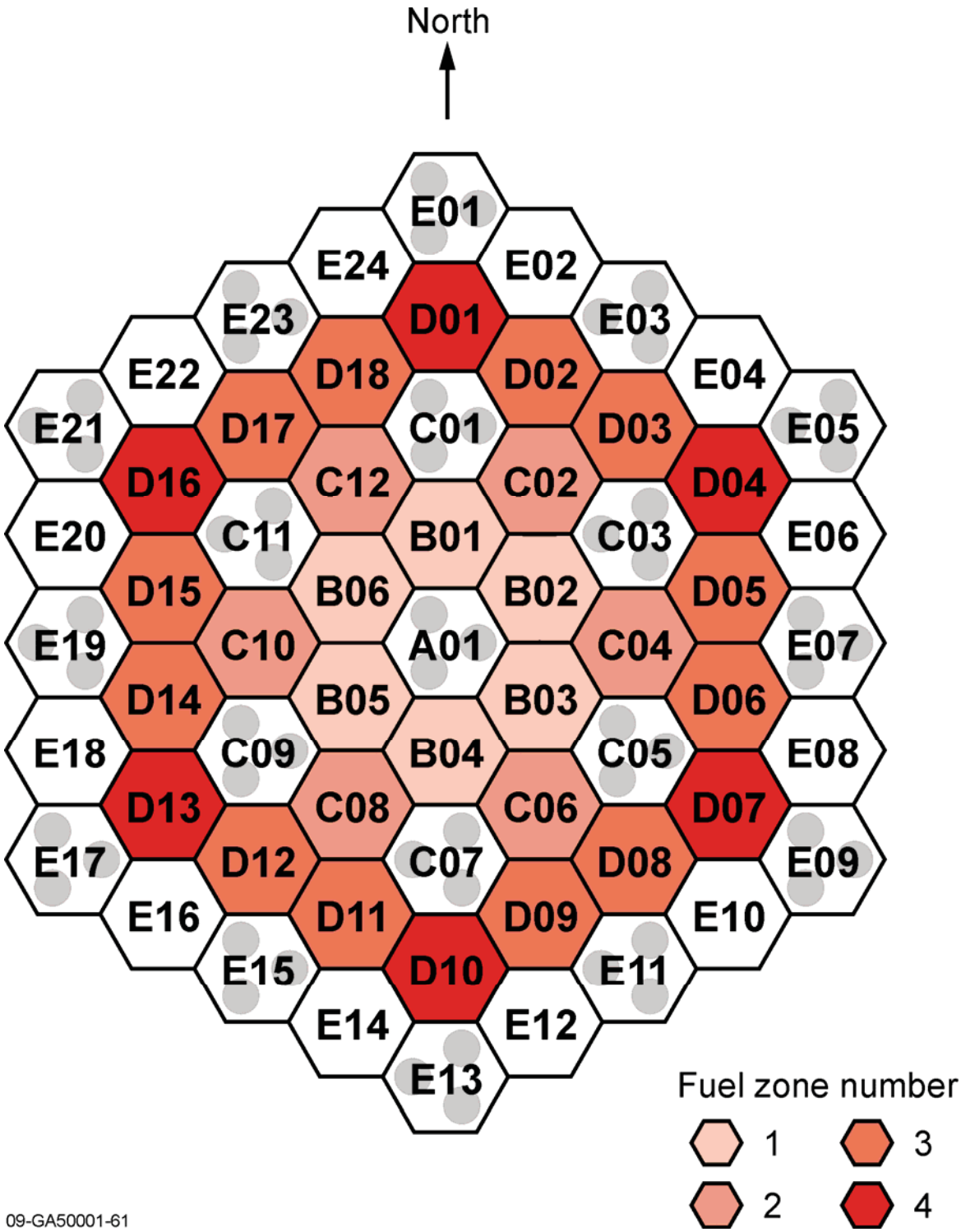

Figure 2.5. Fuel Column Name and Zone Number in the HTTR Core (adapted from Ref. 2, p. 12).

2.1.2.7 Graphite Blocks

Block Dimensions

An uncertainty in the block dimensions was unreported. The uncertainty in the flat-to-flat distance and the height were each varied ±1 mm from their nominal values of 360 and 580 cm (Tables 1.13 and 1.16 of HTTR-GCR-RESR-001), respectively, and their effects on the uncertainty of k_{eff} were determined. The average gap between columns was reported as approximately 2 mm (Ref. 2, p. 13), allowing room for the flat-to-flat uncertainty. All graphite blocks were varied with this analysis: fuel, reflector, control, instrumentation, and dummy. Results are shown in Tables 2.25 and 2.26.

Because of the tight manufacturing tolerances of the fuel compacts and graphite sleeves (Sections 2.1.2.2 and 2.1.2.3, respectively) it is believed that similar tolerances apply to other graphite and boron carbide components of the HTTR. Therefore, the graphite block dimensions are treated with a tolerance (with uniform probability) of ±0.1 mm. The appropriate corrections to the scaling factors have been incorporated into the uncertainty analysis of these parameters.

The total number of graphite blocks used in all core configurations is 549. For determining the random component of the uncertainty, the results in Tables 2.25 and 2.26 would be divided by $\sqrt{549}$.

Table 2.25. Effect of Uncertainty in Graphite Block Dimensions (Flat-to-Flat Distance).

Case	Deviation	Δk	±	$\sigma_{\Delta k}$	Scaling Factor	Δk_{eff} (1σ)	±	$\sigma_{\Delta keff}$
1	-1 mm (10 × limit)	-0.00263	±	0.00016	10√3	-0.00015	±	0.00001
	+1 mm (10 × limit)	0.00238	±	0.00017	10√3	0.00014	±	0.00001
2	-1 mm (10 × limit)	-0.00242	±	0.00016	10√3	-0.00014	±	0.00001
	+1 mm (10 × limit)	0.00222	±	0.00017	10√3	0.00013	±	0.00001
3	-1 mm (10 × limit)	-0.00335	±	0.00017	10√3	-0.00019	±	0.00001
	+1 mm (10 × limit)	0.00247	±	0.00016	10√3	0.00014	±	0.00001
4	-1 mm (10 × limit)	-0.00385	±	0.00017	10√3	-0.00022	±	0.00001
	+1 mm (10 × limit)	0.00308	±	0.00017	10√3	0.00018	±	0.00001
5	-1 mm (10 × limit)	-0.00384	±	0.00016	10√3	-0.00022	±	0.00001
	+1 mm (10 × limit)	0.00311	±	0.00016	10√3	0.00018	±	0.00001

Table 2.26. Effect of Uncertainty in Graphite Block Dimensions (Height).

Case	Deviation	Δk	±	$\sigma_{\Delta k}$	Scaling Factor	Δk_{eff} (1σ)	±	$\sigma_{\Delta keff}$
1	-1 mm (10 × limit)	0.00006	±	0.00017	10√3	0.00000	±	0.00001
	+1 mm (10 × limit)	-0.00004	±	0.00016	10√3	0.00000	±	0.00001
2	-1 mm (10 × limit)	0.00005	±	0.00017	10√3	0.00000	±	0.00001
	+1 mm (10 × limit)	0.00010	±	0.00017	10√3	0.00001	±	0.00001
3	-1 mm (10 × limit)	0.00006	±	0.00017	10√3	0.00000	±	0.00001
	+1 mm (10 × limit)	0.00001	±	0.00017	10√3	0.00000	±	0.00001
4	-1 mm (10 × limit)	-0.00010	±	0.00017	10√3	-0.00001	±	0.00001
	+1 mm (10 × limit)	-0.00015	±	0.00017	10√3	-0.00001	±	0.00001
5	-1 mm (10 × limit)	-0.00002	±	0.00016	10√3	0.00000	±	0.00001
	+1 mm (10 × limit)	-0.00006	±	0.00016	10√3	0.00000	±	0.00001

Dowel/Socket Dimensions

Insufficient information is available to completely model and evaluate the uncertainties and biases related to the incorporation of dowels and sockets in the HTTR. Uncertainty in the volume fraction will be included as part of the assessment of the uncertainty in the total density of the graphite blocks.

Coolant Channel Diameter

An assumed variation of ±2 mm in the diameter of the coolant channels of the fuel blocks (nominally 41 mm, Table 1.13 of HTTR-GCR-RESR-001) and reflector blocks (nominally 23 mm) in the fuel columns was performed to determine the effective uncertainty in k_{eff}. Results are shown in Tables 2.27 and 2.28.

Insufficient information was available to determine the dimensions of the coolant channels of the lowest reflector blocks. They were modeled similar to the other reflector blocks utilized in the fuel columns. No bias or biased uncertainty was assessed.

Because of the tight manufacturing tolerances of the fuel compacts and graphite sleeves (Sections 2.1.2.2 and 2.1.2.3, respectively) it is believed that similar tolerances apply to other graphite and boron carbide components of the HTTR. Therefore, the coolant channel diameters are treated with a tolerance (with uniform probability) of ±0.1 mm. The appropriate corrections to the scaling factors have been incorporated into the uncertainty analysis of these parameters.

The total number of fuel coolant channels used in the fully-loaded core is 4,770. For determining the random component of the uncertainty, the results in Table 2.27 would be divided by √N. The total number of reflector coolant channels in all core configurations is 3,816. For determining the random component of the uncertainty, the results in Table 2.28 would be divided by √3,816.

Table 2.27. Effect of Uncertainty in Coolant Channel Diameter (Fuel Blocks).

Case	Deviation	Δk	±	$\sigma_{\Delta k}$	Scaling Factor	Δk_{eff} (1σ)	±	$\sigma_{\Delta keff}$	N
1	-2 mm (20 × limit)	0.00620	±	0.00017	20√3	0.00018	±	0.00000	2,955
	+2 mm (20 × limit)	-0.00644	±	0.00017	20√3	-0.00019	±	0.00000	
2	-2 mm (20 × limit)	0.00694	±	0.00016	20√3	0.00020	±	0.00000	3,285
	+2 mm (20 × limit)	-0.00705	±	0.00017	20√3	-0.00020	±	0.00000	
3	-2 mm (20 × limit)	0.00730	±	0.00016	20√3	0.00021	±	0.00000	3,780
	+2 mm (20 × limit)	-0.00814	±	0.00016	20√3	-0.00023	±	0.00000	
4	-2 mm (20 × limit)	0.00837	±	0.00016	20√3	0.00024	±	0.00000	3,780
	+2 mm (20 × limit)	-0.00929	±	0.00017	20√3	-0.00027	±	0.00000	
5	-2 mm (20 × limit)	0.00787	±	0.00016	20√3	0.00023	±	0.00000	4,275
	+2 mm (20 × limit)	-0.00889	±	0.00016	20√3	-0.00026	±	0.00000	

Table 2.28. Effect of Uncertainty in Coolant Channel Diameter (Reflector Blocks).

Case	Deviation	Δk	±	$\sigma_{\Delta k}$	Scaling Factor	Δk_{eff} (1σ)	±	$\sigma_{\Delta keff}$
1	-2 mm (20 × limit)	0.00039	±	0.00016	20√3	0.00001	±	0.00000
	+2 mm (20 × limit)	-0.00072	±	0.00017	20√3	-0.00002	±	0.00000
2	-2 mm (20 × limit)	0.00045	±	0.00017	20√3	0.00001	±	0.00000
	+2 mm (20 × limit)	-0.00008	±	0.00016	20√3	0.00000	±	0.00000
3	-2 mm (20 × limit)	0.00028	±	0.00016	20√3	0.00001	±	0.00000
	+2 mm (20 × limit)	-0.00072	±	0.00016	20√3	-0.00002	±	0.00000
4	-2 mm (20 × limit)	0.00009	±	0.00017	20√3	0.00000	±	0.00000
	+2 mm (20 × limit)	-0.00054	±	0.00017	20√3	-0.00002	±	0.00000
5	-2 mm (20 × limit)	0.00026	±	0.00016	20√3	0.00001	±	0.00000
	+2 mm (20 × limit)	-0.00045	±	0.00016	20√3	-0.00001	±	0.00000

Fuel and Coolant Channel Pitch

An uncertainty in the fuel and coolant channel pitches in the fuel columns was not reported. For the evaluation of this uncertainty, the channels were modeled closer together then further apart by adjusting the pitch between them. A variation of ±2.0 mm from the nominal pitch of 51.5 mm (Figures 1.52 and 1.53 of HTTR-GCR-RESR-001) was assumed and the effects on the uncertainty of k_{eff} were determined. Results are shown in Table 2.29.

Because of the tight manufacturing tolerances of the fuel compacts and graphite sleeves (Sections 2.1.2.2 and 2.1.2.3, respectively) it is believed that similar tolerances apply to other graphite and boron carbide components of the HTTR. Therefore, the coolant channel pitch is treated with a tolerance (with uniform

probability) of ±0.1 mm. The appropriate corrections to the scaling factors have been incorporated into the uncertainty analysis of these parameters.

The total number of pitch positions used in the fully-loaded core is 8,586. For determining the random component of the uncertainty, the results in Table 2.29 would be divided by √N, where N for each case is shown in Table 2.29.

Table 2.29. Effect of Uncertainty in Fuel and Coolant Channel Pitch.

Case	Deviation	Δk	±	$\sigma_{\Delta k}$	Scaling Factor	Δk_{eff} (1σ)	±	$\sigma_{\Delta keff}$	N
1	-2 mm (20 × limit)	-0.00620	±	0.00017	20√3	-0.00018	±	0.00000	6,771
	+2 mm (20 × limit)	0.00628	±	0.00017	20√3	0.00018	±	0.00000	
2	-2 mm (20 × limit)	-0.00584	±	0.00016	20√3	-0.00017	±	0.00000	7,101
	+2 mm (20 × limit)	0.00583	±	0.00016	20√3	0.00017	±	0.00000	
3	-2 mm (20 × limit)	-0.00510	±	0.00016	20√3	-0.00015	±	0.00000	7,596
	+2 mm (20 × limit)	0.00472	±	0.00017	20√3	0.00014	±	0.00000	
4	-2 mm (20 × limit)	-0.00485	±	0.00017	20√3	-0.00014	±	0.00000	7,596
	+2 mm (20 × limit)	0.00474	±	0.00017	20√3	0.00014	±	0.00000	
5	-2 mm (20 × limit)	-0.00413	±	0.0016	20√3	-0.00012	±	0.00000	8,091
	+2 mm (20 × limit)	0.00411	±	0.00016	20√3	0.00012	±	0.00000	

Handling Socket Dimensions

The handling sockets were not included in the model as there was insufficient information to model them completely. The calculated volume of the socket (estimated using dimensions in Figure 1.52 of HTTR-GCR-RESR-001) is roughly 0.5 vol. % of the complete block envelope. This volume reduction is included as a reduction in total block density in the benchmark model. A bias has not been assessed. Uncertainty in the volume fraction will be included as part of the assessment of the uncertainty in the total density of the graphite blocks.

Column Pitch

An uncertainty in column pitch was assumed based upon the average distance between blocks of approximately 2 mm. For the evaluation of this uncertainty, the columns were modeled closer together then further apart by adjusting the pitch between them. A variation of ±2 mm (2 × bounding limit) from the nominal value of 362 mm was analyzed and the effects on the uncertainty of k_{eff} were determined. Results are shown in Table 2.30.

The total number of columns used in all core configurations is 61. For determining the random component of the uncertainty, the results in Table 2.30 would be divided by √61.

Table 2.30. Effect of Uncertainty in Column Pitch.

Case	Deviation	Δk	±	$\sigma_{\Delta k}$	Scaling Factor	Δk_{eff} (1σ)	±	$\sigma_{\Delta keff}$
1	-2 mm	0.00204	±	0.00017	2√3	0.00059	±	0.00005
	+2 mm	-0.00249	±	0.00017	2√3	-0.00072	±	0.00005
2	-2 mm	0.00215	±	0.00017	2√3	0.00062	±	0.00005
	+2 mm	-0.00231	±	0.00017	2√3	-0.00067	±	0.00005
3	-2 mm	0.00203	±	0.00017	2√3	0.00059	±	0.00005
	+2 mm	-0.00251	±	0.00017	2√3	-0.00072	±	0.00005
4	-2 mm	0.00185	±	0.00017	2√3	0.00053	±	0.00005
	+2 mm	-0.00267	±	0.00017	2√3	-0.00077	±	0.00005
5	-2 mm	0.00219	±	0.00016	2√3	0.00063	±	0.00005
	+2 mm	-0.00224	±	0.00016	2√3	-0.00065	±	0.00004

Control-Rod Channel Diameter

An assumed variation of ±2 mm in the diameter of the control-rod coolant channels (nominal value of 123 mm, Figure 1.64 of HTTR-GCR-RESR-001) in the control block columns was performed to determine the effective uncertainty in k_{eff}. Results are shown in Table 2.31.

Because of the tight manufacturing tolerances of the fuel compacts and graphite sleeves (Sections 2.1.2.2 and 2.1.2.3, respectively) it is believed that similar tolerances apply to other graphite and boron carbide components of the HTTR. Therefore, the control-rod channel diameter is treated with a tolerance (with uniform probability) of ±0.1 mm. The appropriate corrections to the scaling factors have been incorporated into the uncertainty analysis of these parameters.

The total number of control-rod channels (including empty instrumentation channels) in blocks used in all core configurations is approximately 437. For determining the random component of the uncertainty, the results in Table 2.31 would be divided by √437.

Table 2.31. Effect of Uncertainty in CR Channel Diameter.

Case	Deviation	Δk	±	$\sigma_{\Delta k}$	Scaling Factor	Δk_{eff} (1σ)	±	$\sigma_{\Delta keff}$
1	-2 mm (20 × limit)	0.00111	±	0.00017	20√3	0.00003	±	0.00000
	+2 mm (20 × limit)	-0.00142	±	0.00017	20√3	-0.00004	±	0.00000
2	-2 mm (20 × limit)	0.00136	±	0.00017	20√3	0.00004	±	0.00000
	+2 mm (20 × limit)	-0.00126	±	0.00016	20√3	-0.00004	±	0.00000
3	-2 mm (20 × limit)	0.00131	±	0.00016	20√3	0.00004	±	0.00000
	+2 mm (20 × limit)	-0.00148	±	0.00016	20√3	-0.00004	±	0.00000
4	-2 mm (20 × limit)	0.00122	±	0.00017	20√3	0.00004	±	0.00000
	+2 mm (20 × limit)	-0.00169	±	0.00017	20√3	-0.00005	±	0.00000
5	-2 mm (20 × limit)	0.00144	±	0.00016	20√3	0.00004	±	0.00000
	+2 mm (20 × limit)	-0.00149	±	0.00016	20√3	-0.00004	±	0.00000

Control-Rod Channel Pitch

An uncertainty in control-rod coolant channel pitch in the fuel and reflector blocks was not reported. For the evaluation of this uncertainty, the channels were modeled closer together then further apart by adjusting the pitch between them. A variation of ±2 mm from the nominal distance of 108 mm from the block axis (Figure 1.64 of HTTR-GCR-RESR-001) was assumed and the effects on the uncertainty of k_{eff} were determined. Results are shown in Table 2.32.

Because of the tight manufacturing tolerances of the fuel compacts and graphite sleeves (Sections 2.1.2.2 and 2.1.2.3, respectively) it is believed that similar tolerances apply to other graphite and boron carbide components of the HTTR. Therefore, the control-rod channel pitch is treated with a tolerance (with uniform probability) of ±0.1 mm. The appropriate corrections to the scaling factors have been incorporated into the uncertainty analysis of these parameters.

The total number of control-rod channels (including empty instrumentation channels) in blocks used in the all core configurations is approximately 437. For determining the random component of the uncertainty, the results in Table 2.32 would be divided by √437.

Table 2.32. Effect of Uncertainty in Control-Rod Channel Pitch.

Case	Deviation	Δk	±	$\sigma_{\Delta k}$	Scaling Factor	Δk_{eff} (1σ)	±	$\sigma_{\Delta keff}$
1	-2 mm (20 × limit)	-0.00009	±	0.00016	20√3	0.00000	±	0.00000
	+2 mm (20 × limit)	-0.00004	±	0.00017	20√3	0.00000	±	0.00000
2	-2 mm (20 × limit)	0.00044	±	0.00017	20√3	0.00001	±	0.00000
	+2 mm (20 × limit)	0.00010	±	0.00016	20√3	0.00000	±	0.00000
3	-2 mm (20 × limit)	-0.00005	±	0.00017	20√3	0.00000	±	0.00000
	+2 mm (20 × limit)	-0.00023	±	0.00017	20√3	-0.00001	±	0.00000
4	-2 mm (20 × limit)	-0.00007	±	0.00017	20√3	0.00000	±	0.00000
	+2 mm (20 × limit)	-0.00031	±	0.00017	20√3	-0.00001	±	0.00000
5	-2 mm (20 × limit)	-0.00002	±	0.00016	20√3	0.00000	±	0.00000
	+2 mm (20 × limit)	0.00012	±	0.00016	20√3	0.00000	±	0.00000

2.1.2.8 Permanent Reflectors

Insufficient information is available to model in detail the permanent reflector of the HTTR. A bias was not assessed for any simplification of the permanent reflector. The actual reflector is in the shape of a dodecagon block with an overall diameter and length of 4250 mm and 5250 mm, respectively. It is unclear as to whether the diameter is inscribed within or circumscribed around the polygon.

A radial representation of the permanent reflector had the outer diameter varied ±10 cm to determine the effective change in Δk. The difference between the reported diameter and an equivalent diameter circle representative of an inscribed or circumscribed dodecagon would by -10 cm and +5 cm, respectively. This uncertainty is treated as a bounding uncertainty. Any uncertainty in the unreported manufacturing tolerances would be negligible. Results are shown in Table 2.33.

The permanent reflector is comprised of 12 circumferential segments in eight axial layers for a total of 96 blocks. However, the uncertainty in the diameter of the model's permanent reflector is not adjusted for random uncertainty and treated as 100% systematic because of the uncertainty in the overall detail of the permanent reflector.

Table 2.33. Effect of Uncertainty in Permanent Reflector Diameter.

Case	Deviation	Δk	±	$\sigma_{\Delta k}$	Scaling Factor	Δk_{eff} (1σ)	±	$\sigma_{\Delta keff}$
1	-10 cm	-0.00202	±	0.00017	√3	-0.00117	±	0.00010
	+10 cm	0.00155	±	0.00016	2√3	0.00045	±	0.00005
2	-10 cm	-0.00144	±	0.00016	√3	-0.00083	±	0.00009
	+10 cm	0.00150	±	0.00017	2√3	0.00043	±	0.00005
3	-10 cm	-0.00145	±	0.00016	√3	-0.00084	±	0.00009
	+10 cm	0.00119	±	0.00016	2√3	0.00034	±	0.00005
4	-10 cm	-0.00093	±	0.00017	√3	-0.00054	±	0.00010
	+10 cm	0.00050	±	0.00017	2√3	0.00014	±	0.00005
5	-10 cm	-0.00144	±	0.00016	√3	-0.00083	±	0.00009
	+10 cm	0.00083	±	0.00016	2√3	0.00024	±	0.00005

2.1.2.9 Dummy Blocks

The uncertainty in the outer dimensions of the dummy blocks was included with the graphite block analysis in Section 2.1.2.7. There are two types of dummy blocks, one with a hole pattern similar to that of a control block, and the other with three holes but of smaller diameter (Ref. 2, p. 14). Because the true dimensions of the smaller hole design is unknown, the dummy blocks will all be modeled with the holes of the control blocks but an additional uncertainty will be added to account for this discrepancy. This uncertainty will be assessed by completely filling the holes of the dummy blocks with IG-11 graphite material (Section 2.1.3.9).

2.1.3 Compositional Variations

2.1.3.1 Coated Fuel Particles

Uranium Enrichment

The concentration of ^{234}U expected in the TRISO fuel had to be determined, as it was not provided. First the weight fractions of isotopes in natural uranium dioxide were determined. Then the enriched weight percent of ^{235}U was multiplied by the natural weight percent of ^{234}U (0.0055 at.%) and divided by the natural weight percent of ^{235}U (0.72 at.%). Thus an approximate concentration of "enriched" ^{234}U content could be determined for this evaluation, which may slightly underestimate the actual ^{234}U content.

$$\gamma_{^{234}U}^{Enriched} = \frac{\gamma_{^{234}U}^{Natural}}{\gamma_{^{235}U}^{Natural}} \gamma_{^{235}U}^{Enriched} .$$

Information was not provided regarding the uncertainty in the uranium enrichment of the TRISO kernels. It is reported elsewhere that the manufacturing tolerance limit for the enrichment is 4.5% of the reported weight percent.[a] For example, the enrichment of 3.4 wt.% is bound within a tolerance of ±0.153 wt.%.

[a] S. Maruyama, K. Yamashita, N. Fujimoto, I. Murata, R. Shindo, and Y. Sudo, "Determination of Hot Spot Factors for Calculation of the Maximum Fuel Temperatures in the Core Thermal and Hydraulic Design of HTTR," JAERI-M 88-250, JAEA (November 18, 1988). [in Japanese].

The ^{234}U content adjusted to match the effective increase or decrease in enrichment of ^{235}U, to determine the effective uncertainty in k_{eff}. The nominal enrichment values are shown in Figure 1.46 and Table 1.11 of HTTR-GCR-RESR-001. Results are shown in Tables 2.34 through 2.38. The actual uncertainty in the uranium enrichment is much smaller than the manufacturing limits; however this information is not publicly available. Therefore, the bounding limits are treated with a normal distribution instead of one with uniform probability.

Configurations 1 through 4 do not contain uranium fuel with the enrichments of 3.40 and 6.70 wt.%.

The uncertainty in the uranium enrichment is considered all systematic with no random component.

Table 2.34. Effect of Uncertainty in Uranium Enrichment (Case 1).

Deviation	Δk	±	$\sigma_{\Delta k}$	Scaling Factor	Δk_{eff} (1σ)	±	$\sigma_{\Delta keff}$
-0.1755 wt.% of 3.9 wt.%	-0.00012	±	0.00016	3	-0.00004	±	0.00005
+0.1755 wt.% of 3.9 wt.%	0.00035	±	0.00016	3	0.00012	±	0.00005
-0.1935 wt.% of 4.3 wt.%	-0.00163	±	0.00016	3	-0.00054	±	0.00005
+0.1935 wt.% of 4.3 wt.%	0.00162	±	0.00016	3	0.00054	±	0.00005
-0.216 wt.% of 4.8 wt.%	-0.00069	±	0.00016	3	-0.00023	±	0.00005
+0.216 wt.% of 4.8 wt.%	0.00066	±	0.00016	3	0.00022	±	0.00005
-0.234 wt.% of 5.2 wt.%	-0.00018	±	0.00016	3	-0.00006	±	0.00005
+0.234 wt.% of 5.2 wt.%	0.00023	±	0.00016	3	0.00008	±	0.00005
-0.2655 wt.% of 5.9 wt.%	-0.00189	±	0.00016	3	-0.00063	±	0.00005
+0.2655 wt.% of 5.9 wt.%	0.00180	±	0.00016	3	0.00060	±	0.00005
-0.2835 wt.% of 6.3 wt.%	-0.00127	±	0.00016	3	-0.00042	±	0.00005
+0.2835 wt.% of 6.3 wt.%	0.00101	±	0.00016	3	0.00034	±	0.00005
-0.324 wt.% of 7.2 wt.%	-0.00221	±	0.00016	3	-0.00074	±	0.00005
+0.324 wt.% of 7.2 wt.%	0.00238	±	0.00016	3	0.00079	±	0.00005
-0.3555 wt.% of 7.9 wt.%	-0.00114	±	0.00016	3	-0.00038	±	0.00005
+0.3555 wt.% of 7.9 wt.%	0.00143	±	0.00016	3	0.00048	±	0.00005
-0.423 wt.% of 9.4 wt.%	-0.00166	±	0.00016	3	-0.00055	±	0.00005
+0.423 wt.% of 9.4 wt.%	0.00186	±	0.00016	3	0.00062	±	0.00005
-0.4455 wt.% of 9.9 wt.%	-0.00093	±	0.00016	3	-0.00031	±	0.00005
+0.4455 wt.% of 9.9 wt.%	0.00081	±	0.00016	3	0.00027	±	0.00005

Table 2.35. Effect of Uncertainty in Uranium Enrichment (Case 2).

Deviation	Δk	$\pm$	$\sigma_{\Delta k}$	Scaling Factor	Δk_{eff} (1σ)	$\pm$	$\sigma_{\Delta keff}$
-0.1755 wt.% of 3.9 wt.%	-0.00091	±	0.00016	3	-0.00030	±	0.00005
+0.1755 wt.% of 3.9 wt.%	0.00068	±	0.00016	3	0.00023	±	0.00005
-0.1935 wt.% of 4.3 wt.%	-0.00244	±	0.00016	3	-0.00081	±	0.00005
+0.1935 wt.% of 4.3 wt.%	0.00220	±	0.00016	3	0.00073	±	0.00005
-0.216 wt.% of 4.8 wt.%	-0.00124	±	0.00016	3	-0.00041	±	0.00005
+0.216 wt.% of 4.8 wt.%	0.00110	±	0.00016	3	0.00037	±	0.00005
-0.234 wt.% of 5.2 wt.%	-0.00099	±	0.00016	3	-0.00033	±	0.00005
+0.234 wt.% of 5.2 wt.%	0.00051	±	0.00016	3	0.00017	±	0.00005
-0.2655 wt.% of 5.9 wt.%	-0.00229	±	0.00016	3	-0.00076	±	0.00005
+0.2655 wt.% of 5.9 wt.%	0.00227	±	0.00016	3	0.00076	±	0.00005
-0.2835 wt.% of 6.3 wt.%	-0.00202	±	0.00016	3	-0.00067	±	0.00005
+0.2835 wt.% of 6.3 wt.%	0.00140	±	0.00016	3	0.00047	±	0.00005
-0.324 wt.% of 7.2 wt.%	-0.00213	±	0.00016	3	-0.00071	±	0.00005
+0.324 wt.% of 7.2 wt.%	0.00180	±	0.00016	3	0.00060	±	0.00005
-0.3555 wt.% of 7.9 wt.%	-0.00114	±	0.00016	3	-0.00038	±	0.00005
+0.3555 wt.% of 7.9 wt.%	0.00093	±	0.00016	3	0.00031	±	0.00005
-0.423 wt.% of 9.4 wt.%	-0.00078	±	0.00016	3	-0.00026	±	0.00005
+0.423 wt.% of 9.4 wt.%	0.00048	±	0.00016	3	0.00016	±	0.00005
-0.4455 wt.% of 9.9 wt.%	-0.00044	±	0.00016	3	-0.00015	±	0.00005
+0.4455 wt.% of 9.9 wt.%	0.00013	±	0.00016	3	0.00004	±	0.00005

Table 2.36. Effect of Uncertainty in Uranium Enrichment (Case 3).

Deviation	Δk	$\pm$	$\sigma_{\Delta k}$	Scaling Factor	Δk_{eff} (1σ)	$\pm$	$\sigma_{\Delta keff}$
-0.1755 wt.% of 3.9 wt.%	-0.00193	±	0.00016	3	-0.00064	±	0.00005
+0.1755 wt.% of 3.9 wt.%	0.00231	±	0.00016	3	0.00077	±	0.00005
-0.1935 wt.% of 4.3 wt.%	-0.00277	±	0.00016	3	-0.00092	±	0.00005
+0.1935 wt.% of 4.3 wt.%	0.00293	±	0.00016	3	0.00098	±	0.00005
-0.216 wt.% of 4.8 wt.%	-0.00130	±	0.00016	3	-0.00043	±	0.00005
+0.216 wt.% of 4.8 wt.%	0.00157	±	0.00016	3	0.00052	±	0.00005
-0.234 wt.% of 5.2 wt.%	-0.00137	±	0.00016	3	-0.00046	±	0.00005
+0.234 wt.% of 5.2 wt.%	0.00148	±	0.00016	3	0.00049	±	0.00005
-0.2655 wt.% of 5.9 wt.%	-0.00175	±	0.00016	3	-0.00058	±	0.00005
+0.2655 wt.% of 5.9 wt.%	0.00212	±	0.00016	3	0.00071	±	0.00005
-0.2835 wt.% of 6.3 wt.%	-0.00135	±	0.00016	3	-0.00045	±	0.00005
+0.2835 wt.% of 6.3 wt.%	0.00155	±	0.00016	3	0.00052	±	0.00005
-0.324 wt.% of 7.2 wt.%	-0.00094	±	0.00016	3	-0.00031	±	0.00005
+0.324 wt.% of 7.2 wt.%	0.00108	±	0.00016	3	0.00036	±	0.00005
-0.3555 wt.% of 7.9 wt.%	-0.00034	±	0.00016	3	-0.00011	±	0.00005
+0.3555 wt.% of 7.9 wt.%	0.00051	±	0.00016	3	0.00017	±	0.00005
-0.423 wt.% of 9.4 wt.%	-0.00008	±	0.00016	3	-0.00003	±	0.00005
+0.423 wt.% of 9.4 wt.%	0.00039	±	0.00016	3	0.00013	±	0.00005
-0.4455 wt.% of 9.9 wt.%	0.00003	±	0.00016	3	0.00001	±	0.00005
+0.4455 wt.% of 9.9 wt.%	0.00003	±	0.00016	3	0.00001	±	0.00005

Table 2.37. Effect of Uncertainty in Uranium Enrichment (Case 4).

Deviation	Δk	$\pm$	$\sigma_{\Delta k}$	Scaling Factor	Δk_{eff} (1σ)	$\pm$	$\sigma_{\Delta keff}$
-0.1755 wt.% of 3.9 wt.%	-0.00159	±	0.00017	3	-0.00053	±	0.00006
+0.1755 wt.% of 3.9 wt.%	0.00176	±	0.00017	3	0.00059	±	0.00006
-0.1935 wt.% of 4.3 wt.%	-0.00193	±	0.00017	3	-0.00064	±	0.00006
+0.1935 wt.% of 4.3 wt.%	0.00238	±	0.00016	3	0.00079	±	0.00005
-0.216 wt.% of 4.8 wt.%	-0.00091	±	0.00017	3	-0.00030	±	0.00006
+0.216 wt.% of 4.8 wt.%	0.00108	±	0.00017	3	0.00036	±	0.00006
-0.234 wt.% of 5.2 wt.%	-0.00135	±	0.00017	3	-0.00045	±	0.00006
+0.234 wt.% of 5.2 wt.%	0.00154	±	0.00017	3	0.00051	±	0.00006
-0.2655 wt.% of 5.9 wt.%	-0.00145	±	0.00017	3	-0.00048	±	0.00006
+0.2655 wt.% of 5.9 wt.%	0.00124	±	0.00017	3	0.00041	±	0.00006
-0.2835 wt.% of 6.3 wt.%	-0.00190	±	0.00017	3	-0.00063	±	0.00006
+0.2835 wt.% of 6.3 wt.%	0.00197	±	0.00017	3	0.00066	±	0.00006
-0.324 wt.% of 7.2 wt.%	-0.00103	±	0.00016	3	-0.00034	±	0.00005
+0.324 wt.% of 7.2 wt.%	0.00099	±	0.00017	3	0.00033	±	0.00006
-0.3555 wt.% of 7.9 wt.%	-0.00112	±	0.00017	3	-0.00037	±	0.00006
+0.3555 wt.% of 7.9 wt.%	0.00133	±	0.00016	3	0.00044	±	0.00005
-0.423 wt.% of 9.4 wt.%	-0.00042	±	0.00016	3	-0.00014	±	0.00005
+0.423 wt.% of 9.4 wt.%	0.00055	±	0.00017	3	0.00018	±	0.00006
-0.4455 wt.% of 9.9 wt.%	-0.00013	±	0.00017	3	-0.00004	±	0.00006
+0.4455 wt.% of 9.9 wt.%	0.00032	±	0.00017	3	0.00011	±	0.00006

Table 2.38. Effect of Uncertainty in Uranium Enrichment (Case 5).

Deviation	Δk	±	$\sigma_{\Delta k}$	Scaling Factor	Δk_{eff} (1σ)	±	$\sigma_{\Delta keff}$
-0.153 wt.% of 3.4 wt.%	-0.00162	±	0.00017	3	-0.00054	±	0.00006
+0.153 wt.% of 3.4 wt.%	0.00125	±	0.00016	3	0.00042	±	0.00005
-0.1755 wt.% of 3.9 wt.%	-0.00238	±	0.00016	3	-0.00079	±	0.00005
+0.1755 wt.% of 3.9 wt.%	0.00238	±	0.00017	3	0.00079	±	0.00006
-0.1935 wt.% of 4.3 wt.%	-0.00399	±	0.00016	3	-0.00133	±	0.00005
+0.1935 wt.% of 4.3 wt.%	0.00398	±	0.00017	3	0.00133	±	0.00006
-0.216 wt.% of 4.8 wt.%	-0.00155	±	0.00017	3	-0.00052	±	0.00006
+0.216 wt.% of 4.8 wt.%	0.00152	±	0.00016	3	0.00051	±	0.00005
-0.234 wt.% of 5.2 wt.%	-0.00118	±	0.00017	3	-0.00039	±	0.00006
+0.234 wt.% of 5.2 wt.%	0.00111	±	0.00016	3	0.00037	±	0.00005
-0.2655 wt.% of 5.9 wt.%	-0.00157	±	0.00017	3	-0.00052	±	0.00006
+0.2655 wt.% of 5.9 wt.%	0.00142	±	0.00016	3	0.00047	±	0.00005
-0.2835 wt.% of 6.3 wt.%	-0.00091	±	0.00016	3	-0.00030	±	0.00005
+0.2835 wt.% of 6.3 wt.%	0.00078	±	0.00016	3	0.00026	±	0.00005
-0.3015 wt.% of 6.7 wt.%	0.00009	±	0.00017	3	0.00003	±	0.00006
+0.3015 wt.% of 6.7 wt.%	0.00007	±	0.00016	3	0.00002	±	0.00005
-0.324 wt.% of 7.2 wt.%	-0.00037	±	0.00017	3	-0.00012	±	0.00006
+0.324 wt.% of 7.2 wt.%	0.00033	±	0.00017	3	0.00011	±	0.00006
-0.3555 wt.% of 7.9 wt.%	-0.00025	±	0.00017	3	-0.00008	±	0.00006
+0.3555 wt.% of 7.9 wt.%	0.00019	±	0.00016	3	0.00006	±	0.00005
-0.423 wt.% of 9.4 wt.%	0.00003	±	0.00017	3	0.00001	±	0.00006
+0.423 wt.% of 9.4 wt.%	-0.00005	±	0.00016	3	-0.00002	±	0.00005
-0.4455 wt.% of 9.9 wt.%	-0.00002	±	0.00017	3	-0.00001	±	0.00006
+0.4455 wt.% of 9.9 wt.%	0.00022	±	0.00016	3	0.00007	±	0.00005

Oxygen to Uranium Ratio

The oxygen to uranium ratio was varied by a best judgment value of ±0.06 (3 × bounding limit) from the nominal value of 2.00 to determine the effective uncertainty in k_{eff}. Results are shown in Table 2.39.

The uncertainty in the oxygen to uranium ratio is considered all systematic with no random component.

Table 2.39. Effect of Uncertainty in Oxygen to Uranium Ratio.

Case	Deviation	Δk	$\pm$	$\sigma_{\Delta k}$	Scaling Factor	Δk_{eff} (1σ)	$\pm$	$\sigma_{\Delta keff}$	N
1	-0.06	0.00044	$\pm$	0.00017	3$\sqrt{3}$	0.00008	$\pm$	0.00003	5.38×10^8
	+0.06	-0.00047	$\pm$	0.00016	3$\sqrt{3}$	-0.00009	$\pm$	0.0003	
2	-0.06	0.00074	$\pm$	0.00016	3$\sqrt{3}$	0.00014	$\pm$	0.00003	5.98×10^8
	+0.06	-0.00036	$\pm$	0.00016	3$\sqrt{3}$	-0.00007	$\pm$	0.00003	
3	-0.06	0.00035	$\pm$	0.00016	3$\sqrt{3}$	0.00007	$\pm$	0.00003	6.88×10^8
	+0.06	-0.00086	$\pm$	0.00017	3$\sqrt{3}$	-0.00017	$\pm$	0.00003	
4	-0.06	0.00055	$\pm$	0.00016	3$\sqrt{3}$	0.00011	$\pm$	0.00003	6.88×10^8
	+0.06	-0.00060	$\pm$	0.00017	3$\sqrt{3}$	-0.00012	$\pm$	0.00003	
5	-0.06	0.00048	$\pm$	0.00016	3$\sqrt{3}$	0.00009	$\pm$	0.00003	7.78×10^8
	+0.06	-0.00063	$\pm$	0.00016	3$\sqrt{3}$	-0.00012	$\pm$	0.00003	

UO_2 Density

Because of the overspecification of the TRISO particles in Table 1.14 (HTTR-GCR-RESR-001) and the correlation of uranium kernel diameter, density, TRISO packing fraction, and mass, the effect of the uncertainty in the fuel density is not included in the total uncertainty. However, an analysis of the uncertainty based upon the fuel mass is performed in Section 2.1.6.

UO_2 Impurity

The kernel impurity was varied from 0-3 ppm by weight of equivalent natural-boron content to determine the bounding uncertainty in k_{eff}. The maximum limit was multiplied 10-fold so as to quantify the effective upper uncertainty in the UO_2 impurity. The average value is 1.5 ppm by weight (Tables 1.13 and 1.14 of HTTR-GCR-RESR-001). Results are shown in Table 2.40.

The uncertainty in the UO_2 impurity is considered all systematic with no random component.

Table 2.40. Effect of Uncertainty in UO_2 Impurity.

Case	Deviation	Δk	±	$\sigma_{\Delta k}$	Scaling Factor	Δk_{eff} (1σ)	±	$\sigma_{\Delta keff}$
1	0 ppm	0.00055	±	0.00016	√3	0.00032	±	0.00009
	30 ppm	-0.00963	±	0.00017	10√3	-0.00056	±	0.00001
2	0 ppm	0.00081	±	0.00016	√3	0.00047	±	0.00009
	30 ppm	-0.01034	±	0.00017	10√3	-0.00060	±	0.00001
3	0 ppm	0.00042	±	0.00016	√3	0.00024	±	0.00009
	30 ppm	-0.01176	±	0.00016	10√3	-0.00068	±	0.00001
4	0 ppm	0.00045	±	0.00016	√3	0.00026	±	0.00009
	30 ppm	-0.01090	±	0.00016	10√3	-0.00063	±	0.00001
5	0 ppm	0.00082	±	0.00016	√3	0.00047	±	0.00009
	30 ppm	-0.01260	±	0.00016	10√3	-0.00073	±	0.00001

Buffer Density

The buffer density was varied ±0.30 g/cm^3 from the nominal value of 1.10 g/cm^3 (Table 1.14 of HTTR-GCR-RESR-001) to determine the effective uncertainty in k_{eff}. This value is three times the bounding limit. Results are shown in Table 2.41.

The total number of TRISO particles used in the fully-loaded core is approximately 868,140,000. For determining the random component of the uncertainty, the results in Table 2.41 would be divided by √N, where N for each case is shown in Table 2.41.

Table 2.41. Effect of Uncertainty in Buffer Density.

Case	Deviation	Δk	±	$\sigma_{\Delta k}$	Scaling Factor	Δk_{eff} (1σ)	±	$\sigma_{\Delta keff}$	N
1	-0.30 g/cm^3	-0.00005	±	0.00017	3√3	-0.00001	±	0.00003	5.38×10^8
	+0.30 g/cm^3	0.00014	±	0.00017	3√3	0.00003	±	0.00003	
2	-0.30 g/cm^3	-0.00009	±	0.00017	3√3	-0.00002	±	0.00003	5.98×10^8
	+0.30 g/cm^3	0.00026	±	0.00016	3√3	0.00005	±	0.00003	
3	-0.30 g/cm^3	-0.00021	±	0.00017	3√3	-0.00004	±	0.00003	6.88×10^8
	+0.30 g/cm^3	0.00006	±	0.00017	3√3	0.00001	±	0.00003	
4	-0.30 g/cm^3	-0.00001	±	0.00017	3√3	0.00000	±	0.00003	6.88×10^8
	+0.30 g/cm^3	-0.00019	±	0.00016	3√3	-0.00004	±	0.00003	
5	-0.30 g/cm^3	-0.00002	±	0.00016	3√3	0.00000	±	0.00003	7.78×10^8
	+0.30 g/cm^3	0.00007	±	0.00016	3√3	0.00001	±	0.00003	

Buffer Impurity

The buffer impurity was varied from 0-3 ppm by weight of equivalent natural-boron content to determine the bounding uncertainty in k_{eff}. The average value is 1.5 ppm by weight (Table 1.13 of HTTR-GCR-RESR-001). Results are shown in Table 2.42.

The uncertainty in the buffer impurity is considered all systematic with no random component.

Table 2.42. Effect of Uncertainty in Buffer Impurity.

Case	Deviation	Δk	±	$\sigma_{\Delta k}$	Scaling Factor	Δk_{eff} (1σ)	±	$\sigma_{\Delta keff}$
1	0 ppm	0.00004	±	0.00017	√3	0.00002	±	0.00010
	3 ppm	0.00001	±	0.00017	√3	0.00001	±	0.00010
2	0 ppm	0.00014	±	0.00017	√3	0.00008	±	0.00010
	3 ppm	0.00000	±	0.00017	√3	0.00000	±	0.00010
3	0 ppm	0.00014	±	0.00016	√3	0.00008	±	0.00009
	3 ppm	-0.00021	±	0.00017	√3	-0.00012	±	0.00010
4	0 ppm	-0.00005	±	0.00017	√3	-0.00003	±	0.00010
	3 ppm	-0.00017	±	0.00017	√3	-0.00010	±	0.00010
5	0 ppm	0.00014	±	0.00016	√3	0.00008	±	0.00009
	3 ppm	-0.00020	±	0.00016	√3	-0.00012	±	0.00009

IPyC Density

The IPyC density was varied +0.30 and -0.15 g/cm^3 from the nominal value of 1.85 g/cm^3 (Table 1.14 of HTTR-GCR-RESR-001) to determine the effective uncertainty in k_{eff}. These values are three times the bounding limit. Results are shown in Table 2.43.

The total number of TRISO particles used in the fully-loaded core is approximately 868,140,000. For determining the random component of the uncertainty, the results in Table 2.43 would be divided by √N, where N for each case is shown in Table 2.43.

Table 2.43. Effect of Uncertainty in IPyC Density.

Case	Deviation	Δk	±	$\sigma_{\Delta k}$	Scaling Factor	Δk_{eff} (1σ)	±	$\sigma_{\Delta keff}$	N
1	-0.15 g/cm^3	0.00000	±	0.00016	3√3	0.00000	±	0.00003	5.38×10^8
	+0.30 g/cm^3	0.00017	±	0.00017	3√3	0.00003	±	0.00003	
2	-0.15 g/cm^3	0.00012	±	0.00016	3√3	0.00002	±	0.00003	5.98×10^8
	+0.30 g/cm^3	0.00027	±	0.00017	3√3	0.00005	±	0.00003	
3	-0.15 g/cm^3	0.00006	±	0.00016	3√3	0.00001	±	0.00003	6.88×10^8
	+0.30 g/cm^3	0.00010	±	0.00017	3√3	0.00002	±	0.00003	
4	-0.15 g/cm^3	-0.00011	±	0.00017	3√3	-0.00002	±	0.00003	6.88×10^8
	+0.30 g/cm^3	-0.00005	±	0.00017	3√3	-0.00001	±	0.00003	
5	-0.15 g/cm^3	0.00015	±	0.00016	3√3	0.00003	±	0.00003	7.78×10^8
	+0.30 g/cm^3	0.00010	±	0.00016	3√3	0.00002	±	0.00003	

IPyC Impurity

The IPyC impurity was varied from 0-3 ppm by weight of equivalent natural-boron content to determine the bounding uncertainty in k_{eff}. The average value is 1.5 ppm by weight (Table 1.13 of HTTR-GCR-RESR-001). Results are shown in Table 2.28.

The uncertainty in the IPyC impurity is considered all systematic with no random component.

Table 2.28. Effect of Uncertainty in IPyC Impurity.

Case	Deviation	Δk	±	$\sigma_{\Delta k}$	Scaling Factor	Δk_{eff} (1σ)	±	$\sigma_{\Delta keff}$
1	0 ppm	0.00006	±	0.00017	√3	0.00003	±	0.00010
	3 ppm	-0.00006	±	0.00017	√3	-0.00003	±	0.00010
2	0 ppm	0.00002	±	0.00016	√3	0.00001	±	0.00009
	3 ppm	0.00008	±	0.00017	√3	0.00005	±	0.00010
3	0 ppm	-0.00019	±	0.00016	√3	-0.00011	±	0.00009
	3 ppm	-0.00027	±	0.00017	√3	-0.00016	±	0.00010
4	0 ppm	0.00005	±	0.00017	√3	0.00003	±	0.00010
	3 ppm	-0.00005	±	0.00017	√3	-0.00003	±	0.00010
5	0 ppm	0.00023	±	0.00016	√3	0.00013	±	0.00009
	3 ppm	-0.00011	±	0.00016	√3	-0.00006	±	0.00009

SiC Density

The SiC density was increased by 0.06 g/cm^3, where 0.02 g/cm^3 is typical for SiC material, from the nominal value of 3.20 g/cm^3 (Table 1.14 of HTTR-GCR-RESR-001) to determine the effective

uncertainty in k_{eff}. This value is three times the bounding limit. The density was not decreased because of the minimum requirement for SiC density. Results are shown in Table 2.44.

The total number of TRISO particles used in the fully-loaded core is approximately 868,140,000. For determining the random component of the uncertainty, the results in Table 2.44 would be divided by √N, where N for each case is shown in Table 2.44.

Table 2.44. Effect of Uncertainty in SiC Density.

Case	Deviation	Δk	±	$\sigma_{\Delta k}$	Scaling Factor	Δk_{eff} (1σ)	±	$\sigma_{\Delta keff}$	N
1	+0.06 g/cm^3	0.00003	±	0.00016	6√3	0.00000	±	0.00002	5.38×10^8
2	+0.06 g/cm^3	0.00029	±	0.00017	6√3	0.00003	±	0.00002	5.98×10^8
3	+0.06 g/cm^3	-0.00014	±	0.00017	6√3	-0.00001	±	0.00002	6.88×10^8
4	+0.06 g/cm^3	-0.00026	±	0.00017	6√3	-0.00003	±	0.00002	6.88×10^8
5	+0.06 g/cm^3	-0.00018	±	0.00016	6√3	-0.00002	±	0.00002	7.78×10^8

SiC Impurity

The SiC impurity was varied from 0-3 ppm by weight of equivalent natural-boron content to determine the bounding uncertainty in k_{eff}. The average value is 1.5 ppm by weight (Table 1.13 of HTTR-GCR-RESR-001). Results are shown in Table 2.45.

The uncertainty in the SiC impurity is considered all systematic with no random component.

Table 2.45. Effect of Uncertainty in SiC Impurity.

Case	Deviation	Δk	±	$\sigma_{\Delta k}$	Scaling Factor	Δk_{eff} (1σ)	±	$\sigma_{\Delta keff}$
1	0 ppm	0.00007	±	0.00017	√3	0.00004	±	0.00010
	3 ppm	0.00001	±	0.00017	√3	0.00001	±	0.00010
2	0 ppm	0.00017	±	0.00016	√3	0.00010	±	0.00009
	3 ppm	-0.00013	±	0.00016	√3	-0.00008	±	0.00009
3	0 ppm	-0.00012	±	0.00017	√3	-0.00007	±	0.00010
	3 ppm	-0.00014	±	0.00017	√3	-0.00008	±	0.00010
4	0 ppm	0.00000	±	0.00016	√3	0.00000	±	0.00009
	3 ppm	-0.00019	±	0.00017	√3	-0.00011	±	0.00010
5	0 ppm	0.00000	±	0.00016	√3	0.00000	±	0.00009
	3 ppm	-0.00027	±	0.00016	√3	-0.00016	±	0.00009

OPyC Density

The OPyC density was varied +0.30 and -0.15 g/cm^3 from the nominal value of 1.85 g/cm^3 (Table 1.14 of HTTR-GCR-RESR-001) to determine the effective uncertainty in k_{eff}. This value is three times the bounding limit. Results are shown in Table 2.46.

The total number of TRISO particles used in the fully-loaded core is approximately 868,140,000. For determining the random component of the uncertainty, the results in Table 2.46 would be divided by $\sqrt{N}$, where N for each case is shown in Table 2.46.

Table 2.46. Effect of Uncertainty in OPyC Density.

Case	Deviation	Δk	$\pm$	$\sigma_{\Delta k}$	Scaling Factor	Δk_{eff} (1σ)	$\pm$	$\sigma_{\Delta keff}$	N
1	-0.15 g/cm^3	-0.00012	$\pm$	0.00017	3$\sqrt{3}$	-0.00002	$\pm$	0.00003	5.38 × 10^8
	+0.30 g/cm^3	0.00009	$\pm$	0.00017	3$\sqrt{3}$	-0.00002	$\pm$	0.00003	
2	-0.15 g/cm^3	0.00005	$\pm$	0.00017	3$\sqrt{3}$	0.00001	$\pm$	0.00003	5.98 × 10^8
	+0.30 g/cm^3	0.00026	$\pm$	0.00016	3$\sqrt{3}$	0.00005	$\pm$	0.00003	
3	-0.15 g/cm^3	-0.00018	$\pm$	0.00016	3$\sqrt{3}$	-0.00003	$\pm$	0.00003	6.88 × 10^8
	+0.30 g/cm^3	-0.00026	$\pm$	0.00016	3$\sqrt{3}$	-0.00005	$\pm$	0.00003	
4	-0.15 g/cm^3	-0.00012	$\pm$	0.00017	3$\sqrt{3}$	-0.00011	$\pm$	0.00010	6.88 × 10^8
	+0.30 g/cm^3	-0.00004	$\pm$	0.00017	3$\sqrt{3}$	-0.00001	$\pm$	0.00003	
5	-0.15 g/cm^3	-0.00010	$\pm$	0.00016	3$\sqrt{3}$	-0.00002	$\pm$	0.00003	7.78 × 10^8
	+0.30 g/cm^3	0.00009	$\pm$	0.00016	3$\sqrt{3}$	0.00002	$\pm$	0.00003	

OPyC Impurity

The OPyC impurity was varied from 0-3 ppm by weight of equivalent natural-boron content to determine the bounding uncertainty in k_{eff}. The average value is 1.5 ppm by weight (Table 1.13 of HTTR-GCR-RESR-001). Results are shown in Table 2.47.

The uncertainty in the OPyC impurity is considered all systematic with no random component.

Table 2.47. Effect of Uncertainty in OPyC Impurity.

Case	Deviation	Δk	±	$\sigma_{\Delta k}$	Scaling Factor	Δk_{eff} (1σ)	±	$\sigma_{\Delta keff}$
1	0 ppm	0.00009	±	0.00017	√3	0.00005	±	0.00010
	3 ppm	0.00009	±	0.00017	√3	0.00005	±	0.00010
2	0 ppm	0.00041	±	0.00016	√3	0.00024	±	0.00009
	3 ppm	-0.00026	±	0.00016	√3	-0.00015	±	0.00009
3	0 ppm	-0.00018	±	0.00016	√3	-0.00003	±	0.00003
	3 ppm	-0.00026	±	0.00016	√3	-0.00005	±	0.00003
4	0 ppm	-0.00020	±	0.00017	√3	-0.00012	±	0.00010
	3 ppm	-0.00005	±	0.00017	√3	-0.00003	±	0.00010
5	0 ppm	0.00034	±	0.00016	√3	0.000020	±	0.00009
	3 ppm	-0.00040	±	0.00016	√3	-0.00023	±	0.00009

Overcoat Density

Because insufficient data is available for the final composition and density of the graphite overcoat, this layer is being treated with equal properties to that of the surrounding compact graphite matrix. The overcoat density was varied ±0.15 g/cm^3 to determine the effective uncertainty in k_{eff}. This value is three times the bounding limit. Results are shown in Table 2.48.

The total number of TRISO particles used in the fully-loaded core is approximately 868,140,000. For determining the random component of the uncertainty, the results in Table 2.48 would be divided by √N, where N for each case is shown in Table 2.48.

Table 2.48. Effect of Uncertainty in Overcoat Density.

Case	Deviation	Δk	±	$\sigma_{\Delta k}$	Scaling Factor	Δk_{eff} (1σ)	±	$\sigma_{\Delta keff}$	N
1	-0.15 g/cm^3	-0.00030	±	0.00017	3√3	-0.00006	±	0.00003	5.38×10^8
	+0.15 g/cm^3	0.00034	±	0.00017	3√3	0.00007	±	0.00003	
2	-0.15 g/cm^3	-0.00018	±	0.00017	3√3	-0.00003	±	0.00003	5.98×10^8
	+0.15 g/cm^3	0.00039	±	0.00016	3√3	0.00008	±	0.00003	
3	-0.15 g/cm^3	-0.00050	±	0.00016	3√3	-0.00010	±	0.00003	6.88×10^8
	+0.15 g/cm^3	0.00014	±	0.00017	3√3	0.00003	±	0.00003	
4	-0.15 g/cm^3	-0.00058	±	0.00016	3√3	-0.00011	±	0.00003	6.88×10^8
	+0.15 g/cm^3	0.00032	±	0.00017	3√3	0.00006	±	0.00003	
5	-0.15 g/cm^3	-0.00024	±	0.00016	3√3	-0.00005	±	0.00003	7.78×10^8
	+0.15 g/cm^3	0.00025	±	0.00016	3√3	0.00005	±	0.00003	

Overcoat Composition

Because insufficient data is available for the final composition and density of the graphite overcoat, this layer is being treated with equal properties to that of the surrounding compact graphite matrix. In essence, the uncertainty has already been accounted for, as the surrounding graphite matrix has been characterized for uncertainties, and the overcoat has been demonstrated elsewhere to have negligible impact on the calculation of k_{eff} when it is not explicitly modeled, but included in the surrounding matrix.[a]

Overcoat Impurity

The overcoat impurity was varied from 0-5 ppm by weight of equivalent natural-boron content to determine the bounding uncertainty in k_{eff}. The average value of the coated fuel particles is 1.5 ppm by weight (Table 1.13 of HTTR-GCR-RESR-001); it is assumed that the overcoat would have a comparable impurity amount. The alternative is to use the impurity of the compact (matrix) material, which is 0.82 ppm by weight (Table 1.27 of HTTR-GCR-RESR-001). The larger amount is selected, i.e. 1.5 ppm. Results are shown in Table 2.49.

The uncertainty in the overcoat impurity is considered all systematic with no random component.

Table 2.49. Effect of Uncertainty in Overcoat Impurity.

Case	Deviation	Δk	±	$\sigma_{\Delta k}$	Scaling Factor	Δk_{eff} (1σ)	±	$\sigma_{\Delta keff}$
1	0 ppm	0.00046	±	0.00017	√3	0.00027	±	0.00010
	5 ppm	-0.00069	±	0.00017	√3	-0.00040	±	0.00010
2	0 ppm	0.00052	±	0.00017	√3	0.00030	±	0.00010
	5 ppm	-0.00103	±	0.00017	√3	-0.00059	±	0.00010
3	0 ppm	0.00077	±	0.00016	√3	0.00044	±	0.00009
	5 ppm	-0.00122	±	0.00017	√3	-0.00070	±	0.00010
4	0 ppm	0.00044	±	0.00017	√3	0.00025	±	0.00010
	5 ppm	-0.00132	±	0.00017	√3	-0.00076	±	0.00010
5	0 ppm	0.00055	±	0.00016	√3	0.00032	±	0.00009
	5 ppm	-0.00119	±	0.00016	√3	-0.00069	±	0.00009

2.1.3.2 Prismatic Fuel Compact

Density

The compact matrix density was varied ±0.15 g/cm^3 from the nominal value of 1.70 g/cm^3 (Table 1.14 of HTTR-GCR-RESR-001) to determine the effective uncertainty in k_{eff}. This value is three times the bounding limit. Results are shown in Table 2.50.

[a] W. Ji, J. L. Conlin, W. R. Martin, J. C. Lee, and F. B. Brown, "Explicit Modeling of Particle Fuel for the Very-High Temperature Gas-Cooled Reactor," *Trans. Am. Nucl. Soc.*, **92** (June 2005).

The total number of fuel compacts used in the fully-loaded core is 66,780. For determining the random component of the uncertainty, the results in Table 2.50 would be divided by √N, where N for each case is shown in Table 2.50.

Table 2.50. Effect of Uncertainty in Compact Matrix Density.

Case	Deviation	Δk	±	$\sigma_{\Delta k}$	Scaling Factor	Δk_{eff} (1σ)	±	$\sigma_{\Delta keff}$	N
1	-0.15 g/cm^3	-0.00009	±	0.00016	3√3	-0.00002	±	0.00003	41,370
	+0.15 g/cm^3	-0.00012	±	0.00017	3√3	-0.00002	±	0.00003	
2	-0.15 g/cm^3	0.00016	±	0.00017	3√3	0.00003	±	0.00003	45,990
	+0.15 g/cm^3	0.00016	±	0.00016	3√3	0.00003	±	0.00003	
3	-0.15 g/cm^3	-0.00023	±	0.00016	3√3	-0.00004	±	0.00003	52,920
	+0.15 g/cm^3	0.00000	±	0.00016	3√3	0.00000	±	0.00003	
4	-0.15 g/cm^3	-0.00028	±	0.00017	3√3	0.00005	±	0.00003	52,920
	+0.15 g/cm^3	0.00022	±	0.00017	3√3	0.00004	±	0.00003	
5	-0.15 g/cm^3	-0.00011	±	0.00016	3√3	-0.00002	±	0.00003	59,850
	+0.15 g/cm^3	0.00028	±	0.00016	3√3	0.00005	±	0.00003	

Impurity

The compact matrix impurity was varied from 0-5 ppm by weight of equivalent natural-boron content (Table 1.14 of HTTR-GCR-RESR-001) to determine the bounding uncertainty in k_{eff}. The nominal impurity is 0.82 ppm of natural boron by weight (Table 1.27 of HTTR-GCR-RESR-001). Results are shown in Table 2.51.

The uncertainty in the fuel compact impurity is considered all systematic with no random component.

Table 2.51. Effect of Uncertainty in Compact Matrix Impurity.

Case	Deviation	Δk	±	$\sigma_{\Delta k}$	Scaling Factor	Δk_{eff} (1σ)	±	$\sigma_{\Delta keff}$
1	0 ppm	0.00007	±	0.00016	√3	0.00004	±	0.00009
	5 ppm	-0.00074	±	0.00017	√3	-0.00043	±	0.00010
2	0 ppm	0.00023	±	0.00016	√3	0.00013	±	0.00009
	5 ppm	-0.00072	±	0.00016	√3	-0.00042	±	0.00009
3	0 ppm	0.00008	±	0.00017	√3	0.00005	±	0.00010
	5 ppm	-0.00115	±	0.00016	√3	-0.00066	±	0.00009
4	0 ppm	0.00014	±	0.00017	√3	0.00008	±	0.00010
	5 ppm	-0.00104	±	0.00017	√3	-0.00060	±	0.00010
5	0 ppm	0.00003	±	0.00016	√3	0.000002	±	0.00009
	5 ppm	-0.00113	±	0.00016	√3	-0.00065	±	0.00009

Free Uranium Content

The free uranium fraction in the fuel compacts has a maximum bounding limit of 0.000150 (see Table 1.14 of HTTR-GCR-RESR-001). The bounding limit was multiplied by 10 in order to assess the uncertainty in k_{eff}, but the effects were still negligible. The free uranium was assumed to be 100 % ^{235}U so as to assess the maximum uncertainty. The free uranium content in the graphite compact was not included in the benchmark model and a bias was not applied because the effect was negligible. Results are shown in Table 2.52.

The uncertainty in the free uranium content is considered all systematic with no random component.

Table 2.52. Effect of Uncertainty in Compact Free Uranium Content.

Case	Deviation	Δk	$\pm$	$\sigma_{\Delta k}$	Scaling Factor	Δk_{eff} (1σ)	$\pm$	$\sigma_{\Delta keff}$
1	1500 ppm	-0.00003	±	0.00016	20√3	0.00000	±	0.00000
2	1500 ppm	-0.00024	±	0.00016	20√3	-0.00001	±	0.00000
3	1500 ppm	-0.00012	±	0.00017	20√3	0.00000	±	0.00000
4	1500 ppm	0.00009	±	0.00017	20√3	0.00000	±	0.00000
5	1500 ppm	0.00020	±	0.00016	20√3	0.00001	±	0.00000

2.1.3.3 Graphite Sleeves

Density

The graphite sleeve density was varied an assumed ±0.03 g/cm^3 from the nominal value of 1.770 g/cm^3 (Table 1.27 of HTTR-GCR-RESR-001) to determine the effective uncertainty in k_{eff}. This value is the bounding limit. The graphite sleeves are composed of IG-110 graphite, and the assumed uncertainty of 0.03 g/cm^3 encompasses the range of reported densities for IG-110 graphite throughout Section 1. Results are shown in Table 2.53.

The total number of graphite sleeves used in the fully-loaded core is 4,770. For determining the random component of the uncertainty, the results in Table 2.53 would be divided by √N, where N for each case is shown in Table 2.53.

Table 2.53. Effect of Uncertainty in Graphite Sleeve Density.

Case	Deviation	Δk	±	$\sigma_{\Delta k}$	Scaling Factor	Δk_{eff} (1σ)	±	$\sigma_{\Delta keff}$	N
1	-0.03 g/cm^3	-0.00036	±	0.00017	√3	-0.00021	±	0.00010	2,955
	+0.03 g/cm^3	0.00030	±	0.00017	√3	0.00017	±	0.00010	
2	-0.03 g/cm^3	-0.00024	±	0.00016	√3	-0.00014	±	0.00009	3,285
	+0.03 g/cm^3	0.00022	±	0.00017	√3	0.00013	±	0.00010	
3	-0.03 g/cm^3	-0.00052	±	0.00016	√3	-0.00030	±	0.00009	3,780
	+0.03 g/cm^3	0.00026	±	0.00017	√3	0.00015	±	0.00010	
4	-0.03 g/cm^3	-0.00086	±	0.00017	√3	-0.00050	±	0.00010	3,780
	+0.03 g/cm^3	0.00042	±	0.00017	√3	0.00024	±	0.00010	
5	-0.03 g/cm^3	-0.00038	±	0.00016	√3	-0.00022	±	0.00009	4,275
	+0.03 g/cm^3	0.00030	±	0.00016	√3	0.00017	±	0.00009	

Impurity

The graphite sleeve impurity was varied from 0-1 ppm by weight of equivalent natural-boron content (Table 1.13 of HTTR-GCR-RESR-001) to determine the bounding uncertainty in k_{eff}. The nominal impurity is 0.37 ppm of natural boron by weight (Table 1.27 of HTTR-GCR-RESR-001). Results are shown in Table 2.54.

The uncertainty in the graphite sleeve impurity is considered all systematic with no random component.

Table 2.54. Effect of Uncertainty in Graphite Sleeve Impurity.

Case	Deviation	Δk	±	$\sigma_{\Delta k}$	Scaling Factor	Δk_{eff} (1σ)	±	$\sigma_{\Delta keff}$
1	0 ppm	0.00007	±	0.00017	√3	0.00004	±	0.00010
	1 ppm	-0.00055	±	0.00017	√3	-0.00032	±	0.00010
2	0 ppm	0.00032	±	0.00016	√3	0.00018	±	0.00009
	1 ppm	-0.00037	±	0.00017	√3	-0.00021	±	0.00010
3	0 ppm	0.00011	±	0.00017	√3	0.00006	±	0.00010
	1 ppm	-0.00084	±	0.00017	√3	-0.00048	±	0.00010
4	0 ppm	0.00012	±	0.00016	√3	0.00007	±	0.00009
	1 ppm	-0.00058	±	0.00017	√3	-0.00033	±	0.00010
5	0 ppm	0.00054	±	0.00016	√3	0.00031	±	0.00009
	1 ppm	-0.00053	±	0.00016	√3	-0.00031	±	0.00009

2.1.3.4 Burnable Poisons

Absorber Density

The absorber density was varied ±0.03 g/cm^3 from the average value of 1.8 g/cm^3 to determine the effective uncertainty in k_{eff}. This value is the bounding limit. The density uncertainty is based upon uncertainty typically found in sintered B_4C/C pellets (Table 1.29 of HTTR-GCR-RESR-001). Results are shown in Table 2.55.

The total number of burnable poison pellets used in the fully-loaded core is 5,520. For determining the random component of the uncertainty, the results in Table 2.55 would be divided by √N, where N for each case is shown in Table 2.55.

Table 2.55. Effect of Uncertainty in BP Absorber Density.

Case	Deviation	Δk	±	$\sigma_{\Delta k}$	Scaling Factor	Δk_{eff} (1σ)	±	$\sigma_{\Delta keff}$	N
1	-0.03 g/cm^3	0.00085	±	0.00016	√3	0.00049	±	0.00009	3,496
	+0.03 g/cm^3	-0.00083	±	0.00017	√3	-0.00048	±	0.00010	
2	-0.03 g/cm^3	0.00101	±	0.00017	√3	0.00058	±	0.00010	3,864
	+0.03 g/cm^3	-0.00048	±	0.00017	√3	-0.00028	±	0.00010	
3	-0.03 g/cm^3	0.00066	±	0.00017	√3	0.00038	±	0.00010	4,416
	+0.03 g/cm^3	-0.00081	±	0.00017	√3	-0.00047	±	0.00010	
4	-0.03 g/cm^3	0.00064	±	0.00017	√3	0.00037	±	0.00010	4,416
	+0.03 g/cm^3	-0.00084	±	0.00016	√3	-0.00048	±	0.00009	
5	-0.03 g/cm^3	0.00065	±	0.00016	√3	0.00038	±	0.00009	4,968
	+0.03 g/cm^3	-0.00077	±	0.00016	√3	-0.00044	±	0.00009	

Absorber Content

The uncertainty in the absorber content was not provided and the variation provided in Table 1.29 of HTTR-GCR-RESR-001 appears too excessive for the quantities utilized in the BP pellets. A variation of approximately ±0.25 % by weight was assumed for each of the two absorber pellet types, and the effective uncertainty in k_{eff} was determined. This value is treated as a bounding limit. The uncertainty of ±0.25 % is based upon the assumption that burnable poison pellets with boron contents between 1.75 and 2.25 wt.% would have an average content of 2.00 wt.% and boron contents between 2.25 and 2.75 wt.% would have an average content of 2.50 wt.%. Further information would be necessary to reduce the range of the uncertainty. Results are shown in Tables 2.56 and 2.57.

The total number of burnable poison pellets with weight percents of 2.00 and 2.50 used in the fully-loaded core is 3,600 and 1,920, respectively. For determining the random component of the uncertainty, the results in Tables 2.56 and 2.57 would be divided by their respective √N value, where N for each case is shown in Tables 2.56 and 2.57.

Table 2.56. Effect of Uncertainty in BP Absorber Content (nominal 2.00 wt.%).

Case	Deviation	Δk	±	$\sigma_{\Delta k}$	Scaling Factor	Δk_{eff} (1σ)	±	$\sigma_{\Delta keff}$	N
1	-0.25 wt.%	0.00265	±	0.00016	√3	0.000153	±	0.00009	2,280
	+0.25 wt.%	-0.00234	±	0.00017	√3	-0.00135	±	0.00010	
2	-0.25 wt.%	0.00304	±	0.00017	√3	0.00176	±	0.00010	2,520
	+0.25 wt.%	-0.00234	±	0.00016	√3	-0.00135	±	0.00009	
3	-0.25 wt.%	0.00394	±	0.00017	√3	0.00227	±	0.00010	2,880
	+0.25 wt.%	-0.00342	±	0.00017	√3	-0.00197	±	0.00010	
4	-0.25 wt.%	0.00379	±	0.00016	√3	-0.00219	±	0.00009	2,880
	+0.25 wt.%	-0.00346	±	0.00017	√3	-0.00200	±	0.00010	
5	-0.25 wt.%	0.00518	±	0.00016	√3	0.00299	±	0.00009	3,240
	+0.25 wt.%	-0.00455	±	0.00016	√3	-0.00263	±	0.00009	

Table 2.57. Effect of Uncertainty in BP Absorber Content (nominal 2.50 wt.%).

Case	Deviation	Δk	±	$\sigma_{\Delta k}$	Scaling Factor	Δk_{eff} (1σ)	±	$\sigma_{\Delta keff}$	N
1	-0.25 wt.%	0.00250	±	0.00017	√3	0.00144	±	0.00010	1,216
	+0.25 wt.%	-0.00240	±	0.00017	√3	-0.00139	±	0.00010	
2	-0.25 wt.%	0.00284	±	0.00016	√3	0.00164	±	0.00009	1,344
	+0.25 wt.%	-0.00249	±	0.00017	√3	-0.00144	±	0.00010	
3	-0.25 wt.%	0.00249	±	0.00017	√3	0.00144	±	0.00010	1,536
	+0.25 wt.%	-0.00240	±	0.00016	√3	-0.00139	±	0.00009	
4	-0.25 wt.%	0.00284	±	0.00017	√3	0.00164	±	0.00010	1,536
	+0.25 wt.%	-0.00251	±	0.00016	√3	-0.00145	±	0.00009	
5	-0.25 wt.%	0.00200	±	0.00016	√3	0.00115	±	0.00009	1,728
	+0.25 wt.%	-0.00187	±	0.00016	√3	-0.00108	±	0.00009	

Absorber Impurity

No information was available regarding any impurities present in the sintered B_4C/C material for the BP pellets. However, the impurity limits provided in Table 1.29 of HTTR-GCR-RESR-001 can be applied to approximate a rough estimate of the impact of additional impurities. Sodium and manganese were added with a concentrations of 100 and 10 ppm (by weight), respectively. Concentrations of 1000 ppm (by weight) of aluminum, silicon, calcium, and titanium were also included. The effective uncertainty in k_{eff} was determined and is shown in Table 2.58. This value is treated as a bounding limit.

The uncertainty in the absorber impurity is considered all systematic with no random component.

Table 2.58. Effect of Uncertainty in Absorber Impurity.

Case	Deviation	Δk	±	$\sigma_{\Delta k}$	Scaling Factor	Δk_{eff} (1σ)	±	$\sigma_{\Delta keff}$
1	Added Impurities	0.00048	±	0.00016	2√3	0.00014	±	0.00005
2	Added Impurities	0.00081	±	0.00017	2√3	0.00023	±	0.00005
3	Added Impurities	0.00072	±	0.00016	2√3	0.00021	±	0.00005
4	Added Impurities	0.00064	±	0.00017	2√3	0.00018	±	0.00005
5	Added Impurities	0.00082	±	0.00016	2√3	0.00024	±	0.00004

Absorber Isotopic Abundance

According to the 16th edition of the Chart of the Nuclides, the natural isotopic abundance of ^{10}B has been measured between 19.1 and 20.3 at.% with a nominal value of 19.9 at.%.[a] The abundance of ^{10}B in the BPs was therefore evaluated at the minimum and maximum bounding values to determine the effective uncertainty in k_{eff}. Table 1.28 of HTTR-GCR-RESR-001 states that the abundance of ^{10}B is 18.7 wt.%, which correlates to approximately 20.2 at.%. The benchmark model was evaluated at 19.9 at.%. Results are shown in Table 2.58.

The uncertainty in the absorber isotopic abundance is considered all systematic with no random component.

Table 2.58. Effect of Uncertainty in BP Isotopic Abundance of ^{10}B.

Case	Deviation	Δk	±	$\sigma_{\Delta k}$	Scaling Factor	Δk_{eff} (1σ)	±	$\sigma_{\Delta keff}$
1	19.1%	0.00178	±	0.00016	√3	0.00014	±	0.00005
	20.3%	-0.00101	±	0.00016	√3	-0.00058	±	0.00009
2	19.1%	0.00227	±	0.00017	√3	0.00131	±	0.00010
	20.3%	-0.00073	±	0.00017	√3	-0.00042	±	0.00010
3	19.1%	0.00219	±	0.00017	√3	0.00126	±	0.00010
	20.3%	-0.00107	±	0.00016	√3	-0.00062	±	0.00009
4	19.1%	0.00220	±	0.00016	√3	0.00127	±	0.00009
	20.3%	-0.00139	±	0.00017	√3	-0.00080	±	0.00010
5	19.1%	0.00236	±	0.00016	√3	0.00136	±	0.00009
	20.3%	-0.00133	±	0.00016	√3	-0.00077	±	0.00009

Graphite Disk Density

An uncertainty in the density of the graphite disks was not reported. A variation of ±0.09 g/cm^3 was assumed and the effects on the uncertainty of k_{eff} were determined. This value is three times the bounding limit. The graphite disks are composed of IG-110 graphite, and the assumed uncertainty of

[a] Nuclides and Isotopes: Chart of the Nuclides, 16th edition, (2002).

0.03 g/cm^3 encompasses the range of reported densities for IG-110 graphite throughout Section 1 of HTTR-GCR-RESR-001. Results are shown in Table 2.59.

The total number of graphite disk stacks used in the fully-loaded core is 300. For determining the random component of the uncertainty, the results in Table 2.59 would be divided by $\sqrt{N}$, where N for each case is shown in Table 2.59.

Table 2.59. Effect of Uncertainty in Graphite Disk Density.

Case	Deviation	Δk	±	$\sigma_{\Delta k}$	Scaling Factor	Δk_{eff} (1σ)	±	$\sigma_{\Delta keff}$	N
1	-0.09 g/cm^3	0.00015	±	0.00017	3$\sqrt{3}$	0.00003	±	0.00003	190
	+0.09 g/cm^3	0.00003	±	0.00016	3$\sqrt{3}$	0.00001	±	0.00003	
2	-0.09 g/cm^3	0.00008	±	0.00017	3$\sqrt{3}$	0.000004	±	0.00003	210
	+0.09 g/cm^3	0.00022	±	0.00017	3$\sqrt{3}$	0.00004	±	0.00003	
3	-0.09 g/cm^3	-0.00017	±	0.00017	3$\sqrt{3}$	-0.00003	±	0.00003	240
	+0.09 g/cm^3	-0.00005	±	0.00017	3$\sqrt{3}$	-0.00001	±	0.00003	
4	-0.09 g/cm^3	-0.00027	±	0.00017	3$\sqrt{3}$	-0.00005	±	0.00003	240
	+0.09 g/cm^3	-0.00006	±	0.00017	3$\sqrt{3}$	-0.00001	±	0.00003	
5	-0.09 g/cm^3	0.00001	±	0.00016	3$\sqrt{3}$	0.00000	±	0.00003	270
	+0.09 g/cm^3	0.00001	±	0.00016	3$\sqrt{3}$	0.00000	±	0.00003	

Graphite Disk Impurity

The assumed graphite disk impurity was varied from 0-5 ppm by weight of equivalent natural-boron content to determine the bounding uncertainty in k_{eff}. The nominal impurity is 0.37 ppm of natural boron by weight (Table 1.28 of HTTR-GCR-RESR-001). Results are shown in Table 2.60.

The uncertainty in the graphite disk impurity is considered all systematic with no random component.

Table 2.60. Effect of Uncertainty in Graphite Disk Impurity.

Case	Deviation	Δk	±	$\sigma_{\Delta k}$	Scaling Factor	Δk_{eff} (1σ)	±	$\sigma_{\Delta keff}$
1	0 ppm	-0.00018	±	0.00017	√3	-0.00010	±	0.00010
	5 ppm	-0.00006	±	0.00017	√3	-0.00003	±	0.00010
2	0 ppm	0.00004	±	0.00016	√3	0.00002	±	0.00009
	5 ppm	0.00016	±	0.00017	√3	0.00009	±	0.00010
3	0 ppm	-0.00016	±	0.00017	√3	-0.00009	±	0.00010
	5 ppm	-0.00017	±	0.00016	√3	-0.00010	±	0.00009
4	0 ppm	-0.00017	±	0.00017	√3	-0.00010	±	0.00010
	5 ppm	-0.00007	±	0.00017	√3	-0.00004	±	0.00010
5	0 ppm	-0.00001	±	0.00016	√3	-0.00001	±	0.00009
	5 ppm	-0.00011	±	0.00016	√3	-0.00006	±	0.00009

2.1.3.5 Control Rods

Absorber Density

The absorber density was varied ±0.09 g/cm^3 from the nominal value of 1.9 g/cm^3 (Table 1.15 of HTTR-GCR-RESR-001) to determine the effective uncertainty in k_{eff}. This value is three times the bounding limit. The uncertainty is taken from Table 1.29 of HTTR-GCR-RESR-001. Results are shown in Table 2.46.

The total number of control rod absorber pellets used in the fully-loaded core is approximately 975, as approximately 30% of the control rods are actually inserted into the core. For determining the random component of the uncertainty, the results in Table 2.61 would be divided by √N, where N for each case is shown in Table 2.61.

Table 2.61. Effect of Uncertainty in CR Absorber Density.

Case	Deviation	Δk	±	$\sigma_{\Delta k}$	Scaling Factor	Δk_{eff} (1σ)	±	$\sigma_{\Delta keff}$	N
1	-0.09 g/cm^3	0.00004	±	0.00017	3√3	0.00001	±	0.00003	225
	+0.09 g/cm^3	-0.00023	±	0.00016	3√3	0.00003	±	0.00003	
2	-0.09 g/cm^3	0.00013	±	0.00016	3√3	0.00003	±	0.00003	585
	+0.09 g/cm^3	0.00007	±	0.00016	3√3	0.00001	±	0.00003	
3	-0.09 g/cm^3	0.00020	±	0.00016	3√3	0.00004	±	0.00003	780
	+0.09 g/cm^3	-0.00009	±	0.00016	3√3	-0.00002	±	0.00003	
4	-0.09 g/cm^3	-0.00002	±	0.00016	3√3	0.00000	±	0.00003	720
	+0.09 g/cm^3	-0.00025	±	0.00016	3√3	-0.00005	±	0.00003	
5	-0.09 g/cm^3	-0.00013	±	0.00016	3√3	-0.00003	±	0.00003	910
	+0.09 g/cm^3	-0.00024	±	0.00016	3√3	-0.00005	±	0.00003	

Absorber Content

The boron content was varied ±9 wt.% from the nominal value of 30 wt.% (Table 1.15 of HTTR-GCR-RESR-001) and the effect on the uncertainty in k_{eff} was determined. This value is three times the bounding limit. The uncertainty is taken from Table 1.29 of HTTR-GCR-RESR-001. Results are shown in Table 2.62.

The total number of control rod absorber pellets used in the fully-loaded core is approximately 975, as approximately 30% of the control rods are actually inserted into the core. For determining the random component of the uncertainty, the results in Table 2.62 would be divided by √N, where N for each case is shown in Table 2.62.

Table 2.62. Effect of Uncertainty in CR Absorber Content.

Case	Deviation	Δk	±	$\sigma_{\Delta k}$	Scaling Factor	Δk_{eff} (1σ)	±	$\sigma_{\Delta keff}$	N
1	-9 wt.%	0.00002	±	0.00017	3√3	0.00000	±	0.00003	225
	+9 wt.%	-0.00016	±	0.00017	3√3	-0.00003	±	0.00003	
2	-9 wt.%	0.00055	±	0.00017	3√3	0.00011	±	0.00003	585
	+9 wt.%	-0.00030	±	0.00016	3√3	-0.00006	±	0.00003	
3	-9 wt.%	0.00045	±	0.00017	3√3	0.00009	±	0.00003	780
	+9 wt.%	-0.00045	±	0.00017	3√3	-0.00009	±	0.00003	
4	-9 wt.%	0.00064	±	0.00017	3√3	0.00012	±	0.00003	720
	+9 wt.%	-0.00066	±	0.00017	3√3	-0.00013	±	0.00003	
5	-9 wt.%	0.00045	±	0.00016	3√3	0.00009	±	0.00003	910
	+9 wt.%	-0.00053	±	0.00016	3√3	-0.00010	±	0.00003	

Absorber Impurity

No information was available regarding any impurities present in the sintered B_4C/C material for the control rod absorbers. However, the impurity limits provided in Table 1.29 of HTTR-GCR-RESR-001 can be applied to approximate a rough estimate of the impact of additional impurities. Sodium and manganese were added with a concentrations of 100 and 10 ppm (by weight), respectively. Concentrations of 1000 ppm (by weight) of aluminum, silicon, calcium, and titanium were also included. The effective uncertainty in k_{eff} was determined and is shown in Table 2.63. This value is treated as a bounding limit.

The uncertainty in the absorber impurity is considered all systematic with no random component.

Table 2.63. Effect of Uncertainty in Absorber Impurity.

Case	Deviation	Δk	±	$\sigma_{\Delta k}$	Scaling Factor	Δk_{eff} (1σ)	±	$\sigma_{\Delta keff}$
1	Added Impurities	-0.00007	±	0.00016	2√3	-0.00002	±	0.00005
2	Added Impurities	-0.00017	±	0.00016	2√3	-0.00005	±	0.00005
3	Added Impurities	-0.00009	±	0.00017	2√3	-0.00003	±	0.00005
4	Added Impurities	-0.00005	±	0.00017	2√3	-0.00013	±	0.00003
5	Added Impurities	-0.00005	±	0.00016	2√3	-0.00001	±	0.00004

Absorber Isotopic Abundance

According to the 16th edition of the Chart of the Nuclides, the natural isotopic abundance of ^{10}B has been measured between 19.1 and 20.3% with a nominal value of 19.9%.[a] The abundance of ^{10}B in the control rods was therefore evaluated at the minimum and maximum bounding values to determine the effective uncertainty in k_{eff}. Table 1.28 of HTTR-GCR-RESR-001 states that the abundance of ^{10}B is 18.7 wt.%, which correlates to approximately 20.2 at.%. The model was not evaluated for a ^{10}B abundance of 18.7 wt.%. The benchmark model was evaluated at 19.9 at.%. Results are shown in Table 2.64.

The uncertainty in the absorber isotopic abundance is considered all systematic with no random component.

Table 2.64. Effect of Uncertainty in CR Isotopic Abundance of ^{10}B.

Case	Deviation	Δk	±	$\sigma_{\Delta k}$	Scaling Factor	Δk_{eff} (1σ)	±	$\sigma_{\Delta keff}$
1	19.1%	0.00008	±	0.00017	√3	0.00005	±	0.00010
	20.3%	0.00013	±	0.00017	√3	0.00008	±	0.00010
2	19.1%	0.00009	±	0.00017	√3	0.00005	±	0.00010
	20.3%	0.00000	±	0.00017	√3	0.00000	±	0.00010
3	19.1%	0.00022	±	0.00016	√3	0.00013	±	0.00009
	20.3%	-0.00009	±	0.00016	√3	-0.00005	±	0.00009
4	19.1%	-0.00013	±	0.00017	√3	-0.00008	±	0.00010
	20.3%	-0.00018	±	0.00016	√3	-0.00010	±	0.00009
5	19.1%	-0.00011	±	0.00016	√3	-0.00006	±	0.00009
	20.3%	0.00036	±	0.00016	√3	0.00021	±	0.00009

[a] Nuclides and Isotopes: Chart of the Nuclides, 16th edition, (2002).

Clad Density

Two references were compared to confirm the composition and density of the Alloy 800H material.[ab] The density of Alloy 800H is taken to be 8.03 g/cm^3 with an estimated uncertainty of ±0.03 g/cm^3, which is the difference between the reported density values in the two references. This value is the bounding limit. The effective change in k_{eff} was determined. Results are shown in Table 2.65.

The total number of control rod sections used in the fully-loaded core is approximately 97.5, as approximately 30% of the control rods are actually inserted into the core. For determining the random component of the uncertainty, the results in Table 2.65 would be divided by √N, where N for each case is shown in Table 2.65.

Table 2.65. Effect of Uncertainty in Clad Density.

Case	Deviation	Δk	±	$\sigma_{\Delta k}$	Scaling Factor	Δk_{eff} (1σ)	±	$\sigma_{\Delta keff}$	N
1	-0.03 g/cm^3 (1σ)	0.00028	±	0.00017	√3	0.00016	±	0.00010	22.5
	+0.03 g/cm^3 (1σ)	-0.00012	±	0.00016	√3	-0.00007	±	0.00009	
2	-0.03 g/cm^3 (1σ)	0.00012	±	0.00017	√3	0.00007	±	0.00010	58.5
	+0.03 g/cm^3 (1σ)	0.00001	±	0.00017	√3	0.00001	±	0.00010	
3	-0.03 g/cm^3 (1σ)	0.00006	±	0.00016	√3	0.00003	±	0.00009	78.0
	+0.03 g/cm^3 (1σ)	-0.00023	±	0.00016	√3	-0.00013	±	0.00009	
4	-0.03 g/cm^3 (1σ)	-0.00032	±	0.00017	√3	-0.00018	±	0.00010	72.0
	+0.03 g/cm^3 (1σ)	-0.00005	±	0.00017	√3	-0.00003	±	0.00010	
5	-0.03 g/cm^3 (1σ)	0.00004	±	0.00016	√3	0.00002	±	0.00009	91.0
	+0.03 g/cm^3 (1σ)	0.00007	±	0.00016	√3	0.00004	±	0.00009	

Clad Composition

The clad composition used in the benchmark model is derived from the aforementioned references for Alloy 800H, where the second reference provides a composition range and the first reference provides a nominal composition. A summary of the composition of Alloy 800H is provided in Table 2.66. The nominal distribution is used in the benchmark model. The composition of the clad material was varied from the nominal value. In the first case, the minimum compositions of all elements were used with iron as the remaining balance. The second case uses the maximum weights of all the elements with a reduction in the iron content until the minimum value is achieved; then nickel is reduced to achieve a total of 100 wt.%. The effective change in k_{eff} for these two cases was determined. Results are shown in Table 2.67.

The uncertainty in the clad composition is considered all systematic with no random component.

[a] Specification Sheet: Alloy 800, 800H, and 800AT, Sandmeyer Steel Company (April 2004).

[b] Material Characteristics: Alloy 800H, PhilipCornes, http://www.cornes.com.sg/a800h.htm (Accessed August 5, 2008).

Table 2.66. Composition of Alloy 800H.

Element	Minimum wt.%	Maximum wt.%	Nominal wt.%
C	0.06	0.1	0.08
Al	0.15	0.6	0.375
Si	--	1.0	0.35
P	--	--	0.02
S	--	0.015	0.01
Ti	0.15	0.6	0.375
Cr	19	23	21
Mn	--	1.5	1
Fe	39.5	--	43.99
Ni	30	35	32.5
Cu	--	0.75	0.3
Total	--	--	100.000

Table 2.67. Effect of Uncertainty in Clad Composition.

Case	Deviation	Δk	$\pm$	$\sigma_{\Delta k}$	Scaling Factor	Δk_{eff} (1σ)	$\pm$	$\sigma_{\Delta keff}$
1	Minimum Fe	-0.00010	±	0.00016	√3	-0.00006	±	0.00009
	Maximum Fe	-0.00004	±	0.00016	√3	-0.00002	±	0.00009
2	Minimum Fe	0.00014	±	0.00017	√3	0.00009	±	0.00010
	Maximum Fe	0.00016	±	0.00017	√3	0.00009	±	0.00010
3	Minimum Fe	-0.00009	±	0.00017	√3	-0.00005	±	0.00010
	Maximum Fe	-0.00020	±	0.00016	√3	-0.00012	±	0.00009
4	Minimum Fe	-0.00014	±	0.00017	√3	-0.00008	±	0.00010
	Maximum Fe	-0.00012	±	0.00017	√3	-0.00007	±	0.00010
5	Minimum Fe	-0.00012	±	0.00016	√3	-0.00007	±	0.00009
	Maximum Fe	-0.00007	±	0.00016	√3	-0.00004	±	0.00009

Clad Impurity

No information was available regarding any impurities present in the Alloy 800H metal. Concentrations of minor and trace elements found commonly in nickel alloy[a] were added to the clad material in the benchmark model (a neutron cross-section library was unavailable for Ytterbium) to determine the effective uncertainty in k_{eff}. Because these impurities are not necessarily those that would have been in the alloy, and the total amount is ~10 wt.%, the atom density of the primary alloy composition was not

[a] J. H. Zaidi, S. Waheed, and S. Ahmed, "Determination of Trace Impurities in Nickel-Based Alloy using Neutron Activation Analysis," *J. Radioanal. Nucl. Ch.*, **242**: 259-263 (1999).

reduced. Thus the total atom density of the material was increased by including the additional materials. A list of the additional impurities is shown in Table 2.68, and results are shown in Table 2.69. This value is treated as a bounding limit.

The uncertainty in the clad impurity is considered all systematic with no random component.

Table 2.68. Concentration (by weight) of Minor and Trace Elements in Nickel Alloy.

Element	Concentration	Element	Concentration
As	63.7 µg/g	Mo	9.8 µg/g
Ba	215 µg/g	Na	0.45 %
Br	8.9 µg/g	Nd	16.2 µg/g
Ca	5.9 %	Rb	24 ng/g
Ce	0.33 %	Sb	2.2 µg/g
Co	9.96 µg/g	Sc	0.13 µg/g
Cs	4.34 µg/g	Se	0.16 µg/g
Dy	6.12 µg/g	Sm	0.23 µg/g
Er	2.8 µg/g	Sn	0.25 µg/g
Eu	1.17 µg/g	Sr	371 µg/g
Ga	107.5 µg/g	Ta	1.21 µg/g
Gd	1.7 µg/g	Tb	1.24 µg/g
Hf	19.5 µg/g	Th	18.3 µg/g
Hg	6 ng/g	U	4.3 µg/g
In	245 ng/g	Yb[(a)]	2.48 µg/g
La	2.34 µg/g	V	0.75 %
Lu	1.16 µg/g	Zn	93.4 µg/g
Mg	2.14 %		

(a) A neutron cross-section library was unavailable to include this element in the analysis.

Table 2.69. Effect of Uncertainty in Clad Impurity.

Case	Deviation	Δk	±	$\sigma_{\Delta k}$	Scaling Factor	Δk_{eff} (1σ)	±	$\sigma_{\Delta keff}$
1	Added Impurities	0.00015	±	0.00016	2√3	0.00004	±	0.00005
2	Added Impurities	-0.00005	±	0.00016	2√3	-0.00001	±	0.00005
3	Added Impurities	0.00015	±	0.00016	2√3	0.00004	±	0.00005
4	Added Impurities	-0.00001	±	0.00016	2√3	0.00000	±	0.00005
5	Added Impurities	-0.00002	±	0.00016	2√3	-0.00001	±	0.00004

2.1.3.6 Instrumentation

Insufficient information is available to model and comprehensively evaluate the uncertainties and biases related to the utility of instrumentation in the HTTR. A basic analysis of the general description of the instrumentation was performed, as discussed in Section 2.1.2.6.

2.1.3.7 Graphite Blocks

Density

The IG-110 graphite density was varied ±0.04 g/cm^3 from a nominal value selected as 1.76 g/cm^3 (ranging from 1.75 to 1.78 g/cm^3, Tables 1.13, 1.19, and 1.27 of HTTR-GCR-RESR-001) to determine the effective uncertainty in k_{eff}. A variation of 0.03 g/cm^3 accounts for the difference in density between the various samples of IG-110 blocks, and a variation of 0.01 g/cm^3 is assumed to encompass the variability in the volume fraction caused by eliminating various features such as the dowels, sockets, fuel handling position, and ridged features on the fuel rods. The assumed uncertainty of 0.03 g/cm^3 for the IG-110 graphite encompasses the range of reported densities found throughout Section 1 of HTTR-GCR-RESR-001. Results are shown in Table 2.70. This value is treated as a bounding limit.

Previous results[a] state that a graphite weight difference of less than 1% should result in a bias of -0.3 % Δk/k. Scaling the results provided in Table 2.70 provides an uncertainty comparable to the previously published information.

The total number of IG-110 graphite blocks used in the fully-loaded core is 549. For determining the random component of the uncertainty, the results in Table 2.70 would be divided by √N, where N for each case is shown in Table 2.70.

Table 2.70. Effect of Uncertainty in IG-110 Density in Graphite Blocks.

Case	Deviation	Δk	±	$\sigma_{\Delta k}$	Scaling Factor	Δk_{eff} (1σ)	±	$\sigma_{\Delta keff}$	N
1	-0.04 g/cm^3	-0.00418	±	0.00016	√3	-0.00241	±	0.00009	494
	+0.04 g/cm^3	0.00422	±	0.00017	√3	0.00244	±	0.00010	
2	-0.04 g/cm^3	-0.00424	±	0.00016	√3	-0.00245	±	0.00009	504
	+0.04 g/cm^3	0.00455	±	0.00016	√3	0.00263	±	0.00009	
3	-0.04 g/cm^3	-0.00507	±	0.00016	√3	-0.00293	±	0.00009	519
	+0.04 g/cm^3	0.00439	±	0.00016	√3	0.00253	±	0.00009	
4	-0.04 g/cm^3	-0.00575	±	0.00017	√3	-0.00332	±	0.00010	519
	+0.04 g/cm^3	0.00553	±	0.00016	√3	0.00319	±	0.00009	
5	-0.04 g/cm^3	-0.00513	±	0.00016	√3	-0.00296	±	0.00009	534
	+0.04 g/cm^3	0.00473	±	0.00016	√3	0.00273	±	0.00009	

[a] Fujimoto, N., Nakano, M., Takeuchi, M., Fujisaki, S., and Yamashita, K., "Start-Up Core Physics Tests of High Temperature Engineering Test Reactor (HTTR), (II): First Criticality by an Annular Form Fuel Loading and Its Criticality Prediction Method," *J. Atomic Energy Society Japan*, **42**(5), 458-464 (2000).

Impurity

The graphite block impurity was varied from 0-3 ppm by weight of equivalent natural-boron content (Table 1.13 of HTTR-GCR-RESR-001), where the 3 ppm value is 3 times the bounding limit, to determine the bounding uncertainty in k_{eff}. The nominal impurity is 0.40 ppm or 0.37 ppm of natural boron by weight for the fuel/control blocks and reflector blocks, respectively (Table 1.27 of HTTR-GCR-RESR-001). However, characterization of the graphite first loaded into the reactor determined the equivalent boron content for IG-110 graphite to be 0.59 ppm.[a] This latter value is used in the benchmark model. Results are shown in Table 2.71.

It has been reported that the estimated air content in the graphite blocks would provide -0.4 % Δk/k to the computational model.[b] Reference 1 states that an uncertainty factor of ~0.52 % Δk/k should be used. The inclusion of air in the benchmark model did not produce a noticeable change in reactivity; this was done by modeling air, at atmospheric pressure, distributed throughout the block in the quantity equivalent to the volume fraction to the void space generated for the dowels, sockets, fuel handling position, and other miscellaneous block features. However, it is unclear exactly how much air would be entrapped within the graphite blocks. Air can be entrapped during the graphitization process or absorbed onto the graphite surface. Typically, significant contribution to the equivalent boron content in a graphite block is caused by impurities in the graphite. Methods to measure the impurity content in graphite have improved over the past several years, and the impurity content of the HTTR graphite may need to be reassessed.[c]

Graphite is also somewhat hydroscopic and can absorb water into its pores after fabrication. At low temperatures, the water would still be present in the graphite. Information regarding possible water content in the graphite blocks is unavailable, however.

The uncertainty in the graphite block impurity is considered all systematic with no random component.

Table 2.71. Effect of Uncertainty in IG-110 Impurity in Graphite Blocks.

Case	Deviation	Δk	±	$\sigma_{\Delta k}$	Scaling Factor	Δk_{eff} (1σ)	±	$\sigma_{\Delta keff}$
1	0 ppm	0.00921	±	0.00016	√3	0.00532	±	0.00009
	3 ppm	-0.03424	±	0.00016	3√3	-0.00659	±	0.00003
2	0 ppm	0.00842	±	0.00016	√3	0.00486	±	0.00009
	3 ppm	-0.03204	±	0.00016	3√3	-0.00617	±	0.00003
3	0 ppm	0.00800	±	0.00016	√3	0.00462	±	0.00009
	3 ppm	-0.03122	±	0.00016	3√3	-0.00601	±	0.00003
4	0 ppm	0.00727	±	0.00016	√3	0.00420	±	0.00009
	3 ppm	-0.02822	±	0.00017	3√3	-0.00543	±	0.00003
5	0 ppm	0.00848	±	0.00016	√3	0.00490	±	0.00009
	3 ppm	-0.03036	±	0.00016	3√3	-0.00584	±	0.00003

[a] Sumita, J., Shibata, T., Hanawa, S., Ishihara, M., Iyoku, T., and Sawa, K., "Characteristics of First Loaded IG-110 Graphite in HTTR Core," *JAEA Technol 2006-048*, October (2006).

[b] Fujimoto, N., Nakano, M., Takeuchi, M., Fujisaki, S., and Yamashita, K., "Start-Up Core Physics Tests of High Temperature Engineering Test Reactor (HTTR), (II): First Criticality by an Annular Form Fuel Loading and Its Criticality Prediction Method," *J. Atomic Energy Society Japan*, **42**(5), 458-464 (2000).

[c] Private communication with Rob Bratton at Idaho National Laboratory (November 20, 2008).

2.1.3.8 Permanent Reflectors

Density

The PGX graphite density was varied ±0.04 g/cm^3 from a nominal value selected as 1.73 g/cm^3 (ranging from 1.73 to 1.74 g/cm^3, Tables 1.19, 1.20, and 1.27 of HTTR-GCR-RESR-001) to determine the effective uncertainty in k_{eff}. A variation of 0.03 g/cm^3 accounts for the PGX, and a variation of 0.01 g/cm^3 is assumed to encompass the variability in the volume fraction, which is not provided. The assumed uncertainty of 0.03 g/cm^3 for the PGX graphite encompasses the range of reported densities found throughout Section 1 of HTTR-GCR-RESR-001. Results are shown in Table 2.72. This value is treated as a bounding limit.

The total number of permanent reflector blocks used in all core configurations is 96. For determining the random component of the uncertainty, the results in Table 2.72 would be divided by √96.

Table 2.72. Effect of Uncertainty in PGX Density in Permanent Reflector.

Case	Deviation	Δk	±	$\sigma_{\Delta k}$	Scaling Factor	Δk_{eff} (1σ)	±	$\sigma_{\Delta keff}$
1	-0.04 g/cm^3	-0.00068	±	0.00017	√3	-0.00039	±	0.00010
	+0.04 g/cm^3	0.00080	±	0.00016	√3	0.00046	±	0.00009
2	-0.04 g/cm^3	-0.00070	±	0.00016	√3	-0.00040	±	0.00009
	+0.04 g/cm^3	0.00098	±	0.00016	√3	0.00057	±	0.00009
3	-0.04 g/cm^3	-0.00060	±	0.00016	√3	-0.00035	±	0.00009
	+0.04 g/cm^3	0.00031	±	0.00016	√3	0.00018	±	0.00009
4	-0.04 g/cm^3	-0.00047	±	0.00017	√3	-0.00027	±	0.00010
	+0.04 g/cm^3	0.00033	±	0.00017	√3	0.00019	±	0.00010
5	-0.04 g/cm^3	-0.00059	±	0.00016	√3	-0.00034	±	0.00009
	+0.04 g/cm^3	0.00040	±	0.00016	√3	0.00023	±	0.00009

Impurity

The permanent reflector impurity was varied from 0-5 ppm by weight of equivalent natural-boron content (Table 1.16 of HTTR-GCR-RESR-001) to determine the bounding uncertainty in k_{eff}. The nominal impurity is 1.91 ppm of natural boron by weight (Table 1.27 of HTTR-GCR-RESR-001). Results are shown in Table 2.73.

The uncertainty in the permanent reflector impurity is considered all systematic with no random component.

Table 2.73. Effect of Uncertainty in PGX Impurity in Permanent Reflector.

Case	Deviation	Δk	±	$\sigma_{\Delta k}$	Scaling Factor	Δk_{eff} (1σ)	±	$\sigma_{\Delta keff}$
1	0 ppm	0.00765	±	0.00017	√3	0.00442	±	0.00010
	5 ppm	-0.01014	±	0.00016	√3	-0.00585	±	0.00009
2	0 ppm	0.00656	±	0.00016	√3	0.00379	±	0.00009
	5 ppm	-0.00864	±	0.00017	√3	-0.00499	±	0.00010
3	0 ppm	0.00543	±	0.00016	√3	0.00314	±	0.00009
	5 ppm	-0.00752	±	0.00017	√3	-0.00434	±	0.00010
4	0 ppm	0.00296	±	0.00016	√3	0.00171	±	0.00009
	5 ppm	-0.00427	±	0.00017	√3	-0.00247	±	0.00010
5	0 ppm	0.00466	±	0.00016	√3	0.00269	±	0.00009
	5 ppm	-0.00598	±	0.00016	√3	-0.00345	±	0.00009

2.1.3.9 Dummy Blocks

Density

The IG-11 graphite density was varied ±0.04 g/cm^3 from a nominal value of 1.75 g/cm^3 (Table 1.20 of HTTR-GCR-RESR-001) to determine the effective uncertainty in k_{eff}. A variation of 0.03 g/cm^3 was selected as the density uncertainty because IG-11 graphite is essentially impure IG-110 graphite. An additional variation of 0.01 g/cm^3 is assumed to encompass the variability in the volume fraction caused by eliminating various features such as the dowels, sockets, and fuel handling position. Results are shown in Table 2.74. This value is treated as a bounding limit.

The total number of IG-11 graphite blocks used in the fully-loaded core is approximately zero; there are IG-11 graphite blocks in the annular core configurations. For determining the random component of the uncertainty, the results in Table 2.74 would be divided by √N, where N for each case is shown in Table 2.74.

Table 2.74. Effect of Uncertainty in IG-11 Density in Dummy Blocks.

Case	Deviation	Δk	±	$\sigma_{\Delta k}$	Scaling Factor	Δk_{eff} (1σ)	±	$\sigma_{\Delta keff}$	N
1	-0.04 g/cm^3	0.00008	±	0.00017	√3	0.00005	±	0.00010	55
	+0.04 g/cm^3	-0.00050	±	0.00017	√3	-0.00029	±	0.00010	
2	-0.04 g/cm^3	0.00054	±	0.00017	√3	0.00031	±	0.00010	45
	+0.04 g/cm^3	-0.00057	±	0.00016	√3	-0.00033	±	0.00009	
3	-0.04 g/cm^3	0.00008	±	0.00016	√3	0.00005	±	0.00009	30
	+0.04 g/cm^3	-0.00046	±	0.00017	√3	-0.00027	±	0.00010	
4	-0.04 g/cm^3	0.00016	±	0.00017	√3	0.00009	±	0.00010	30
	+0.04 g/cm^3	-0.00051	±	0.00017	√3	-0.00029	±	0.00010	
5	-0.04 g/cm^3	-0.00016	±	0.00016	√3	0.00009	±	0.00009	15
	+0.04 g/cm^3	-0.00011	±	0.00016	√3	-0.00006	±	0.00009	

Impurity

The graphite block impurity was varied from 0-5 ppm by weight of equivalent natural-boron content to determine the bounding uncertainty in k_{eff}. The nominal impurity is 3.1 ppm natural boron by weight (Ref 1, p. 314). The dummy blocks in the HTTR are created from the same graphite material, IG-11, as the reflector graphite in the HTR-10 reactor.[ab] The maximum impurity content was derived from the reflector graphite in the HTR-10 reactor (HTR10-GCR-RESR-001), which has a nominal boron concentration of 4.8366 ±0.09673 ppm (±2 %). Results are shown in Table 2.75.

The uncertainty in the graphite block impurity is considered all systematic with no random component.

[a] L. Xiaowei, R. Jean-Charles, and Y. Suyuan, "Effect of Temperature on Graphite Oxidation Behavior," *Nucl. Eng. Des.*, **227**: 273-280 (2004).

[b] X. Luo, J-C. Robin, and S. Yu, "Comparison of Oxidation Behaviors of Different Grades of Nuclear Graphite," *Nucl. Sci. Eng.*, **151**, 121-127 (2005).

Table 2.75. Effect of Uncertainty in IG-11 Impurity in Dummy Blocks.

Case	Deviation	Δk	$\pm$	$\sigma_{\Delta k}$	Scaling Factor	Δk_{eff} (1σ)	$\pm$	$\sigma_{\Delta keff}$
1	0 ppm	0.01219	±	0.00017	√3	0.00704	±	0.00010
	5 ppm	-0.00671	±	0.00017	√3	-0.00387	±	0.00010
2	0 ppm	0.01278	±	0.00016	√3	0.00738	±	0.00009
	5 ppm	-0.00674	±	0.00017	√3	-0.00389	±	0.00010
3	0 ppm	0.00797	±	0.00017	√3	0.00460	±	0.00010
	5 ppm	-0.00457	±	0.00017	√3	-0.00264	±	0.00010
4	0 ppm	0.01037	±	0.00017	√3	0.00599	±	0.00010
	5 ppm	-0.00580	±	0.00017	√3	-0.00335	±	0.00010
5	0 ppm	0.00376	±	0.00016	√3	0.00217	±	0.00009
	5 ppm	-0.00215	±	0.00016	√3	-0.00124	±	0.00009

Block Type

There are two types of dummy blocks, one with a hole pattern similar to that of a control block, and the other with three holes but of smaller diameter (Ref. 2, p. 14). Elsewhere the source of eight types of dummy blocks are specified (most likely having one of the two hole patterns).[a] Because the true dimensions of the smaller hole design is unknown, the dummy blocks will all be modeled with the holes of the control blocks but an additional uncertainty will be assessed to account for this discrepancy. This uncertainty will be determined by completely filling the holes of the dummy blocks with IG-11 graphite material as a bounding limit (i.e., maximizing the amount of graphite material mass) representing the minimum dimensions of three infinitely thin holes in the dummy blocks. The volume fraction of the simulated control channels in a dummy blocks is approximately 31.76 %, representing an increase in graphite mass of 36 kg per block when the holes are completely filled (based on a graphite density of 1.75 g/cm^3 with an 0.005 % reduction for void volume). Results are shown in Table 2.76.

There are no IG-11 graphite blocks used in the fully-loaded core; there are IG-11 graphite blocks in the annular core configurations. For determining the random component of the uncertainty, the results in Table 2.76 would be divided by √N, where N for each case is shown in Table 2.76.

[a] N. Fujimoto, N. Nojiri, and K. Yamashita, "HTTR's Benchmark Calculation of Start-Up Core Physics Tests," Report of the 3rd Research Coordination Meeting on the CRP, IAEA, Oarai, Japan, March 12-16 (2001).

Table 2.76. Effect of Uncertainty in Dummy Blocks Type.

Case	Deviation	Δk	±	$\sigma_{\Delta k}$	Scaling Factor	Δk_{eff} (1σ)	±	$\sigma_{\Delta keff}$	N
1	Filled Holes	-0.00058	±	0.00017	2√3	-0.00017	±	0.00005	55
2	Filled Holes	-0.00507	±	0.00017	2√3	-0.00146	±	0.00005	45
3	Filled Holes	-0.00200	±	0.00017	2√3	-0.00058	±	0.00005	30
4	Filled Holes	-0.00893	±	0.00017	2√3	-0.00258	±	0.00005	30
5	Filled Holes	0.00234	±	0.00016	2√3	0.00068	±	0.00005	15

2.1.3.10 Helium Coolant

Density

The density of helium gas was evaluated using the ideal gas law, PV=nRT, at a pressure of 1 atm and temperature of 25 ºC. The helium coolant was modeled with an atom density of 2.4616×10^{-4} atoms/b-cm (mass density of 1.6361×10^{-4} g/cm^3).

The helium density was varied approximately ±35% (10 × bounding limit) to determine the effective uncertainty in k_{eff}. Results are shown in Table 2.77.

The effect of neglecting the helium content and replacing it with an empty void was also performed. The effective change in change in k_{eff} was determined. Results are shown in Table 2.77.

The uncertainty in the helium density is considered all systematic with no random component.

Table 2.77. Effect of Uncertainty in Helium Coolant Density.

Case	Deviation	Δk	±	$\sigma_{\Delta k}$	Scaling Factor	Δk_{eff} (1σ)	±	$\sigma_{\Delta keff}$
1	void	-0.00006	±	0.00016	1	-0.00006	±	0.00016
	-35% (10σ)	-0.00007	±	0.00017	10√3	0.00000	±	0.00001
	+35% (10σ)	0.00005	±	0.00017	10√3	0.00000	±	0.00001
2	void	0.00014	±	0.00017	1	0.00014	±	0.00017
	-35% (10σ)	0.00004	±	0.00017	10√3	0.00000	±	0.00001
	+35% (10σ)	0.00021	±	0.00016	10√3	0.00001	±	0.00001
3	void	-0.00014	±	0.00016	1	-0.00014	±	0.00016
	-35% (10σ)	-0.00003	±	0.00016	10√3	0.00000	±	0.00000
	+35% (10σ)	0.00004	±	0.00017	10√3	0.00000	±	0.00000
4	void	-0.00005	±	0.00016	1	-0.00005	±	0.00016
	-35% (10σ)	-0.00022	±	0.00017	10√3	-0.00001	±	0.00001
	+35% (10σ)	-0.00016	±	0.00017	10√3	-0.00001	±	0.00001
5	void	0.00018	±	0.00016	1	0.00018	±	0.00016
	-35% (10σ)	-0.00010	±	0.00016	10√3	-0.00001	±	0.00001
	+35% (10σ)	0.00001	±	0.00016	10√3	0.00000	±	0.00001

Impurity

The upper impurity limit in the helium coolant was included in the model to determine its effect upon the uncertainty in k_{eff}. Upper concentration limits from Table 1.10 of HTTR-GCR-RESR-001 were included although the impurity content in helium at room temperature would be considerably less (and practically nonexistent); therefore it will be treated as a bounding limit. The bounding limit was multiplied by 10 for each component in order to assess the uncertainty, but the effects were still negligible. Results are shown in Table 2.78.

The uncertainty in the helium impurity is considered all systematic with no random component.

Table 2.78. Effect of Uncertainty in Helium Coolant Impurity.

Case	Deviation	Δk	±	$\sigma_{\Delta k}$	Scaling Factor	Δk_{eff} (1σ)	±	$\sigma_{\Delta keff}$
1	Added Impurities (×10)	-0.00004	±	0.00017	20√3	0.00000	±	0.00000
2	Added Impurities (×10)	0.00024	±	0.00017	20√3	0.00001	±	0.00000
3	Added Impurities (×10)	0.00011	±	0.00016	20√3	0.00000	±	0.00000
4	Added Impurities (×10)	0.00003	±	0.00017	20√3	0.00000	±	0.00000
5	Added Impurities (×10)	0.00005	±	0.00016	20√3	0.00000	±	0.00000

2.1.4 Additional Analyses

2.1.4.1 Room Return

Insufficient information is available to model and evaluate the uncertainties and biases related to any room return effects in the HTTR. Shielding plugs, plates, and blocks are incorporated within the HTTR vessel and would considerably reduce room return effects from the surrounding reactor vessel, reactor internals, and HTTR infrastructure and facility due to the content of sintered B_4C/C neutron absorber.

A conservative analysis of the HTTR benchmark model of the fully-loaded core (HTTR-GCR-RESR-001) surrounded by shielding material, steel, and concrete provided an insignificant effect because the slight increase in the effective multiplication factor was well below the range of statistical uncertainty for the analysis. Actual room return effects would be assumed quite negligible.

2.1.4.2 TRISO Particle Placement

Currently MCNP has a limited capability for modeling stochastic geometries. The HTTR core is unique in the fact that it has 12 different enrichments throughout the core. MCNP could effectively model randomness for only two types of TRISO particles at once because the URAN card used to create stochastic models has a maximum limit of two universes per model. A comparison of using the URAN analysis with multiple input decks to represent pairs of enriched TRISO particles was performed for the fully-loaded core configuration (HTTR-GCR-RESR-001) and shown to provide equivalent results to the approach performed below.

To approximate the bounding uncertainty in the effects of random TRISO placement, the fuel compacts were modeled with a uniform cell lattice of TRISO particles, which effectively creates partial particles along the compact borders. Figures 2.6 and 2.7 show a cross section of the fuel compacts with ordered and uniformly-filled TRISO distributions, respectively. The effective difference in the multiplication factor is shown in Table 2.79. The 30 vol. % packing fraction and uranium mass per fuel rod is conserved in this comparison. In order to conserve the uranium mass, the volume was estimated for the uranium kernels along the edges of the fuel compacts (using linear approximation of the cylindrical surface and spherical dome formulas)[a] to determine the approximate fuel content in each compact. Then the uniform cell lattice was adjusted such that the modeled fuel content matched the reported HTTR value. The reduction in resonance shielding effects in partial particles (i.e. fuel kernels not completely surrounded by graphite coatings) along the edges is not considered in this analysis. There is a slight mass uncertainty that is unaccounted for in this approximation. Because this is a bounding application, the results in Table 2.79 need to be divided by the square-root of three.

An analysis performed at the University of Michigan to look at the effects of explicitly modeling particle fuel in a very-high temperature gas-cooled reactor found that in a full core model, the effect of modeling with a uniform lattice and clipped TRISO particles would have a reduced k_{eff} of approximately 0.1 % compared to a heterogeneous core design containing only complete TRISO particles.[b] The results shown in Table 2.79 are approximately 0.1 % for the fully-loaded core configuration and slightly less for these annular configurations. The values calculated in Table 2.79 are used to represent the uncertainty in random TRISO particle placement in the HTTR. This uncertainty is treated as 100% systematic to capture the complete uncertainty in random particle placement.

A driver for this phenomenon might be explained by the Dancoff-Ginsberg factor, where in a lattice, the closer the lumps of fissionable material are to each other, the greater the shadowing effect and the smaller

---

[a] "Spherical and Ellipsoid Dome Formulas," Monolithic Dome Institute, Italy, Texas (2001).

[b] W. Ji, J. L. Conlin, W. R. Martin, J. C. Lee, and F. B. Brown, "Explicit Modeling of Particle Fuel for the Very-High Temperature Gas-Cooled Reactor," *Trans. Am. Nucl. Soc.*, **92** (June 2005).

the resonance integral for the interacting lattice, which results in an increase in the non-leakage probability and net increase in k_{eff}.[a]

A competing argument is that self-shielding and shadowing effects are quite negligible (2nd-order effect) and that small variations in fuel conservation actually lead to the difference in the calculated value of k_{eff}.[bc] Further discussion of the relevance of fuel particle parameters upon the reactivity of the system can be read elsewhere.[d] It remains up to the user's discretion to assess whether and how an uncertainty might apply to the modeling of this reactor system.

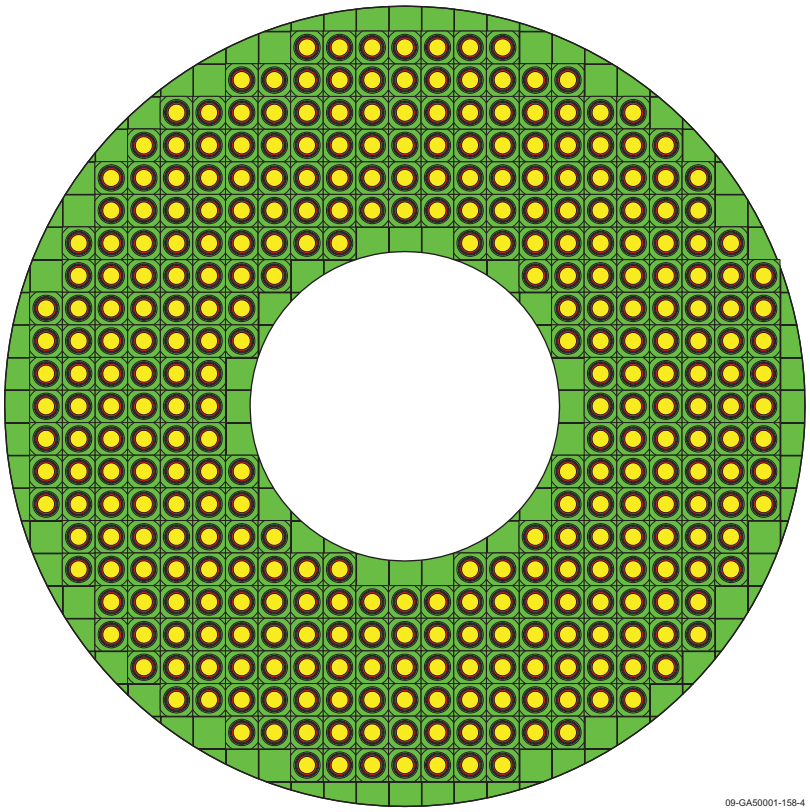

Figure 2.6. MCNP Ordered TRISO Lattice within the Fuel Compacts.

[a] J. R. Lamarsh, *Introduction to Nuclear Reactor Theory*, Addison-Wesley Publishing Company, Reading, Massachusetts, pp. 399-400 (1966).

[b] Personal communication between Luka Snoj and Forrest Brown from Los Alamos National Laboratory (November 20, 2008).

[c] F. B. Brown, "Monte Carlo Advances & Challenges," *Proc. Frederic Joliot and Otto Hahn Summer School 2005*, Karlsruhe, Germany, August 24 – September 2 (2005).

[d] L. Snoj and M. Ravnik, "Effect of Fuel Particles' Size and Position Variations on Multiplication Factor in Pebble-Bed Nuclear Reactors," *Kerntechnik*, **72** (2007).

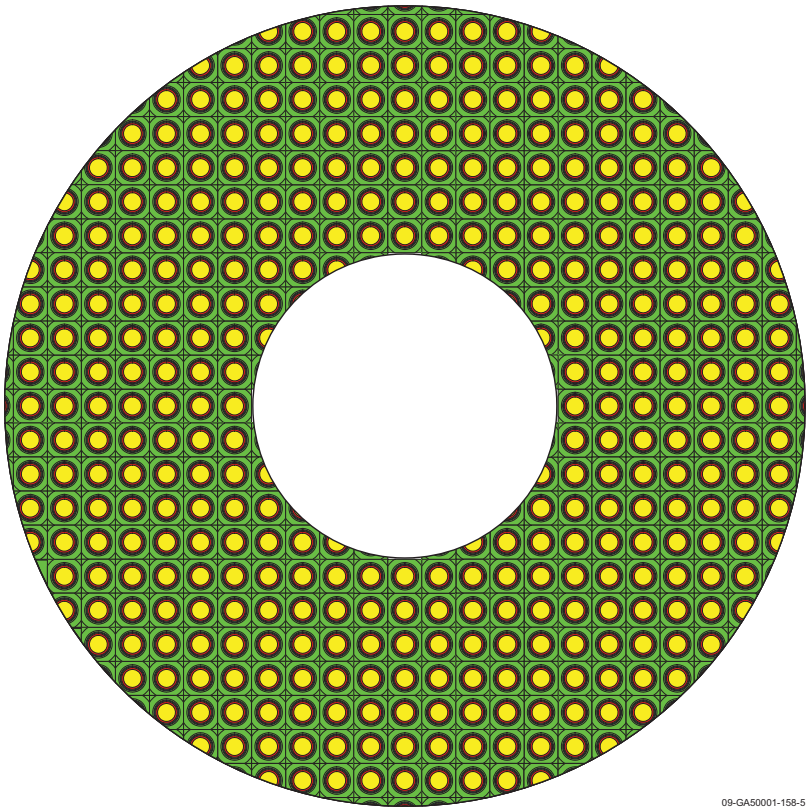

Figure 2.7. MCNP Uniformly-Filled TRISO Lattice within the Fuel Compacts.

Table 2.79. Comparison of Uniform and Organized TRISO Fill in Fuel Compacts.

Case	Organized Distribution (Figure 2.6)			Uniform Fill (Figure 2.7)			Bounding Difference			1σ Uncertainty		
	k_{eff}	±	σ_k	k_{eff}	±	σ_k	Δk	±	$\sigma_{\Delta k}$	Δk	±	$\sigma_{\Delta k}$
1	1.03123	±	0.00012	1.03087	±	0.00011	0.00036	±	0.00016	0.00021	±	0.00009
2	1.03290	±	0.00012	1.03233	±	0.00011	0.00057	±	0.00016	0.00033	±	0.00009
3	1.02847	±	0.00012	1.02758	±	0.00012	0.00089	±	0.00017	0.00051	±	0.00010
4	1.03193	±	0.00012	1.03101	±	0.00012	0.00092	±	0.00017	0.00053	±	0.00009
5	1.02516	±	0.00011	1.02399	±	0.00012	0.00117	±	0.00016	0.00068	±	0.00009

2.1.4.3 Block Stack Alignment

As discussed in the previous section, MCNP has a limited capability for modeling stochastic geometries for systems with multiple unique components. Whereas the HTTR core model is comprised of 61 columns each containing 9 bricks, a comprehensive analysis of the stochastic nature of block stacking could not be easily evaluated.

2.1.4.4 MCNP Random Number Generation

The random number seed was changed for the benchmark model and compared with the original to determine the uncertainty in utilizing Monte Carlo analysis methods. Results are shown in Table 2.80. The uncertainty in the average is the standard deviation of the six averaged eigenvalues.

Table 2.80. Analysis of the Effect of Random Number Generation in MCNP.

Seed	Case 1			Case 2			Case 3		
	k_{eff}	±	σ_{keff}	k_{eff}	±	σ_{keff}	k_{eff}	±	σ_{keff}
123456787	1.03121	±	0.00012	1.03304	±	0.00012	1.02831	±	0.00012
9876543279	1.03145	±	0.00012	1.03292	±	0.00012	1.02850	±	0.00012
198765432799	1.03111	±	0.00011	1.03293	±	0.00012	1.02841	±	0.00011
17623486105893	1.03131	±	0.00011	1.03308	±	0.00012	1.02847	±	0.00012
19073486328125[(a)]	1.03123	±	0.00012	1.03290	±	0.00012	1.02847	±	0.00012
32160231045432797	1.03107	±	0.00011	1.03291	±	0.00011	1.02844	±	0.00012
Average	1.03123	±	0.00014	1.03296	±	0.00008	1.02843	±	0.00007

Table 2.80 (cont'd.). Analysis of the Effect of Random Number Generation in MCNP.

Seed	Case 4			Case 5		
	k_{eff}	±	σ_{keff}	k_{eff}	±	σ_{keff}
123456787	1.03186	±	0.00012	1.02511	±	0.00011
9876543279	1.03169	±	0.00012	1.02495	±	0.00011
198765432799	1.03177	±	0.00012	1.02539	±	0.00012
17623486105893	1.03192	±	0.00012	1.02513	±	0.00012
19073486328125[(a)]	1.03193	±	0.00012	1.02516	±	0.00011
32160231045432797	1.03204	±	0.00012	1.02536	±	0.00011
Average	1.03187	±	0.00012	1.02518	±	0.00017

(a) Primary seed value for evaluation.

2.1.4.5 Simplification Biases and Uncertainties

Whereas insufficient information is publicly available, a comprehensive analysis of simplification biases and their respective uncertainties could not be appropriately assessed. Currently only an approximate bias for the instrumentation components in the reactor has been assessed (Section 2.1.2.6). As additional

information becomes available, highly detailed and simplified benchmark models can be generated and their biases can be adequately determined.

2.1.5 Systematic Biases and Uncertainties

There was no information regarding systematic biases or uncertainties publicly available for these experiments. Previous efforts of the Japanese in analyzing the 19-fuel-column core (Case 1) obtained an analytical excess reactivity of 2.7 % Δk/k, with an estimated Monte Carlo calculation overestimate of 1.2 % Δk/k.[a] Additional information would be necessary to completely verify published results to generate an analytical bias for MCNP.

As discussed at the beginning of Section 2, all uncertainties are treated as 25% systematic, with no reduction in uncertainty due to the multiplicity of core components, and as 75% random.

2.1.6 Analysis of HTTR Uranium Content

The parameters (dimensions, density, etc.) of the TRISO particles fabricated during the manufacturing process are very normally distributed, except for any defective particles. The fuel content, or mass, is the most well-known specification and measured with the highest accuracy.[b]

Because of the overspecification of the TRISO particles in Table 1.14 of HTTR-GCR-RESR-001 and the correlation of uranium kernel diameter, density, packing fraction, and mass, the effect of the uncertainties in the kernel diameter, density, and packing fraction are not included in the total uncertainty as separate entities. The uranium content of the fuel rods of 188.58 ± 5.66 g (Table 1.14 of HTTR-GCR-RESR-001) is the parameter most likely known with the greatest accuracy. Therefore, the diameter of the kernels will be fixed at 600 μm, and the density will be varied ± 0.32 g/cm^3 from a nominal value of 10.39 g/cm^3 to determine the effective uncertainty in k_{eff} due to the uranium mass uncertainty. Results are shown in Table 2.81. This value is treated as a bounding limit.

The total number of fuel rods used in the fully-loaded core is approximately 4,770. For determining the random component of the uncertainty, the results in Table 2.81 would be divided by √N.

[a] Fujimoto, N., Nakano, M., Takeuchi, M., Fujisaki, S., and Yamashita, K., "Start-Up Core Physics Tests of High Temperature Engineering Test Reactor (HTTR), (II): First Criticality by an Annular Form Fuel Loading and Its Criticality Prediction Method," *J. Atomic Energy Society Japan*, **42**(5), 458-464 (2000).

[b] Personal communication with David Petti from the Idaho National Laboratory (September 28, 2009).

Table 2.81. Effect of Uncertainty in Uranium Mass.

Case	Deviation	Δk	±	$\sigma_{\Delta k}$	Scaling Factor	Δk_{eff} (1σ)	±	$\sigma_{\Delta keff}$	N
1	-0.32 g/cm^3	-0.00509	±	0.00017	√3	-0.00294	±	0.00010	2,955
	+0.32 g/cm^3	0.00482	±	0.00016	√3	0.00278	±	0.00009	
2	-0.32 g/cm^3	-0.00487	±	0.00017	√3	-0.00281	±	0.00010	3,285
	+0.32 g/cm^3	0.00511	±	0.00017	√3	0.00295	±	0.00010	
3	-0.32 g/cm^3	-0.00535	±	0.00017	√3	-0.00309	±	0.00010	3,780
	+0.32 g/cm^3	0.00492	±	0.00017	√3	0.00284	±	0.00010	
4	-0.32 g/cm^3	-0.00520	±	0.00017	√3	-0.00300	±	0.00010	3,780
	+0.32 g/cm^3	0.00498	±	0.00017	√3	0.00288	±	0.00010	
5	-0.32 g/cm^3	-0.00519	±	0.00016	√3	-0.00300	±	0.00009	4,275
	+0.32 g/cm^3	0.00507	±	0.00016	√3	0.00293	±	0.00009	

2.1.7 Total Experimental Uncertainty

A compilation of the total evaluated uncertainty in the HTTR model is shown in Tables 2.82 through 2.86 for configurations 1 through 5, respectively. As discussed earlier, each of the evaluated uncertainties is divided into a systematic component (25%) and random component (75%), where appropriate. The random component is then divided by the square-root of the number of random objects reported in the subsection containing the calculated base uncertainty values. The root-mean square of each subcomponent is taken to determine the uncertainty in either the random or systematic components of the total evaluated uncertainty. The total evaluated uncertainty is then the root-mean square of the random and systematic uncertainties.

Uncertainties less than 0.00001 are reported as negligible (neg). When calculated uncertainties in Δk_{eff} are less than their statistical uncertainties, the statistical uncertainties are used in the calculation of the total uncertainty. Table listings where calculations were not performed or otherwise not available are labeled with 'NA'. For uncertainties where a random component is not applicable, the uncertainty is denoted with '--'.

The most significant contributions to the overall uncertainty from the systematic uncertainties include the impurities in the IG-110 graphite blocks, PGX graphite reflector blocks, and IG-11 graphite dummy blocks. All uncertainties providing at least 0.1 % Δk_{eff} are highlighted in gray in Tables 2.82 through 2.86. All of the random uncertainties are less than 0.1 % Δk_{eff}. The overall uncertainty is less than 1% Δk_{eff} (except for Cases 1 and 2); it is expected that the total uncertainty will be reduced as additional parameters that characterize the HTTR are obtained.

Table 2.82. Total Experimental Uncertainty (Case 1).

Varied Parameter	Systematic Uncertainty		Random Uncertainty	
	$-\Delta k_{eff}$ (1σ)	$+\Delta k_{eff}$ (1σ)	$-\Delta k_{eff}$ (1σ)	$+\Delta k_{eff}$ (1σ)
Temperature	0.00013	-0.00013	--	--
Control Rod Positions	-0.00003	0.00003	-0.00002	0.00003
Measured Value of k_{eff}	neg	neg	neg	neg
Kernel Diameter	Correlated Parameter (see Section 2.1.6)			
Buffer Diameter	neg	neg	neg	neg
IPyC Diameter	neg	0.00001	neg	neg
SiC Diameter	0.00002	-0.00005	neg	neg
OPyC Diameter	neg	neg	neg	neg
Overcoat Diameter	NA	NA	NA	NA
Compact Inner Diameter	neg	neg	neg	neg
Compact Outer Diameter	-0.00002	0.00003	neg	neg
Compact Height	-0.00005	0.00005	neg	neg
Compact Packing Fraction	Correlated Parameter (see Section 2.1.6)			
Sleeve Inner Diameter	0.00002	-0.00003	neg	neg
Sleeve Outer Diameter	-0.00004	0.00004	neg	neg
Sleeve Height	-0.00001	0.00001	neg	neg
BP Diameter	0.00015	-0.00014	0.00001	-0.00001
BP Stack Height	0.00009	-0.00007	0.00001	-0.00001
BP Hole Diameter	0.00001	-0.00001	neg	neg
Graphite Disk Diameter	neg	neg	neg	neg
Disk Stack Height	0.00003	0.00003	neg	neg
CR Absorber Inner Diameter	neg	neg	neg	neg
CR Absorber Outer Diameter	neg	neg	neg	neg
CR Absorber Height	neg	neg	neg	neg
CR Clad Inner Diameter	neg	neg	neg	neg
CR Clad Outer Diameter	neg	neg	neg	neg
CR Clad Height	neg	neg	neg	neg
CR Spine Diameter	neg	neg	neg	neg
Instrumentation Dimensions	-0.00139	0.00139	--	--
Block Flat-to-Flat Distance	-0.00004	0.00003	neg	neg
Graphite Block Height	neg	neg	neg	neg
Dowel/Socket Dimensions	NA	NA	NA	NA
Fuel Channel Diameter	0.00004	-0.00005	neg	neg
Reflector Channel Diameter	neg	neg	neg	neg
Channel Pitch	-0.00004	0.00005	neg	neg

Table 2.82 (cont'd.). Total Experimental Uncertainty (Case 1).

Varied Parameter	Systematic Uncertainty		Random Uncertainty	
	$-\Delta k_{eff}$ (1σ)	$+\Delta k_{eff}$ (1σ)	$-\Delta k_{eff}$ (1σ)	$+\Delta k_{eff}$ (1σ)
Handling Socket Dimensions	NA	NA	NA	NA
Column Pitch	0.00015	-0.00018	0.00006	-0.00007
CR Channel Diameter	neg	-0.00001	neg	neg
CR Channel Pitch	neg	neg	neg	neg
Permanent Reflector Diameter	-0.00117	0.00045	--	--
Dummy Block Dimensions	See Sections 2.1.2.7 and 2.1.3.9			
3.4 wt.% Enrichment	NA	NA	NA	NA
3.9 wt.% Enrichment	0.00005	0.00012	--	--
4.3 wt.% Enrichment	-0.00054	0.00054	--	--
4.8 wt.% Enrichment	-0.00023	0.00022	--	--
5.2 wt.% Enrichment	-0.00006	0.00008	--	--
5.9 wt.% Enrichment	-0.00063	0.00060	--	--
6.3 wt.% Enrichment	-0.00042	0.00034	--	--
6.7 wt.% Enrichment	NA	NA	NA	NA
7.2 wt.% Enrichment	-0.00074	0.00079	--	--
7.9 wt.% Enrichment	-0.00038	0.00048	--	--
9.4 wt.% Enrichment	-0.00055	0.00062	--	--
9.9 wt.% Enrichment	-0.00031	0.00027	--	--
Oxygen to Uranium Ratio	0.00008	-0.00009	--	--
UO_2 Density	Correlated Parameter (see Section 2.1.6)			
UO_2 Impurity	0.00032	-0.00056	--	--
Buffer Density	neg	neg	neg	neg
Buffer Impurity	0.00010	neg	--	--
IPyC Density	neg	neg	neg	neg
IPyC Impurity	0.00010	0.00010	--	--
SiC Density	NA	neg	NA	neg
SiC Impurity	0.00010	neg	--	--
OPyC Density	neg	neg	neg	neg
OPyC Impurity	0.00005	0.00010	--	--
Overcoat Density	-0.00001	0.00002	neg	neg
Overcoat Composition	NA	NA	NA	NA
Overcoat Impurity	0.00027	-0.00040	--	--
Compact Density	neg	neg	neg	neg
Compact Impurity	0.00009	-0.00043	--	--
Compact Free U Content	NA	neg	--	--

Table 2.82 (cont'd.). Total Experimental Uncertainty (Case 1).

Varied Parameter	Systematic Uncertainty		Random Uncertainty	
	$-\Delta k_{eff}$ (1σ)	$+\Delta k_{eff}$ (1σ)	$-\Delta k_{eff}$ (1σ)	$+\Delta k_{eff}$ (1σ)
Sleeve Density	-0.00005	0.00004	neg	neg
Sleeve Impurity	0.00010	-0.00032	--	--
BP Absorber Density	0.00012	-0.00012	neg	neg
BP Absorber Content, 2.0 wt.%	0.00038	-0.00034	0.00002	-0.00002
BP Absorber Content, 2.5 wt.%	0.00036	-0.00035	0.00003	-0.00003
BP Absorber Impurity	NA	0.00014	--	--
BP Isotopic Abundance of ^{10}B	0.00103	-0.00058	--	--
Graphite Disk Density	neg	neg	neg	neg
Graphite Disk Impurity	-0.00010	0.00010	--	--
CR Absorber Density	neg	-0.00001	neg	neg
CR Absorber Content	neg	neg	neg	neg
CR Absorber Impurity	NA	0.00005	--	--
CR Isotopic Abundance of ^{10}B	0.00010	0.00010	--	--
CR Clad Density	0.00004	0.00002	0.00003	0.00003
CR Clad Composition	0.00009	0.00009	--	--
CR Clad Impurity	NA	0.00005	--	--
Instrumentation Composition	See Section 2.1.2.6			
IG-110 Density in Blocks	-0.00060	0.00061	-0.00008	0.00008
IG-110 Impurity in Blocks	0.00532	-0.00659	--	--
PGX Density	-0.00010	0.00012	-0.00003	0.00004
PGX Impurity	0.00442	-0.00585	--	--
Dummy Block Density	0.00002	-0.00007	neg	-0.00003
Dummy Block Impurity	0.00704	-0.00387	--	--
Dummy Block Type	NA	-0.00004	NA	-0.00003
Helium Coolant Density	neg	neg	--	--
Helium Coolant Impurity	NA	neg	--	--
Room Return	neg	neg	neg	neg
TRISO Particle Placement	0.00021	0.00021	neg	neg
Block Stack Alignment	NA	NA	NA	NA
MCNP Random Number Seed	--	--	0.00014	0.00014
Uranium Fuel Mass (Sec. 2.1.6)	-0.00073	0.00070	-0.00004	0.00004
Uncertainty of Components	0.01026	0.00997	0.00019	0.00019
Total Evaluation Uncertainty	**0.01026**	**0.00997**		

Table 2.83. Total Experimental Uncertainty (Case 2).

Varied Parameter	Systematic Uncertainty		Random Uncertainty	
	$-\Delta k_{eff}$ (1σ)	$+\Delta k_{eff}$ (1σ)	$-\Delta k_{eff}$ (1σ)	$+\Delta k_{eff}$ (1σ)
Temperature	0.00013	-0.00013	--	--
Control Rod Positions	-0.00011	0.00012	-0.00008	0.00009
Measured Value of k_{eff}	neg	neg	neg	neg
Kernel Diameter	Correlated Parameter (see Section 2.1.6)			
Buffer Diameter	neg	0.00001	neg	neg
IPyC Diameter	neg	neg	neg	neg
SiC Diameter	0.00006	-0.00002	neg	neg
OPyC Diameter	0.00002	0.00003	neg	neg
Overcoat Diameter	NA	NA	NA	NA
Compact Inner Diameter	neg	neg	neg	neg
Compact Outer Diameter	-0.00002	0.00002	neg	neg
Compact Height	-0.00005	0.00004	neg	neg
Compact Packing Fraction	Correlated Parameter (see Section 2.1.6)			
Sleeve Inner Diameter	0.00002	-0.00002	neg	neg
Sleeve Outer Diameter	-0.00004	0.00004	neg	neg
Sleeve Height	-0.00001	0.00001	neg	neg
BP Diameter	0.00016	-0.00015	0.00001	-0.00001
BP Stack Height	0.00008	-0.00009	neg	neg
BP Hole Diameter	0.00002	-0.00001	neg	neg
Graphite Disk Diameter	neg	neg	neg	neg
Disk Stack Height	0.00002	0.00002	neg	neg
CR Absorber Inner Diameter	neg	neg	neg	neg
CR Absorber Outer Diameter	neg	neg	neg	neg
CR Absorber Height	0.00001	-0.00001	0.00001	-0.00001
CR Clad Inner Diameter	neg	neg	neg	neg
CR Clad Outer Diameter	neg	neg	neg	neg
CR Clad Height	-0.00003	-0.00003	-0.00001	-0.00001
CR Spine Diameter	neg	neg	neg	neg
Instrumentation Dimensions	-0.00116	0.00116	--	--
Block Flat-to-Flat Distance	-0.00003	0.00003	neg	neg
Graphite Block Height	neg	0.00002	neg	neg
Dowel/Socket Dimensions	NA	NA	NA	NA
Fuel Channel Diameter	0.00005	-0.00005	neg	neg
Reflector Channel Diameter	neg	neg	neg	neg
Channel Pitch	-0.00004	0.00004	neg	neg

Table 2.83 (cont'd.). Total Experimental Uncertainty (Case 2).

Varied Parameter	Systematic Uncertainty		Random Uncertainty	
	$-\Delta k_{eff}$ (1σ)	$+\Delta k_{eff}$ (1σ)	$-\Delta k_{eff}$ (1σ)	$+\Delta k_{eff}$ (1σ)
Handling Socket Dimensions	NA	NA	NA	NA
Column Pitch	0.00016	-0.00017	0.00006	-0.00006
CR Channel Diameter	neg	neg	neg	neg
CR Channel Pitch	neg	neg	neg	neg
Permanent Reflector Diameter	-0.00083	0.00043	--	--
Dummy Block Dimensions	See Sections 2.1.2.7 and 2.1.3.9			
3.4 wt.% Enrichment	NA	NA	NA	NA
3.9 wt.% Enrichment	-0.00030	0.00023	--	--
4.3 wt.% Enrichment	-0.00081	0.00073	--	--
4.8 wt.% Enrichment	-0.00041	0.00037	--	--
5.2 wt.% Enrichment	-0.00033	0.00017	--	--
5.9 wt.% Enrichment	-0.00076	0.00076	--	--
6.3 wt.% Enrichment	-0.00067	0.00047	--	--
6.7 wt.% Enrichment	NA	NA	NA	NA
7.2 wt.% Enrichment	-0.00071	0.00060	--	--
7.9 wt.% Enrichment	-0.00038	0.00031	--	--
9.4 wt.% Enrichment	-0.00026	0.00016	--	--
9.9 wt.% Enrichment	-0.00015	0.00005	--	--
Oxygen to Uranium Ratio	0.00014	-0.00007	--	--
UO_2 Density	Correlated Parameter (see Section 2.1.6)			
UO_2 Impurity	0.00047	-0.00060	--	--
Buffer Density	neg	0.00001	neg	neg
Buffer Impurity	0.00010	neg	--	--
IPyC Density	neg	0.00001	neg	neg
IPyC Impurity	0.00009	0.00010	--	--
SiC Density	NA	neg	NA	neg
SiC Impurity	0.00010	0.00009	--	--
OPyC Density	neg	0.00001	neg	neg
OPyC Impurity	0.00024	-0.00015	--	--
Overcoat Density	neg	0.00002	neg	neg
Overcoat Composition	NA	NA	NA	NA
Overcoat Impurity	0.00030	-0.00059	--	--
Compact Density	neg	neg	neg	neg
Compact Impurity	0.00013	-0.00042	--	--
Compact Free U Content	NA	neg	--	--

Table 2.83 (cont'd.). Total Experimental Uncertainty (Case 2).

Varied Parameter	Systematic Uncertainty		Random Uncertainty	
	$-\Delta k_{eff}$ (1σ)	$+\Delta k_{eff}$ (1σ)	$-\Delta k_{eff}$ (1σ)	$+\Delta k_{eff}$ (1σ)
Sleeve Density	-0.00003	0.00003	neg	neg
Sleeve Impurity	0.00018	-0.00021	--	--
BP Absorber Density	0.00015	-0.00007	neg	neg
BP Absorber Content, 2.0 wt.%	0.00044	-0.00034	0.00003	-0.00002
BP Absorber Content, 2.5 wt.%	0.00041	-0.00036	0.00003	-0.00003
BP Absorber Impurity	NA	0.00023	--	--
BP Isotopic Abundance of ^{10}B	0.00131	-0.00042	--	--
Graphite Disk Density	neg	0.00001	neg	neg
Graphite Disk Impurity	0.00009	0.00010	--	--
CR Absorber Density	neg	neg	neg	neg
CR Absorber Content	0.00003	-0.00001	neg	neg
CR Absorber Impurity	NA	-0.00005	--	--
CR Isotopic Abundance of ^{10}B	0.00010	neg	--	--
CR Clad Density	0.00002	neg	neg	neg
CR Clad Composition	0.00010	0.00010	--	--
CR Clad Impurity	NA	0.00005	--	--
Instrumentation Composition	See Section 2.1.2.6			
IG-110 Density in Blocks	-0.00061	0.00066	-0.00008	0.00009
IG-110 Impurity in Blocks	0.00486	-0.00617	--	--
PGX Density	-0.00010	0.00014	-0.00003	0.00004
PGX Impurity	0.00379	-0.00499	--	--
Dummy Block Density	0.00008	-0.00008	0.00003	-0.00004
Dummy Block Impurity	0.00738	-0.00389	--	--
Dummy Block Type	NA	-0.00037	NA	-0.00016
Helium Coolant Density	neg	0.00001	--	--
Helium Coolant Impurity	NA	neg	--	--
Room Return	neg	neg	neg	neg
TRISO Particle Placement	0.00033	0.00033	neg	neg
Block Stack Alignment	NA	NA	NA	NA
MCNP Random Number Seed	--	--	0.00008	0.00008
Uranium Fuel Mass (Sec. 2.1.6)	-0.00070	0.00074	-0.00004	0.00004
Uncertainty of Components	0.01005	0.00919	0.00017	0.00024
Total Evaluation Uncertainty	**0.01004**	**0.00919**		

Table 2.84. Total Experimental Uncertainty (Case 3).

Varied Parameter	Systematic Uncertainty		Random Uncertainty	
	$-\Delta k_{eff}$ (1σ)	$+\Delta k_{eff}$ (1σ)	$-\Delta k_{eff}$ (1σ)	$+\Delta k_{eff}$ (1σ)
Temperature	0.00013	-0.00013	--	--
Control Rod Positions	-0.00015	0.00013	-0.00011	0.00010
Measured Value of k_{eff}	neg	neg	neg	neg
Kernel Diameter	Correlated Parameter (see Section 2.1.6)			
Buffer Diameter	-0.00002	0.00001	neg	neg
IPyC Diameter	-0.00001	neg	neg	neg
SiC Diameter	0.00005	-0.00005	neg	neg
OPyC Diameter	-0.00002	neg	neg	neg
Overcoat Diameter	NA	NA	NA	NA
Compact Inner Diameter	neg	neg	neg	neg
Compact Outer Diameter	-0.00004	0.00003	neg	neg
Compact Height	-0.00005	0.00004	neg	neg
Compact Packing Fraction	Correlated Parameter (see Section 2.1.6)			
Sleeve Inner Diameter	0.00002	-0.00003	neg	neg
Sleeve Outer Diameter	-0.00004	0.00005	neg	neg
Sleeve Height	-0.00001	0.00001	neg	neg
BP Diameter	0.00017	-0.00017	0.00001	-0.00001
BP Stack Height	0.00006	-0.00011	0.00001	-0.00002
BP Hole Diameter	0.00001	-0.00002	neg	neg
Graphite Disk Diameter	neg	neg	neg	neg
Disk Stack Height	neg	neg	neg	neg
CR Absorber Inner Diameter	neg	neg	neg	neg
CR Absorber Outer Diameter	neg	neg	neg	neg
CR Absorber Height	0.00001	-0.00001	neg	neg
CR Clad Inner Diameter	neg	neg	neg	neg
CR Clad Outer Diameter	-0.00001	0.00001	neg	neg
CR Clad Height	-0.00004	-0.00003	-0.00001	-0.00001
CR Spine Diameter	neg	neg	neg	neg
Instrumentation Dimensions	-0.00100	0.00100	--	--
Block Flat-to-Flat Distance	-0.00005	0.00004	-0.00001	neg
Graphite Block Height	neg	neg	neg	neg
Dowel/Socket Dimensions	NA	NA	NA	NA
Fuel Channel Diameter	0.00005	-0.00006	neg	neg
Reflector Channel Diameter	neg	neg	neg	neg
Channel Pitch	-0.00004	0.00003	neg	neg

Table 2.84 (cont'd.). Total Experimental Uncertainty (Case 3).

Varied Parameter	Systematic Uncertainty		Random Uncertainty	
	$-\Delta k_{eff}$ (1σ)	$+\Delta k_{eff}$ (1σ)	$-\Delta k_{eff}$ (1σ)	$+\Delta k_{eff}$ (1σ)
Handling Socket Dimensions	NA	NA	NA	NA
Column Pitch	0.00015	-0.00018	0.00006	-0.00007
CR Channel Diameter	0.00001	-0.00001	neg	neg
CR Channel Pitch	neg	neg	neg	neg
Permanent Reflector Diameter	-0.00084	0.00034	--	--
Dummy Block Dimensions	See Sections 2.1.2.7 and 2.1.3.9			
3.4 wt.% Enrichment	NA	NA	NA	NA
3.9 wt.% Enrichment	-0.00064	0.00077	--	--
4.3 wt.% Enrichment	-0.00092	0.00098	--	--
4.8 wt.% Enrichment	-0.00043	0.00052	--	--
5.2 wt.% Enrichment	-0.00046	0.00049	--	--
5.9 wt.% Enrichment	-0.00058	0.00071	--	--
6.3 wt.% Enrichment	-0.00045	0.00052	--	--
6.7 wt.% Enrichment	NA	NA	NA	NA
7.2 wt.% Enrichment	-0.00031	0.00036	--	--
7.9 wt.% Enrichment	-0.00011	0.00017	--	--
9.4 wt.% Enrichment	0.00005	0.00013	--	--
9.9 wt.% Enrichment	0.00005	0.00005	--	--
Oxygen to Uranium Ratio	0.00007	-0.00017	--	--
UO_2 Density	Correlated Parameter (see Section 2.1.6)			
UO_2 Impurity	0.00024	-0.00068	--	--
Buffer Density	-0.00001	neg	neg	neg
Buffer Impurity	0.00009	-0.00012	--	--
IPyC Density	neg	neg	neg	neg
IPyC Impurity	0.00011	-0.00016	--	--
SiC Density	NA	neg	NA	neg
SiC Impurity	0.00010	0.00010	--	--
OPyC Density	neg	-0.00001	neg	neg
OPyC Impurity	0.00005	0.00010	--	--
Overcoat Density	-0.00002	neg	neg	neg
Overcoat Composition	NA	NA	NA	NA
Overcoat Impurity	0.00044	-0.00070	--	--
Compact Density	-0.00001	neg	neg	neg
Compact Impurity	0.00010	-0.00066	--	--
Compact Free U Content	NA	neg	--	--

Table 2.84 (cont'd.). Total Experimental Uncertainty (Case 3).

Varied Parameter	Systematic Uncertainty		Random Uncertainty	
	$-\Delta k_{eff}$ (1σ)	$+\Delta k_{eff}$ (1σ)	$-\Delta k_{eff}$ (1σ)	$+\Delta k_{eff}$ (1σ)
Sleeve Density	-0.00008	0.00004	neg	neg
Sleeve Impurity	0.00010	-0.00048	--	--
BP Absorber Density	0.00010	-0.00012	neg	neg
BP Absorber Content, 2.0 wt.%	0.00057	-0.00049	0.00003	-0.00003
BP Absorber Content, 2.5 wt.%	0.00036	-0.00035	0.00003	-0.00003
BP Absorber Impurity	NA	0.00021	--	--
BP Isotopic Abundance of ^{10}B	0.00126	-0.00062	--	--
Graphite Disk Density	neg	neg	neg	neg
Graphite Disk Impurity	0.00010	-0.00010	--	--
CR Absorber Density	neg	neg	neg	neg
CR Absorber Content	0.00002	-0.00002	neg	neg
CR Absorber Impurity	NA	0.00005	--	--
CR Isotopic Abundance of ^{10}B	0.00013	0.00009	--	--
CR Clad Density	neg	-0.00003	neg	-0.00001
CR Clad Composition	0.00010	-0.00012	--	--
CR Clad Impurity	NA	0.00005	--	--
Instrumentation Composition	See Section 2.1.2.6			
IG-110 Density in Blocks	-0.00073	0.00063	-0.00010	0.00008
IG-110 Impurity in Blocks	0.00462	-0.00601	--	--
PGX Density	-0.00009	0.00004	-0.00003	0.00001
PGX Impurity	0.00314	-0.00434	--	--
Dummy Block Density	0.00002	-0.00007	neg	-0.00004
Dummy Block Impurity	0.00460	-0.00264	--	--
Dummy Block Type	NA	-0.00014	NA	-0.00008
Helium Coolant Density	neg	neg	--	--
Helium Coolant Impurity	NA	neg	--	--
Room Return	neg	neg	neg	Neg
TRISO Particle Placement	0.00051	0.00051	neg	neg
Block Stack Alignment	NA	NA	NA	NA
MCNP Random Number Seed	--	--	0.00007	0.00007
Uranium Fuel Mass (Sec. 2.1.6)	-0.00077	0.00071	-0.00004	0.00003
Uncertainty of Components	0.00776	0.00836	0.00018	0.00019
Total Evaluation Uncertainty	**0.00777**	**0.00836**		

Table 2.85. Total Experimental Uncertainty (Case 4).

Varied Parameter	Systematic Uncertainty		Random Uncertainty	
	$-\Delta k_{eff}$ (1σ)	$+\Delta k_{eff}$ (1σ)	$-\Delta k_{eff}$ (1σ)	$+\Delta k_{eff}$ (1σ)
Temperature	0.00013	-0.00013	--	--
Control Rod Positions	-0.00009	0.00006	-0.00007	0.00005
Measured Value of k_{eff}	neg	neg	neg	neg
Kernel Diameter	Correlated Parameter (see Section 2.1.6)			
Buffer Diameter	neg	-0.00004	neg	neg
IPyC Diameter	neg	neg	neg	neg
SiC Diameter	0.00002	-0.00007	neg	neg
OPyC Diameter	0.00001	-0.00003	neg	neg
Overcoat Diameter	NA	NA	NA	NA
Compact Inner Diameter	neg	-0.00002	neg	neg
Compact Outer Diameter	-0.00004	0.00003	neg	neg
Compact Height	-0.00006	0.00004	neg	neg
Compact Packing Fraction	Correlated Parameter (see Section 2.1.6)			
Sleeve Inner Diameter	0.00003	-0.00003	neg	neg
Sleeve Outer Diameter	-0.00005	0.00005	neg	neg
Sleeve Height	-0.00002	0.00001	neg	neg
BP Diameter	0.00017	-0.00017	0.00001	-0.00001
BP Stack Height	0.00007	-0.00013	0.00001	-0.00002
BP Hole Diameter	0.00001	-0.00002	neg	neg
Graphite Disk Diameter	neg	neg	neg	neg
Disk Stack Height	neg	0.00002	neg	neg
CR Absorber Inner Diameter	neg	neg	neg	neg
CR Absorber Outer Diameter	neg	neg	neg	neg
CR Absorber Height	0.00001	-0.00001	neg	neg
CR Clad Inner Diameter	neg	neg	neg	neg
CR Clad Outer Diameter	-0.00002	0.00002	neg	neg
CR Clad Height	-0.00002	-0.00002	neg	neg
CR Spine Diameter	neg	neg	neg	neg
Instrumentation Dimensions	-0.00091	0.00091	--	--
Block Flat-to-Flat Distance	-0.00006	0.00004	-0.00001	0.00001
Graphite Block Height	neg	neg	neg	neg
Dowel/Socket Dimensions	NA	NA	NA	NA
Fuel Channel Diameter	0.00006	-0.00007	neg	neg
Reflector Channel Diameter	neg	neg	neg	neg
Channel Pitch	-0.00004	0.00003	neg	neg

Table 2.85 (cont'd.). Total Experimental Uncertainty (Case 4).

Varied Parameter	Systematic Uncertainty		Random Uncertainty	
	$-\Delta k_{eff}$ (1σ)	$+\Delta k_{eff}$ (1σ)	$-\Delta k_{eff}$ (1σ)	$+\Delta k_{eff}$ (1σ)
Handling Socket Dimensions	NA	NA	NA	NA
Column Pitch	0.00013	-0.00019	0.00005	-0.00007
CR Channel Diameter	0.00001	-0.00001	neg	neg
CR Channel Pitch	neg	neg	neg	neg
Permanent Reflector Diameter	-0.00054	0.00014	--	--
Dummy Block Dimensions	See Sections 2.1.2.7 and 2.1.3.9			
3.4 wt.% Enrichment	NA	NA	NA	NA
3.9 wt.% Enrichment	-0.00053	0.00059	--	--
4.3 wt.% Enrichment	-0.00064	0.00079	--	--
4.8 wt.% Enrichment	-0.00030	0.00036	--	--
5.2 wt.% Enrichment	-0.00045	0.00051	--	--
5.9 wt.% Enrichment	-0.00048	0.00041	--	--
6.3 wt.% Enrichment	-0.00063	0.00066	--	--
6.7 wt.% Enrichment	NA	NA	NA	NA
7.2 wt.% Enrichment	-0.00034	0.00033	--	--
7.9 wt.% Enrichment	-0.00037	0.00044	--	--
9.4 wt.% Enrichment	-0.00014	0.00018	--	--
9.9 wt.% Enrichment	0.00006	0.00011	--	--
Oxygen to Uranium Ratio	0.00011	-0.00012	--	--
UO_2 Density	Correlated Parameter (see Section 2.1.6)			
UO_2 Impurity	0.00026	-0.00063	--	--
Buffer Density	neg	neg	neg	neg
Buffer Impurity	0.00010	-0.00010	--	--
IPyC Density	neg	neg	neg	neg
IPyC Impurity	0.00010	0.00010	--	--
SiC Density	NA	neg	NA	neg
SiC Impurity	neg	-0.00011	--	--
OPyC Density	neg	neg	neg	neg
OPyC Impurity	-0.00012	0.00010	--	--
Overcoat Density	-0.00003	0.00002	neg	neg
Overcoat Composition	NA	NA	NA	NA
Overcoat Impurity	0.00025	-0.00076	--	--
Compact Density	-0.00001	0.00001	neg	neg
Compact Impurity	0.00010	-0.00060	--	--
Compact Free U Content	NA	neg	--	--

Table 2.85 (cont'd.). Total Experimental Uncertainty (Case 4).

Varied Parameter	Systematic Uncertainty		Random Uncertainty	
	$-\Delta k_{eff}$ (1σ)	$+\Delta k_{eff}$ (1σ)	$-\Delta k_{eff}$ (1σ)	$+\Delta k_{eff}$ (1σ)
Sleeve Density	-0.00012	0.00006	neg	neg
Sleeve Impurity	0.00009	-0.00033	--	--
BP Absorber Density	0.00009	-0.00012	neg	neg
BP Absorber Content, 2.0 wt.%	0.00055	-0.00050	0.00003	-0.00003
BP Absorber Content, 2.5 wt.%	0.00041	-0.00036	0.00003	-0.00003
BP Absorber Impurity	NA	0.00018	--	--
BP Isotopic Abundance of ^{10}B	0.00127	-0.00080	--	--
Graphite Disk Density	-0.00001	neg	neg	neg
Graphite Disk Impurity	-0.00010	0.00010	--	--
CR Absorber Density	neg	-0.00001	neg	neg
CR Absorber Content	0.00003	-0.00003	neg	neg
CR Absorber Impurity	NA	0.00005	--	--
CR Isotopic Abundance of ^{10}B	0.00010	-0.00010	--	--
CR Clad Density	-0.00005	neg	-0.00002	neg
CR Clad Composition	0.00010	0.00010	--	--
CR Clad Impurity	NA	neg	--	--
Instrumentation Composition	See Section 2.1.2.6			
IG-110 Density in Blocks	-0.00083	0.00080	-0.00011	0.00011
IG-110 Impurity in Blocks	0.00420	-0.00543	--	--
PGX Density	-0.00007	0.00005	-0.00002	0.00001
PGX Impurity	0.00171	-0.00247	--	--
Dummy Block Density	0.00002	-0.00007	0.00001	-0.00004
Dummy Block Impurity	0.00599	-0.00335	--	--
Dummy Block Type	NA	-0.00064	NA	-0.00035
Helium Coolant Density	-0.00001	neg	--	--
Helium Coolant Impurity	NA	neg	--	--
Room Return	neg	neg	neg	neg
TRISO Particle Placement	0.00053	0.00053	neg	neg
Block Stack Alignment	NA	NA	NA	NA
MCNP Random Number Seed	--	--	0.00012	0.00012
Uranium Fuel Mass (Sec. 2.1.6)	-0.00075	0.00072	-0.00004	0.00004
Uncertainty of Components	0.00796	0.00739	0.00020	0.00040
Total Evaluation Uncertainty	**0.00796**	**0.00740**		

Table 2.86. Total Experimental Uncertainty (Case 5).

Varied Parameter	Systematic Uncertainty		Random Uncertainty	
	$-\Delta k_{eff}$ (1σ)	$+\Delta k_{eff}$ (1σ)	$-\Delta k_{eff}$ (1σ)	$+\Delta k_{eff}$ (1σ)
Temperature	0.00013	-0.00013	--	--
Control Rod Positions	-0.00014	0.00016	-0.00011	0.00012
Measured Value of k_{eff}	neg	neg	neg	neg
Kernel Diameter	Correlated Parameter (see Section 2.1.6)			
Buffer Diameter	0.00002	-0.00002	neg	neg
IPyC Diameter	neg	neg	neg	neg
SiC Diameter	0.00006	-0.00006	neg	neg
OPyC Diameter	neg	neg	neg	neg
Overcoat Diameter	NA	NA	NA	NA
Compact Inner Diameter	0.00001	-0.00001	neg	neg
Compact Outer Diameter	-0.00003	0.00003	neg	neg
Compact Height	-0.00006	0.00004	neg	neg
Compact Packing Fraction	Correlated Parameter (see Section 2.1.6)			
Sleeve Inner Diameter	0.00003	-0.00004	neg	neg
Sleeve Outer Diameter	-0.00005	0.00005	neg	neg
Sleeve Height	-0.00002	0.00001	neg	neg
BP Diameter	0.00019	-0.00018	0.00001	-0.00001
BP Stack Height	0.00008	-0.00009	0.00001	-0.00001
BP Hole Diameter	0.00002	-0.00001	neg	neg
Graphite Disk Diameter	neg	neg	neg	neg
Disk Stack Height	0.00002	0.00003	neg	neg
CR Absorber Inner Diameter	neg	neg	neg	neg
CR Absorber Outer Diameter	neg	neg	neg	neg
CR Absorber Height	0.00001	-0.00002	0.00001	-0.00001
CR Clad Inner Diameter	neg	neg	neg	neg
CR Clad Outer Diameter	-0.00001	0.00001	neg	neg
CR Clad Height	-0.00003	-0.00004	-0.00001	-0.00001
CR Spine Diameter	neg	neg	neg	neg
Instrumentation Dimensions	-0.00084	0.00084	--	--
Block Flat-to-Flat Distance	-0.00006	0.00004	-0.00001	0.00001
Graphite Block Height	neg	neg	neg	neg
Dowel/Socket Dimensions	NA	NA	NA	NA
Fuel Channel Diameter	0.00006	-0.00006	neg	neg
Reflector Channel Diameter	neg	neg	neg	neg
Channel Pitch	-0.00003	0.00003	neg	neg

Table 2.86 (cont'd.). Total Experimental Uncertainty (Case 5).

Varied Parameter	Systematic Uncertainty		Random Uncertainty	
	$-\Delta k_{eff}$ (1σ)	$+\Delta k_{eff}$ (1σ)	$-\Delta k_{eff}$ (1σ)	$+\Delta k_{eff}$ (1σ)
Handling Socket Dimensions	NA	NA	NA	NA
Column Pitch	0.00001	-0.00001	neg	neg
CR Channel Diameter	neg	neg	neg	neg
CR Channel Pitch	neg	neg	neg	neg
Permanent Reflector Diameter	-0.00083	0.00024	--	--
Dummy Block Dimensions	See Sections 2.1.2.7 and 2.1.3.9			
3.4 wt.% Enrichment	-0.00054	0.00042	--	--
3.9 wt.% Enrichment	-0.00079	0.00079	--	--
4.3 wt.% Enrichment	-0.00133	0.00133	--	--
4.8 wt.% Enrichment	-0.00052	0.00051	--	--
5.2 wt.% Enrichment	-0.00039	0.00037	--	--
5.9 wt.% Enrichment	-0.00052	0.00047	--	--
6.3 wt.% Enrichment	-0.00030	0.00026	--	--
6.7 wt.% Enrichment	0.00006	0.00005	--	--
7.2 wt.% Enrichment	-0.00012	0.00011	--	--
7.9 wt.% Enrichment	-0.00008	0.00006	--	--
9.4 wt.% Enrichment	0.00006	0.00005	--	--
9.9 wt.% Enrichment	0.00006	0.00007	--	--
Oxygen to Uranium Ratio	0.00009	-0.00012	--	--
UO_2 Density	Correlated Parameter (see Section 2.1.6)			
UO_2 Impurity	0.00047	-0.00073	--	--
Buffer Density	neg	neg	neg	neg
Buffer Impurity	0.00009	-0.00012	--	--
IPyC Density	neg	neg	neg	neg
IPyC Impurity	0.00013	0.00009	--	--
SiC Density	NA	neg	NA	neg
SiC Impurity	neg	-0.00016	--	--
OPyC Density	neg	neg	neg	neg
OPyC Impurity	0.00020	-0.00023	--	--
Overcoat Density	-0.00001	0.00001	neg	neg
Overcoat Composition	NA	NA	NA	NA
Overcoat Impurity	0.00032	-0.00069	--	--
Compact Density	neg	0.00001	neg	neg
Compact Impurity	0.00009	-0.00065	--	--
Compact Free U Content	NA	neg	--	--

Table 2.86 (cont'd.). Total Experimental Uncertainty (Case 5).

Varied Parameter	Systematic Uncertainty		Random Uncertainty	
	$-\Delta k_{eff}$ (1σ)	$+\Delta k_{eff}$ (1σ)	$-\Delta k_{eff}$ (1σ)	$+\Delta k_{eff}$ (1σ)
Sleeve Density	-0.00005	0.00004	neg	neg
Sleeve Impurity	0.00031	-0.00031	--	--
BP Absorber Density	0.00009	-0.00011	neg	neg
BP Absorber Content, 2.0 wt.%	0.00075	-0.00066	0.00004	-0.00003
BP Absorber Content, 2.5 wt.%	0.00029	-0.00027	0.00002	-0.00002
BP Absorber Impurity	NA	0.00024	--	--
BP Isotopic Abundance of ^{10}B	0.00136	-0.00077	--	--
Graphite Disk Density	neg	neg	neg	neg
Graphite Disk Impurity	neg	0.00009	--	--
CR Absorber Density	neg	-0.00001	neg	neg
CR Absorber Content	0.00002	-0.00003	neg	neg
CR Absorber Impurity	NA	0.00004	--	--
CR Isotopic Abundance of ^{10}B	0.00009	0.00021	--	--
CR Clad Density	neg	0.00002	neg	neg
CR Clad Composition	0.00009	0.00009	--	--
CR Clad Impurity	NA	neg	--	--
Instrumentation Composition	See Section 2.1.2.6			
IG-110 Density in Blocks	-0.00074	0.00068	-0.00010	0.00009
IG-110 Impurity in Blocks	0.00490	-0.00584	--	--
PGX Density	-0.00009	0.00006	-0.00003	0.00002
PGX Impurity	0.00269	-0.00345	--	--
Dummy Block Density	0.00002	0.00002	-0.00002	-0.00001
Dummy Block Impurity	0.00217	-0.00124	--	--
Dummy Block Type	NA	0.00017	NA	0.00013
Helium Coolant Density	neg	neg	--	--
Helium Coolant Impurity	NA	neg	--	--
Room Return	neg	neg	neg	neg
TRISO Particle Placement	0.00068	0.00068	neg	neg
Block Stack Alignment	NA	NA	NA	NA
MCNP Random Number Seed	--	--	0.00017	0.00017
Uranium Fuel Mass (Sec. 2.1.6)	-0.00075	0.00073	-0.00003	0.00003
Uncertainty of Components	0.00675	0.00749	0.00024	0.00027
Total Evaluation Uncertainty	**0.00675**	**0.00750**		

2.2 Evaluation of Buckling and Extrapolation Length Data

Buckling and extrapolation length measurements were not made.

2.3 Evaluation of Spectral Characteristics Data

Spectral characteristics measurements were not made.

2.4 Evaluation of Reactivity Effects Data

Evaluation of the excess reactivity measurements of the HTTR annular core configurations is provided in Section 2.4.1 of HTTR-GCR-RESR-001.

2.5 Evaluation of Reactivity Coefficient Data

Reactivity coefficient measurements were not made.

2.6 Evaluation of Kinetics Measurements Data

Kinetics measurements were not made.

2.7 Evaluation of Reaction-Rate Distributions

The benchmark model for the critical configuration analyzed in Section 2.1 and described in Section 3.1 was utilized in the analysis of the reactor physics experiments in Section 1.7.

Monte Carlo n-Particle (MCNP) version 5.1.40 was utilized to predict the biases and uncertainties associated with the experimental results for HTTR critical configurations in this evaluation. MCNP is a general-purpose, continuous-energy, generalized-geometry, time-dependent, coupled n-particle, Monte Carlo transport code. The Evaluated Neutron Data File library, ENDF/B-VII.0, was utilized in analysis of the benchmark model biases and uncertainties.

It should be noted that the neutron flux could not be measured directly in the core, but the fission chambers (FCs), containing ^{235}U, were used to indirectly measure the flux as fission reaction rates. A fixed FC in one of the instrumentation columns was used to normalize the reaction-rate measurements from the FC that was moved to various positions in another column. This was to account for variation in the flux due to movement effects of the detector and its respective components.

2.7.1 Axial Reaction Rate Distribution

The axial fission neutron reaction-rate distribution in Figures 1.5 for the two annular 24-fuel-column cores were digitized and renormalized to allow for further comparative analysis with computational results. The digitization of the charts was performed by Chris White at the Idaho National Laboratory using Marisoft Digitizer.[a] The chart is imported into the program and bound within a grid system; each individual data point is then marked and exported as numerical data. Table 2.87 and Figures 2.8 and 2.9 represent the digitized data. A comprehensive analysis of the axial neutron reaction-rate distribution in the instrumentation columns of the fully-loaded, 30-fuel-column core has already been performed

[a] M. Mitchell, Marisoft Digitizer Application Version 3.3, http://digitizer.sourceforge.net/, © 1997.

(Section 2.7.1 of HTTR-GCR-RESR-001). The uncertainty in the reaction-rate measurements of the fully-loaded core were used to generate an estimate of the uncertainties in the 24-fuel-column core measurements by fitting the data to a trend, as shown in Figure 2.10. The uncertainty in the normalized reaction rates is proportional to the magnitude of the ratio. There is less uncertainty in values near the peak of the neutron flux and significantly more uncertainty for lower fluxes near the edge of the core. A log trend fit is obtained to approximate the uncertainty as a function of normalized reaction rate. The uncertainties in the 24-fuel-column core reaction rates were then estimated using this trend and provided in Table 2.87.

Table 2.87. Axial Neutron Fission Reaction-Rate Distribution Data for the Annular 24-Fuel-Column Core Configurations.

Data Point	Configuration 3[a]					Configuration 4[a]				
	Normalized Reaction Rate	±	1σ	1σ (%)	Height (cm)[b]	Normalized Reaction Rate	±	1σ	1σ (%)	Height (cm)[b]
1	0.6946	±	0.0199	2.87	18.89	0.7030	±	0.0199	2.83	18.79
2	0.7304	±	0.0198	2.70	27.86	0.7383	±	0.0197	2.67	28.40
3	0.9555	±	0.0173	1.81	86.07	0.9523	±	0.0174	1.83	86.36
4	1.0000	±	0.0166	1.66	130.96	1.0000	±	0.0166	1.66	115.79
5	0.9854	±	0.0169	1.71	137.15	0.9749	±	0.0170	1.75	137.45
6	0.9750	±	0.0170	1.75	143.96	0.9562	±	0.0173	1.81	144.57
7	0.6735	±	0.0200	2.97	202.48	0.7915	±	0.0193	2.44	202.72
8	0.2818	±	0.0165	5.86	260.99	0.5582	±	0.0201	3.59	260.85
9	0.1041	±	0.0095	9.16	318.58	0.3312	±	0.0176	5.32	318.37

(a) The 24-fuel-column core reaction-rate data are from the top and middle charts, respectively, in Figure 1.6.
(b) The height is in reference to the position relative to the bottom of the fifth layer of fuel.

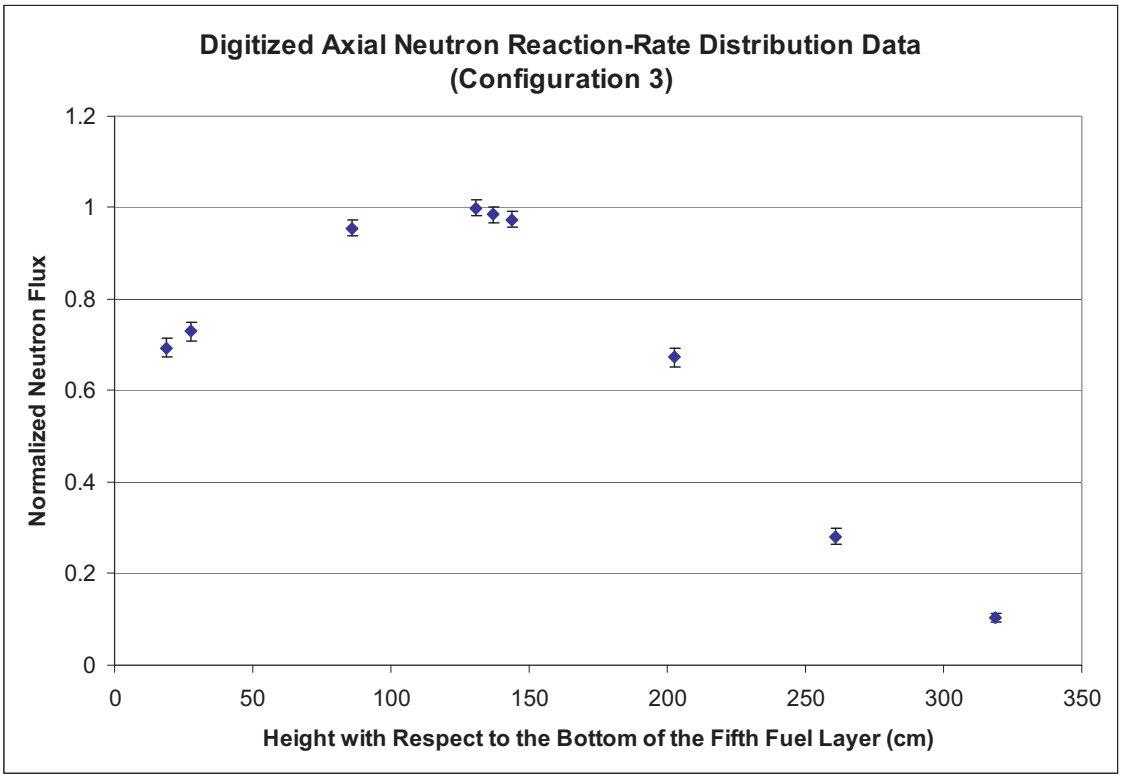

Figure 2.8. Axial Neutron Reaction-Rate Distribution for the Annular 24-Fuel-Column Core (Configuration 3).

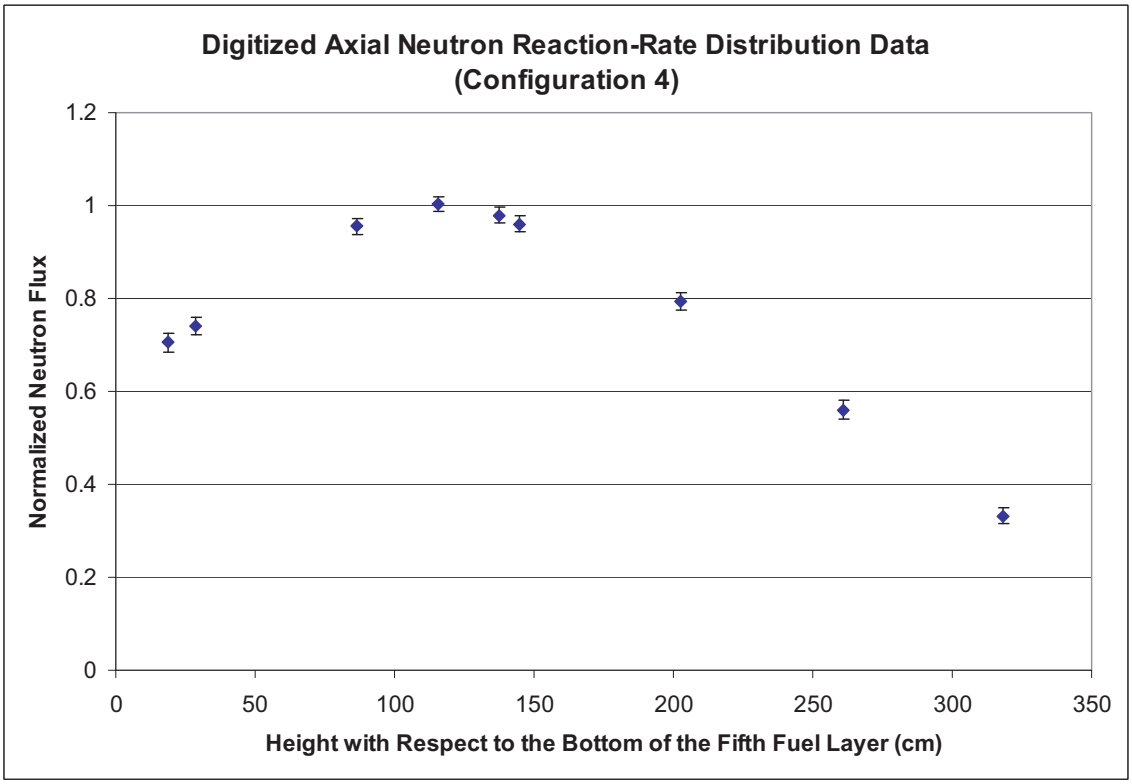

Figure 2.9. Axial Neutron Reaction-Rate Distribution for the Annular 24-Fuel-Column Core (Configuration 4).

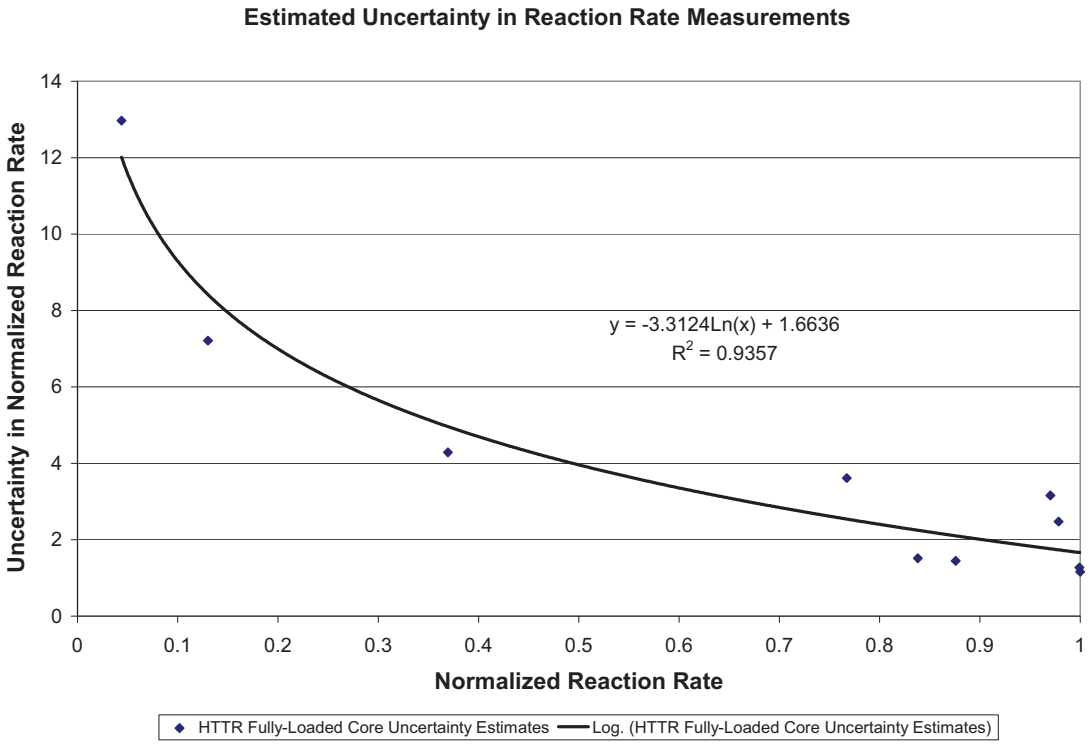

Figure 2.10. Uncertainty Trend Estimated with HTTR Fully-Loaded-Core Analysis.

The axial neutron fission reaction rate in the instrumentation columns were calculated by taking the benchmark model of the 24-fuel-column cores (configurations 3 and 4) in Section 3.1 and superimposing a flux tally over each of the instrumentation column positions: E05, E13, and E21. The flux was computed for 6.15-cm radius discs with a thickness of 1 cm located at the center of one instrumentation channel in each instrumentation column (see Figure 2.11). A total of 522 cm, representing the total height of the core fuel and reflector blocks, was modeled. The (x, y) coordinates used for columns E05, E13, and E21, are (114.6005, 72.4), (5.4, -135.447), and (-120, 63.04693), respectively, where the origin is located at the radial center of the core.

The F4 flux tally is used in MCNP, which determines the flux across a cell volume by tabulating the average track length of the neutrons.[a] The tally is then modified by a tally multiplier card, Fm, that accounts for the total fission cross section of ^{235}U, the fissile material in the fission chambers, to obtain the neutron reaction-rate in each instrumentation column.

The calculated neutron fission reaction rates are obtained by taking the variance-weighted average of results obtained using six variations of the input deck (Appendix A.1) with different random number seeds and tallies of the neutron reaction rate (Appendix A.3). This approach was used to reduce the statistical uncertainty in the neutron flux tallies because the relative error values obtained can underpredict the true uncertainty in the calculated neutron flux.[b] Therefore, the final calculated values are obtained from a total of 18 reaction-rate tallies (6 input decks with 3 instrumentation columns each).

[a] X-5 Monte Carlo Team, "MCNP – A General Monte Carlo N-Particle Transport Code, Version 5, Volume II: User's Guide," LA-CP-03-0245 (April 24, 2003; revised October 2, 2005).

[b] F. B. Brown, "A Review of Best Practices for Monte Carlo Criticality Calculations," *Proc. NCSD 2009*, Richland, WA, September 13-17 (2009).

The average of the neutron reaction rate in each position is taken and normalized to represent the calculated axial neutron reaction-rate profile.

$$\phi(z)_{normalized} = \frac{\phi(z)}{\phi_{maximum}},$$

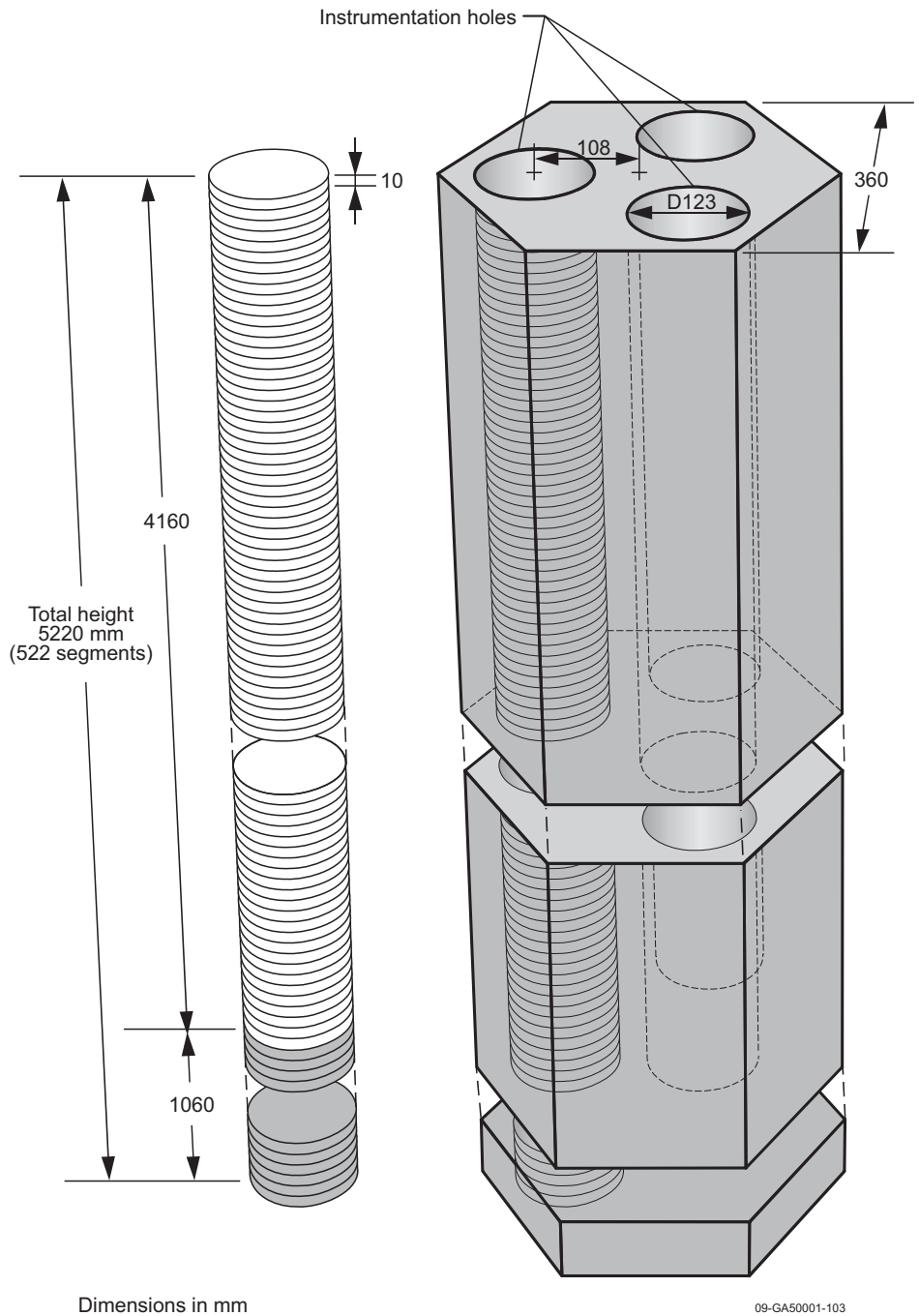

Fig 2.11. Placement of Axial Flux Tally in the Instrumentation Column.

2.8 Evaluation of Power Distribution Data

Power distribution measurements were not made.

2.9 Evaluation of Isotopic Measurements

Isotopic measurements were not made.

2.10 Evaluation of Other Miscellaneous Types of Measurements

Other miscellaneous types of measurements were not made.

3.0 BENCHMARK SPECIFICATIONS

3.1 Benchmark-Model Specifications for Critical and / or Subcritical Measurements

Whereas insufficient information is publicly available, a finely-detailed benchmark model could not be established. A benchmark of the HTTR was prepared and analyzed with as much detail as feasible. The simplification bias for this model could also not be fully determined. However, the uncertainties in the benchmark model are believed to be of sufficient magnitude to encompass any biases incurred due to the simplification process of the benchmark model and a bias for the removal of the core instrumentation has been estimated. It is currently difficult to obtain the necessary information to improve the confidence in the benchmark model; the necessary data is proprietary and its released is being restricted, because the benchmark configuration of the HTTR core is the same that is currently in operation. Once this information is made available, the HTTR benchmark can be adjusted as appropriate.

Models for all five configurations of the annular HTTR core are provided. The five configurations, or cases, in this benchmark analysis use four core layouts, with the third core layout implementing two different control rod positionings. Configuration 1 has 19 fuel columns. Configuration 2 has 21 fuel columns. Configurations 3 and 4 have 24 fuel columns. Configuration 5 has 27 fuel columns. Analysis of the fully-loaded, 30-fuel-column, core can be found in HTTR-GCR-RESR-001.

3.1.1 Description of the Benchmark Model Simplifications

Significant simplifications were incurred to develop a benchmark model of the HTTR because of a lack of information publicly available to determine dimensions and compositions. Simplifications will be discussed where applicable in the descriptions of the dimension and material properties of the model.

As stated previously, biases of the model were not assessed but will be addressed as additional HTTR information becomes available. Biases that have been partially investigated are listed in Section 3.1.1.1.

The fuel handling positions, dowels, and sockets were not included in the model due to insufficient data specifications, but were accounted for with a void fraction of 0.5 % reduction in graphite density (based upon volume calculations using dimensions provided in Figure 1.52 of HTTR-GCR-RESR-001). The burnable poison insertion holes were placed on the same pitch as the fuel channels to simplify the model.

It is apparent from a comparison of Figures 1.65 and 1.67 of HTTR-GCR-RESR-001 that the depth to which the control rod, reserve shutdown system, and instrumentation holes are drilled varies. A depth of 1060 mm above the bottom of the core was selected for all positions to simplify the model. No bias was assessed.

Insufficient information was available to model the bottom-most reflector block according to actual design; therefore it was modeled with the same design as the two top reflector blocks and the other bottom reflector block. The top and bottom of each coolant channel is expected to taper from the 21-mm diameter to the 41-mm diameter of the fuel assemblies, but information was unavailable to describe the taper in the model. Therefore channels in the reflector blocks were modeled with 21-mm diameters.

Individual sections of the dodecagon-block-shaped permanent reflector were not modeled due to insufficient information. It was modeled as a cylindrical region surrounding the core columns. A bias could not be assessed.

Insufficient information was available to model the shielding blocks surrounding the core and shielding plugs in the core. Therefore, they were not included in the benchmark model. It is assumed that all neutrons reaching the core boundaries are lost and not scattered back by the shielding material. A conservative estimate of room-return effects demonstrated a negligible change in k_{eff}.

In the materials section, impurity contents in the materials are based upon natural boron equivalency. In the model, however, only the ^{10}B component is included, as the effect of the ^{11}B content would be insignificant.

The density is the same (1.80 g/cm^3) for both types of burnable poison pellets. The boron content in the pellets is based on the reported weight percents instead of the atomic percents.

Partially-withdrawn control rod positions represent the average height of the values reported in Table 1.1, which are reported in Table 1.2 except for configuration 4. The average height for the partially-withdrawn rods in configuration 4 is taken to be 1592 mm. Fully-withdrawn rod positions are 4050 mm for all rods except those in the R2 positions; their maximum withdrawal height is 3325 mm.

Too much information was available to specify parameters for the TRISO particle fuel. Because the fuel mass of an individual rod would most probably be the most accurate measured parameter, it was preserved in the benchmark model with some variation to other parameters as necessary. The TRISO kernel diameter is maintained at the nominal value of 600 μm and the density of the fuel is 10.39 g/cm^3, which is within approximately 95% of the theoretical density of UO_2. The number of TRISO particles in a given compact was reduced from 13,000 to 12,987, with a packing fraction of 30 %, in order to conserve a nominal fuel mass per rod of 188.58 g.

3.1.1.1 Assessed Biases

Although some biases have been partially investigated, there is incomplete information regarding the HTTR to properly address simplification biases in order to adjust the benchmark k_{eff}. As stated previously, a conservative estimate of potential room-return effects provided negligible results. As shown in Section 2.1.3.2 in Table 2.52, the effect of neglecting the free uranium content of the fuel compacts was negligible. Finally, the effect of modeling the helium coolant as void material was also negligible (as shown in Section 2.1.3.10, Table 2.77). The reported literature bias for air content in the graphite could not be verified (Section 2.1.3.7).

Previous efforts of the Japanese in analyzing the 19-fuel-column core (Case 1) obtained an analytical excess reactivity of 2.7 % Δk/k, with an estimated Monte Carlo calculation overestimate of 1.2 % Δk/k.[a] Additional information would be necessary to completely verify published results

An approximate bias for the removal of reactor instrumentation from the three instrumentation columns in the core was calculated, as discussed in Section 2.1.2.6. Calculated biases with uncertainties are shown in Table 3.1.

[a] Fujimoto, N., Nakano, M., Takeuchi, M., Fujisaki, S., and Yamashita, K., "Start-Up Core Physics Tests of High Temperature Engineering Test Reactor (HTTR), (II): First Criticality by an Annular Form Fuel Loading and Its Criticality Prediction Method," *J. Atomic Energy Society Japan*, **42**(5), 458-464 (2000).

Table 3.1. Estimated Bias for the Removal of Instrumentation Components.

Case	Δk	$\pm$	$\sigma_{\Delta k}$
1	0.00483	±	0.00139
2	0.00403	±	0.00116
3	0.00348	±	0.00100
4	0.00315	±	0.00091
5	0.00291	±	0.00084

3.1.2 Dimensions

3.1.2.1 Prismatic Pin-in-Block Fuel

TRISO Particles

The basic ingredient for HTTR fuel is the TRISO particle. A UO_2 kernel is surrounded by four coatings: a low density porous pyrolytic carbon (PyC) buffer layer, a high density inner isotropic PyC layer, a SiC layer, and a final outer PyC layer. A resinated graphite overcoat is then deposited around each TRISO particle. Figure 3.1 depicts the TRISO layers and their respective dimensions.

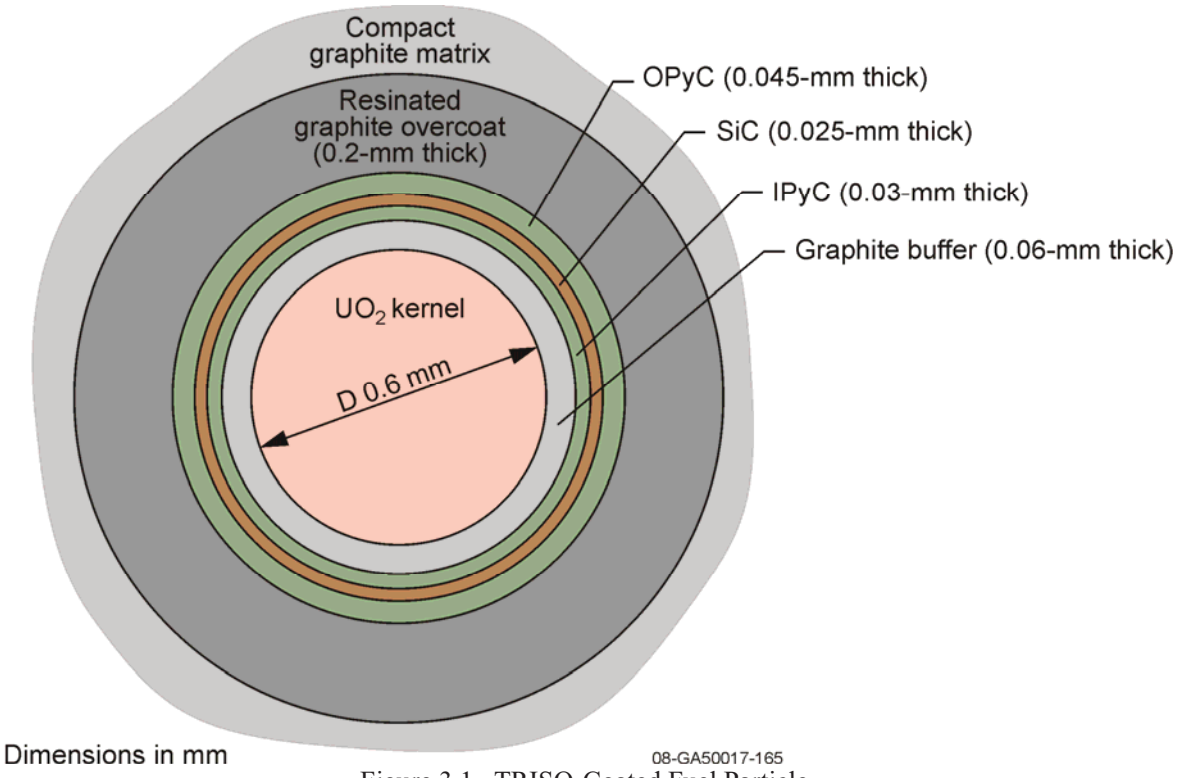

Figure 3.1. TRISO-Coated Fuel Particle.

Compacts

All fourteen fuel compacts in a single fuel pin are modeled as a single unit filled with the TRISO lattice. The stacked compacts have an inner diameter of 1 cm, an outer diameter of 2.6 cm, and an overall height of 54.6 cm.

A horizontal cross section of the compacts is shown in Figure 3.2. In the benchmark model, 12,987 TRISO particles are randomly distributed throughout the compact matrix in a single compact. For a stack of 14 compacts, as modeled in this benchmark, the total number of TRISO particles is 181,818.

A key parameter is that the total fuel mass of a single fuel rod (14 stacked compacts) is approximately 188.58 g.

While the benchmark model retains randomness in distribution, many computer codes cannot properly model such configurations. It is up to the user to determine which method is most appropriate while accounting for its impact on the reactivity of the model. Example means for analyzing this model are provided in Section 4.1. The difference in methods for accurately modeling random TRISO particles in a full-core reactor has been discussed in Section 2.1.4.2.

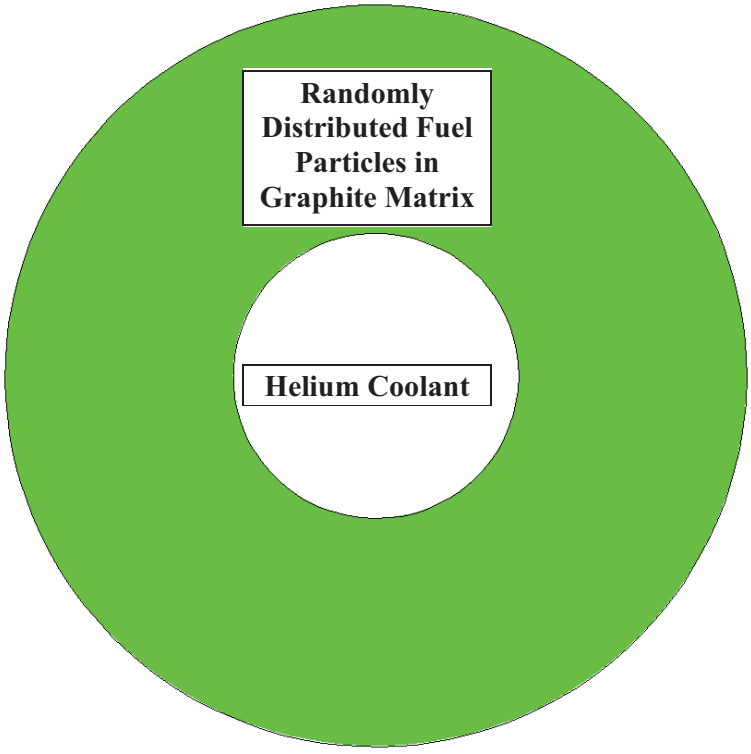

Figure 3.2. Fuel Compact Filled with Randomly Distributed TRISO Particles (Particles Not Shown).

Fuel Element

A description of the HTTR fuel element is modeled (Figure 3.3).

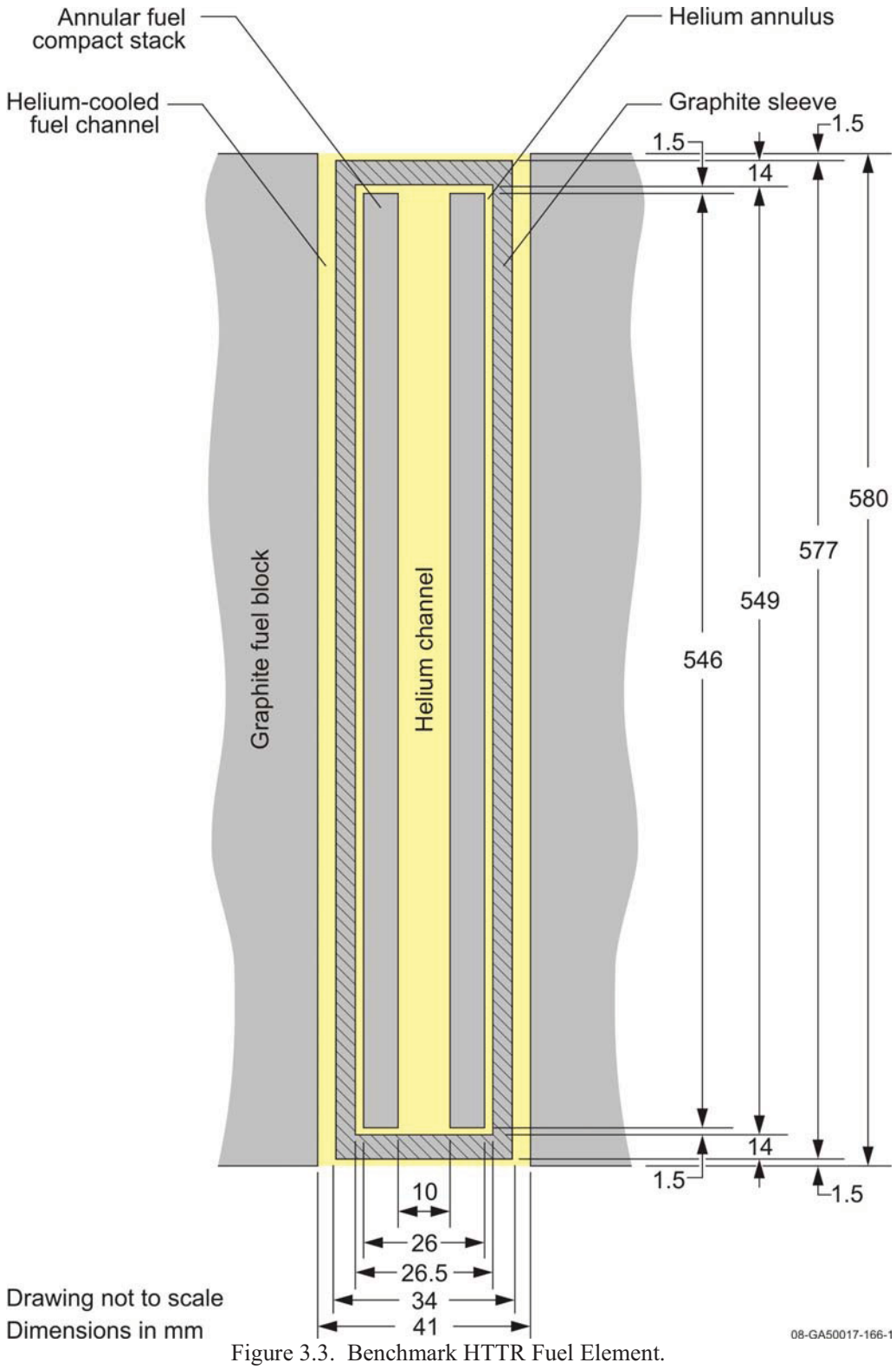

Figure 3.3. Benchmark HTTR Fuel Element.

3.1.2.2 Burnable Poisons

The burnable poison pellets and graphite disks were modeled as individual stacks contained within a pin position in the fuel blocks (Figure 3.4). Each fuel block contained two BP pins and one empty pin position.

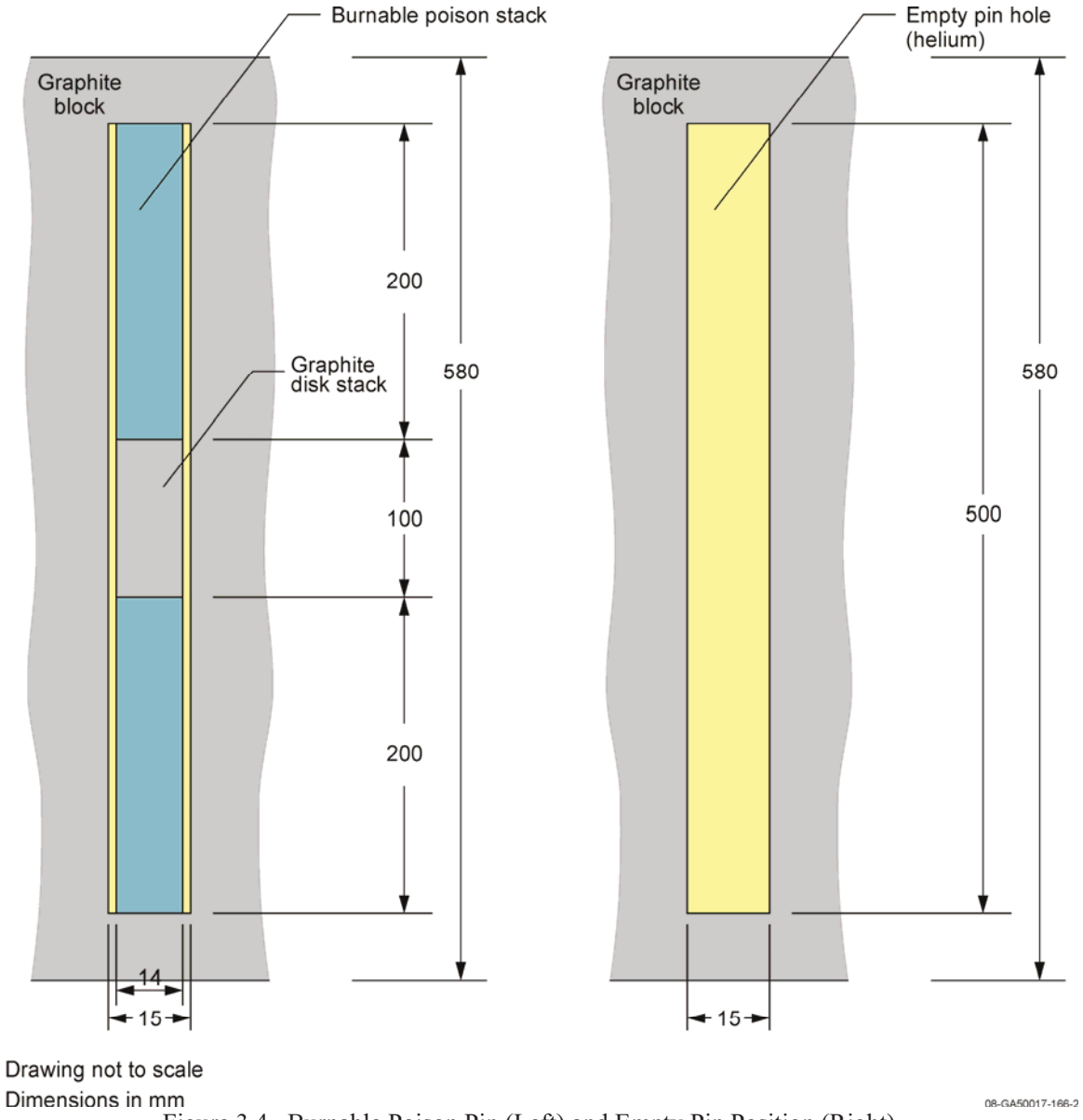

Figure 3.4. Burnable Poison Pin (Left) and Empty Pin Position (Right).

3.1.2.3 Fuel Blocks

The HTTR contains two types of regular hexagonal fuel blocks: 33-pin (Zones 1 and 2) and 31-pin (Zones 3 and 4). Diagrams of each fuel block design implemented in the benchmark model are shown in Figures 3.5 and 3.6, respectively. The pitch for all positions is 51.5 mm.

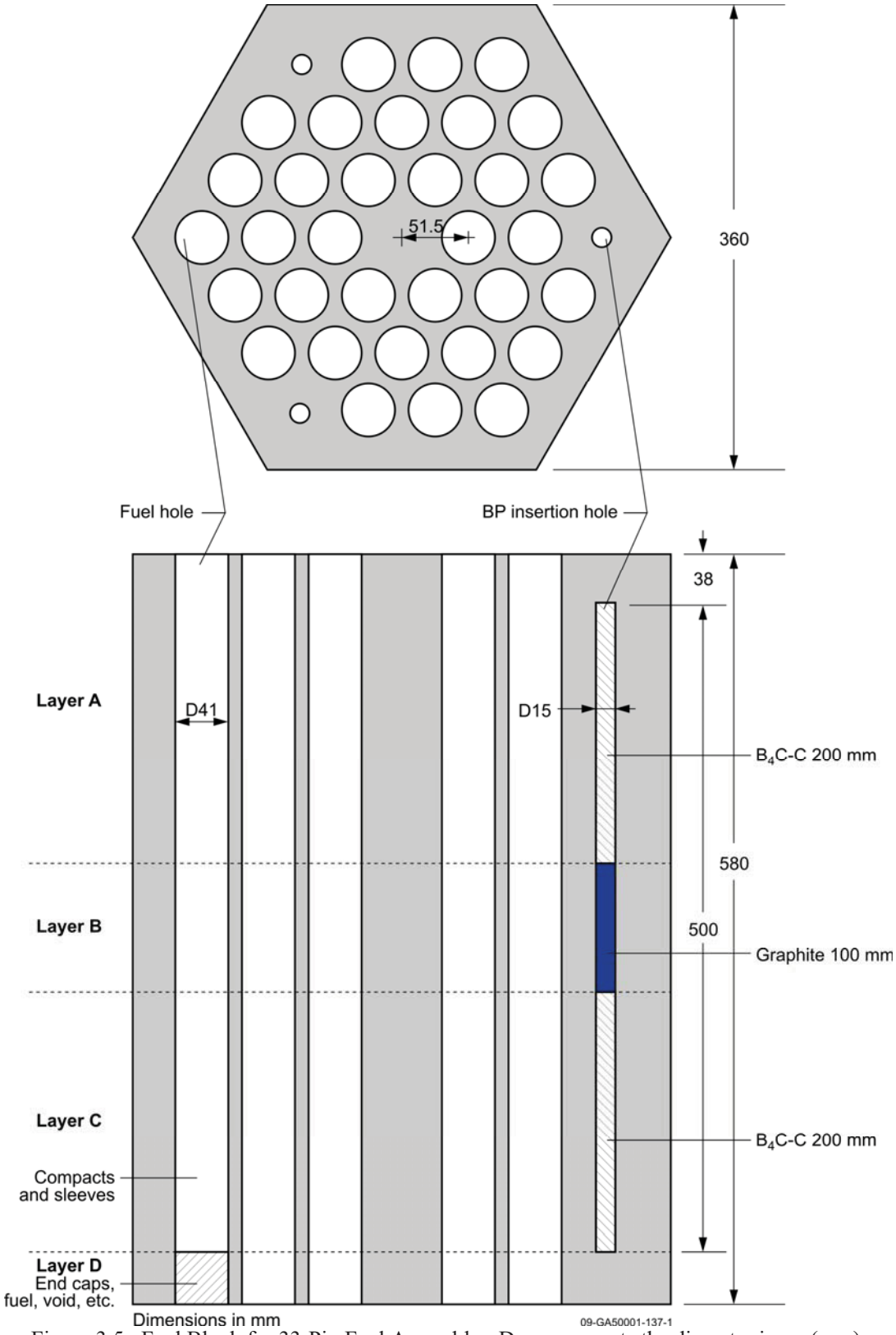

Figure 3.5. Fuel Block for 33-Pin Fuel Assembly. Dxx represents the diameter in xx (mm).

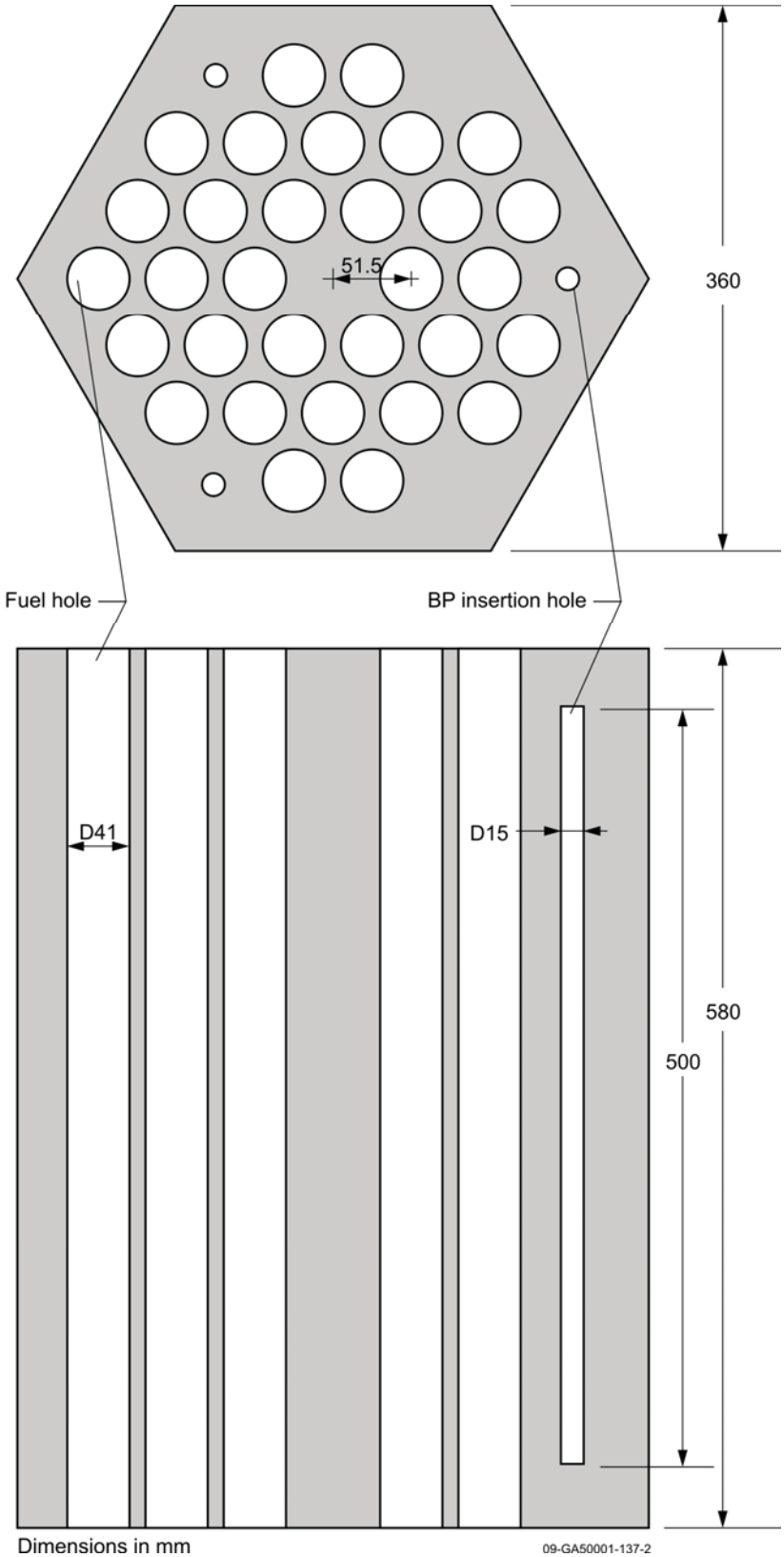

Figure 3.6. Fuel Block for 31-Pin Fuel Assembly. Dxx represents the diameter in xx (mm).

3.1.2.4 Dummy Blocks

The HTTR contains regular hexagonal dummy blocks. A diagram of the dummy block design implemented in the benchmark model is shown in Figure 3.7.

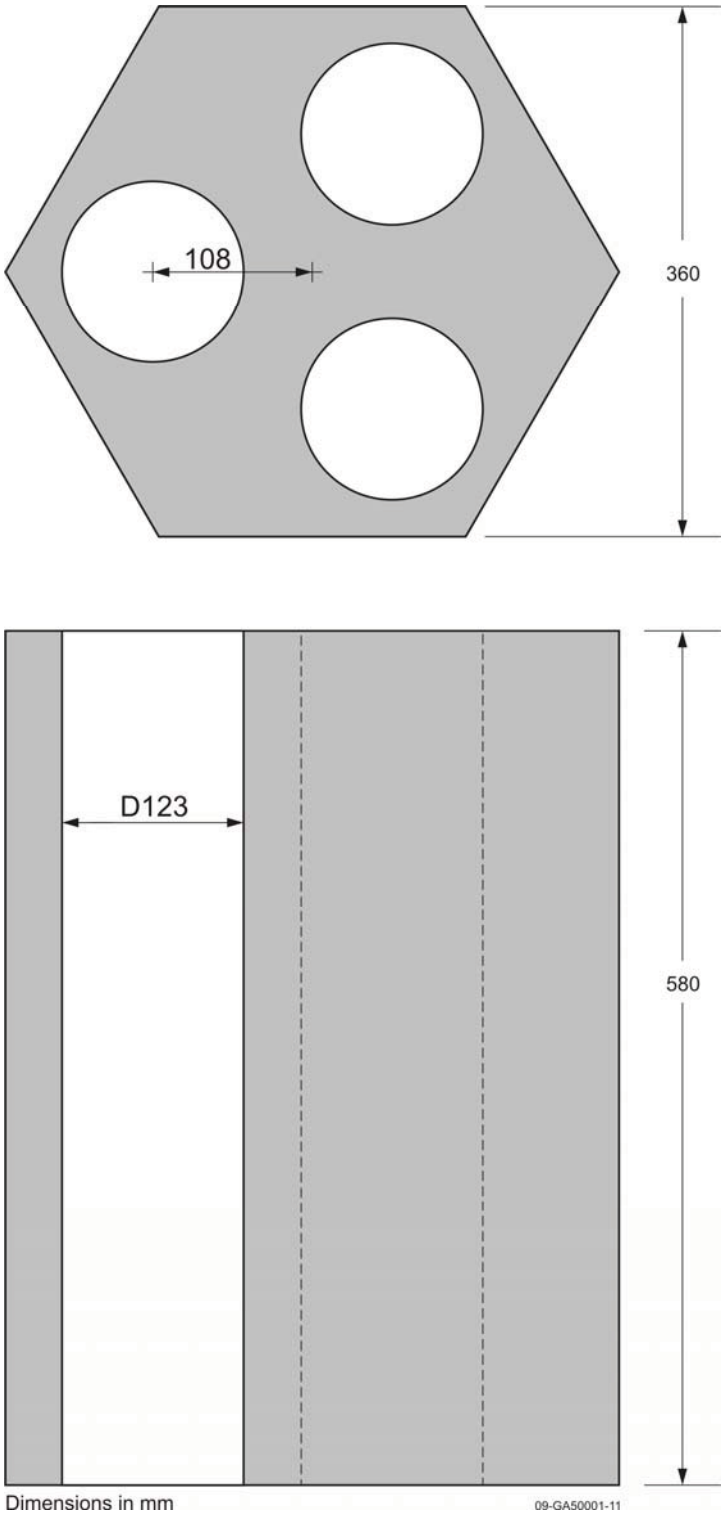

Figure 3.7. Dummy Block. Dxx represents the diameter in xx (mm).

3.1.2.5 Control Rod System

Control Rods

A diagram of a control rod section is shown in Figure 3.8. The absorber compacts are modeled as a single unit. Detailed dimensions regarding the cladding infrastructure for each section was unavailable, and the clad is therefore modeled without detail. A single control rod is comprised of ten sections (Figure 3.9) with a total height of 3.1 m.

The control rods are divided up into four sets: center position (C), ring 1 (R1), ring 2 (R2), and ring 3 (R3). The center position contains two control rods. The other rings are comprised of six, six, and three positions, containing a total of twelve, twelve, and six control rods, respectively. Control rods in each set are synchronously moved.

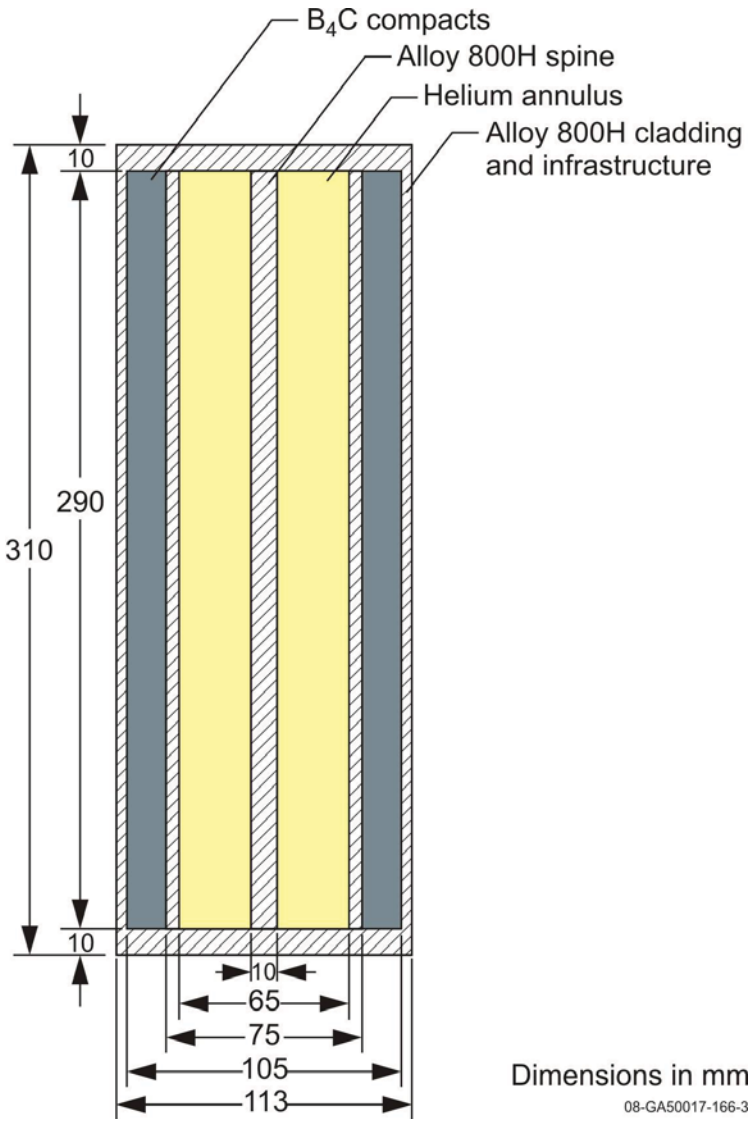

Figure 3.8. Control Rod Section.

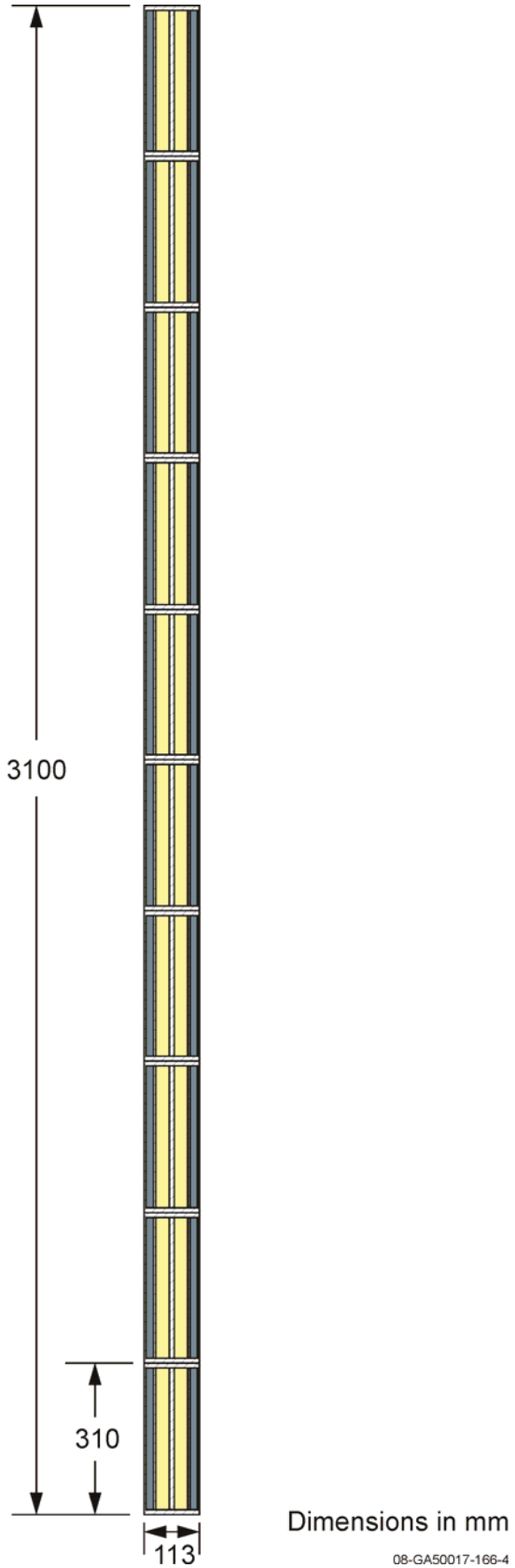

Figure 3.9. Control Rod Comprised of Ten Sections.

Control Rod Columns

Individual control rod blocks were not modeled. A single control rod column was modeled with three holes to accommodate two control rods and an empty position (for the reserved shutdown system). A diagram of a generic control column (without control rods) is shown in Figure 3.10. The holes in the control rod and instrumentation columns are equidistant from each other, with an angle of 120º.

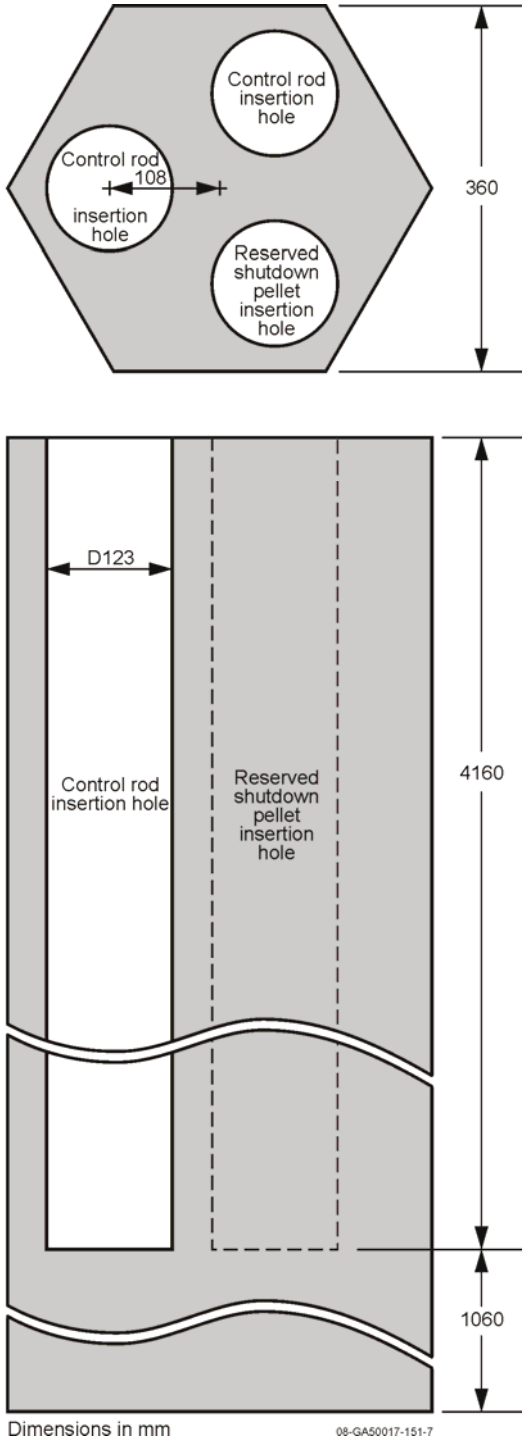

Figure 3.10. Control Rod Column. Dxx represents the diameter in xx (mm).

3.1.2.6 Instrumentation

Instrumentation Components

Instrumentation was not included in the benchmark model of the HTTR. An approximate bias with uncertainty was determined applied to the benchmark model (see Sections 2.1.2.6 and 3.1.1.1).

Instrumentation Columns

Instrumentation columns are modeled as a single unit without blocks, similar to the control rod columns. However, all three positions are empty (Figure 3.11).

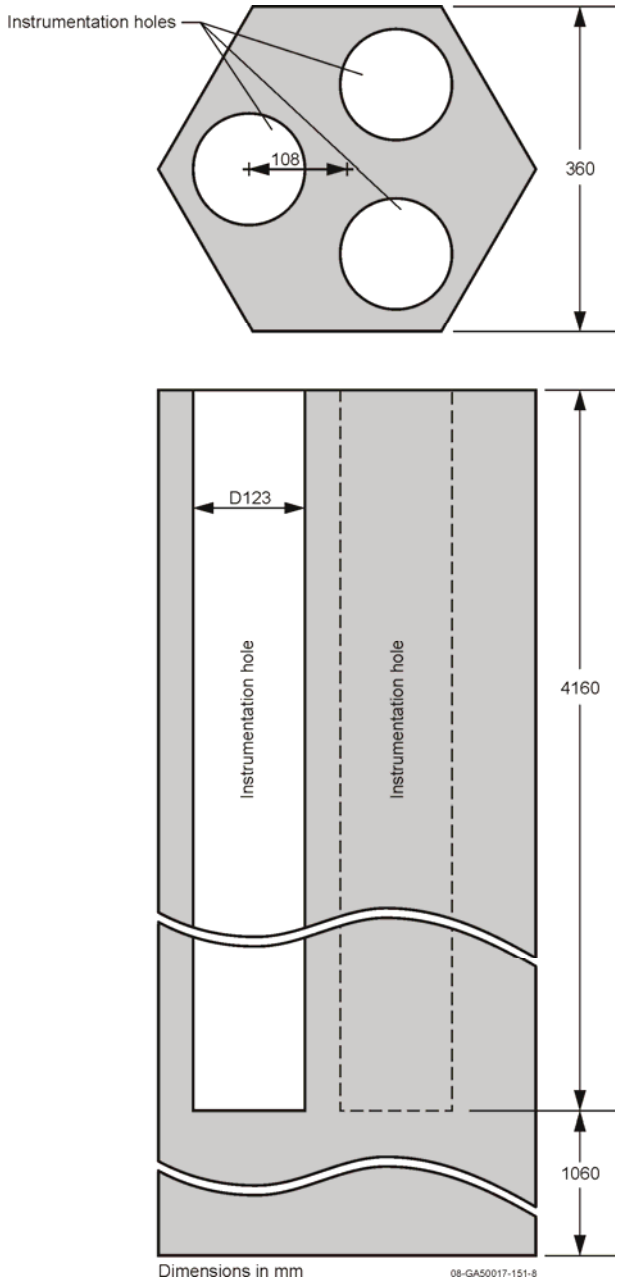

Figure 3.11. Instrumentation Column. Dxx represents the diameter in xx (mm).

3.1.2.7 Replaceable Reflector Columns

The replaceable reflector columns are modeled as a solid unit and not as individual blocks, similar to the control rod and instrumentation columns but without any channels (Figure 3.12).

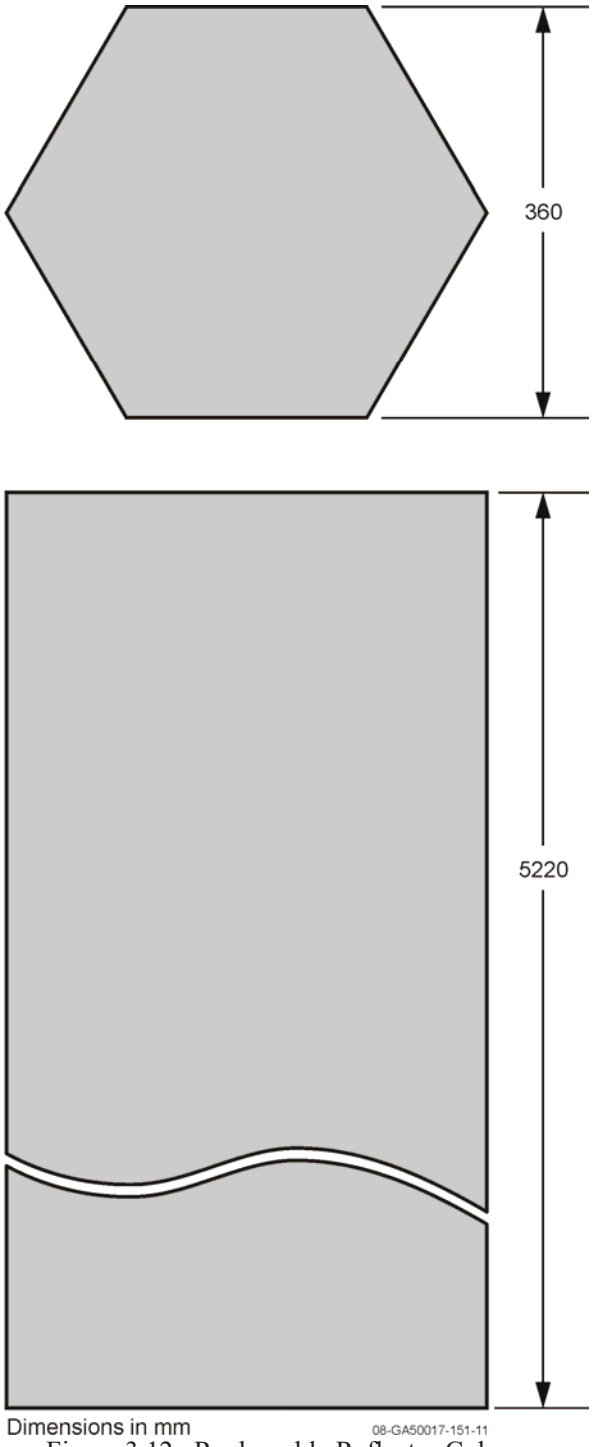

Figure 3.12. Replaceable Reflector Column.

3.1.2.8 Replaceable Reflectors Blocks in Fuel Columns

The replaceable reflector blocks, located at the top and the bottom fuel columns, are shown in Figures 3.13 and 3.14, for the 33-pin and 31-pin fuel assemblies, respectively. The replaceable reflector blocks have the same regular hexagonal shape and pitch as described for the fuel blocks.

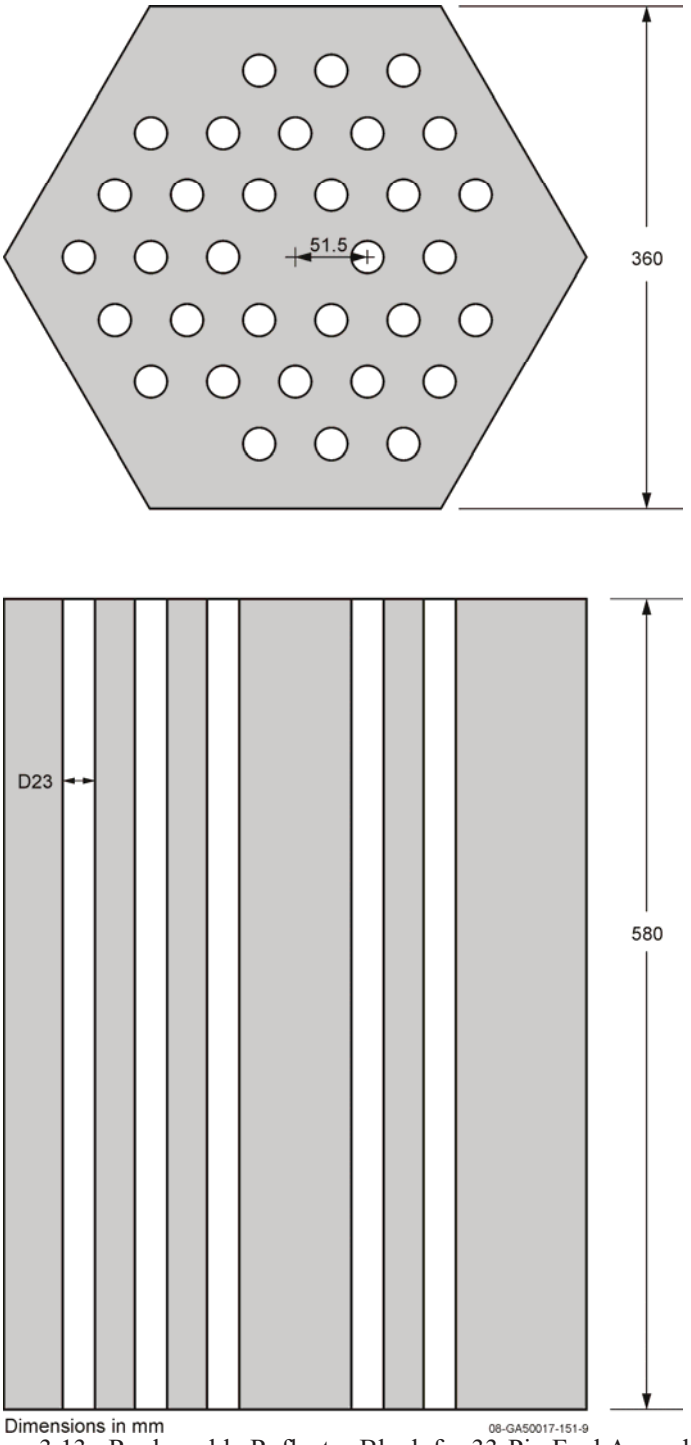

Figure 3.13. Replaceable Reflector Block for 33-Pin Fuel Assembly.
Dxx represents the diameter in xx (mm).

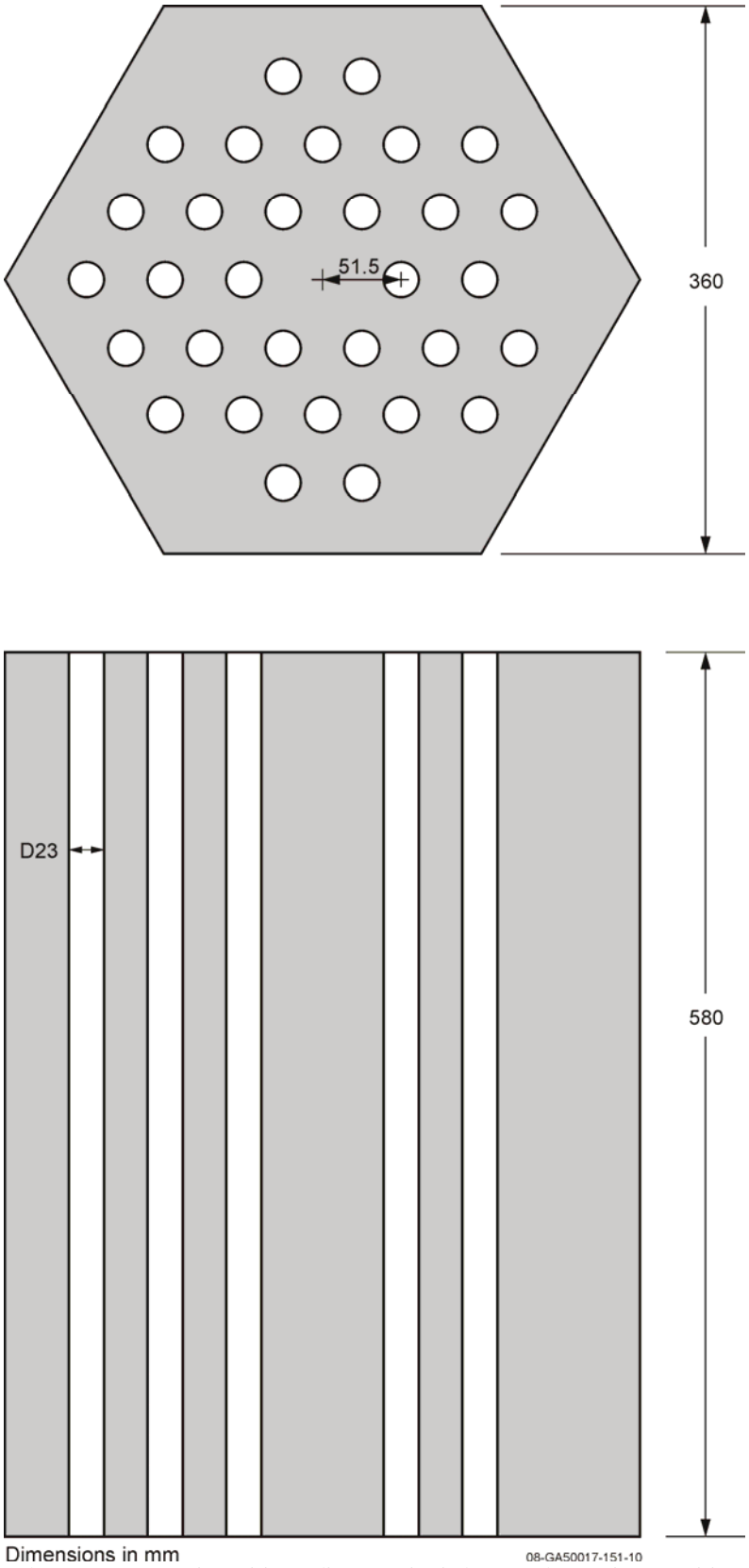

Figure 3.14. Replaceable Reflector Block for 31-Pin Fuel Assembly. Dxx represents the diameter in xx (mm).

3.1.2.9 Fuel Columns

The fuel columns are separated into four zones (as shown in Figure 1.46 of HTTR-GCR-RESR-001). Each zone has a specified pattern of uranium enrichment. Each column contains two top replaceable reflector blocks (Figure 3.13 for Zones 1 and 2 or Figure 3.14 for Zones 3 and 4), five fuel blocks (Figure 3.5 for Zones 1 and 2 and Figure 3.6 for Zones 3 and 4), and two bottom replaceable reflector blocks (Figure 3.13 for Zones 1 and 2 or Figure 3.14 for Zones 3 and 4). The second and third fuel blocks from the top contain burnable poison pellets that are more enriched than the pellets in the other three positions. Figure 3.15 shows the enrichment of the uranium (wt.%) in the TRISO fuel (upper left) and the natural boron content (wt.%) in the burnable pellets (lower right).

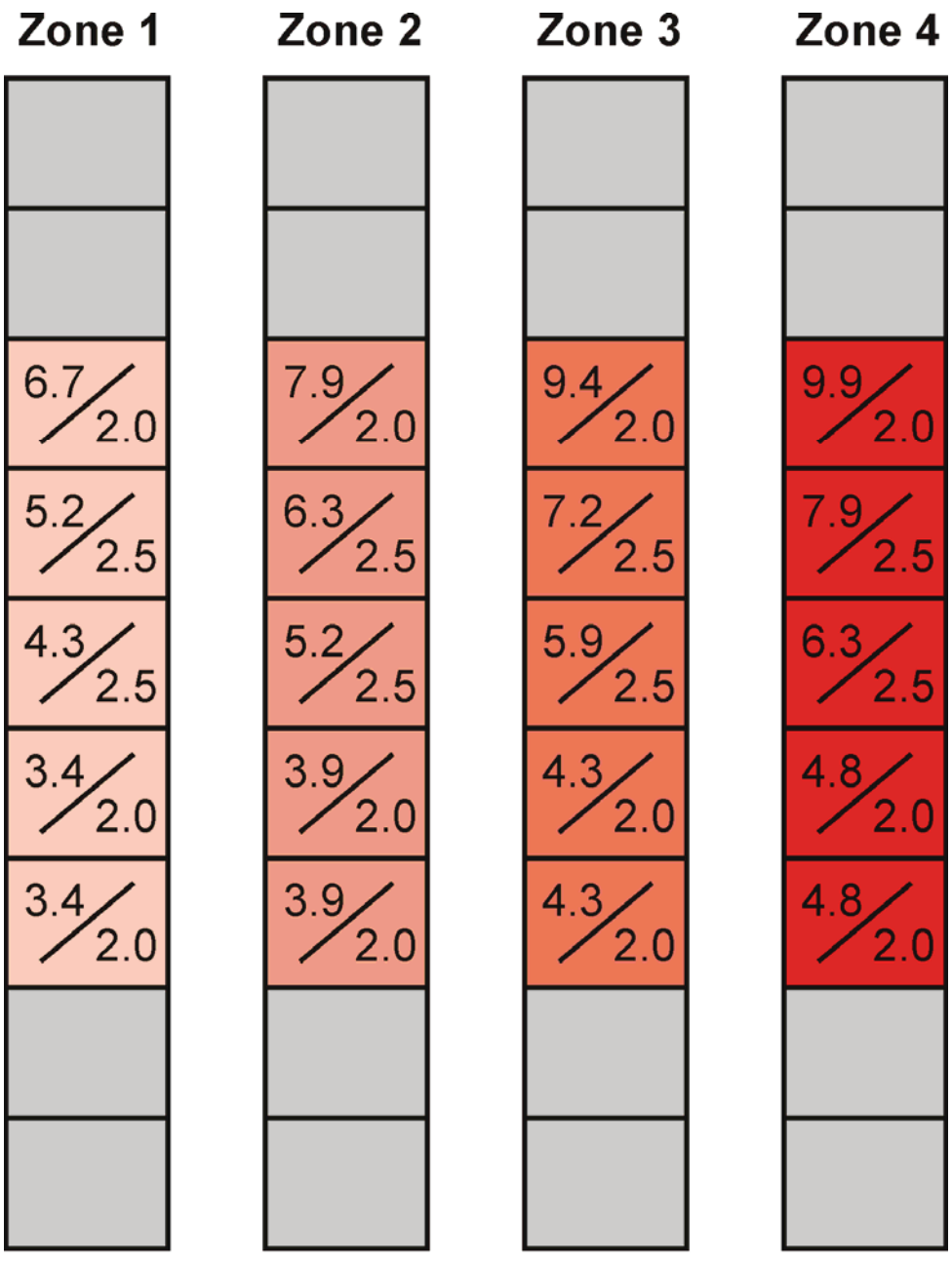

Figure 3.15. HTTR Fuel Zones.

3.1.2.10 Dummy Fuel Columns

The dummy fuel columns are similar to the fuel columns shown in Figure 3.15 except that the fueled blocks are replaced with dummy fuel blocks. Each column therefore contains two top replaceable reflector blocks (Figures 3.13 or 3.14 if replacing Zones 1 and 2 or Zones 3 and 4, respectively), five dummy blocks (Figure 3.7), and two bottom replaceable reflector blocks (Figures 3.13 or 3.14). A dummy fuel column is shown in Figure 3.16.

Figure 3.16. HTTR Dummy Fuel Zone.

3.1.2.11 Reactor Core Configuration

Figures 3.17 through 3.20 are included to provide an understanding of the final configuration of the reactor. All of the annular core configurations have the same configuration and orientation as the fully-loaded core, but with dummy fuel columns in place of some of the fuel columns, as shown in Figures 3.21 through 3.24.

The HTTR fully-loaded, 30-fuel-column, core configuration (HTTR-GCR-RESR-001) is shown in Figures 3.17, 3.18, 3.19. The first figure identifies the positions in the core for a given column type. The second figure provides the orientation of each column within its respective position in the core. The third figure shows the column identification number for each position in the core. Figure 3.20 shows a basic cross section of the HTTR fully-loaded core generated in MCNP.

The five configurations in this benchmark analysis use four core layouts, with the third core layout implementing two different control rod positions. Configuration 1 (Figure 3.21) has 19 fuel columns and 11 dummy fuel columns. Configuration 2 (Figure 3.22) has 21 fuel columns and 9 dummy fuel columns. Configurations 3 and 4 (Figure 3.23) have 24 fuel columns and 6 dummy fuel columns. Configuration 5 (Figure 3.24) has 27 fuel columns and 3 dummy fuel columns.

The permanent reflector surrounding the core has been circularized with a radius of 2125 mm and height of 5220 mm.

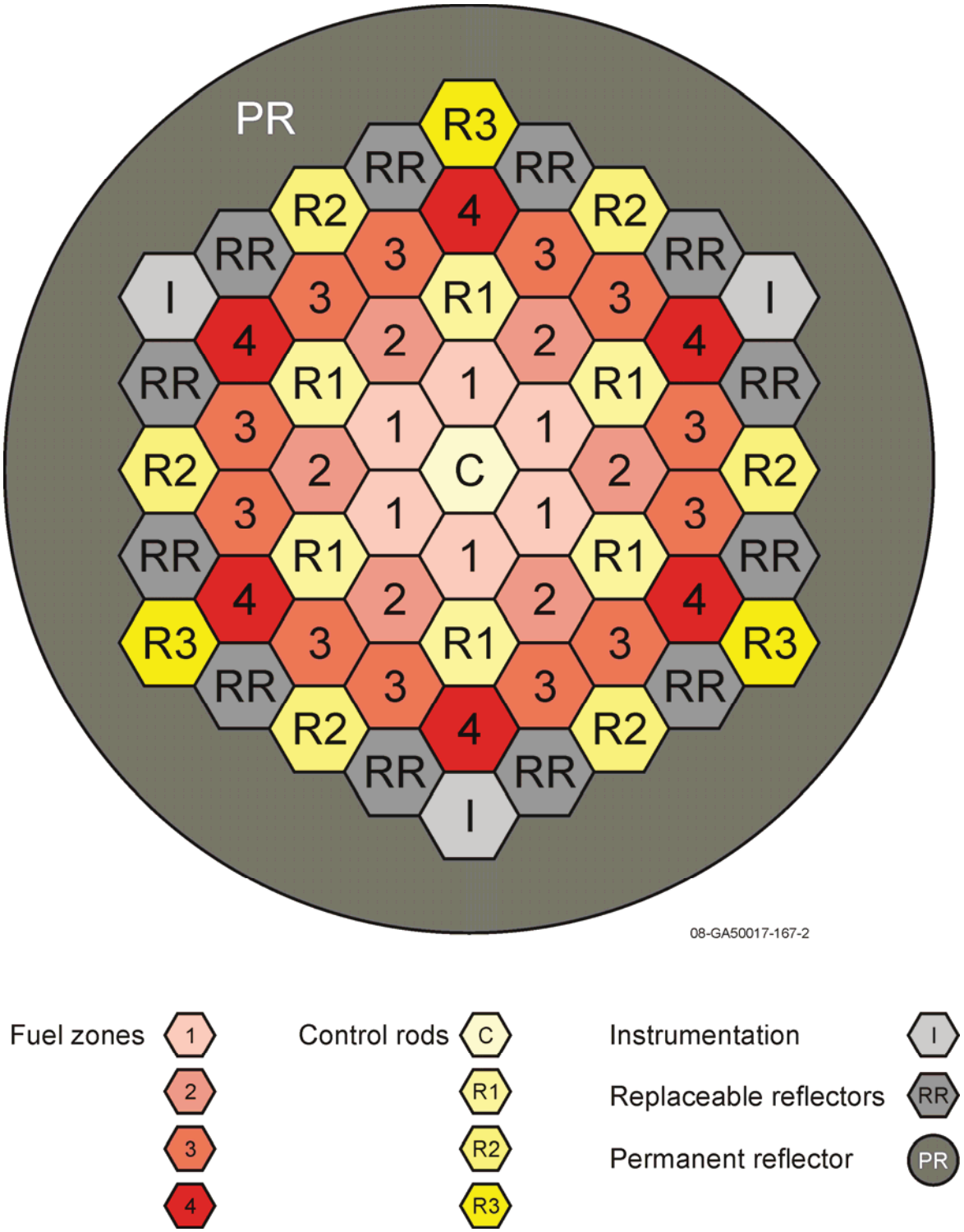

Figure 3.17. HTTR Core Positions (Fully-Loaded, 30-Fuel-Column Core – No Dummy Fuel Columns).

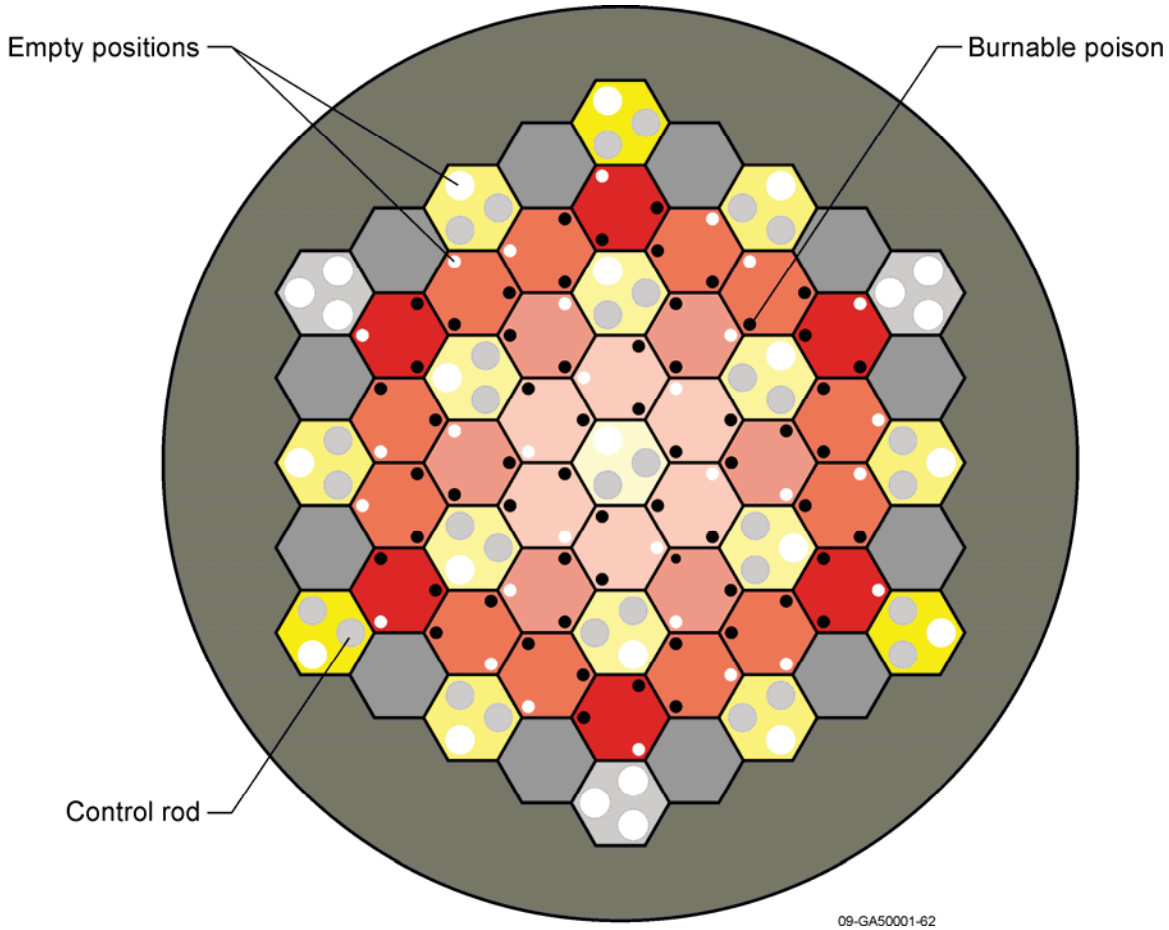

Figure 3.18. Fuel and Control Rod Column Orientations.

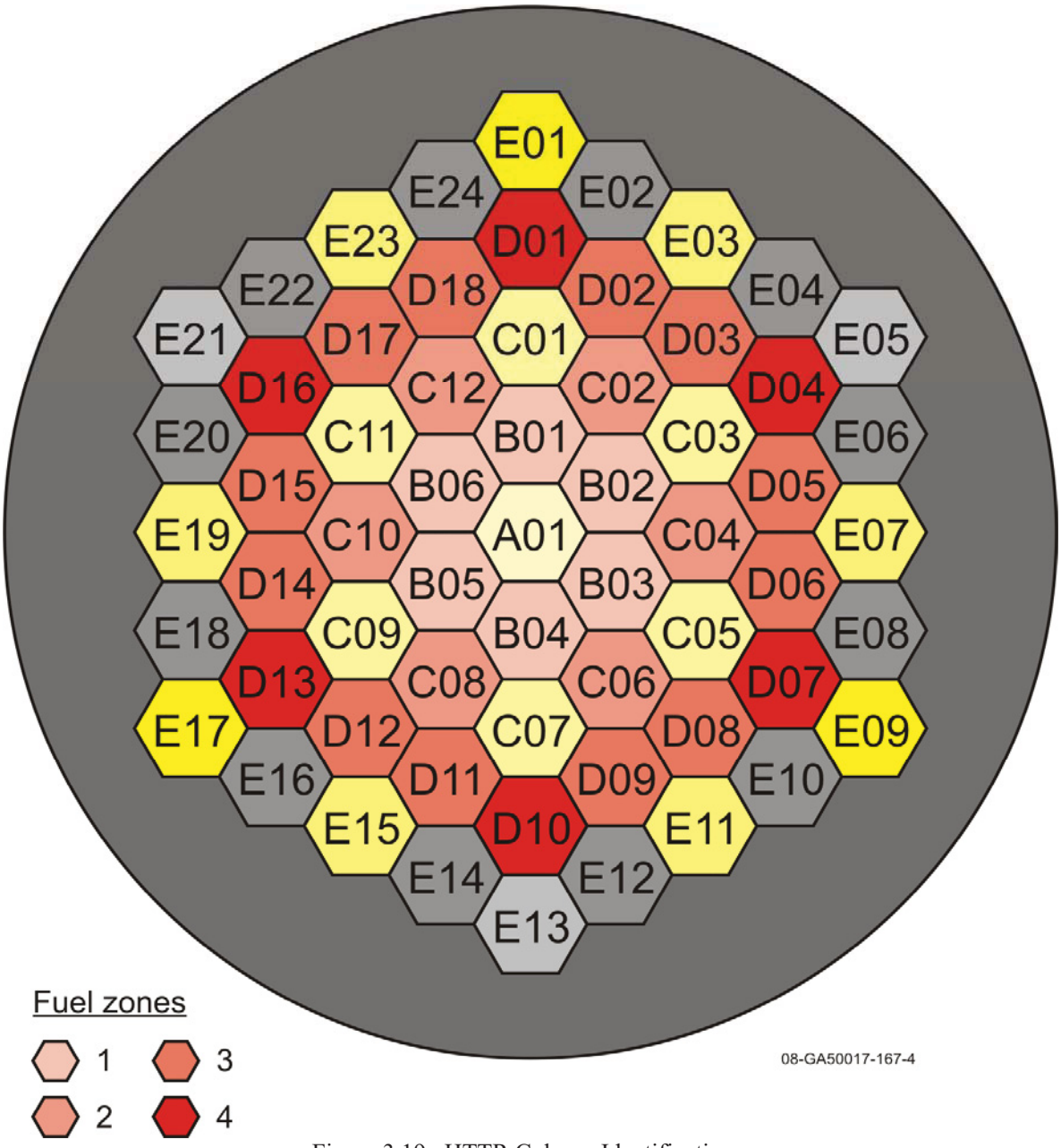

Figure 3.19. HTTR Column Identification.

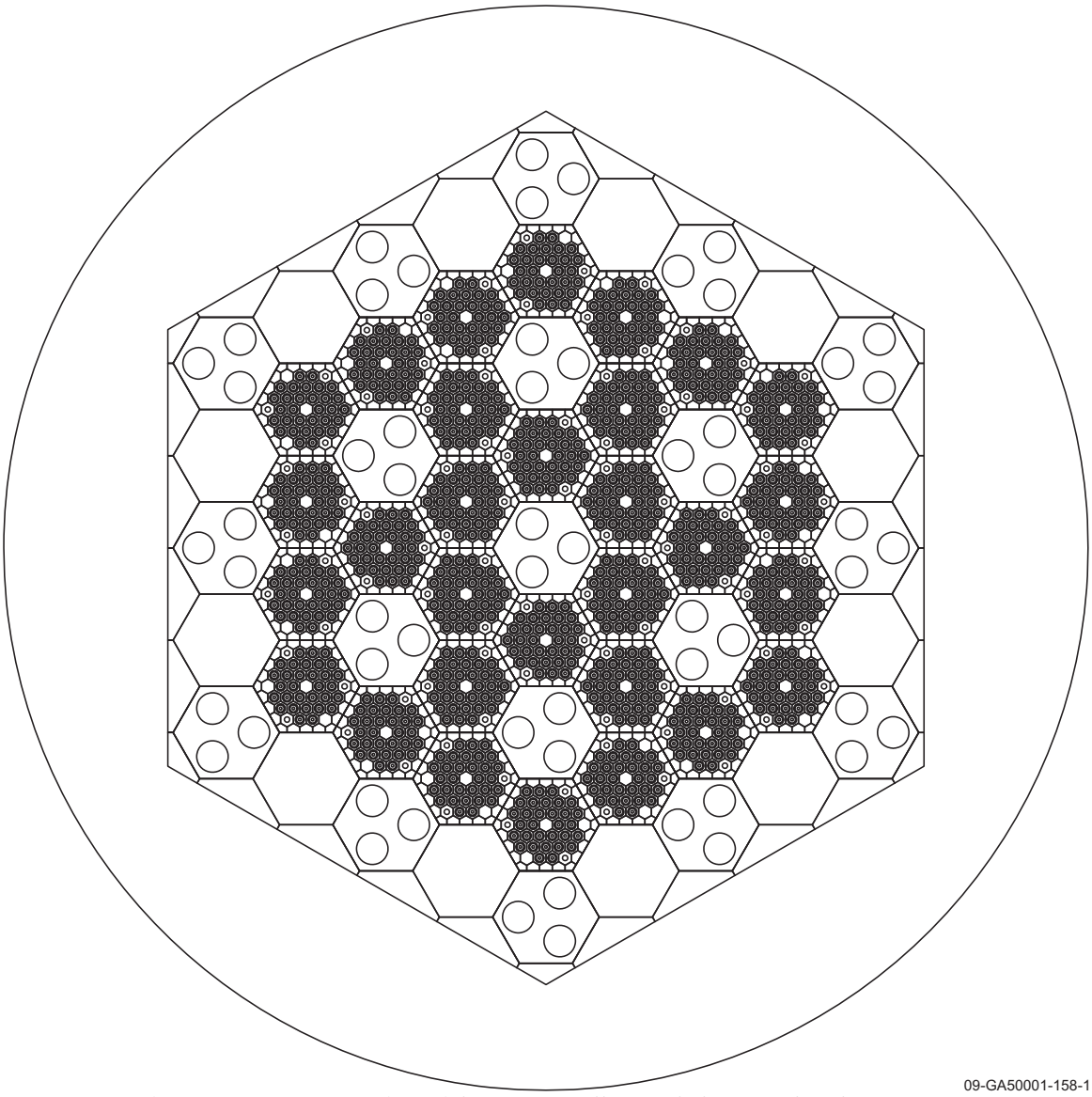

09-GA50001-158-1

Figure 3.20. Cross Section of the HTTR Fully-Loaded, 30-Fuel-Column Core.

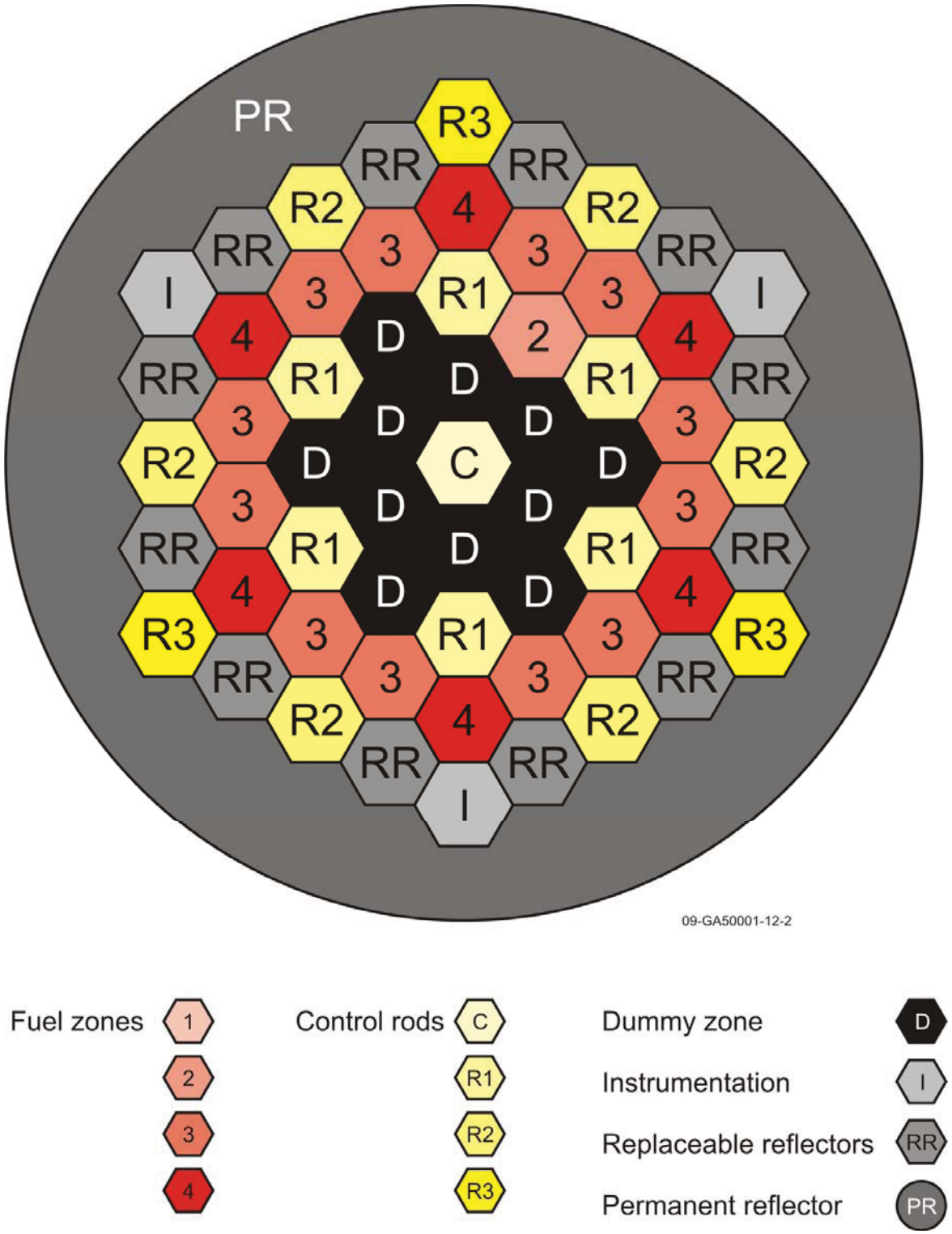

Figure 3.21. HTTR Core Positions (Configuration 1, 19-Fuel-Columns).

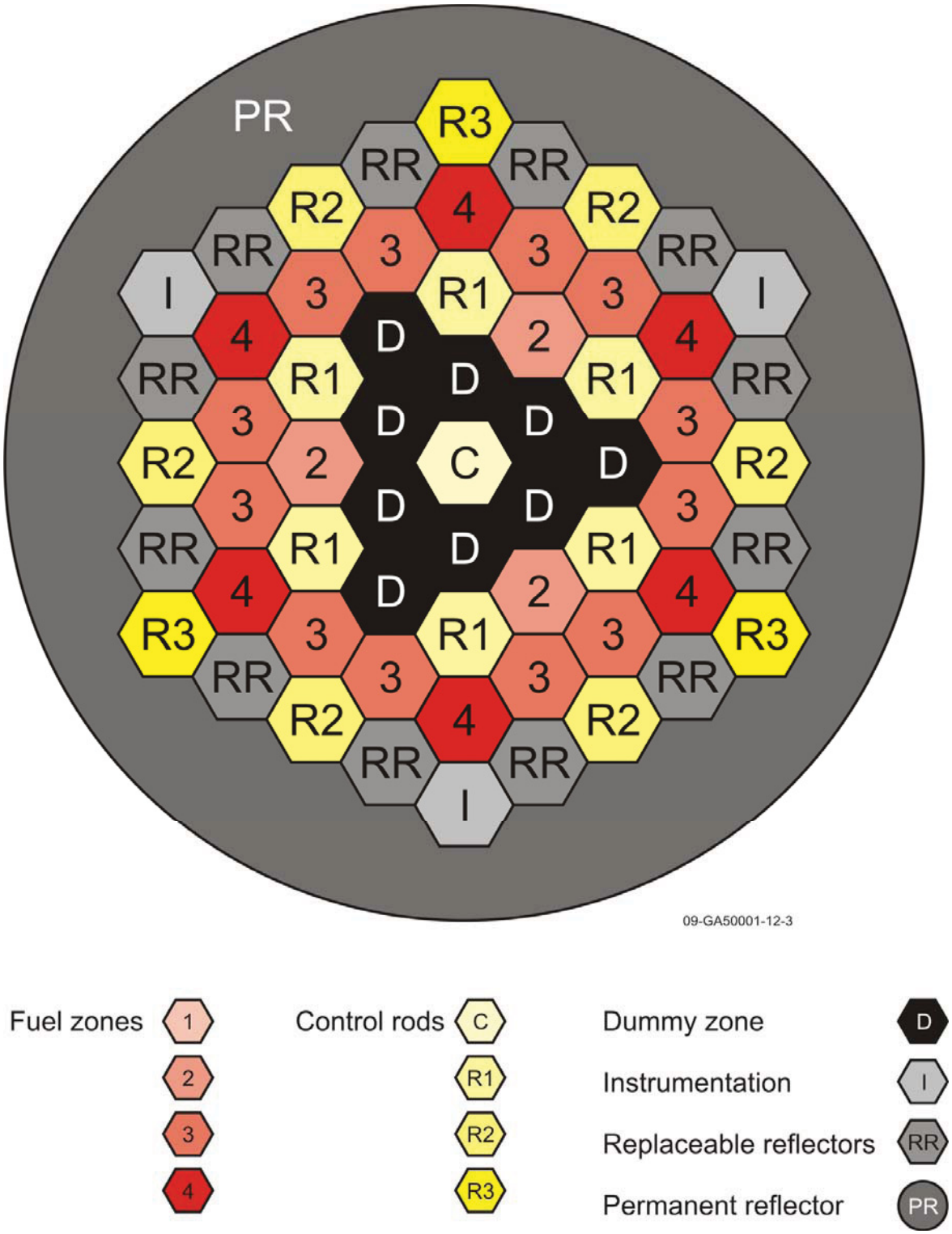

Figure 3.22. HTTR Core Positions (Configuration 2, 21-Fuel-Columns).

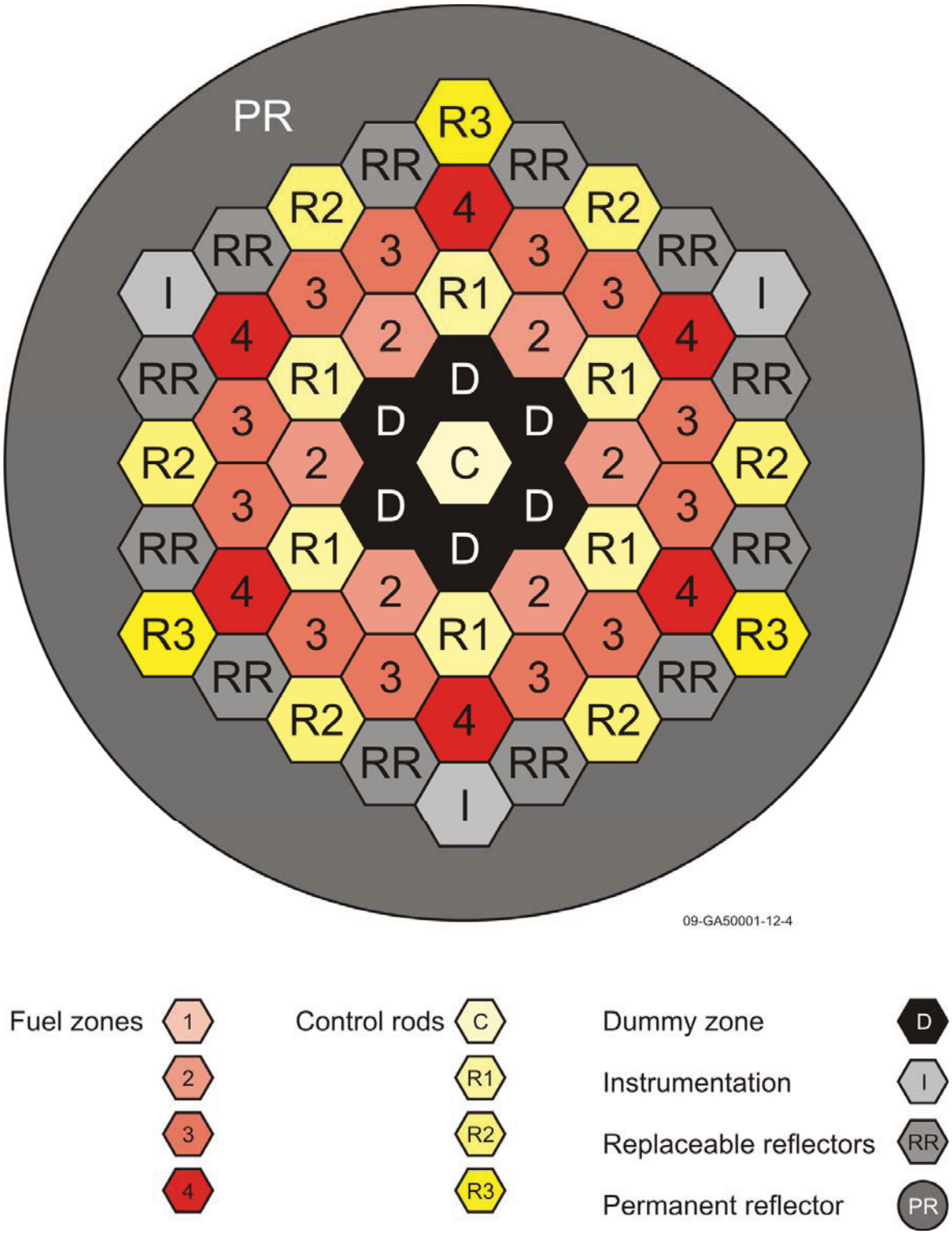

Figure 3.23. HTTR Core Positions (Configurations 3 and 4, 24-Fuel-Columns).

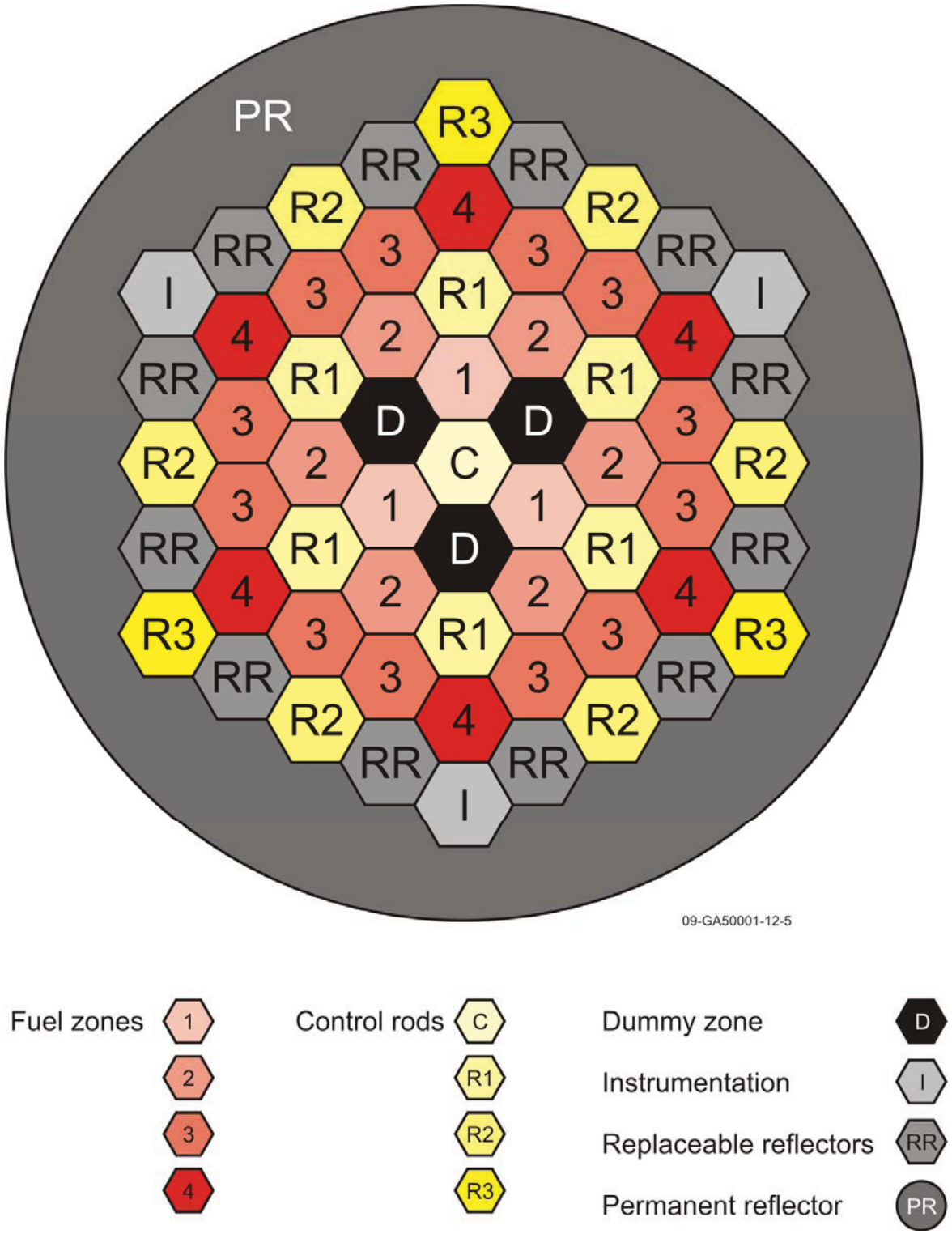

Figure 3.24. HTTR Core Positions (Configuration 5, 27-Fuel-Columns).

3.1.2.12 Critical Rod Positions

The critical rod positions for configurations 1 through 5 are shown in Figures 3.25 through 3.29, respectively. Control rod positions are described with the zero position defined as level with the bottom place of the lowest fuel block (i.e. 1160 mm from the bottom of the core graphite, the lowest fuel block). These figures provide reference between the various column types in the core and the control rod positions; the dummy fuel column and fuel column are interchangeable in these figures, with no change in the dimensions.

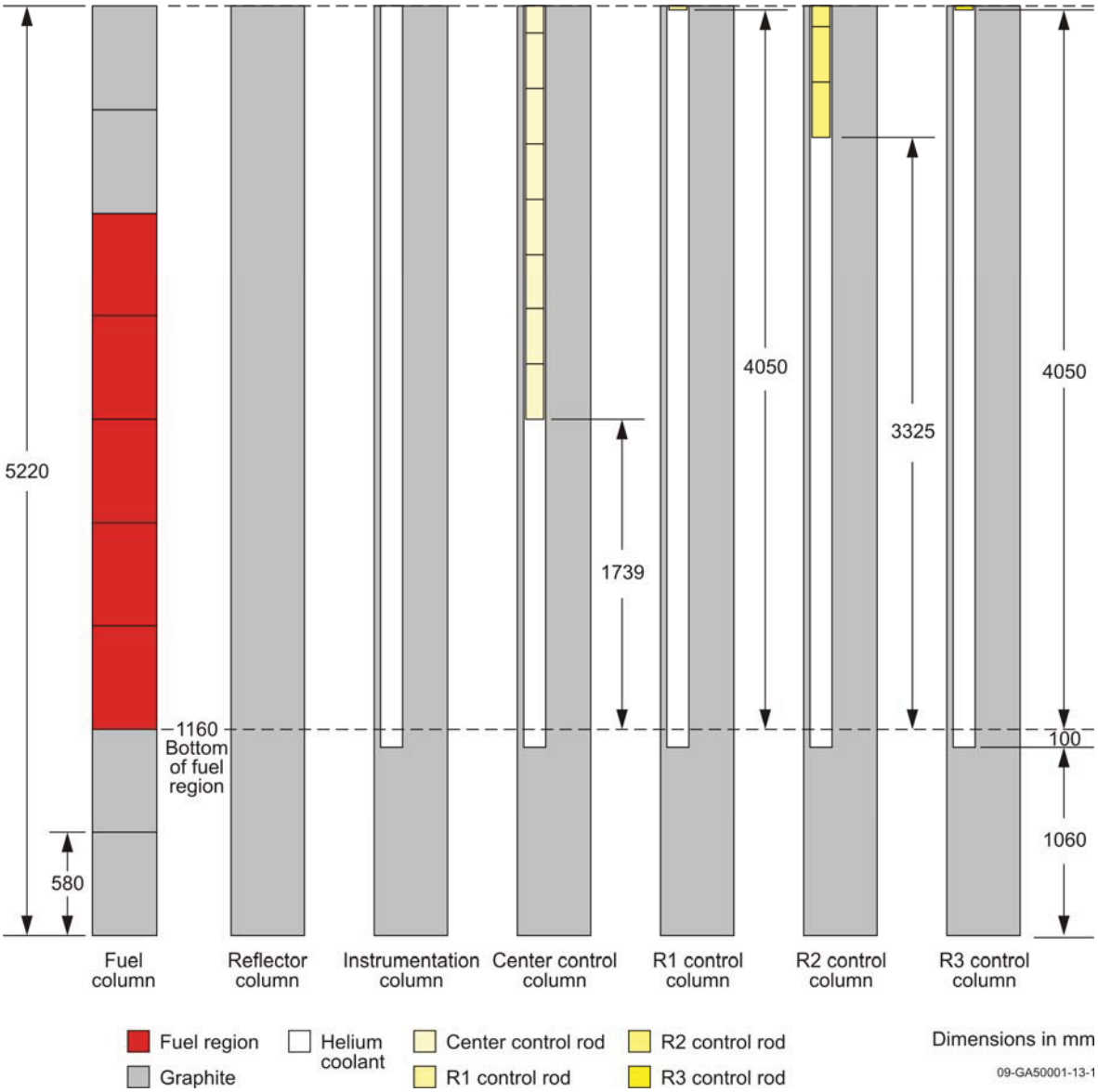

Figure 3.25. Axial Profile of Columns and Control Rod Positions (Configuration 1).

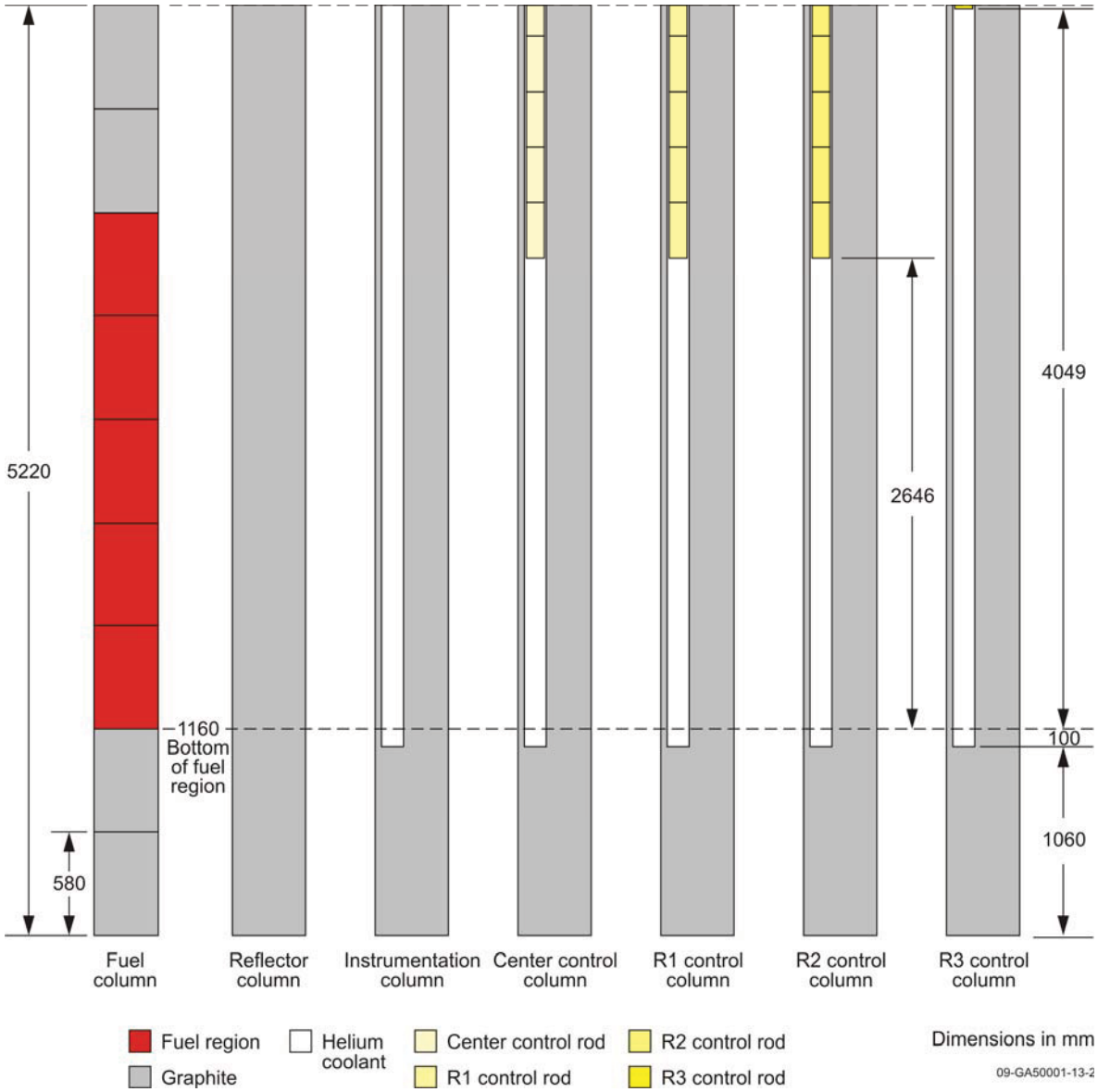

Figure 3.26. Axial Profile of Columns and Control Rod Positions (Configuration 2).

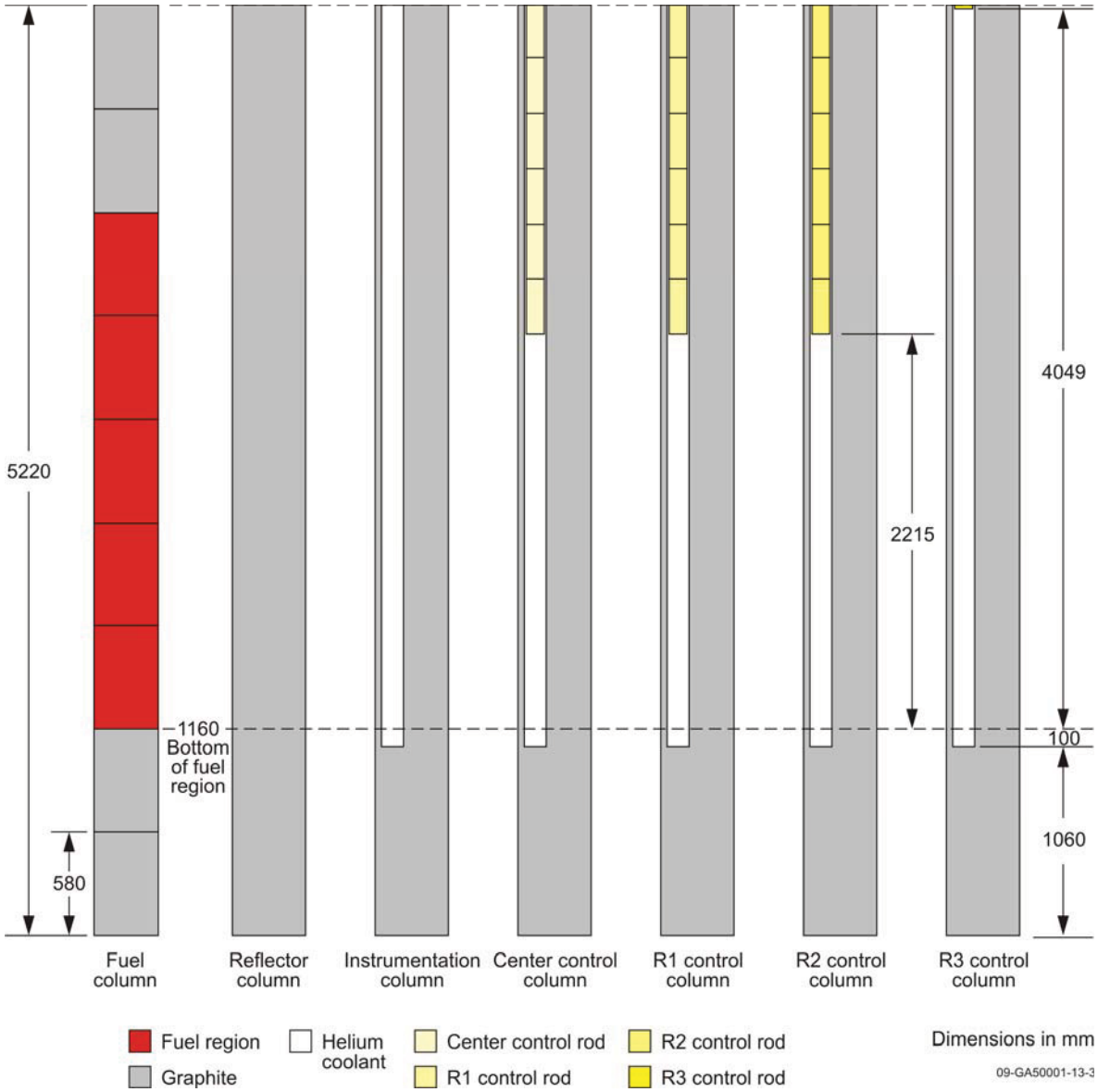

Figure 3.27. Axial Profile of Columns and Control Rod Positions (Configuration 3).

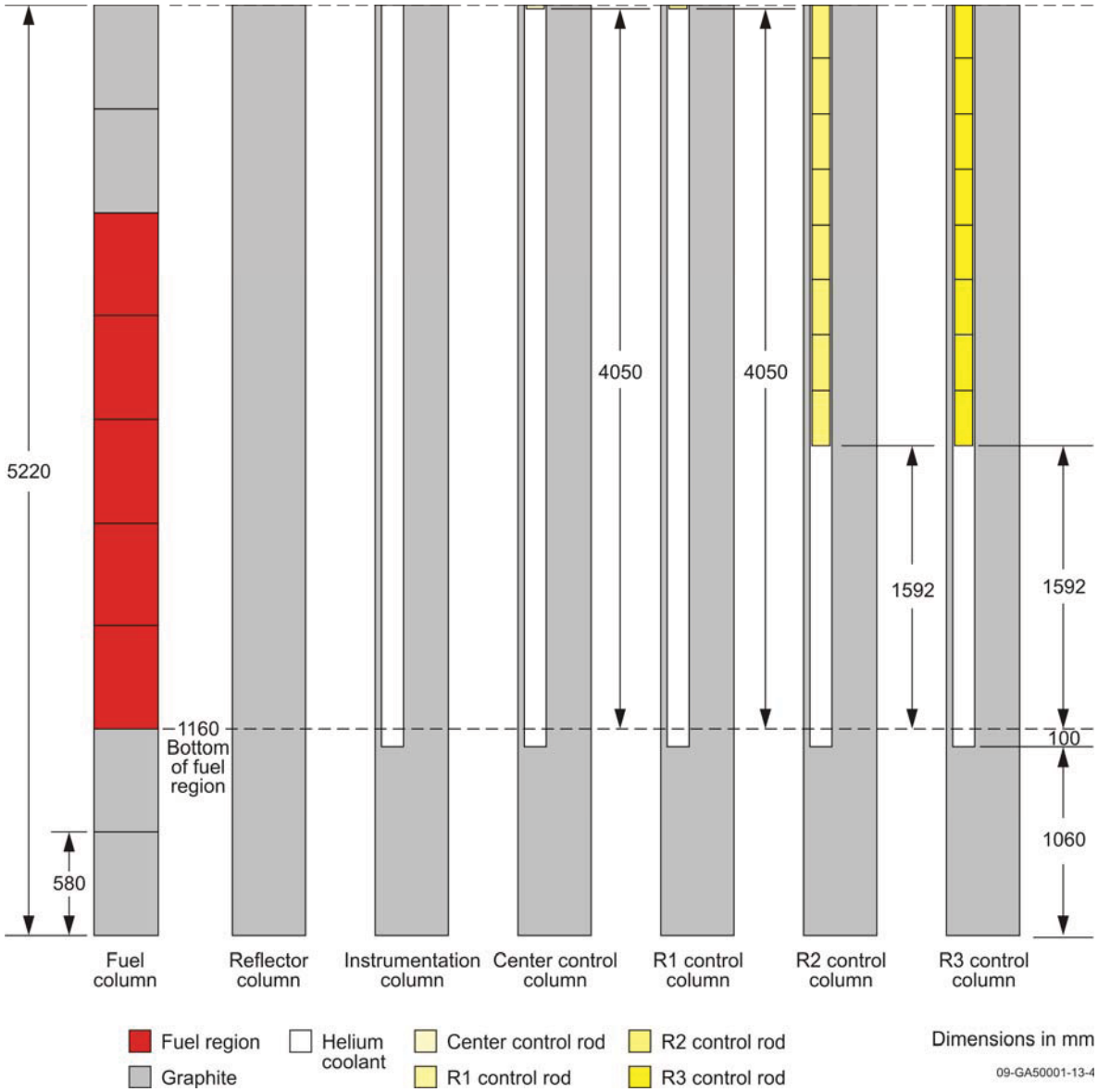

Figure 3.28. Axial Profile of Columns and Control Rod Positions (Configuration 4).

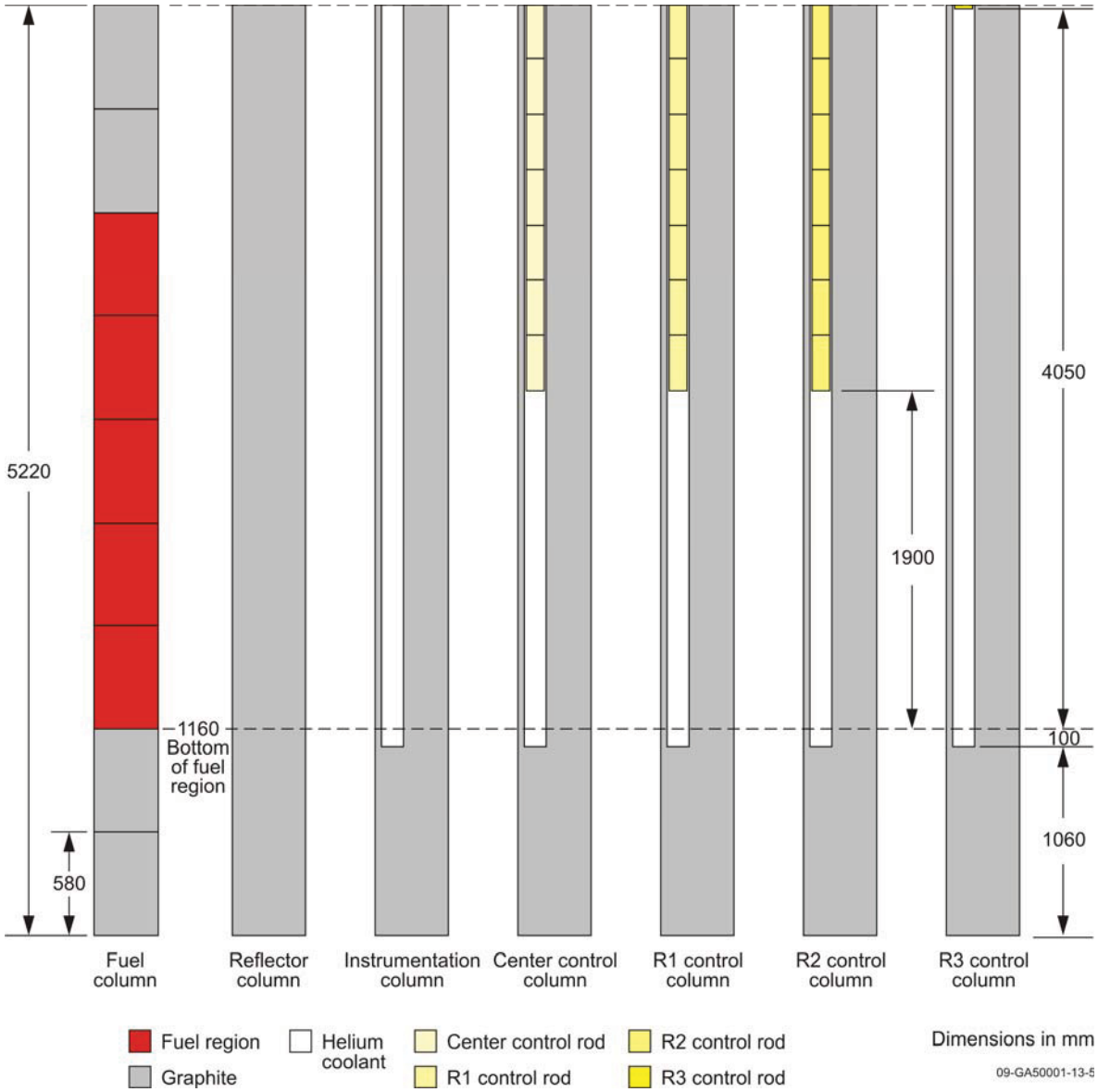

Figure 3.29. Axial Profile of Columns and Control Rod Positions (Configuration 5).

3.1.3 Material Data

3.1.3.1 Pin-in-Block Fuel

TRISO Particles

The mass density of the TRISO-coated UO_2 fuel kernels is 10.40363 g/cm^3 (such that the total uranium mass per fuel rod is 188.58 g) with an O/U ratio of ~2.00 and an equivalent natural-boron impurity content of 0.00015 wt.%. A summary of the atomic densities and compositions for the twelve enrichments found throughout the core are provided in Table 3.2.

Table 3.2. Atomic Densities (atoms/b-cm) of the UO_2 Kernels for Varying Enrichments.

Isotope	3.40 wt.%	3.90 wt.%	4.30 wt.%	4.80 wt.%	5.20 wt.%	5.90 wt.%
^{10}B	1.7299E-07	1.7299E-07	1.7299E-07	1.7299E-07	1.7299E-07	1.7299E-07
O	4.6404E-02	4.6404E-02	4.6404E-02	4.6404E-02	4.6404E-02	4.6404E-02
^{234}U	6.1026E-06	7.0000E-06	7.7180E-06	8.6154E-06	9.3334E-06	1.0590E-05
^{235}U	7.9888E-04	9.1637E-04	1.0104E-03	1.1278E-03	1.2218E-03	1.3863E-03
^{238}U	2.2405E-02	2.2288E-02	2.2195E-02	2.2078E-02	2.1984E-02	2.1821E-02
Total	6.9614E-02	6.9616E-02	6.9617E-02	6.9618E-02	6.9619E-02	6.9622E-02

Table 3.2 (cont'd.). Atomic Densities (atoms/b-cm) of the UO_2 Kernels for Varying Enrichments.

Isotope	6.30 wt.%	6.70 wt.%	7.20 wt.%	7.90 wt.%	9.40 wt.%	9.90 wt.%
^{10}B	1.7299E-07	1.7299E-07	1.7299E-07	1.7299E-07	1.7299E-07	1.7299E-07
O	4.6404E-02	4.6404E-02	4.6404E-02	4.6404E-02	4.6404E-02	4.6404E-02
^{234}U	1.1308E-05	1.2026E-05	1.2923E-05	1.4180E-05	1.6872E-05	1.7769E-05
^{235}U	1.4803E-03	1.5743E-03	1.6918E-03	1.8562E-03	2.2087E-03	2.3262E-03
^{238}U	2.1727E-02	2.1634E-02	2.1517E-02	2.1353E-02	2.1002E-02	2.0886E-02
Total	6.9623E-02	6.9624E-02	6.9625E-02	6.9628E-02	6.9632E-02	6.9634E-02

The material properties of the TRISO layers and graphite overcoat are provided in Table 3.3.

Table 3.3. Material Properties of the TRISO Coatings and Graphite Overcoat.

Property	Buffer	IPyC	SiC	OPyC	Overcoat
Mass Density (g/cm^3)	1.1	1.85	3.2	1.85	1.7
B-nat Impurity (wppm)	1.5	1.5	1.5	1.5	1.5
Atomic Density (atoms/b-cm)	5.5153E-02	9.2758E-02	9.6122E-02	9.2758E-02	8.5237E-02
^{10}B	1.8290E-08	3.0761E-08	5.3208E-08	3.0761E-08	2.8267E-08
C-nat	5.5153E-02	9.2758E-02	4.8061E-02	9.2758E-02	8.5237E-02
Si	--	--	4.8061E-02	--	--

Compacts

A key parameter is that the total fuel mass of a single fuel rod (14 stacked compacts) is approximately 188.58 g.

The mass density of the fuel compact graphite matrix is 1.7 g/cm^3 with an equivalent natural-boron impurity content of 0.000082 wt.%. The atomic density and composition of the compact matrix is shown in Table 3.4.

Table 3.4. Atomic Densities of the Fuel Compact Graphite Matrix.

Isotope	Atoms/b-cm
^{10}B	1.5452E-08
C-nat	8.5237E-02
Total	8.5237E-02

Fuel Element

The IG-110 graphite sleeve and end caps for the fuel pins have a mass density of 1.77 g/cm^3 and an equivalent natural-boron content of 0.000037 wt.%. The atomic density and composition of the graphite used in the fuel element is shown in Table 3.5.

Table 3.5. Atomic Densities of the Graphite Fuel Sleeve.

Isotope	Atoms/b-cm
^{10}B	7.2596E-09
C-nat	8.8747E-02
Total	8.8747E-02

3.1.3.2 Burnable Poisons

The burnable poison pellets have a mass density of 1.80 g/cm^3; a summary of the atomic densities and compositions for the two natural-boron concentrations employed in the core are provided in Table 3.6. The mass density of the graphite disks used to separate the burnable poison pellets is 1.77 g/cm^3 with an equivalent natural-boron content of 0.000037 wt.%. The atomic density and composition of the graphite disks is also found in Table 3.6

Table 3.6. Atomic Densities (atoms/b-cm) of the Burnable Poison Pellets and Graphite Disks.

Isotope	2.00 wt.%	2.50 wt.%	Disks
^{10}B	3.9906E-04	4.9882E-04	7.2596E-09
^{11}B	1.6063E-03	2.0078E-03	--
C-nat	8.8446E-02	8.7995E-02	8.8747E-02
Total	9.0451E-02	9.0501E-02	8.8747E-02

3.1.3.3 Fuel Blocks

The IG-110 graphite fuel blocks have a mass density of 1.7512 g/cm^3 (1.76 g/cm^3 base density decreased by a calculated 0.5 % void fraction) and an equivalent natural-boron content of 0.000059 wt.%. The atomic density and composition of the graphite fuel blocks is shown in Table 3.7.

Table 3.7. Atomic Densities of the Graphite Fuel Blocks.

Isotope	Atoms/b-cm
^{10}B	1.1453E-08
C-nat	8.7804E-02
Total	8.7804E-02

3.1.3.4 Dummy Blocks

The IG-11 graphite fuel blocks have a mass density of 1.7413 g/cm^3 (1.75 g/cm^3 base density decreased by a calculated 0.5 % void fraction) and an equivalent natural-boron content of 0.00031 wt.%. The atomic density and composition of the graphite dummy blocks is shown in Table 3.8.

Table 3.8. Atomic Densities of the Graphite Dummy Blocks.

Isotope	Atoms/b-cm
^{10}B	5.9835E-08
C-nat	8.7305E-02
Total	8.7305E-02

3.1.3.5 Control Rod System

Control Rods

The absorber compacts have a mass density of 1.9 g/cm^3 and have a composition and atomic density as described in Table 3.9.

Table 3.9. Atomic Densities of the Absorber Compacts.

Isotope	Atoms/b-cm
^{10}B	6.3184E-03
^{11}B	2.5432E-02
C-nat	6.6685E-02
Total	9.8436E-02

The Alloy 800H cladding of the control rods has a mass density of 8.03 g/cm^3 with a composition and atomic density as shown in Table 3.10.

Table 3.10. Atomic Densities of the Alloy 800H Clad.

Isotope	Atoms/b-cm
C-nat	3.2210E-04
Al	6.7209E-04
Si	6.0263E-04
P	3.1225E-05
S	1.5081E-05
Ti	3.7884E-04
Cr	1.9530E-02
Mn	8.8022E-04
Fe	3.8092E-02
Ni	2.6777E-02
Cu	2.2830E-04
Total	8.7530E-02

Control Rod Columns

The IG-110 graphite fuel columns are modeled with the same physical properties as the fuel blocks in Section 3.1.3.3 and Table 3.7.

3.1.3.6 Instrumentation

Instrumentation Components

Insufficient information was available to adequately model instrumentation in the HTTR. An approximate bias with uncertainty was determined applied to the benchmark model (see Sections 2.1.2.6 and 3.1.1.1).

Instrumentation Columns

The IG-110 graphite instrumentation columns are modeled with the same physical properties as the fuel blocks in Section 3.1.3.3 and Table 3.7.

3.1.3.7 Replaceable Reflector Columns

The IG-110 replaceable reflector columns are modeled with the same physical properties as the fuel blocks in Section 3.1.3.3 and Table 3.7.

3.1.3.8 Replaceable Reflectors Blocks in Fuel Columns

The IG-110 replaceable reflector blocks are modeled with the same physical properties as the fuel blocks in Section 3.1.3.3 and Table 3.7.

3.1.3.9 Permanent Reflector

The PGX graphite permanent reflector has a mass density of 1.71789 g/cm^3 (1.76 g/cm^3 base density decreased by a provided 0.7 % void fraction) and an equivalent natural-boron content of 0.000191 wt.%. The atomic density and composition of the permanent reflector is shown in Table 3.11.

Table 3.11. Atomic Densities of the Permanent Reflector.

Isotope	Atoms/b-cm
^{10}B	3.6372E-08
C-nat	8.6134E-02
Total	8.6134E-02

3.1.3.10 Helium Coolant

The helium coolant has an atomic density of 2.4616E-05 atoms/b-cm (mass density of 1.6361 × 10^{-4} g/cm^3). No impurities are modeled in the coolant.

$$\frac{n}{V}=\frac{P\cdot N_A}{R\cdot T}=\frac{(1atm)\cdot\left(0.60221\frac{atoms\cdot cm^2}{mol\cdot b}\right)}{\left(0.082054\frac{L\cdot atm}{mol\cdot K}\right)\cdot(298.15K)}\cdot\left(\frac{1L}{1000cm^3}\right)=2.4616\times10^{-5}\frac{atoms}{b\cdot cm}.$$

$$\rho=\frac{n}{V}\cdot\frac{M}{N_A}=2.4616\times10^{-5}\frac{atoms}{b\cdot cm}\cdot\frac{4.002602\frac{g}{mol}}{\left(0.60221\frac{atoms\cdot cm^2}{mol\cdot b}\right)}=1.6361\times10^{-4}\frac{g}{cm^3}.$$

3.1.4 Temperature Data

The benchmark model temperature is 300 K.

3.1.5 Experimental and Benchmark-Model k_{eff} and / or Subcritical Parameters

The experimental k_{eff} was approximately at unity, made to delayed critical. A comprehensive bias assessment could not be performed; therefore, the experimental k_{eff} values were adjusted only for the bias incurred by removing the instrumentation in the core (Table 3.1). Furthermore, the uncertainty in the benchmark models (Tables 2.64 through 2.68) is the same as the uncertainty evaluated for the experimental, as the bias uncertainty for instrumentation has already been included. The benchmark eigenvalues for the annular HTTR core loadings are shown in Table 3.12.

Table 3.12. HTTR Benchmark Values.

Case	Fuel Columns	Control[(a)]	k_{eff}	-σ	+σ
1	19	C	1.0048	0.0103	0.0100
2	21	FS	1.0040	0.0100	0.0092
3	24	FS	1.0035	0.0078	0.0084
4	24	F23	1.0032	0.0080	0.0074
5	27	FS	1.0029	0.0068	0.0075

(a) C = criticality obtained using central control rod only.
FS = flat standard pattern where C, R1, and R2 CRs were inserted into the core at the same levels while R3 CRs were fully withdrawn.
F23 = only R2 and R3 CRs were used for control while C and R1 CRs were fully withdrawn.

3.2 Benchmark-Model Specifications for Buckling and Extrapolation-Length Measurements

Buckling and extrapolation length measurements were not made.

3.3 Benchmark-Model Specifications for Spectral Characteristics Measurements

Spectral characteristics measurements were not made.

3.4 Benchmark-Model Specifications for Reactivity Effects Measurements

Benchmark specifications for the excess reactivity measurements pertaining to the annular core configurations are provided in Section 3.4 of HTTR-GCR-RESR-001.

3.5 Benchmark-Model Specifications for Reactivity Coefficient Measurements

Reactivity coefficient measurements were not made.

3.6 Benchmark-Model Specifications for Kinetics Measurements

Kinetics measurements were not made.

3.7 Benchmark-Model Specifications for Reaction-Rate Distribution Measurements

3.7.1 Description of the Benchmark Model Simplifications

The simplifications of the benchmark model for determination of the axial neutron fission reaction-rate in the instrumentation columns of the HTTR (described in Section 1.7) are identical to those of the critical annular 24-fuel-column core configurations 3 and 4 described in Section 3.1.1.

3.7.2 Dimensions

The dimensions of the benchmark model for determination of the axial neutron reaction-rate in the instrumentation columns of the HTTR are identical to those of the critical annular 24-fuel-column core configurations 3 and 4 described in Section 3.1.2.

The axial neutron fission reaction-rate in the instrumentation columns is calculated by taking the benchmark model of the fully-loaded 30-fuel-column core and superimposing a flux tally over one of the instrumentation column positions: E05, E13, or E21. The flux is computed for 6.15-cm radius discs with a thickness of 1 cm located at the center of one instrumentation channel in each instrumentation column (see Figure 3.30). A total of 522 cm, representing the total height of the core fuel and reflector blocks, was modeled. The (x, y) coordinates used for columns E05, E13, and E21, are (114.6005, 72.4), (5.4, -135.447), and (-120, 63.04693), respectively, where the origin is located at the radial center of the core.

The F4 flux tally is used in MCNP, which determines the flux across a cell volume by tabulating the average track length of the neutrons.[a] The tally is then modified by a tally multiplier card, Fm, that accounts for the total fission cross section of ^{235}U, the fissile material in the fission chambers, to obtain the neutron reaction-rate in each instrumentation column.

The calculated neutron fission reaction rates are obtained by taking the variance-weighted average of results obtained using six variations of the input deck (Appendix A.1) with different random number seeds and tallies of the neutron reaction rate (Appendix A.3). This approach was used to reduce the statistical uncertainty in the neutron flux tallies because the relative error values obtained can underpredict the true uncertainty in the calculated neutron flux.[b] Therefore, the final calculated values are obtained from a total of 18 reaction-rate tallies (6 input decks with 3 instrumentation columns each).

The average of the neutron reaction-rate in each position is taken and normalized to represent the calculated axial neutron reaction-rate profile:

$$\phi(z)_{normalized} = \frac{\phi(z)}{\phi_{maximum}},$$

[a] X-5 Monte Carlo Team, "MCNP – A General Monte Carlo N-Particle Transport Code, Version 5, Volume II: User's Guide," LA-CP-03-0245 (April 24, 2003; revised October 2, 2005).

[b] F. B. Brown, "A Review of Best Practices for Monte Carlo Criticality Calculations," *Proc. NCSD 2009*, Richland, WA, September 13-17 (2009).

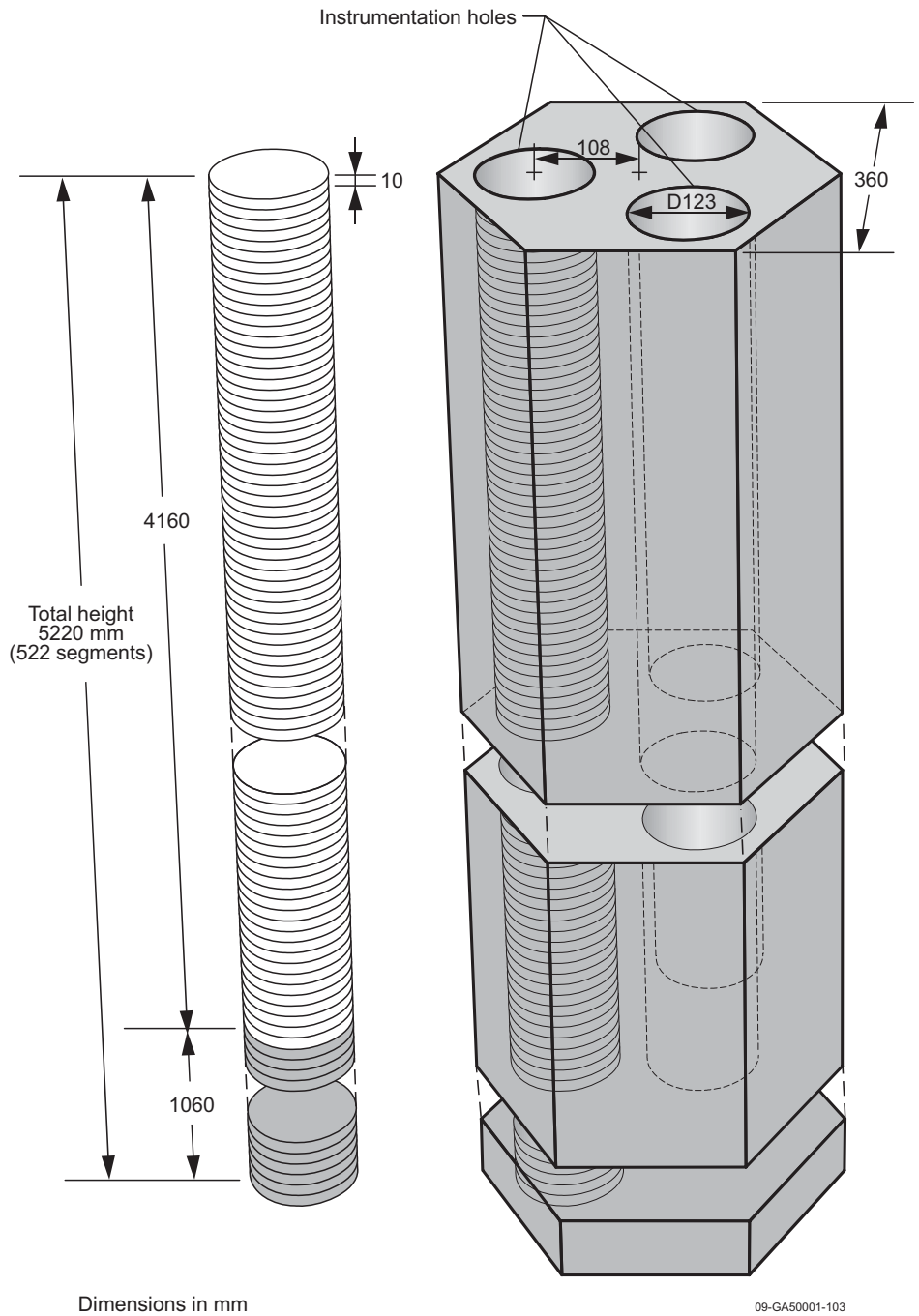

Figure 3.30. Placement of Axial Flux Tally in the Instrumentation Column

3.7.3 Material Data

The materials in the benchmark model for determination of the axial neutron reaction-rate in the instrumentation columns of the HTTR are identical to those in the critical annular 24-fuel-column core configurations 3 and 4 described in Section 3.1.3.

3.7.4 Temperature Data

The benchmark model temperature is 300 K.

3.7.5 Benchmark-Model Specification for Reaction-Rate Distribution Measurements

The expected benchmark values for the normalized axial neutron reaction-rate in the instrumentation columns of the HTTR, with their respective uncertainties (from Section 2.7.1), are shown in Table 3.13 and 3.14 for core configurations 3 and 4, respectively. The normalization is to the highest reaction-rate value, which is data point 4 at a height of 130.96 and 115.79 cm for core configurations 3 and 4, respectively.

Table 3.13. Axial Neutron Fission Reaction Rate in the Instrumentation Columns of the HTTR (Configuration 3).

Data Point	Height (cm)[(a)]	Normalized Benchmark Reaction Rate	±	1σ	1σ (%)
1	18.89	0.6946	±	0.0199	2.87
2	27.86	0.7304	±	0.0198	2.70
3	86.07	0.9555	±	0.0173	1.81
4	130.96	1.0000	±	0.0166	1.66
5	137.15	0.9854	±	0.0169	1.71
6	143.96	0.9750	±	0.0170	1.75
7	202.48	0.6735	±	0.0200	2.97
8	260.99	0.2818	±	0.0165	5.86
9	318.58	0.1041	±	0.0095	9.16

(a) The height is in reference to the position relative to the bottom of the fifth layer of fuel.

Table 3.14. Axial Neutron Fission Reaction Rate in the Instrumentation Columns of the HTTR (Configuration 4).

Data Point	Height (cm)[(a)]	Normalized Benchmark Reaction Rate	±	1σ	1σ (%)
1	18.79	0.7030	±	0.0199	2.83
2	28.40	0.7383	±	0.0197	2.67
3	86.36	0.9523	±	0.0174	1.83
4	115.79	1.0000	±	0.0166	1.66
5	137.45	0.9749	±	0.0170	1.75
6	144.57	0.9562	±	0.0173	1.81
7	202.72	0.7915	±	0.0193	2.44
8	260.85	0.5582	±	0.0201	3.59
9	318.37	0.3312	±	0.0176	5.32

(a) The height is in reference to the position relative to the bottom of the fifth layer of fuel.

3.8 Benchmark-Model Specifications for Power Distribution Measurements

Power distribution measurements were not made.

3.9 Benchmark-Model Specifications for Isotopic Measurements

Isotopic measurements were not made.

3.10 Benchmark-Model Specifications for Other Miscellaneous Types of Measurements

Other miscellaneous types of measurements were not made.

4.0 RESULTS OF SAMPLE CALCULATIONS

4.1 Results of Calculations of the Critical or Subcritical Configurations

Random particles cannot be easily modeled in MCNP. Therefore an ordered-lattice approach for modeling the benchmark was implemented, and results are provided

The computed k_{eff} values for the benchmark model of the annular cores were evaluated with MCNP using the ENDF/B-V.2, -VI.8, and -VII.0, JEFF-3.1, and JENDL-3.3 cross section libraries. All benchmark model calculations are compared against the expected benchmark value reported in Section 3.1.5. The total uncertainty in the expected value of k_{eff} is taken from Section 2.1.7. The JENDL-3.3 analysis was performed with the inclusion of ENDF/B-VII.0 thermal neutron scattering data because it was not included in the JENDL-3.3 library. Thermal neutron scattering, or $S(\alpha,\beta)$, adjusts the neutron cross sections for neutron upscatter at thermal energies and provides scattering data for elements bound within specific materials. The k_{eff} values were also calculated using ENDF/B-VII.0 and MCNPX. The MCNP5 calculations were performed with 1,050 generations (skipping the first 50) and 50,000 neutrons per generation.

It is currently difficult to obtain the necessary information to further improve the confidence in the benchmark model and effectively reduce the overall uncertainty; the necessary data is proprietary and its released is being restricted, because the benchmark configuration of the HTTR core is the same that is currently in operation. Once this information is made available, the HTTR benchmark can be adjusted as appropriate.

4.1.1 Ordered TRISO Lattice within the Fuel Compacts

The TRISO particles are modeled in rectangular lattices with the dimensions of 0.106 cm (length) × 0.106 cm (width) × 0.1 cm (height) to generate a volumetric packing fraction of 30 % (not including the graphite overcoat) when only complete particles are placed within the compact. A cross-sectional view of the TRISO lattice block is shown in Figure 4.1. The graphite overcoat isn't completely represented in the lattice.

A horizontal cross section of the compacts is shown in Figure 4.2. As can be seen, selective placement of TRISO particles was necessary to conserve the fuel rod mass of 188.58 g. For the current configuration, 12,987 TRISO particles are present within a standard fuel compact; this value is slightly less than the reported value of approximately 13,000.

The effective multiplication factor for configurations 1 through 5 are shown in Table 4.1 through 4.5, respectively. Calculated values of k_{eff} differ from the benchmark model values by between 1.4 to 2.7 %. Reevaluation of the HTTR model as additional information becomes available might improve the quality of this benchmark. The benchmark models are most sensitive to graphite impurities, and graphite cross section data may also contributed to the bias.

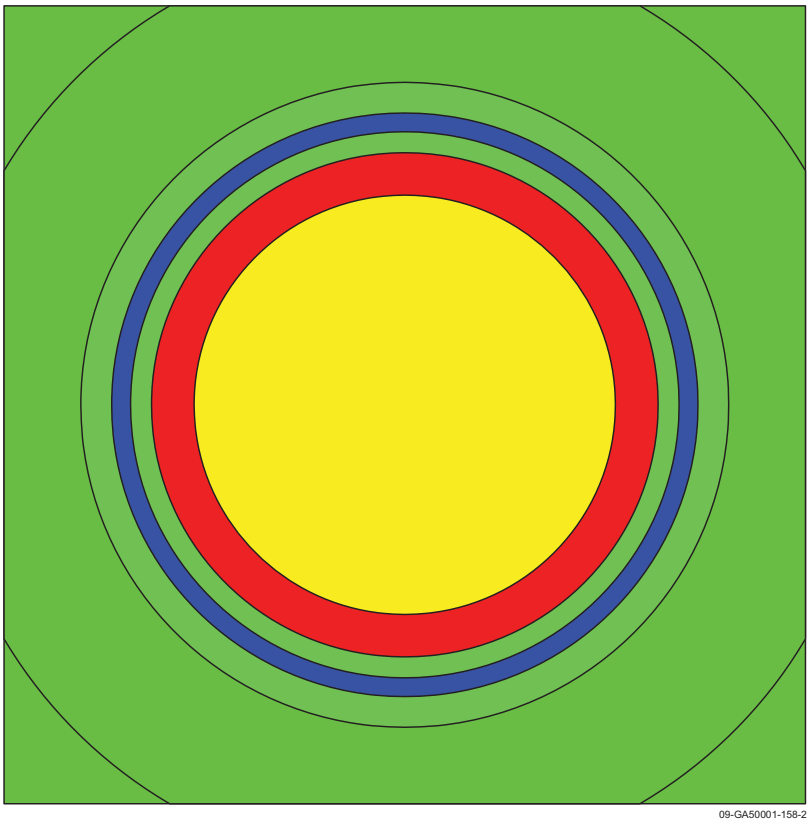

Figure 4.1. MCNP TRISO Lattice Unit Cell.

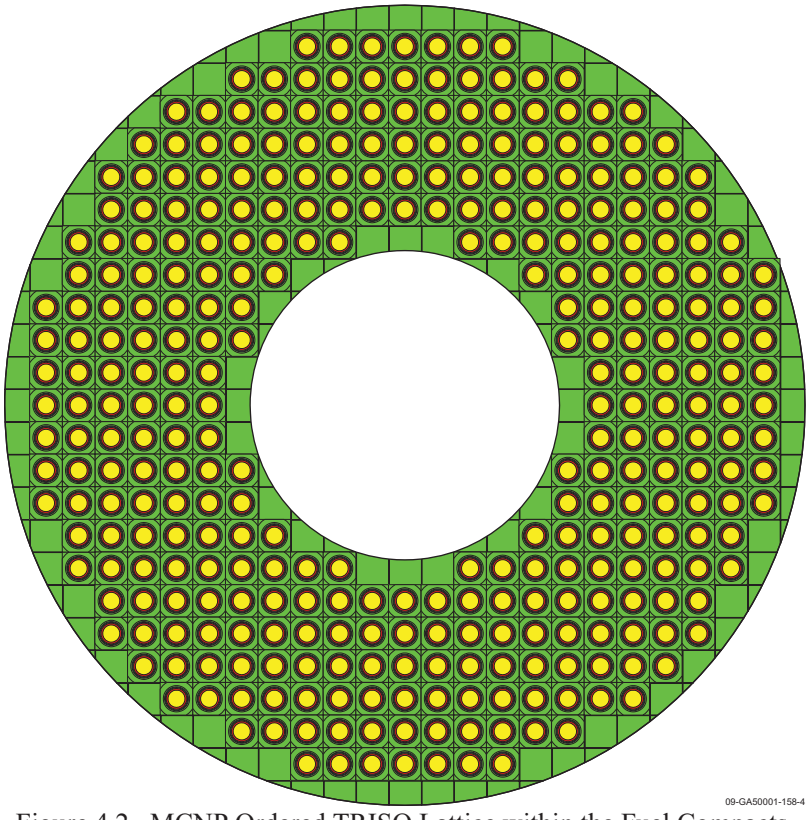

Figure 4.2. MCNP Ordered TRISO Lattice within the Fuel Compacts.

Table 4.1. Final Results for the HTTR Benchmark Model Evaluation using an Ordered Lattice (Configuration 1).

Neutron Cross-Section Library	Calculated k_{eff}	±	σ	Benchmark k_{eff}	Uncertainty -σ (%)	Uncertainty +σ (%)	(C-E)/E (%)
ENDF/B-V.2	1.0250	±	0.0001	1.0048[(a)]	0.0103	0.0100	2.00
ENDF/B-VI.8	1.0267	±	0.0001	1.0048[(a)]	0.0103	0.0100	2.17
END/B-VII.0	1.0276	±	0.0001	1.0048[(a)]	0.0103	0.0100	2.27
JEFF-3.1	1.0280	±	0.0001	1.0048[(a)]	0.0103	0.0100	2.31
JENDL-3.3 with ENDF/B-VII.0 S(α,β)	1.0222	±	0.0001	1.0048[(a)]	0.0103	0.0100	1.73
ENDF/B-VII.0 (MCNPX)	1.0273	±	0.0001	1.0048[(a)]	0.0103	0.0100	2.24

(a) No biases have been currently evaluated for correcting the expected experimental k_{eff}, besides the bias for removing the reactor instrumentation in the instrumentation columns.

Table 4.2. Final Results for the HTTR Benchmark Model Evaluation using an Ordered Lattice (Configuration 2).

Neutron Cross-Section Library	Calculated k_{eff}	±	σ	Benchmark k_{eff}	Uncertainty -σ (%)	Uncertainty +σ (%)	(C-E)/E (%)
ENDF/B-V.2	1.0268	±	0.0001	1.0040[(a)]	0.0100	0.0092	2.27
ENDF/B-VI.8	1.0289	±	0.0001	1.0040[(a)]	0.0100	0.0092	2.48
END/B-VII.0	1.0297	±	0.0001	1.0040[(a)]	0.0100	0.0092	2.55
JEFF-3.1	1.0301	±	0.0001	1.0040[(a)]	0.0100	0.0092	2.60
JENDL-3.3 with ENDF/B-VII.0 S(α,β)	1.0241	±	0.0001	1.0040[(a)]	0.0100	0.0092	1.99
ENDF/B-VII.0 (MCNPX)	1.0291	±	0.0001	1.0040[(a)]	0.0100	0.0092	2.50

(a) No biases have been currently evaluated for correcting the expected experimental k_{eff}, besides the bias for removing the reactor instrumentation in the instrumentation columns.

Table 4.3. Final Results for the HTTR Benchmark Model Evaluation using an Ordered Lattice (Configuration 3).

Neutron Cross-Section Library	Calculated k_{eff}	±	σ	Benchmark k_{eff}	Uncertainty -σ (%)	Uncertainty +σ (%)	(C-E)/E (%)
ENDF/B-V.2	1.0224	±	0.0001	1.0035[(a)]	0.0078	0.0084	1.89
ENDF/B-VI.8	1.0243	±	0.0001	1.0035[(a)]	0.0078	0.0084	2.07
END/B-VII.0	1.0249	±	0.0001	1.0035[(a)]	0.0078	0.0084	2.13
JEFF-3.1	1.0257	±	0.0001	1.0035[(a)]	0.0078	0.0084	2.21
JENDL-3.3 with ENDF/B-VII.0 S(α,β)	1.0198	±	0.0001	1.0035[(a)]	0.0078	0.0084	1.62
ENDF/B-VII.0 (MCNPX)	1.0249	±	0.0001	1.0035[(a)]	0.0078	0.0084	2.13

(a) No biases have been currently evaluated for correcting the expected experimental k_{eff}, besides the bias for removing the reactor instrumentation in the instrumentation columns.

Table 4.4. Final Results for the HTTR Benchmark Model Evaluation using an Ordered Lattice (Configuration 4).

Neutron Cross-Section Library	Calculated k_{eff}	±	σ	Benchmark k_{eff}	Uncertainty -σ (%)	Uncertainty +σ (%)	(C-E)/E (%)
ENDF/B-V.2	1.0261	±	0.0001	1.0032[(a)]	0.0080	0.0074	2.29
ENDF/B-VI.8	1.0284	±	0.0001	1.0032[(a)]	0.0080	0.0074	2.52
END/B-VII.0	1.0287	±	0.0001	1.0032[(a)]	0.0080	0.0074	2.54
JEFF-3.1	1.0298	±	0.0001	1.0032[(a)]	0.0080	0.0074	2.65
JENDL-3.3 with ENDF/B-VII.0 S(α,β)	1.0239	±	0.0001	1.0032[(a)]	0.0080	0.0074	2.07
ENDF/B-VII.0 (MCNPX)	1.0287	±	0.0001	1.0032[(a)]	0.0080	0.0074	2.55

(a) No biases have been currently evaluated for correcting the expected experimental k_{eff}, besides the bias for removing the reactor instrumentation in the instrumentation columns.

Table 4.5. Final Results for the HTTR Benchmark Model Evaluation using an Ordered Lattice (Configuration 5).

Neutron Cross-Section Library	Calculated k_{eff}	±	σ	Benchmark k_{eff}	Uncertainty -σ (%)	Uncertainty +σ (%)	(C-E)/E (%)
ENDF/B-V.2	1.0189	±	0.0001	1.0029[(a)]	0.0068	0.0075	1.60
ENDF/B-VI.8	1.0211	±	0.0001	1.0029[(a)]	0.0068	0.0075	1.82
END/B-VII.0	1.0218	±	0.0001	1.0029[(a)]	0.0068	0.0075	1.88
JEFF-3.1	1.0224	±	0.0001	1.0029[(a)]	0.0068	0.0075	1.94
JENDL-3.3 with ENDF/B-VII.0 S(α,β)	1.0167	±	0.0001	1.0029[(a)]	0.0068	0.0075	1.37
ENDF/B-VII.0 (MCNPX)	1.0217	±	0.0001	1.0029[(a)]	0.0068	0.0075	1.88

(a) No biases have been currently evaluated for correcting the expected experimental k_{eff}, besides the bias for removing the reactor instrumentation in the instrumentation columns.

4.2 Results of Buckling and Extrapolation Length Calculations

Buckling and extrapolation length measurements were not made.

4.3 Results of Spectral-Characteristics Calculations

Spectral characteristics measurements were not made.

4.4 Results of Reactivity-Effects Calculations

Sample calculation results for the excess reactivity measurements of the annular core configurations are provided in Section 4.4.1 of HTTR-GCR-RESR-001.

4.5 Results of Reactivity Coefficient Calculations

Reactivity coefficient measurements were not made.

4.6 Results of Kinetics Parameter Calculations

Kinetics measurements were not made.

4.7 Results of Reaction-Rate Distribution Calculations

4.7.1 Axial Reaction Rate Distribution

The benchmark model for the critical annular 24-fuel-column configurations 3 and 4 described in Section 3.1 was utilized in the analysis of the reactor physics experiments in Section 1.7. The modeling approach described in Section 4.1 applies to the analysis in this section except that all calculations were performed only using the ENDF/B-VII.0 neutron cross-section library. Computed axial neutron reaction-rates in the instrumentation columns of the HTTR, averaged and normalized from tallies across the three columns from input decks using six different random number seeds, are summarized in Tables 4.6 and 4.7 as well as depicted in Figures 4.3 and 4.4 for configurations 3 and 4, respectively. The calculated flux with uncertainty bars is shown in Figures 4.5 and 4.6, respectively.

The calculated reaction rates are renormalized such that at data point 4, both the benchmark and calculated values are 1.0000, using Equations 4.1 and 4.2, where the normalized flux at the i^{th} position, $\varphi_{i,n}$, is obtained by dividing the reaction rate at that position by the maximum flux, $\varphi_{i,max}$. Then the calculated reaction rate, subscript C, is renormalized to the maximum reaction rate of the benchmark experiment, subscript E.

$$\varphi_{i,n} = \frac{\varphi_i}{\varphi_{i,\max}} . \tag{4.1}$$

$$\varphi_{i,n,C} = \frac{\varphi_{i,n,C}}{\varphi_{i,n,\max,E}} . \tag{4.2}$$

The calculated axial neutron fission reaction-rate values appear to be in good agreement with the experimental measurements; all values are within 2σ. The values reported in the right-hand column of Tables 4.6 and 4.7 represent the difference between the calculated (C) and the expected benchmark (E) values.

Table 4.6. Calculated Axial Neutron Fission Reaction Rate in the Instrumentation Columns of the HTTR (Configuration 3).

Data Point	Height (cm)[a]	Benchmark Flux	±	1σ	Calculated Flux	±	1σ	C/E
1	18.89	0.6946	±	0.0199	0.6914	±	0.0014	0.995
2	27.86	0.7304	±	0.0198	0.7326	±	0.0014	1.003
3	86.07	0.9555	±	0.0173	0.9650	±	0.0016	1.010
4	130.96	1.0000	±	0.0166	1.0000	±	0.0016	1.000
5	137.15	0.9854	±	0.0169	0.9892	±	0.0016	1.004
6	143.96	0.9750	±	0.0170	0.9761	±	0.0016	1.001
7	202.48	0.6735	±	0.0200	0.6894	±	0.0014	1.024
8	260.99	0.2818	±	0.0165	0.3043	±	0.0009	1.080
9	318.58	0.1041	±	0.0095	0.1111	±	0.0005	1.068

(a) The height is in reference to the position relative to the bottom of the fifth layer of fuel.

Table 4.7. Calculated Axial Neutron Fission Reaction Rate in the Instrumentation Columns of the HTTR (Configuration 4).

Data Point	Height (cm)[a]	Benchmark Reaction Rate	±	1σ	Calculated Reaction Rate	±	1σ	C/E
1	18.79	0.7030	±	0.0199	0.6932	±	0.0015	0.986
2	28.40	0.7383	±	0.0197	0.7380	±	0.0016	1.000
3	86.36	0.9523	±	0.0174	0.9625	±	0.0018	1.011
4	115.79	1.0000	±	0.0166	1.0000	±	0.0018	1.000
5	137.45	0.9749	±	0.0170	0.9704	±	0.0018	0.995
6	144.57	0.9562	±	0.0173	0.9569	±	0.0018	1.001
7	202.72	0.7915	±	0.0193	0.7905	±	0.0016	0.999
8	260.85	0.5582	±	0.0201	0.5625	±	0.0014	1.008
9	318.37	0.3312	±	0.0176	0.3417	±	0.0011	1.032

(a) The height is in reference to the position relative to the bottom of the fifth layer of fuel.

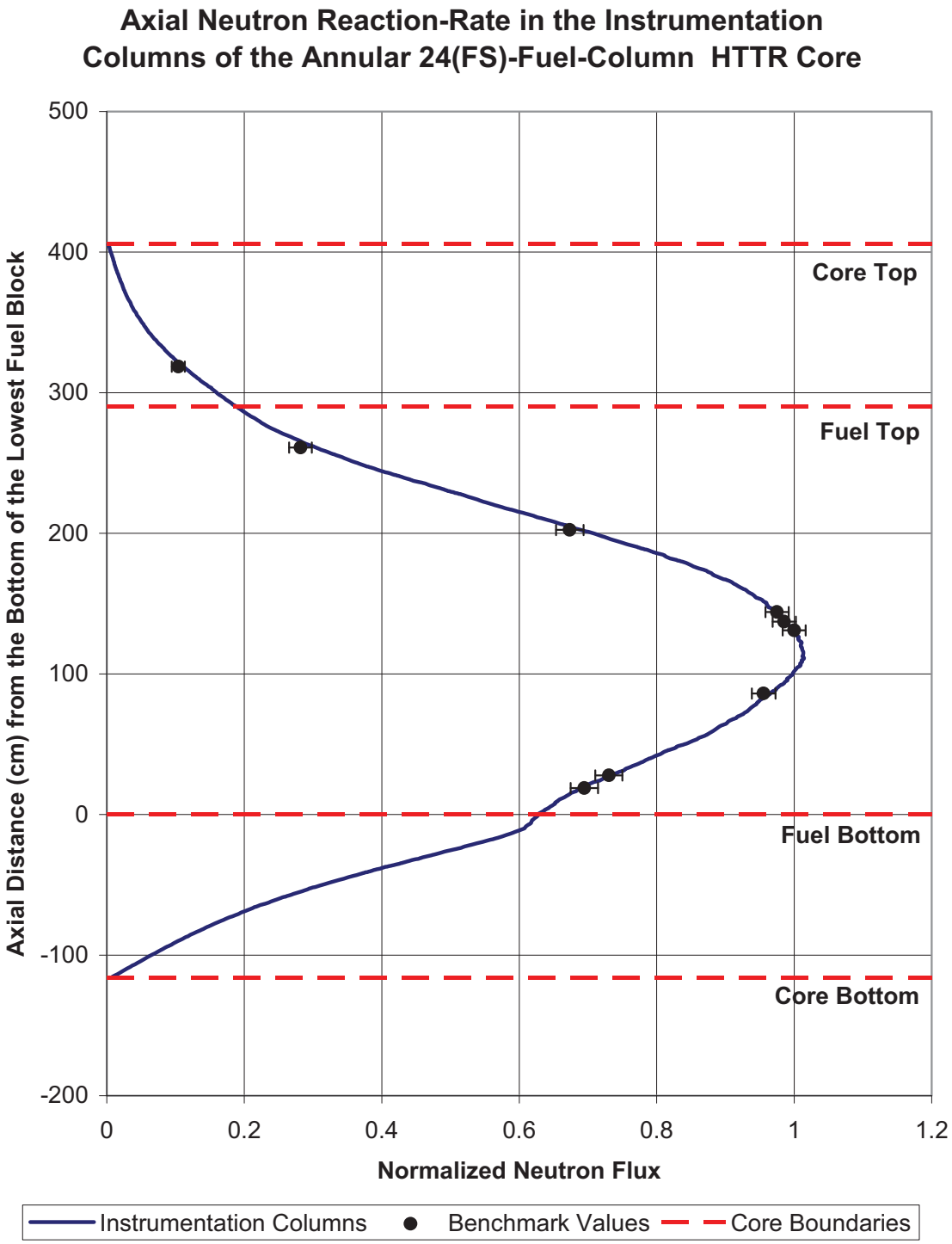

Figure 4.3. Calculated Axial Neutron Reaction Rate in the Instrumentation Columns of the HTTR (Configuration 3).

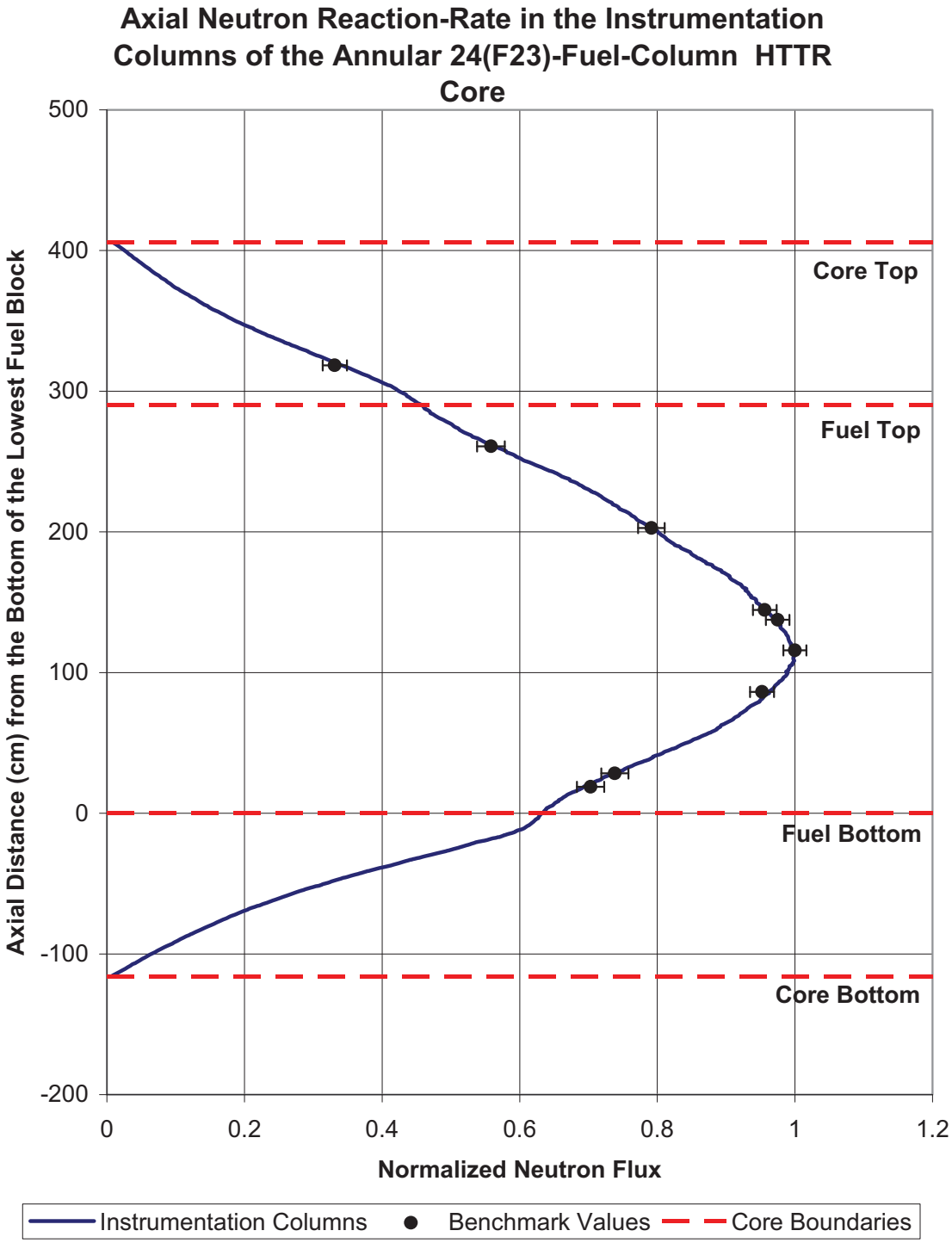

Figure 4.4. Calculated Axial Neutron Reaction Rate in the Instrumentation Columns of the HTTR (Configuration 4).

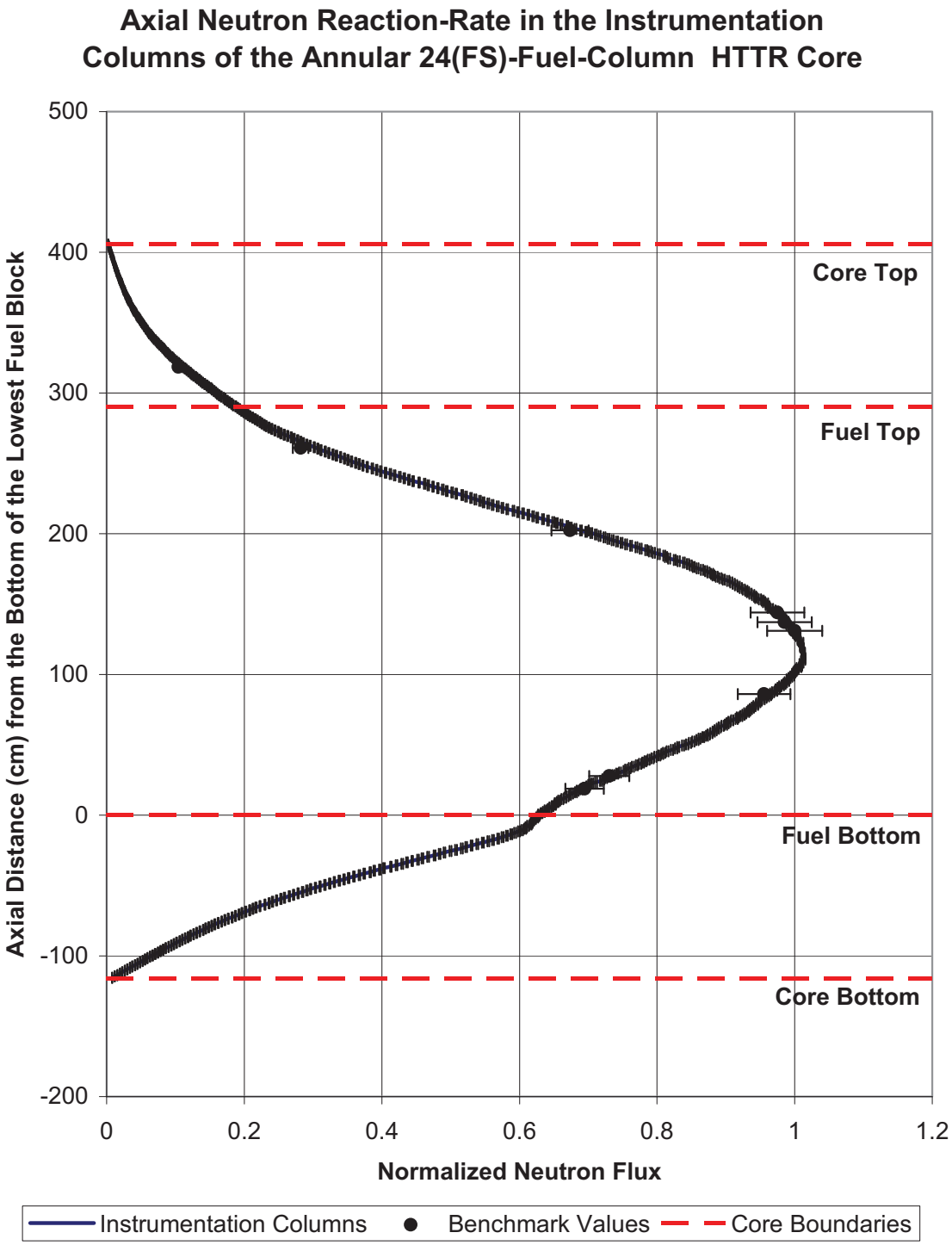

Figure 4.5. Calculated Axial Neutron Reaction Rate with Uncertainty (1σ) for Configuration 3.

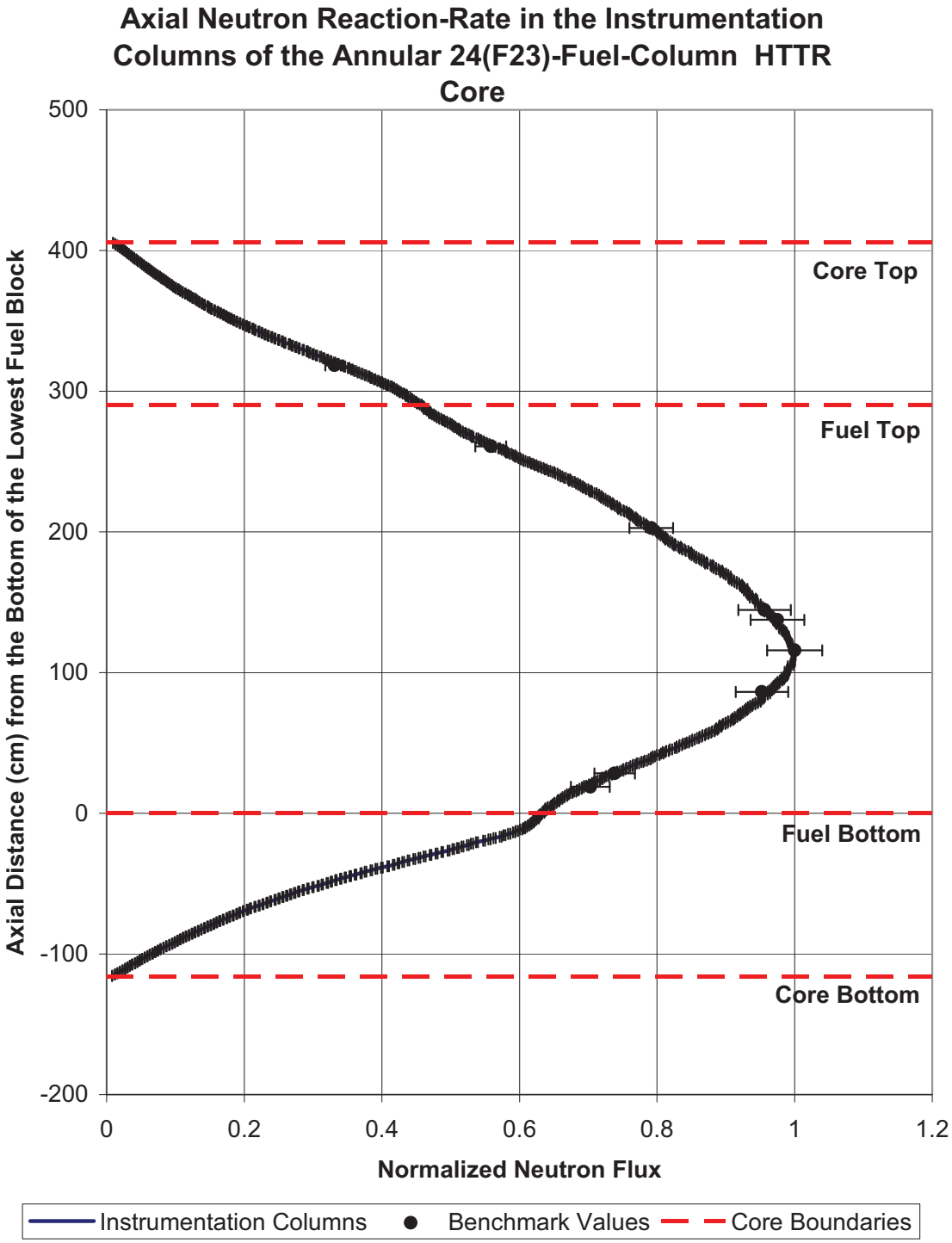

Figure 4.6. Calculated Axial Neutron Reaction Rate with Uncertainty (1σ) for Configuration 4.

4.8 Results of Power Distribution Calculations

Power distribution measurements were not made.

4.9 Results of Isotopic Calculations

Isotopic measurements were not made.

4.10 Results of Calculations for Other Miscellaneous Types of Measurements

Other miscellaneous types of measurements were not made.

5.0 REFERENCES

1. N. Fujimoto, K. Yamashita, N. Nojiri, M. Takeuchi, and S. Fujisaki, "Annular Core Experiments in HTTR's Start-Up Core Physics Tests," *Nucl. Sci. Eng.*, **150**, 310-321 (2005).

2. "Evaluation of High Temperature Gas Cooled Reactor Performance: Benchmark Analysis Related to Initial Testing of the HTTR and HTR-10," IAEA-TECDOC-1382, International Atomic Energy Agency, Vienna, November 2003.

3. S. Shiozawa, S. Fujikawa, T. Iyoku, K. Kunitomi, and Y. Tachibana, "Overview of HTTR Design Features," *Nucl. Eng. Des.*, **233**:11-21 (2004).

4. N. Nojiri, S. Shimakawa, N. Fujimoto, and M. Goto, "Characteristic Test of Initial HTTR Core," *Nucl. Eng. Des.*, **233**: 283-290 (2004).

APPENDIX A: COMPUTER CODES, CROSS SECTIONS, AND TYPICAL INPUT LISTINGS

A.1 Critical Configuration

A.1.1 Name(s) of code system(s) used.

1. Monte Carlo n-Particle, version 5.1.40 (MCNP5)
2. Monte Carlo n-Particle Extensions, version 2.5.0 (MCNPX)

A.1.2 Bibliographic references for the codes used.

1. X-5 Monte Carlo Team, "MCNP – a General Monte Carlo n-Particle Transport Code, version 5," LA-UR-03-1987, Los Alamos National Laboratory (2003).
2. J. S. Hendricks, et al., "MCNPX Extensions," LA-UR-05-2675, Los Alamos National Laboratory (April 2005).

A.1.3 Origin of cross-section data.

The Evaluated Neutron Data File library, ENDF/B-VII.0,[a] was utilized in the benchmark model analysis. Other versions, including ENDF/B-V.2[b] and ENDF/B-VI.8,[c] were used with the benchmark model for a baseline comparison. The European Joint Evaluated Fission and Fusion File, JEFF-3.1[d] and the Japanese Evaluated Nuclear Data Library, JENDL-3.3,[e] were also included for a basic evaluative comparison. Such comparisons are typical.[fg] The JENDL-3.3 analysis was performed with the inclusion of ENDF/B-VII.0 thermal neutron scattering data because it was not included in the JENDL-3.3 library. Thermal neutron scattering, or S(α,β), adjusts the neutron cross sections for neutron upscatter at thermal energies and provides scattering data for elements bound within specific materials.

A.1.4 Spectral calculations and data reduction methods used.

Not applicable

A.1.5 Number of energy groups or if continuous-energy cross sections are used in the different phases of the calculation.

Continuous-energy cross sections

---

[a] M. B. Chadwick, et al., "ENDF/B-VII.0: Next Generation Evaluated Nuclear Data Library for Nuclear Science and Technology," *Nucl. Data Sheets*, **107**: 2931-3060 (2006).

[b] R. Kinsey, Ed., ENDF/B Summary Documentation, BNL-NCS-17542 (ENDF-201), 3rd ed., Brookhaven National Laboratory (1979).

[c] H. D. Lemmel, P. K. McLaughlin, and V. G. Pronyaev, "ENDF/B-VI Release 8 (Last Release of ENDF/B-VI) the U.S. Evaluated Nuclear Data Library for Neutron Reaction Data," IAEA-NDS-100 Rev. 11, International Atomic Energy Agency, Vienna (November 2001).

[d] A. Koning, R. Forrest, M. Kellett, R. Mills, H. Henriksson, and Y. Rugama, "The JEFF-3.1 Nuclear Data Library," JEFF Report 21, Organisation for Economic Co-operation and Development, Paris (2006).

[e] K. Shibata, et al., "Japanese Evaluated Nuclear Data Library Version 3 Revision-3: JENDL-3.3," *J. Nucl. Sci. Tech.*, **39**(11): 1125-1136 (November 2002).

[f] A. C. Kahler, "Monte Carlo Eigenvalue Calculations withENDF/B-VI.8, JEFF-3.0, and JENDL-3.3 Cross Sections for a Selection of International Criticality Safety Benchmark Evaluation Project Handbook Benchmarks," *Nucl. Sci. Eng.*, **145**: 213-224 (2003).

[g] M. Goto, N. Nojiri, and S. Shimakawa, "Neutronics Calculations of HTTR with Several Nuclear Data Libraries," *J. Nucl. Sci. Tech.*, **43**(10): 1237-1244 (2006).

A.1.6 Component calculations.

- Type of cell calculation – Reactor core and reflectors
- Geometry – Cylindrical
- Theory used – Not applicable
- Method used – Monte Carlo
- Calculation characteristics – histories/cycles/cycles skipped = 50,000/1,050/50
  continuous-energy cross sections

A.1.7 Other assumptions and characteristics.

Not applicable

A.1.8 Typical input listings.

MCNP5 and MCNPX Input Deck for the 27-fuel-column core, configuration 5, of the HTTR:

```
HTTR Start-Up Core Critical (27 fuel columns, Configuration 5) --
c
c John Darrell Bess - Idaho National Laboratory
c Last Updated: November 13, 2009
c
c Cell Cards ***********************************************************************
c --- Fuel Column -------------------------------------------------------------
c ------ TRISO Particles ------
1    1  6.9614E-02   -1 imp:n=1 u=13 $ 3.4% kernel
2    13 5.5153E-02 1 -2 imp:n=1 u=13 $ buffer
3    14 9.2758E-02 2 -3 imp:n=1 u=13 $ IPyC
4    15 9.6122E-02 3 -4 imp:n=1 u=13 $ SiC
5    16 9.2758E-02 4 -5 imp:n=1 u=13 $ OPyC
6    17 8.5237E-02 5 -6 imp:n=1 u=13 $ overcoat
7    18 8.5237E-02 6 901 -902 903 -904 905 -906 imp:n=1 u=13 $ compact fill
11   like 1 but mat=2 u=14 rho=6.9616E-02 $ 3.9% kernel ---
12   like 2 but u=14 $ buffer
13   like 3 but u=14 $ IPyC
14   like 4 but u=14 $ SiC
15   like 5 but u=14 $ OPyC
16   like 6 but u=14 $ overcoat
17   like 7 but u=14 $ compact fill
21   like 1 but mat=3 u=15 rho=6.9617E-02 $ 4.3% kernel ---
22   like 2 but u=15 $ buffer
23   like 3 but u=15 $ IPyC
24   like 4 but u=15 $ SiC
25   like 5 but u=15 $ OPyC
26   like 6 but u=15 $ overcoat
27   like 7 but u=15 $ compact fill
31   like 1 but mat=4 u=16 rho=6.9618E-02 $ 4.8% kernel ---
32   like 2 but u=16 $ buffer
33   like 3 but u=16 $ IPyC
34   like 4 but u=16 $ SiC
35   like 5 but u=16 $ OPyC
36   like 6 but u=16 $ overcoat
37   like 7 but u=16 $ compact fill
41   like 1 but mat=5 u=17 rho=6.9619E-02 $ 5.2% kernel ---
42   like 2 but u=17 $ buffer
43   like 3 but u=17 $ IPyC
44   like 4 but u=17 $ SiC
45   like 5 but u=17 $ OPyC
46   like 6 but u=17 $ overcoat
47   like 7 but u=17 $ compact fill
51   like 1 but mat=6 u=18 rho=6.9622E-02 $ 5.9% kernel ---
52   like 2 but u=18 $ buffer
53   like 3 but u=18 $ IPyC
54   like 4 but u=18 $ SiC
55   like 5 but u=18 $ OPyC
56   like 6 but u=18 $ overcoat
57   like 7 but u=18 $ compact fill
61   like 1 but mat=7 u=19 rho=6.9623E-02 $ 6.3% kernel ---
62   like 2 but u=19 $ buffer
```

```
63   like 3 but u=19 $ IPyC
64   like 4 but u=19 $ SiC
65   like 5 but u=19 $ OPyC
66   like 6 but u=19 $ overcoat
67   like 7 but u=19 $ compact fill
71   like 1 but mat=8 u=20 rho=6.9624E-02 $ 6.7% kernel ---
72   like 2 but u=20 $ buffer
73   like 3 but u=20 $ IPyC
74   like 4 but u=20 $ SiC
75   like 5 but u=20 $ OPyC
76   like 6 but u=20 $ overcoat
77   like 7 but u=20 $ compact fill
81   like 1 but mat=9 u=21 rho=6.9625E-02 $ 7.2% kernel ---
82   like 2 but u=21 $ buffer
83   like 3 but u=21 $ IPyC
84   like 4 but u=21 $ SiC
85   like 5 but u=21 $ OPyC
86   like 6 but u=21 $ overcoat
87   like 7 but u=21 $ compact fill
91   like 1 but mat=10 u=22 rho=6.9628E-02 $ 7.9% kernel ---
92   like 2 but u=22 $ buffer
93   like 3 but u=22 $ IPyC
94   like 4 but u=22 $ SiC
95   like 5 but u=22 $ OPyC
96   like 6 but u=22 $ overcoat
97   like 7 but u=22 $ compact fill
101  like 1 but mat=11 u=23 rho=6.9632E-02 $ 9.4% kernel ---
102  like 2 but u=23 $ buffer
103  like 3 but u=23 $ IPyC
104  like 4 but u=23 $ SiC
105  like 5 but u=23 $ OPyC
106  like 6 but u=23 $ overcoat
107  like 7 but u=23 $ compact fill
111  like 1 but mat=12 u=24 rho=6.9634E-02 $ 9.9% kernel ---
112  like 2 but u=24 $ buffer
113  like 3 but u=24 $ IPyC
114  like 4 but u=24 $ SiC
115  like 5 but u=24 $ OPyC
116  like 6 but u=24 $ overcoat
117  like 7 but u=24 $ compact fill
c
c ------ Compacts ------
120  18 8.5237E-02 901 -902 903 -904 905 -906 imp:n=1 u=300 $ compact fill
163  0 911 -912 913 -914 915 -916 imp:n=1 u=25 lat=1 fill=-13:13 -13:13 0:0
     300 26r 300 26r 300 9r 13 6r 300 9r 300 7r 13 10r 300 7r
     300 5r 13 14r 300 5r 300 4r 13 16r 300 4r 300 3r 13 18r 300 3r
     300 3r 13 18r 300 3r 300 2r 13 8r 300 2r 13 8r 300 2r
     300 1r 13 7r 300 6r 13 6r 300 2r 300 1r 13 6r 300 8r 13 6r 300 1r
     300 1r 13 6r 300 8r 13 6r 300 1r 300 1r 13 5r 300 10r 13 5r 300 1r
     300 1r 13 5r 300 10r 13 5r 300 1r 300 1r 13 5r 300 10r 13 5r 300 1r
     300 1r 13 6r 300 8r 13 6r 300 1r 300 1r 13 6r 300 8r 13 6r 300 1r
     300 2r 13 6r 300 6r 13 6r 300 2r 300 2r 13 8r 300 2r 13 8r 300 2r
     300 3r 13 18r 300 3r 300 3r 13 18r 300 3r 300 4r 13 16r 300 4r
     300 5r 13 14r 300 5r 300 7r 13 10r 300 7r 300 9r 13 6r 300 9r
     300 26r 300 26r
164  like 163 but u=26 fill=-13:13 -13:13 0:0
     300 26r 300 26r 300 9r 14 6r 300 9r 300 7r 14 10r 300 7r
     300 5r 14 14r 300 5r 300 4r 14 16r 300 4r 300 3r 14 18r 300 3r
     300 3r 14 18r 300 3r 300 2r 14 8r 300 2r 14 8r 300 2r
     300 1r 14 7r 300 6r 14 6r 300 2r 300 1r 14 6r 300 8r 14 6r 300 1r
     300 1r 14 6r 300 8r 14 6r 300 1r 300 1r 14 5r 300 10r 14 5r 300 1r
     300 1r 14 5r 300 10r 14 5r 300 1r 300 1r 14 5r 300 10r 14 5r 300 1r
     300 1r 14 6r 300 8r 14 6r 300 1r 300 1r 14 6r 300 8r 14 6r 300 1r
     300 2r 14 6r 300 6r 14 6r 300 2r 300 2r 14 8r 300 2r 14 8r 300 2r
     300 3r 14 18r 300 3r 300 3r 14 18r 300 3r 300 4r 14 16r 300 4r
     300 5r 14 14r 300 5r 300 7r 14 10r 300 7r 300 9r 14 6r 300 9r
     300 26r 300 26r
165  like 163 but u=27 fill=-13:13 -13:13 0:0
     300 26r 300 26r 300 9r 15 6r 300 9r 300 7r 15 10r 300 7r
     300 5r 15 14r 300 5r 300 4r 15 16r 300 4r 300 3r 15 18r 300 3r
     300 3r 15 18r 300 3r 300 2r 15 8r 300 2r 15 8r 300 2r
     300 1r 15 7r 300 6r 15 6r 300 2r 300 1r 15 6r 300 8r 15 6r 300 1r
     300 1r 15 6r 300 8r 15 6r 300 1r 300 1r 15 5r 300 10r 15 5r 300 1r
     300 1r 15 5r 300 10r 15 5r 300 1r 300 1r 15 5r 300 10r 15 5r 300 1r
     300 1r 15 6r 300 8r 15 6r 300 1r 300 1r 15 6r 300 8r 15 6r 300 1r
     300 2r 15 6r 300 6r 15 6r 300 2r 300 2r 15 8r 300 2r 15 8r 300 2r
```

```
     300 3r 15 18r 300 3r 300 3r 15 18r 300 3r 300 4r 15 16r 300 4r
     300 5r 15 14r 300 5r 300 7r 15 10r 300 7r 300 9r 15 6r 300 9r
     300 26r 300 26r
166  like 163 but u=28 fill=-13:13 -13:13 0:0
     300 26r 300 26r 300 9r 16 6r 300 9r 300 7r 16 10r 300 7r
     300 5r 16 14r 300 5r 300 4r 16 16r 300 4r 300 3r 16 18r 300 3r
     300 3r 16 18r 300 3r 300 2r 16 8r 300 2r 16 8r 300 2r
     300 1r 16 7r 300 6r 16 6r 300 2r 300 1r 16 6r 300 8r 16 6r 300 1r
     300 1r 16 6r 300 8r 16 6r 300 1r 300 1r 16 5r 300 10r 16 5r 300 1r
     300 1r 16 5r 300 10r 16 5r 300 1r 300 1r 16 5r 300 10r 16 5r 300 1r
     300 1r 16 6r 300 8r 16 6r 300 1r 300 1r 16 6r 300 8r 16 6r 300 1r
     300 2r 16 6r 300 6r 16 6r 300 2r 300 2r 16 8r 300 2r 16 8r 300 2r
     300 3r 16 18r 300 3r 300 3r 16 18r 300 3r 300 4r 16 16r 300 4r
     300 5r 16 14r 300 5r 300 7r 16 10r 300 7r 300 9r 16 6r 300 9r
     300 26r 300 26r
167  like 163 but u=29 fill=-13:13 -13:13 0:0
     300 26r 300 26r 300 9r 17 6r 300 9r 300 7r 17 10r 300 7r
     300 5r 17 14r 300 5r 300 4r 17 16r 300 4r 300 3r 17 18r 300 3r
     300 3r 17 18r 300 3r 300 2r 17 8r 300 2r 17 8r 300 2r
     300 1r 17 7r 300 6r 17 6r 300 2r 300 1r 17 6r 300 8r 17 6r 300 1r
     300 1r 17 6r 300 8r 17 6r 300 1r 300 1r 17 5r 300 10r 17 5r 300 1r
     300 1r 17 5r 300 10r 17 5r 300 1r 300 1r 17 5r 300 10r 17 5r 300 1r
     300 1r 17 6r 300 8r 17 6r 300 1r 300 1r 17 6r 300 8r 17 6r 300 1r
     300 2r 17 6r 300 6r 17 6r 300 2r 300 2r 17 8r 300 2r 17 8r 300 2r
     300 3r 17 18r 300 3r 300 3r 17 18r 300 3r 300 4r 17 16r 300 4r
     300 5r 17 14r 300 5r 300 7r 17 10r 300 7r 300 9r 17 6r 300 9r
     300 26r 300 26r
168  like 163 but u=30 fill=-13:13 -13:13 0:0
     300 26r 300 26r 300 9r 18 6r 300 9r 300 7r 18 10r 300 7r
     300 5r 18 14r 300 5r 300 4r 18 16r 300 4r 300 3r 18 18r 300 3r
     300 3r 18 18r 300 3r 300 2r 18 8r 300 2r 18 8r 300 2r
     300 1r 18 7r 300 6r 18 6r 300 2r 300 1r 18 6r 300 8r 18 6r 300 1r
     300 1r 18 6r 300 8r 18 6r 300 1r 300 1r 18 5r 300 10r 18 5r 300 1r
     300 1r 18 5r 300 10r 18 5r 300 1r 300 1r 18 5r 300 10r 18 5r 300 1r
     300 1r 18 6r 300 8r 18 6r 300 1r 300 1r 18 6r 300 8r 18 6r 300 1r
     300 2r 18 6r 300 6r 18 6r 300 2r 300 2r 18 8r 300 2r 18 8r 300 2r
     300 3r 18 18r 300 3r 300 3r 18 18r 300 3r 300 4r 18 16r 300 4r
     300 5r 18 14r 300 5r 300 7r 18 10r 300 7r 300 9r 18 6r 300 9r
     300 26r 300 26r
169  like 163 but u=31 fill=-13:13 -13:13 0:0
     300 26r 300 26r 300 9r 19 6r 300 9r 300 7r 19 10r 300 7r
     300 5r 19 14r 300 5r 300 4r 19 16r 300 4r 300 3r 19 18r 300 3r
     300 3r 19 18r 300 3r 300 2r 19 8r 300 2r 19 8r 300 2r
     300 1r 19 7r 300 6r 19 6r 300 2r 300 1r 19 6r 300 8r 19 6r 300 1r
     300 1r 19 6r 300 8r 19 6r 300 1r 300 1r 19 5r 300 10r 19 5r 300 1r
     300 1r 19 5r 300 10r 19 5r 300 1r 300 1r 19 5r 300 10r 19 5r 300 1r
     300 1r 19 6r 300 8r 19 6r 300 1r 300 1r 19 6r 300 8r 19 6r 300 1r
     300 2r 19 6r 300 6r 19 6r 300 2r 300 2r 19 8r 300 2r 19 8r 300 2r
     300 3r 19 18r 300 3r 300 3r 19 18r 300 3r 300 4r 19 16r 300 4r
     300 5r 19 14r 300 5r 300 7r 19 10r 300 7r 300 9r 19 6r 300 9r
     300 26r 300 26r
180  like 163 but u=32 fill=-13:13 -13:13 0:0
     300 26r 300 26r 300 9r 20 6r 300 9r 300 7r 20 10r 300 7r
     300 5r 20 14r 300 5r 300 4r 20 16r 300 4r 300 3r 20 18r 300 3r
     300 3r 20 18r 300 3r 300 2r 20 8r 300 2r 20 8r 300 2r
     300 1r 20 7r 300 6r 20 6r 300 2r 300 1r 20 6r 300 8r 20 6r 300 1r
     300 1r 20 6r 300 8r 20 6r 300 1r 300 1r 20 5r 300 10r 20 5r 300 1r
     300 1r 20 5r 300 10r 20 5r 300 1r 300 1r 20 5r 300 10r 20 5r 300 1r
     300 1r 20 6r 300 8r 20 6r 300 1r 300 1r 20 6r 300 8r 20 6r 300 1r
     300 2r 20 6r 300 6r 20 6r 300 2r 300 2r 20 8r 300 2r 20 8r 300 2r
     300 3r 20 18r 300 3r 300 3r 20 18r 300 3r 300 4r 20 16r 300 4r
     300 5r 20 14r 300 5r 300 7r 20 10r 300 7r 300 9r 20 6r 300 9r
     300 26r 300 26r
181  like 163 but u=33 fill=-13:13 -13:13 0:0
     300 26r 300 26r 300 9r 21 6r 300 9r 300 7r 21 10r 300 7r
     300 5r 21 14r 300 5r 300 4r 21 16r 300 4r 300 3r 21 18r 300 3r
     300 3r 21 18r 300 3r 300 2r 21 8r 300 2r 21 8r 300 2r
     300 1r 21 7r 300 6r 21 6r 300 2r 300 1r 21 6r 300 8r 21 6r 300 1r
     300 1r 21 6r 300 8r 21 6r 300 1r 300 1r 21 5r 300 10r 21 5r 300 1r
     300 1r 21 5r 300 10r 21 5r 300 1r 300 1r 21 5r 300 10r 21 5r 300 1r
     300 1r 21 6r 300 8r 21 6r 300 1r 300 1r 21 6r 300 8r 21 6r 300 1r
     300 2r 21 6r 300 6r 21 6r 300 2r 300 2r 21 8r 300 2r 21 8r 300 2r
     300 3r 21 18r 300 3r 300 3r 21 18r 300 3r 300 4r 21 16r 300 4r
     300 5r 21 14r 300 5r 300 7r 21 10r 300 7r 300 9r 21 6r 300 9r
     300 26r 300 26r
182  like 163 but u=34 fill=-13:13 -13:13 0:0
```

```
     300 26r 300 26r 300 9r 22 6r 300 9r 300 7r 22 10r 300 7r
     300 5r 22 14r 300 5r 300 4r 22 16r 300 4r 300 3r 22 18r 300 3r
     300 3r 22 18r 300 3r 300 2r 22 8r 300 2r 22 8r 300 2r
     300 1r 22 7r 300 6r 22 6r 300 2r 300 1r 22 6r 300 8r 22 6r 300 1r
     300 1r 22 6r 300 8r 22 6r 300 1r 300 1r 22 5r 300 10r 22 5r 300 1r
     300 1r 22 5r 300 10r 22 5r 300 1r 300 1r 22 5r 300 10r 22 5r 300 1r
     300 1r 22 6r 300 8r 22 6r 300 1r 300 1r 22 6r 300 8r 22 6r 300 1r
     300 2r 22 6r 300 6r 22 6r 300 2r 300 2r 22 8r 300 2r 22 8r 300 2r
     300 3r 22 18r 300 3r 300 3r 22 18r 300 3r 300 4r 22 16r 300 4r
     300 5r 22 14r 300 5r 300 7r 22 10r 300 7r 300 9r 22 6r 300 9r
     300 26r 300 26r
183  like 163 but u=35 fill=-13:13 -13:13 0:0
     300 26r 300 26r 300 9r 23 6r 300 9r 300 7r 23 10r 300 7r
     300 5r 23 14r 300 5r 300 4r 23 16r 300 4r 300 3r 23 18r 300 3r
     300 3r 23 18r 300 3r 300 2r 23 8r 300 2r 23 8r 300 2r
     300 1r 23 7r 300 6r 23 6r 300 2r 300 1r 23 6r 300 8r 23 6r 300 1r
     300 1r 23 6r 300 8r 23 6r 300 1r 300 1r 23 5r 300 10r 23 5r 300 1r
     300 1r 23 5r 300 10r 23 5r 300 1r 300 1r 23 5r 300 10r 23 5r 300 1r
     300 1r 23 6r 300 8r 23 6r 300 1r 300 1r 23 6r 300 8r 23 6r 300 1r
     300 2r 23 6r 300 6r 23 6r 300 2r 300 2r 23 8r 300 2r 23 8r 300 2r
     300 3r 23 18r 300 3r 300 3r 23 18r 300 3r 300 4r 23 16r 300 4r
     300 5r 23 14r 300 5r 300 7r 23 10r 300 7r 300 9r 23 6r 300 9r
     300 26r 300 26r
184  like 163 but u=36 fill=-13:13 -13:13 0:0
     300 26r 300 26r 300 9r 24 6r 300 9r 300 7r 24 10r 300 7r
     300 5r 24 14r 300 5r 300 4r 24 16r 300 4r 300 3r 24 18r 300 3r
     300 3r 24 18r 300 3r 300 2r 24 8r 300 2r 24 8r 300 2r
     300 1r 24 7r 300 6r 24 6r 300 2r 300 1r 24 6r 300 8r 24 6r 300 1r
     300 1r 24 6r 300 8r 24 6r 300 1r 300 1r 24 5r 300 10r 24 5r 300 1r
     300 1r 24 5r 300 10r 24 5r 300 1r 300 1r 24 5r 300 10r 24 5r 300 1r
     300 1r 24 6r 300 8r 24 6r 300 1r 300 1r 24 6r 300 8r 24 6r 300 1r
     300 2r 24 6r 300 6r 24 6r 300 2r 300 2r 24 8r 300 2r 24 8r 300 2r
     300 3r 24 18r 300 3r 300 3r 24 18r 300 3r 300 4r 24 16r 300 4r
     300 5r 24 14r 300 5r 300 7r 24 10r 300 7r 300 9r 24 6r 300 9r
     300 26r 300 26r
9163 0 921 -922 923 -924 925 -926 imp:n=1 u=925 lat=1 fill=25
9164 like 9163 but u=926 fill=26
9165 like 9163 but u=927 fill=27
9166 like 9163 but u=928 fill=28
9167 like 9163 but u=929 fill=29
9168 like 9163 but u=930 fill=30
9169 like 9163 but u=931 fill=31
9180 like 9163 but u=932 fill=32
9181 like 9163 but u=933 fill=33
9182 like 9163 but u=934 fill=34
9183 like 9163 but u=935 fill=35
9184 like 9163 but u=936 fill=36
185  0 12 -13 imp:n=1 u=37 fill=925
186  like 185 but u=38 fill=926
187  like 185 but u=39 fill=927
188  like 185 but u=40 fill=928
189  like 185 but u=41 fill=929
190  like 185 but u=42 fill=930
191  like 185 but u=43 fill=931
192  like 185 but u=44 fill=932
193  like 185 but u=45 fill=933
194  like 185 but u=46 fill=934
195  like 185 but u=47 fill=935
196  like 185 but u=48 fill=936
c
c ------ Fuel Pins ------
251  27 2.4616E-05 -12 imp:n=1 u=37 $ central hole
252  like 251 but u=38
253  like 251 but u=39
254  like 251 but u=40
255  like 251 but u=41
256  like 251 but u=42
257  like 251 but u=43
258  like 251 but u=44
259  like 251 but u=45
260  like 251 but u=46
261  like 251 but u=47
262  like 251 but u=48
263  27 2.4616E-05 13 -21 imp:n=1 u=37 $ annulus between compact and sleeve
264  like 263 but u=38
265  like 263 but u=39
```

```
266  like 263 but u=40
267  like 263 but u=41
268  like 263 but u=42
269  like 263 but u=43
270  like 263 but u=44
271  like 263 but u=45
272  like 263 but u=46
273  like 263 but u=47
274  like 263 but u=48
275  19 8.8747E-02 21 -22 imp:n=1 u=37 $ graphite sleeve
1275 like 275 but u=38
276  like 275 but u=39
277  like 275 but u=40
278  like 275 but u=41
279  like 275 but u=42
280  like 275 but u=43
281  like 275 but u=44
282  like 275 but u=45
283  like 275 but u=46
284  like 275 but u=47
285  like 275 but u=48
c
c ------ Coolant Channels ------
286  27 2.4616E-05 22 -31 imp:n=1 u=37 $ annulus between sleeve and block
287  like 286 but u=38
288  like 286 but u=39
289  like 286 but u=40
290  like 286 but u=41
291  like 286 but u=42
292  like 286 but u=43
293  like 286 but u=44
294  like 286 but u=45
295  like 286 but u=46
296  like 286 but u=47
297  like 286 but u=48
298  25 8.7804E-02 31 imp:n=1 u=37 $ graphite block
299  like 298 but u=38
300  like 298 but u=39
301  like 298 but u=40
302  like 298 but u=41
303  like 298 but u=42
304  like 298 but u=43
305  like 298 but u=44
306  like 298 but u=45
307  like 298 but u=46
308  like 298 but u=47
309  like 298 but u=48
c
c ------ BP Pins ------
351  20 9.0451E-02 -41 imp:n=1 u=50 $ 2.0%
352  like 351 but mat=21 rho=9.0501E-02 u=51 $ 2.5%
353  22 8.8747E-02 -42 imp:n=1 u=50 $ graphite disks
354  like 353 but u=51
355  20 9.0451E-02 -43 imp:n=1 u=50 $ 2.0%
356  like 355 but mat=21 rho=9.0501E-02 u=51 $ 2.5%
357  27 2.4616E-05 41 42 43 -44 imp:n=1 u=50 $ pin gap
358  like 357 but u=51
359  27 2.4616E-05 -44 imp:n=1 u=52 $ empty pin position
360  25 8.7804E-02 44 imp:n=1 u=50 $ graphite block
361  like 360 but u=51
362  like 360 but u=52
c
c ------ Dummy Blocks ------
380  27 2.4616E-05 -301 imp:n=1 u=400
381  27 2.4616E-05 -302 imp:n=1 u=400
382  27 2.4616E-05 -303 imp:n=1 u=400
383  28 8.7305E-02 301 302 303 -502 imp:n=1 u=400
384  27 2.4616E-05 502 imp:n=1 u=400
c
c ------ Blocks ------
401  25 8.7804E-02 -501 imp:n=1 u=61 lat=2 fill= -5:5 -5:5 0:0 $ Zone 1 Lvl 4/5
     61 10r
     61 10r
     61  4r       50  37  37  37       61 1r
     61  3r     37  37  37  37  37     61 1r
     61  2r   37  37  37  37  37  37   61 1r
```

```
     61  1r 37  37  37  61  37  37  52 61 1r
     61  1r   37  37  37  37  37  37   61 2r
     61  1r     37  37  37  37  37     61 3r
     61  1r       50  37  37  37       61 4r
     61 10r
     61 10r
402  25 8.7804E-02 -501 imp:n=1 u=62 lat=2 fill= -5:5 -5:5 0:0 $ Zone 1 Lvl 3
     62 10r
     62 10r
     62  4r       51  39  39  39       62 1r
     62  3r     39  39  39  39  39     62 1r
     62  2r   39  39  39  39  39  39   62 1r
     62  1r 39  39  39  62  39  39  52 62 1r
     62  1r   39  39  39  39  39  39   62 2r
     62  1r     39  39  39  39  39     62 3r
     62  1r       51  39  39  39       62 4r
     62 10r
     62 10r
403  25 8.7804E-02 -501 imp:n=1 u=63 lat=2 fill= -5:5 -5:5 0:0 $ Zone 1 Lvl 2
     63 10r
     63 10r
     63  4r       51  41  41  41       63 1r
     63  3r     41  41  41  41  41     63 1r
     63  2r   41  41  41  41  41  41   63 1r
     63  1r 41  41  41  63  41  41  52 63 1r
     63  1r   41  41  41  41  41  41   63 2r
     63  1r     41  41  41  41  41     63 3r
     63  1r       51  41  41  41       63 4r
     63 10r
     63 10r
404  25 8.7804E-02 -501 imp:n=1 u=64 lat=2 fill= -5:5 -5:5 0:0 $ Zone 1 Lvl 1
     64 10r
     64 10r
     64  4r       50  44  44  44       64 1r
     64  3r     44  44  44  44  44     64 1r
     64  2r   44  44  44  44  44  44   64 1r
     64  1r 44  44  44  64  44  44  52 64 1r
     64  1r   44  44  44  44  44  44   64 2r
     64  1r     44  44  44  44  44     64 3r
     64  1r       50  44  44  44       64 4r
     64 10r
     64 10r
405  25 8.7804E-02 -501 imp:n=1 u=65 lat=2 fill= -5:5 -5:5 0:0 $ Zone 2 Lvl 4/5
     65 10r
     65 10r
     65  4r       50  38  38  38       65 1r
     65  3r     38  38  38  38  38     65 1r
     65  2r   38  38  38  38  38  38   65 1r
     65  1r 38  38  38  65  38  38  52 65 1r
     65  1r   38  38  38  38  38  38   65 2r
     65  1r     38  38  38  38  38     65 3r
     65  1r       50  38  38  38       65 4r
     65 10r
     65 10r
406  25 8.7804E-02 -501 imp:n=1 u=66 lat=2 fill= -5:5 -5:5 0:0 $ Zone 2 Lvl 3
     66 10r
     66 10r
     66  4r       51  41  41  41       66 1r
     66  3r     41  41  41  41  41     66 1r
     66  2r   41  41  41  41  41  41   66 1r
     66  1r 41  41  41  66  41  41  52 66 1r
     66  1r   41  41  41  41  41  41   66 2r
     66  1r     41  41  41  41  41     66 3r
     66  1r       51  41  41  41       66 4r
     66 10r
     66 10r
407  25 8.7804E-02 -501 imp:n=1 u=67 lat=2 fill= -5:5 -5:5 0:0 $ Zone 2 Lvl 2
     67 10r
     67 10r
     67  4r       51  43  43  43       67 1r
     67  3r     43  43  43  43  43     67 1r
     67  2r   43  43  43  43  43  43   67 1r
     67  1r 43  43  43  67  43  43  52 67 1r
     67  1r   43  43  43  43  43  43   67 2r
     67  1r     43  43  43  43  43     67 3r
     67  1r       51  43  43  43       67 4r
```

```
     67 10r
     67 10r
408  25 8.7804E-02 -501 imp:n=1 u=68 lat=2 fill= -5:5 -5:5 0:0 $ Zone 2 Lvl 1
     68 10r
     68 10r
     68  4r       50  46  46  46       68 1r
     68  3r     46  46  46  46  46     68 1r
     68  2r   46  46  46  46  46  46   68 1r
     68  1r 46  46  46  68  46  46  52 68 1r
     68  1r   46  46  46  46  46  46   68 2r
     68  1r     46  46  46  46  46     68 3r
     68  1r       50  46  46  46       68 4r
     68 10r
     68 10r
409  25 8.7804E-02 -501 imp:n=1 u=69 lat=2 fill= -5:5 -5:5 0:0 $ Zone 3 Lvl 4/5
     69 10r
     69 10r
     69  4r       50  39  39  69       69 1r
     69  3r     39  39  39  39  39     69 1r
     69  2r   39  39  39  39  39  39   69 1r
     69  1r 39  39  39  69  39  39  52 69 1r
     69  1r   39  39  39  39  39  39   69 2r
     69  1r     39  39  39  39  39     69 3r
     69  1r       50  39  39  69       69 4r
     69 10r
     69 10r
410  25 8.7804E-02 -501 imp:n=1 u=70 lat=2 fill= -5:5 -5:5 0:0 $ Zone 3 Lvl 3
     70 10r
     70 10r
     70  4r       51  42  42  70       70 1r
     70  3r     42  42  42  42  42     70 1r
     70  2r   42  42  42  42  42  42   70 1r
     70  1r 42  42  42  70  42  42  52 70 1r
     70  1r   42  42  42  42  42  42   70 2r
     70  1r     42  42  42  42  42     70 3r
     70  1r       51  42  42  70       70 4r
     70 10r
     70 10r
411  25 8.7804E-02 -501 imp:n=1 u=71 lat=2 fill= -5:5 -5:5 0:0 $ Zone 3 Lvl 2
     71 10r
     71 10r
     71  4r       51  45  45  71       71 1r
     71  3r     45  45  45  45  45     71 1r
     71  2r   45  45  45  45  45  45   71 1r
     71  1r 45  45  45  71  45  45  52 71 1r
     71  1r   45  45  45  45  45  45   71 2r
     71  1r     45  45  45  45  45     71 3r
     71  1r       51  45  45  71       71 4r
     71 10r
     71 10r
412  25 8.7804E-02 -501 imp:n=1 u=72 lat=2 fill= -5:5 -5:5 0:0 $ Zone 3 Lvl 1
     72 10r
     72 10r
     72  4r       50  47  47  72       72 1r
     72  3r     47  47  47  47  47     72 1r
     72  2r   47  47  47  47  47  47   72 1r
     72  1r 47  47  47  72  47  47  52 72 1r
     72  1r   47  47  47  47  47  47   72 2r
     72  1r     47  47  47  47  47     72 3r
     72  1r       50  47  47  72       72 4r
     72 10r
     72 10r
413  25 8.7804E-02 -501 imp:n=1 u=73 lat=2 fill= -5:5 -5:5 0:0 $ Zone 4 Lvl 4/5
     73 10r
     73 10r
     73  4r       50  40  40  73       73 1r
     73  3r     40  40  40  40  40     73 1r
     73  2r   40  40  40  40  40  40   73 1r
     73  1r 40  40  40  73  40  40  52 73 1r
     73  1r   40  40  40  40  40  40   73 2r
     73  1r     40  40  40  40  40     73 3r
     73  1r       50  40  40  73       73 4r
     73 10r
     73 10r
414  25 8.7804E-02 -501 imp:n=1 u=74 lat=2 fill= -5:5 -5:5 0:0 $ Zone 4 Lvl 3
     74 10r
```

```
     74 10r
     74  4r       51  43  43  74       74 1r
     74  3r     43  43  43  43  43     74 1r
     74  2r   43  43  43  43  43  43   74 1r
     74  1r 43  43  43  74  43  43  52 74 1r
     74  1r   43  43  43  43  43  43   74 2r
     74  1r     43  43  43  43  43     74 3r
     74  1r       51  43  43  74       74 4r
     74 10r
     74 10r
415  25 8.7804E-02 -501 imp:n=1 u=75 lat=2 fill= -5:5 -5:5 0:0 $ Zone 4 Lvl 2
     75 10r
     75 10r
     75  4r       51  46  46  75       75 1r
     75  3r     46  46  46  46  46     75 1r
     75  2r   46  46  46  46  46  46   75 1r
     75  1r 46  46  46  75  46  46  52 75 1r
     75  1r   46  46  46  46  46  46   75 2r
     75  1r     46  46  46  46  46     75 3r
     75  1r       51  46  46  75       75 4r
     75 10r
     75 10r
416  25 8.7804E-02 -501 imp:n=1 u=76 lat=2 fill= -5:5 -5:5 0:0 $ Zone 4 Lvl 1
     76 10r
     76 10r
     76  4r       50  48  48  76       76 1r
     76  3r     48  48  48  48  48     76 1r
     76  2r   48  48  48  48  48  48   76 1r
     76  1r 48  48  48  76  48  48  52 76 1r
     76  1r   48  48  48  48  48  48   76 2r
     76  1r     48  48  48  48  48     76 3r
     76  1r       50  48  48  76       76 4r
     76 10r
     76 10r
451  0 -502 imp:n=1 u=81 fill=61
452  like 451 but u=82 fill=62
453  like 451 but u=83 fill=63
454  like 451 but u=84 fill=64
455  like 451 but u=85 fill=65
456  like 451 but u=86 fill=66
457  like 451 but u=87 fill=67
458  like 451 but u=88 fill=68
459  like 451 but u=89 fill=69
460  like 451 but u=90 fill=70
461  like 451 but u=91 fill=71
462  like 451 but u=92 fill=72
463  like 451 but u=93 fill=73
464  like 451 but u=94 fill=74
465  like 451 but u=95 fill=75
466  like 451 but u=96 fill=76
467  27 2.4616E-05 502 imp:n=1 u=81
468  like 467 but u=82
469  like 467 but u=83
470  like 467 but u=84
471  like 467 but u=85
472  like 467 but u=86
473  like 467 but u=87
474  like 467 but u=88
475  like 467 but u=89
476  like 467 but u=90
477  like 467 but u=91
478  like 467 but u=92
479  like 467 but u=93
480  like 467 but u=94
481  like 467 but u=95
482  like 467 but u=96
c
c ------ Reflectors ------
483  27 2.4616E-05 -201 imp:n=1 u=97 $ coolant channels
484  25 8.7804E-02  201 imp:n=1 u=97 $ graphite block
485  25 8.7804E-02 -501 imp:n=1 u=98 lat=2 fill= -5:5 -5:5 0:0 $ 33-hole
     98 10r
     98 10r
     98  4r       98  97  97  97       98 1r
     98  3r     97  97  97  97  97     98 1r
     98  2r   97  97  97  97  97  97   98 1r
```

```
     98  1r 97  97  97  98  97  97  98 98 1r
     98  1r   97  97  97  97  97  97   98 2r
     98  1r     97  97  97  97  97     98 3r
     98  1r       98  97  97  97       98 4r
     98 10r
     98 10r
486  25 8.7804E-02 -501 imp:n=1 u=99 lat=2 fill= -5:5 -5:5 0:0 $ 31-hole
     99 10r
     99 10r
     99  4r       99  97  97  99       99 1r
     99  3r     97  97  97  97  97     99 1r
     99  2r   97  97  97  97  97  97   99 1r
     99  1r 97  97  97  99  97  97  99 99 1r
     99  1r   97  97  97  97  97  97   99 2r
     99  1r     97  97  97  97  97     99 3r
     99  1r       99  97  97  99       99 4r
     99 10r
     99 10r
489  0 -502 imp:n=1 u=100 fill=98
490  0 -502 imp:n=1 u=101 fill=99
491  like 467 but u=100
492  like 467 but u=101
c
c ------ Columns ------
500  27 2.4616E-05 -503 imp:n=1 u=401 lat=2 fill= -1:1 -1:1 -5:5 $ Dummy Zone
     401 401 401 401 401 401 401 401 401
     401 401 401 401 100 401 401 401 401
     401 401 401 401 100 401 401 401 401
     401 401 401 401 400 401 401 401 401
     401 401 401 401 400 401 401 401 401
     401 401 401 401 400 401 401 401 401
     401 401 401 401 400 401 401 401 401
     401 401 401 401 400 401 401 401 401
     401 401 401 401 100 401 401 401 401
     401 401 401 401 100 401 401 401 401
     401 401 401 401 401 401 401 401 401
501  27 2.4616E-05 -503 imp:n=1 u=121 lat=2 fill= -1:1 -1:1 -5:5 $ Zone 1
     121 121 121 121 121 121 121 121 121
     121 121 121 121 100 121 121 121 121
     121 121 121 121 100 121 121 121 121
     121 121 121 121  81 121 121 121 121
     121 121 121 121  81 121 121 121 121
     121 121 121 121  82 121 121 121 121
     121 121 121 121  83 121 121 121 121
     121 121 121 121  84 121 121 121 121
     121 121 121 121 100 121 121 121 121
     121 121 121 121 100 121 121 121 121
     121 121 121 121 121 121 121 121 121
502  27 2.4616E-05 -503 imp:n=1 u=122 lat=2 fill= -1:1 -1:1 -5:5 $ Zone 2
     122 122 122 122 122 122 122 122 122
     122 122 122 122 100 122 122 122 122
     122 122 122 122 100 122 122 122 122
     122 122 122 122  85 122 122 122 122
     122 122 122 122  85 122 122 122 122
     122 122 122 122  86 122 122 122 122
     122 122 122 122  87 122 122 122 122
     122 122 122 122  88 122 122 122 122
     122 122 122 122 100 122 122 122 122
     122 122 122 122 100 122 122 122 122
     122 122 122 122 122 122 122 122 122
503  27 2.4616E-05 -503 imp:n=1 u=123 lat=2 fill= -1:1 -1:1 -5:5 $ Zone 3
     123 123 123 123 123 123 123 123 123
     123 123 123 123 100 123 123 123 123
     123 123 123 123 100 123 123 123 123
     123 123 123 123  89 123 123 123 123
     123 123 123 123  89 123 123 123 123
     123 123 123 123  90 123 123 123 123
     123 123 123 123  91 123 123 123 123
     123 123 123 123  92 123 123 123 123
     123 123 123 123 101 123 123 123 123
     123 123 123 123 101 123 123 123 123
     123 123 123 123 123 123 123 123 123
504  27 2.4616E-05 -503 imp:n=1 u=124 lat=2 fill= -1:1 -1:1 -5:5 $ Zone 4
     124 124 124 124 124 124 124 124 124
     124 124 124 124 100 124 124 124 124
     124 124 124 124 100 124 124 124 124
```

```
     124 124 124 124  93 124 124 124 124
     124 124 124 124  93 124 124 124 124
     124 124 124 124  94 124 124 124 124
     124 124 124 124  95 124 124 124 124
     124 124 124 124  96 124 124 124 124
     124 124 124 124 101 124 124 124 124
     124 124 124 124 101 124 124 124 124
     124 124 124 124 124 124 124 124 124
525  0 -950 imp:n=1 u=125 fill=121 $ B04
526  like 525 but u=126 fill=121 *trcl=(0 0 0 180 90 90 270 180 90 90 90 0) $ B01
527  like 525 but u=127 fill=121 *trcl=(0 0 0 120 30 90 210 120 90 90 90 0) $ B02
528  like 525 but u=128 fill=121 *trcl=(0 0 0 60 330 90 150 60 90 90 90 0) $ B03
529  like 525 but u=129 fill=121 *trcl=(0 0 0 300 210 90 30 300 90 90 90 0) $ B05
530  like 525 but u=130 fill=121 *trcl=(0 0 0 240 150 90 330 240 90 90 90 0) $ B06
531  0 -950 imp:n=1 u=131 fill=122 $ C02
532  like 531 but u=132 fill=122 *trcl=(0 0 0 300 210 90 30 300 90 90 90 0) $ C04
533  like 531 but u=133 fill=122 *trcl=(0 0 0 240 150 90 330 240 90 90 90 0) $ C06
534  like 531 but u=134 fill=122 *trcl=(0 0 0 180 90 90 270 180 90 90 90 0) $ C08
535  like 531 but u=135 fill=122 *trcl=(0 0 0 120 30 90 210 120 90 90 90 0) $ C10
536  like 531 but u=136 fill=122 *trcl=(0 0 0 60 330 90 150 60 90 90 90 0) $ C12
537  0 -950 imp:n=1 u=137 fill=123 $ D05/09
538  like 537 but u=138 fill=123 *trcl=(0 0 0 60 330 90 150 60 90 90 90 0) $ D02/06
539  like 537 but u=139 fill=123 *trcl=(0 0 0 120 30 90 210 120 90 90 90 0) $ D03/17
540  like 537 but u=140 fill=123 *trcl=(0 0 0 300 210 90 30 300 90 90 90 0) $ D08/12
541  like 537 but u=141 fill=123 *trcl=(0 0 0 240 150 90 330 240 90 90 90 0) $ D11/15
542  like 537 but u=142 fill=123 *trcl=(0 0 0 180 90 90 270 180 90 90 90 0) $ D14/18
543  0 -950 imp:n=1 u=143 fill=124 $ D07
544  like 543 but u=144 fill=124 *trcl=(0 0 0 120 30 90 210 120 90 90 90 0) $ D01
545  like 543 but u=145 fill=124 *trcl=(0 0 0 60 330 90 150 60 90 90 90 0) $ D04
546  like 543 but u=146 fill=124 *trcl=(0 0 0 300 210 90 30 300 90 90 90 0) $ D10
547  like 543 but u=147 fill=124 *trcl=(0 0 0 240 150 90 330 240 90 90 90 0) $ D13
548  like 543 but u=148 fill=124 *trcl=(0 0 0 180 90 90 270 180 90 90 90 0) $ D16
c
c --- Control Column ------------------------------------------------------------
c ------ Control Rod Segments ------
601  24 8.7530E-02 -103 imp:n=1 u=150 $ spine
602  27 2.4616E-05 103 -104 imp:n=1 u=150 $ helium gap
603  24 8.7530E-02 104 -101 imp:n=1 u=150 $ inner clad
604  23 9.8436E-02 101 -102 imp:n=1 u=150 $ absorber
605  24 8.7530E-02 102 -105 imp:n=1 u=150 $ outer clad
606  27 2.4616E-05 105 imp:n=1 u=150 $ helium
607  0 -151 imp:n=1 u=151 lat=2 fill=150 $ rod segment
608  0 -152 imp:n=1 u=152 fill=151 $ control rod
609  27 2.4616E-05 152 imp:n=1 u=152 $ helium
c
c ------ Positions ------
610  0 -999 imp:n=1 u=153 fill=152 (0 0 189.9) $ C
611  0 -154 imp:n=1 u=154 fill=153 (10.8 0 0)
612  0 -155 imp:n=1 u=154 fill=153 (-5.4 -9.35307 0)
613  27 2.4616E-05 -156 imp:n=1 u=154 $ RSS
614  like 610 but u=155 fill=152 (0 0 189.9) $ R1
615  like 611 but u=156 fill=155 (10.8 0 0)
616  like 612 but u=156 fill=155 (-5.4 -9.35307 0)
617  like 613 but u=156
618  like 610 but u=157 fill=152 (0 0 189.9) $ R2
619  like 611 but u=158 fill=157 (10.8 0 0)
620  like 612 but u=158 fill=157 (-5.4 -9.35307 0)
621  like 613 but u=158
622  like 610 but u=159 fill=152 (0 0 405) $ R3
623  like 611 but u=160 fill=159 (10.8 0 0)
624  like 612 but u=160 fill=159 (-5.4 -9.35307 0)
625  like 613 but u=160
c
c ------ C Column ------
626  25 8.7804E-02 154 155 156 -550 imp:n=1 u=154 $ graphite blocks
627  27 2.4616E-05 550 imp:n=1 u=154
628  0 -950 imp:n=1 u=161 fill=154 $ A01
c
c ------ R1 Columns ------
629  25 8.7804E-02 154 155 156 -550 imp:n=1 u=156 $ graphite blocks
630  like 627 but u=156
631  like 628 but u=162 fill=156 $ C01
632  like 631 but u=163 *trcl=(0 0 0 300 210 90 30 300 90 90 90 0) $ C03
633  like 631 but u=164 *trcl=(0 0 0 240 150 90 330 240 90 90 90 0) $ C05
634  like 631 but u=165 *trcl=(0 0 0 180 90 90 270 180 90 90 90 0) $ C07
635  like 631 but u=166 *trcl=(0 0 0 120 30 90 210 120 90 90 90 0) $ C09
```

```
636  like 631 but u=167 *trcl=(0 0 0 60 330 90 150 60 90 90 90 0) $ C11
c
c ------ R2 Columns ------
637  25 8.7804E-02 154 155 156 -550 imp:n=1 u=158 $ graphite blocks
638  like 627 but u=158
639  like 628 but u=168 fill=158 $ E23
640  like 639 but u=169 *trcl=(0 0 0 300 210 90 30 300 90 90 90 0) $ E03
641  like 639 but u=170 *trcl=(0 0 0 240 150 90 330 240 90 90 90 0) $ E07
642  like 639 but u=171 *trcl=(0 0 0 180 90 90 270 180 90 90 90 0) $ E11
643  like 639 but u=172 *trcl=(0 0 0 120 30 90 210 120 90 90 90 0) $ E15
644  like 639 but u=173 *trcl=(0 0 0 60 330 90 150 60 90 90 90 0) $ E19
c
c ------ R3 Columns ------
645  25 8.7804E-02 154 155 156 -550 imp:n=1 u=160 $ graphite blocks
646  like 627 but u=160
647  like 628 but u=174 fill=160 $ E01
648  like 647 but u=175 *trcl=(0 0 0 240 150 90 330 240 90 90 90 0) $ E09
649  like 647 but u=176 *trcl=(0 0 0 120 30 90 210 120 90 90 90 0) $ E17
c
c --- Instrumentation Column ---------------------------------------------------
c ------ Positions ------
661  27 2.4616E-05 -155 imp:n=1 u=181
662  27 2.4616E-05 -154 imp:n=1 u=181
663  27 2.4616E-05 -156 imp:n=1 u=181
c
c ------ Columns ------
664  25 8.7804E-02 154 155 156 -550 imp:n=1 u=181 $ graphite blocks
665  like 627 but u=181
666  0 -950 imp:n=1 u=182 fill=181
c
c --- Reflector Column ----------------------------------------------------------
c ------ Columns ------
671  25 8.7804E-02 -550 imp:n=1 u=183 $ graphite blocks
672  like 627 but u=183
673  0 -950 imp:n=1 u=184 fill=183
c
c --- HTTR Core -----------------------------------------------------------------
c ------ Core Map ------
701  26 8.6134E-02 -551 imp:n=1 lat=2 u=200 fill=-6:6 -6:6 0:0
     200 12r
     200 12r
     200 5r          175 184 170 184 182          200 1r
     200 4r        184 143 138 137 145 184        200 1r
     200 3r      171 140 164 132 163 139 169      200 1r
     200 2r    184 137 133 128 401 131 138 184    200 1r
     200 1r  182 146 165 401 161 126 162 144 174  200 1r
     200 1r    184 141 134 129 401 136 142 184    200 2r
     200 1r      172 140 166 135 167 139 168      200 3r
     200 1r       184 147 142 141 148 184         200 4r
     200 1r         176 184 173 184 182           200 5r
     200 12r
     200 12r
c
c ------ Core Map Legend ---
c    u 12r
c    u 12r
c    u 5r      Z G Y G I      u 1r
c    u 4r     G 4 3 3 4 G     u 1r
c    u 3r    Y 3 X 2 X 3 Y    u 1r           |
c    u 2r   G 3 2 1 D 2 3 G   u 1r           |     \
c    u 1r  I 4 X D C 1 X 4 Z  u 1r   --------+------> N
c    u 1r   G 3 2 1 D 2 3 G   u 2r           |     /
c    u 1r    Y 3 X 2 X 3 Y    u 3r           |
c    u 1r     G 4 3 3 4 G     u 4r
c    u 1r      Z G Y G I      u 5r
c    u 12r
c    u 12r
c
c    1 = Fuel Columns #1
c    2 = Fuel Columns #2
c    3 = Fuel Columns #3
c    4 = Fuel Columns #4
c    D = Dummy Fuel Columns
c    C = Central Control Column
c    X = R1 Control Columns
c    Y = R2 Control Columns
```

```
c    Z = R3 Control Columns
c    I = Instrumentation Columns
c    G = Removable Reflector Columns
c
702  0  -602 imp:n=1 fill=200
c
c --- Permanent Reflector -------------------------------------------------------
711  26 8.6134E-02 602 -651 imp:n=1
c
c --- The Great Void ------------------------------------------------------------
999  0 651 imp:n=0
c

c Surface Cards ****************************************************************
c --- Fuel Blocks ---------------------------------------------------------------
c ------ TRISO Particles ------
1    so 0.03   $ UO2 kernal
2    so 0.036  $ buffer
3    so 0.039  $ IPyC
4    so 0.0415 $ SiC
5    so 0.046  $ OPyC
6    so 0.066  $ overcoat
901 px -0.125
902 px  0.125
903 py -0.125
904 py  0.125
905 pz -0.125
906 pz  0.125
c
c ------ Compacts ------
911 px -0.053
912 px  0.053
913 py -0.053
914 py  0.053
915 pz -0.05
916 pz 0.05
921 px -1.31
922 px 1.31
923 py -1.31
924 py 1.31
925 pz -0.05
926 pz 0.05
12   rcc 0 0 -27.3 0 0 54.6 0.5 $ inside
13   rcc 0 0 -27.3 0 0 54.6 1.3 $ outside
c
c ------ Fuel Pins ------
21   rcc 0 0 -27.45 0 0 54.9 1.325 $ inside
22   rcc 0 0 -28.85 0 0 57.7 1.7   $ outside
c
c ------ Coolant Channels ------
31   rcc 0 0 -31 0 0 62 2.05
c
c ------ BP Pins ------
41   rcc 0 0 -25 0 0 20 0.7  $ BP
42   rcc 0 0  -5 0 0 10 0.7  $ graphite
43   rcc 0 0   5 0 0 20 0.7  $ BP
44   rcc 0 0 -25 0 0 50 0.75 $ pin
c
c --- Control Blocks ------------------------------------------------------------
c ------ Control Rod Segments ------
101  rcc 0 0 11 0 0 29 3.75 $ inside
102  rcc 0 0 11 0 0 29 5.25 $ outside
103  rcc 0 0 11 0 0 29 0.5 $ spine
104  rcc 0 0 11 0 0 29 3.25 $ inside clad
105  rcc 0 0 10 0 0 31 5.65 $ outside clad
c
c ------ Positions ------
151  hex 0 0 10 0 0 31 10 $ "box"
152  rcc 0 0 -145 0 0 310 6.30 $ control rod
154  rcc 10.8 0 -155 0 0 416 6.15 $ control rod hole
155  rcc -5.4 -9.35307 -155 0 0 416 6.15 $ control rod hole
156  rcc -5.4 9.35307 -155 0 0 416 6.15 $ control rod hole
c
c --- Reflector Blocks ----------------------------------------------------------
c ------ Coolant Channels ------
201  rcc 0 0 -31 0 0 62 1.15
```

```
c
c --- Dummy Blocks ------------------------------------------------------------
c ------ Coolant Channels ------
301  rcc -10.8 0 -29.5 0 0 59 6.15
302  rcc 5.4 9.35307 -29.5 0 0 59 6.15
303  rcc 5.4 -9.35307 -29.5 0 0 59 6.15
c
c --- Blocks ------------------------------------------------------------------
501  hex 0 0 -30 0 0 60 2.575 0 0 $ pitch
502  hex 0 0 -29.5 0 0 59 0 18 0 $ graphite
503  hex 0 0 -29 0 0 58 0 18.2 0 $ helium
c
c --- Columns -----------------------------------------------------------------
550  hex 0 0 -261.5 0 0 523 0 18 0
551  hex 0 0 -261 0 0 522 0 18.1 0
c
c --- HTTR Core ---------------------------------------------------------------
602  hex 0 0 -261 0 0 522 -148 0 0
c
c --- Permanent Reflector -----------------------------------------------------
651  rcc 0 0 -261 0 0 522 212.5
c
c --- Auxiliary Organization --------------------------------------------------
950  rcc 0 0 -1000 0 0 2000 25 $ small cylinder
999  rcc 0 0 -2500 0 0 5000 2500 $ big cylinder
c

c Data Cards ******************************************************************
c --- Material Cards ----------------------------------------------------------
c ------ Kernel (3.4%) ------
m1    5010.00c 1.7299E-07
      8016.00c 4.6386E-02
      8017.00c 1.7633E-05
     92234.00c 6.1026E-06
     92235.00c 7.9888E-04
     92238.00c 2.2405E-02
c    Total     6.9614E-02
mt1   OUO2.00t
      UUO2.00t
c
c ------ Kernel (3.9%) ------
m2    5010.00c 1.7299E-07
      8016.00c 4.6386E-02
      8017.00c 1.7633E-05
     92234.00c 7.0000E-06
     92235.00c 9.1637E-04
     92238.00c 2.2288E-02
c    Total     6.9616E-02
mt2   OUO2.00t
      UUO2.00t
c
c ------ Kernel (4.3%) ------
m3    5010.00c 1.7299E-07
      8016.00c 4.6386E-02
      8017.00c 1.7633E-05
     92234.00c 7.7180E-06
     92235.00c 1.0104E-03
     92238.00c 2.2195E-02
c    Total     6.9617E-02
mt3   OUO2.00t
      UUO2.00t
c
c ------ Kernel (4.8%) ------
m4    5010.00c 1.7299E-07
      8016.00c 4.6386E-02
      8017.00c 1.7633E-05
     92234.00c 8.6154E-06
     92235.00c 1.1278E-03
     92238.00c 2.2078E-02
c    Total     6.9618E-02
mt4   OUO2.00t
      UUO2.00t
c
c ------ Kernel (5.2%) ------
m5    5010.00c 1.7299E-07
      8016.00c 4.6386E-02
```

```
      8017.00c 1.7633E-05
     92234.00c 9.3334E-06
     92235.00c 1.2218E-03
     92238.00c 2.1984E-02
c    Total     6.9619E-02
mt5   OUO2.00t
      UUO2.00t
c
c ------ Kernel (5.9%) ------
m6    5010.00c 1.7299E-07
      8016.00c 4.6386E-02
      8017.00c 1.7633E-05
     92234.00c 1.0590E-05
     92235.00c 1.3863E-03
     92238.00c 2.1821E-02
c    Total     6.9622E-02
mt6   OUO2.00t
      UUO2.00t
c
c ------ Kernel (6.3%) ------
m7    5010.00c 1.7299E-07
      8016.00c 4.6386E-02
      8017.00c 1.7633E-05
     92234.00c 1.1308E-05
     92235.00c 1.4803E-03
     92238.00c 2.1727E-02
c    Total     6.9623E-02
mt7   OUO2.00t
      UUO2.00t
c
c ------ Kernel (6.7%) ------
m8    5010.00c 1.7299E-07
      8016.00c 4.6386E-02
      8017.00c 1.7633E-05
     92234.00c 1.2026E-05
     92235.00c 1.5743E-03
     92238.00c 2.1634E-02
c    Total     6.9624E-02
mt8   OUO2.00t
      UUO2.00t
c
c ------ Kernel (7.2%) ------
m9    5010.00c 1.7299E-07
      8016.00c 4.6386E-02
      8017.00c 1.7633E-05
     92234.00c 1.2923E-05
     92235.00c 1.6918E-03
     92238.00c 2.1517E-02
c    Total     6.9625E-02
mt9   OUO2.00t
      UUO2.00t
c
c ------ Kernel (7.9%) ------
m10   5010.00c 1.7299E-07
      8016.00c 4.6386E-02
      8017.00c 1.7633E-05
     92234.00c 1.4180E-05
     92235.00c 1.8562E-03
     92238.00c 2.1353E-02
c    Total     6.9628E-02
mt10  OUO2.00t
      UUO2.00t
c
c ------ Kernel (9.4%) ------
m11   5010.00c 1.7299E-07
      8016.00c 4.6386E-02
      8017.00c 1.7633E-05
     92234.00c 1.6872E-05
     92235.00c 2.2087E-03
     92238.00c 2.1002E-02
c    Total     6.9632E-02
mt11  OUO2.00t
      UUO2.00t
c
c ------ Kernel (9.9%) ------
m12   5010.00c 1.7299E-07
```

```
      8016.00c 4.6386E-02
      8017.00c 1.7633E-05
     92234.00c 1.7769E-05
     92235.00c 2.3262E-03
     92238.00c 2.0886E-02
c    Total     6.9634E-02
mt12  OUO2.00t
      UUO2.00t
c
c ------ Buffer Layer ------
m13   5010.00c 1.8290E-08
      6000.00c 5.5153E-02
c    Total     5.5153E-02
mt13 Graph.00t
c
c ------ IPyC Layer ------
m14   5010.00c 3.0761E-08
      6000.00c 9.2758E-02
c    Total     9.2758E-02
mt14 Graph.00t
c
c ------ SiC Layer ------
m15   5010.00c 5.3208E-08
      6000.00c 4.8061E-02
     14028.00c 4.4327E-02
     14029.00c 2.2508E-03
     14030.00c 1.4837E-03
c    Total     9.6122E-02
mt15 Graph.00t
c
c ------ OPyC Layer ------
m16   5010.00c 3.0761E-08
      6000.00c 9.2758E-02
c    Total     9.2758E-02
mt16 Graph.00t
c
c ------ Graphite Overcoat ------
m17   5010.00c 2.8267E-08
      6000.00c 8.5237E-02
c    Total     8.5237E-02
mt17 Graph.00t
c
c ------ Graphite Compact ------
m18   5010.00c 1.5452E-08
      6000.00c 8.5237E-02
c    Total     8.5237E-02
mt18 Graph.00t
c
c ------ Graphite Sleeve ------
m19   5010.00c 7.2596E-09
      6000.00c 8.8747E-02
c    Total     8.8747E-02
mt19 Graph.00t
c
c ------ Burnable Poison (2.0%) ------
m20   5010.00c 3.9906E-04
      5011.00c 1.6063E-03
      6000.00c 8.8446E-02
c    Total     9.0451E-02
mt20 Graph.00t
c
c ------ Burnable Poison (2.5%) ------
m21   5010.00c 4.9882E-04
      5011.00c 2.0078E-03
      6000.00c 8.7995E-02
c    Total     9.0501E-02
mt21 Graph.00t
c
c ------ Graphite Disks ------
m22   5010.00c 7.2596E-09
      6000.00c 8.8747E-02
c    Total     8.8747E-02
mt22 Graph.00t
c
c ------ Neutron Absorber ------
m23   5010.00c 6.3184E-03
```

```
      5011.00c 2.5432E-02
      6000.00c 6.6685E-02
c    Total     9.8436E-02
mt23 Graph.00t
c
c ------ Alloy 800H ------
m24   6000.00c 3.2210E-04
     13027.00c 6.7209E-04
     14028.00c 5.5580E-04
     14029.00c 2.8222E-05
     14030.00c 1.8604E-05
     15031.00c 3.1225E-05
     16032.00c 1.4316E-05
     16033.00c 1.1462E-07
     16034.00c 6.4698E-07
     16036.00c 3.0162E-09
     22046.00c 3.1254E-05
     22047.00c 2.8186E-05
     22048.00c 2.7928E-04
     22049.00c 2.0495E-05
     22050.00c 1.9624E-05
     24050.00c 8.4860E-04
     24052.00c 1.6364E-02
     24053.00c 1.8556E-03
     24054.00c 4.6189E-04
     25055.00c 8.8022E-04
     26054.00c 2.2265E-03
     26056.00c 3.4951E-02
     26057.00c 8.0717E-04
     26058.00c 1.0742E-04
     28058.00c 1.8229E-02
     28060.00c 7.0217E-03
     28061.00c 3.0523E-04
     28062.00c 9.7320E-04
     28064.00c 2.4785E-04
     29063.00c 1.5791E-04
     29065.00c 7.0383E-05
c    Total     8.7530E-02
mt24    Fe.00t
        Al.00t
c
c ------ IG-110 Graphite ------
m25   5010.00c 1.1453E-08
      6000.00c 8.7804E-02
c    Total     8.7804E-02
mt25 Graph.00t
c
c ------ PGX Graphite ------
m26   5010.00c 3.6372E-08
      6000.00c 8.6134E-02
c    Total     8.6134E-02
mt26 Graph.00t
c
c ------ Helium Coolant ------
m27   2003.00c 3.3724E-11
      2004.00c 2.4616E-05
c    Total     2.4616E-05
c
c ------ IG-11 Graphite ------
m28   5010.00c 5.9835E-08
      6000.00c 8.7305E-02
c    Total     8.7305E-02
mt28 Graph.00t
c
c --- Control Cards -----------------------------------------------------------
mode  n
kcode 50000 1 50 1050
ksrc  93.545       0 -20  93.545       0 20
     -93.545       0 -20 -93.545       0 20
      55.050  76.350 -20  55.050  76.350 20
     -55.050  76.350 -20 -55.050  76.350 20
      55.050 -76.350 -20  55.050 -76.350 20
     -55.050 -76.350 -20 -55.050 -76.350 20
c print
```

A.2 Buckling and Extrapolation Length Configurations

Buckling and extrapolation length measurements were not made.

A.3 Spectral-Characteristics Configurations

Spectral characteristics measurements were not made.

A.4 Reactivity-Effects Configurations

MCNP5 Input Deck for the excess reactivity measurements of the HTTR:

The input decks from the 30-fuel-column core configuration in HTTR-GCR-RESR-001 and the 19-, 21-, 24-, and 27-fuel-column core configurations in this report are used to determine the excess reactivity of the HTTR core loading. Control rod positions are either fully withdrawn or adjusted to positions already reported in this report and HTTR-GCR-RESR-001.

A.5 Reactivity Coefficient Configurations

Reactivity coefficient measurements have not been evaluated.

A.6 Kinetics Parameter Configurations

Kinetics measurements have not been evaluated.

A.7 Reaction-Rate Configurations

MCNP5 Input Deck for the axial neutron fission reaction rate in the instrumentation columns of the HTTR:

The input deck used to determine the axial reaction rate in the instrumentation columns is that of either configuration 3 or 4 (the 24-fuel-column annular core) with the following appended coding to the end of the input deck:

```
c --- Tally Cards ------------------------------------------------------------
c ------ Plutonium Foil in Fission Chamber ------
m101 92235.00c 1.
c
fmesh4:n geom cyl origin 114.6005 72.4 -261
         imesh 6.15 jmesh 522 jints 522 kmesh 1
fm4  (1 101 -6)
fmesh14:n geom cyl origin 5.4 -135.447 -261
          imesh 6.15 jmesh 522 jints 522 kmesh 1
fm14 (1 101 -6)
fmesh24:n geom cyl origin -120 63.04693 -261
          imesh 6.15 jmesh 522 jints 522 kmesh 1
fm24 (1 101 -6)
c
```

A.8 Power Distribution Configuration

Power distribution measurements were not made.

A.9 Isotopic Configurations

Isotopic measurements were not made.

A.10 Configurations of Other Miscellaneous Types of Measurements

Other miscellaneous types of measurements were not made.

APPENDIX B: CALCULATED SPECTRAL DATA

B.1 Spectral Data for the Critical and Subcritical Configurations

Data generated in the MCNP5 output files include information regarding the energy of the average lethargy causing fission (EALF) and the percentages of fission caused by thermal, intermediate, and fast energy neutrons for each case shown in Tables 4.1 through 4.5; results are shown in Tables B.1 through B.5, respectively. There was no significant difference in the spectra when using different neutron libraries. The MCNP5 calculations were performed with 1,050 generations (skipping the first 50) and 50,000 neutrons per generation. The only significant difference is that the EALF values are slightly elevated and the neutron fission spectra is distributed slightly more in the fast energy range in Case 4. This configuration uses only the control rods in the reflector region to manage core criticality whereas the other configurations typically remove the reflector rods and maintain criticality via the core control systems. The JENDL-3.3 analysis was performed with the inclusion of ENDF/B-VII.0 thermal neutron scattering data because it was not included in the JENDL-3.3 library.

Table B.1. Spectral Data for the HTTR Benchmark Model Evaluation using an Ordered Lattice (Case 1).

Neutron Cross-Section Library	EALF (eV)	Percentage of Neutrons Causing Fission		
		<0.625 eV	0.625 eV – 100 keV	>100 keV
ENDF/B-V.2	0.0776	92.36	6.73	0.91
ENDF/B-VI.8	0.0758	92.53	6.57	0.90
END/B-VII.0	0.0758	92.53	6.57	0.90
JEFF-3.1	0.0755	92.53	6.57	0.90
JENDL-3.3 with ENDF/B-VII.0 S(α,β)	0.0763	92.48	6.60	0.92

Table B.2. Spectral Data for the HTTR Benchmark Model Evaluation using an Ordered Lattice (Case 2).

Neutron Cross-Section Library	EALF (eV)	Percentage of Neutrons Causing Fission		
		<0.625 eV	0.625 eV – 100 keV	>100 keV
ENDF/B-V.2	0.0774	92.39	6.71	0.90
ENDF/B-VI.8	0.0757	92.56	6.55	0.89
END/B-VII.0	0.0758	92.56	6.55	0.90
JEFF-3.1	0.0754	92.56	6.55	0.89
JENDL-3.3 with ENDF/B-VII.0 S(α,β)	0.0761	92.52	6.57	0.91

Table B.3. Spectral Data for the HTTR Benchmark Model Evaluation using an Ordered Lattice (Case 3).

Neutron Cross-Section Library	EALF (eV)	Percentage of Neutrons Causing Fission		
		<0.625 eV	0.625 eV – 100 keV	>100 keV
ENDF/B-V.2	0.0775	92.41	6.69	0.90
ENDF/B-VI.8	0.0759	92.56	6.55	0.89
END/B-VII.0	0.0759	92.57	6.54	0.89
JEFF-3.1	0.0756	92.58	6.54	0.89
JENDL-3.3 with ENDF/B-VII.0 S(α,β)	0.0763	92.53	6.57	0.90

Table B.4. Spectral Data for the HTTR Benchmark Model Evaluation using an Ordered Lattice (Case 4).

Neutron Cross-Section Library	EALF (eV)	Percentage of Neutrons Causing Fission		
		<0.625 eV	0.625 eV – 100 keV	>100 keV
ENDF/B-V.2	0.0813	91.98	7.11	0.91
ENDF/B-VI.8	0.0795	92.15	6.94	0.90
END/B-VII.0	0.0797	92.14	6.95	0.91
JEFF-3.1	0.0792	92.16	6.94	0.90
JENDL-3.3 with ENDF/B-VII.0 S(α,β)	0.0800	92.11	6.98	0.92

Table B.5. Spectral Data for the HTTR Benchmark Model Evaluation using an Ordered Lattice (Case 5).

Neutron Cross-Section Library	EALF (eV)	Percentage of Neutrons Causing Fission		
		<0.625 eV	0.625 eV – 100 keV	>100 keV
ENDF/B-V.2	0.0769	92.52	6.58	0.90
ENDF/B-VI.8	0.0752	92.69	6.42	0.89
END/B-VII.0	0.0753	92.69	6.42	0.89
JEFF-3.1	0.0749	92.70	6.42	0.89
JENDL-3.3 with ENDF/B-VII.0 S(α,β)	0.0756	92.66	6.45	0.90

APPENDIX C: DATA FROM THE 16TH EDITION CHART OF THE NUCLIDES[a]

C.1 Isotopic Abundances and Atomic Weights

This evaluation incorporated atomic weights and isotopic abundances found in the 16th edition of the Chart of the Nuclides. A list of the values used in the benchmark model or in the generation of the MCNP input deck is compiled in Table C.1.

Table C.1. Summary of Data Employed from the 16th Ed. of the Chart of the Nuclides.

Isotope or Element	Atomic Weight	Isotopic Abundance
He	4.002602	--
^{3}He	--	0.000137
^{4}He	--	99.999863
^{10}B	10.0129370	19.9
^{11}B	11.0093055	80.1
C	12.0107	--
N	14.0067	--
^{14}N	--	99.632
^{15}N	--	0.368
O	15.9994	--
^{16}O	--	99.757
^{17}O	--	0.038
^{18}O(a)	--	0.205
Na	22.989770	--
Al	26.981538	--
Si	28.0855	--
^{28}Si	--	92.2297
^{29}Si	--	4.6832
^{30}Si	--	3.0872
P	30.973761	--
S	32.065	--
^{32}S	--	94.93
^{33}S	--	0.76
^{34}S	--	4.29
^{36}S	--	0.02
Ca	40.078	--

[a] Nuclides and Isotopes: Chart of the Nuclides, 16th edition, (2002).

Table C.1 (cont'd.). Summary of Data Employed from the 16th Ed. of the Chart of the Nuclides.

Isotope or Element	Atomic Weight	Isotopic Abundance
^{40}Ca	--	96.941
^{42}Ca	--	0.647
^{43}Ca	--	0.135
^{44}Ca	--	2.086
^{46}Ca	--	0.004
^{48}Ca	--	0.187
Ti	47.867	--
^{46}Ti	--	8.25
^{47}Ti	--	7.44
^{48}Ti	--	73.72
^{49}Ti	--	5.41
^{50}Ti	--	5.18
Cr	51.9961	--
^{50}Cr	--	4.345
^{52}Cr	--	83.789
^{53}Cr	--	9.501
^{54}Cr	--	2.365
Mn	54.938049	--
Fe	55.845	--
^{54}Fe	--	5.845
^{56}Fe	--	91.754
^{57}Fe	--	2.119
^{58}Fe	--	0.282
Ni	58.6934	--
^{58}Ni	--	68.0769
^{60}Ni	--	26.2231
^{61}Ni	--	1.1399
^{62}Ni	--	3.6345
^{64}Ni	--	0.9256
Cu	63.546	--
^{63}Cu	--	69.17
^{65}Cu	--	30.83

Table C.1 (cont'd.). Summary of Data Employed from the 16th Ed. of the Chart of the Nuclides.

Isotope or Element	Atomic Weight	Isotopic Abundance
^{234}U	234.040946	0.0055[(b)]
^{235}U	235.043923	0.7200[(b)]
^{238}U	238.050783	99.2745[(b)]

(a) Neutronically, ^{18}O is treated as ^{16}O.
(b) Natural isotopic abundance of U.